S

S

► Sulfur

Saccharide

► Carbohydrate

Sagan Carl

Florence Raulin-Cerceau
Maître de Conférences, Centre Alexandre Koyré (UMR 8560-CNRS/EHESS/MNHN/CSI)
Muséum National d'Histoire Naturelle, Brunoy, France

History

Carl Edward Sagan (November 9, 1934 – December 20, 1996) pioneered Exobiology since the beginning of planetary exploration and played a leading role in the preparation of experiments intended to detect signs of life on other planets. He was associated with the American space program since its beginning in the 1950s and contributed to the *Mariner*, *Viking*, *Voyager*, and *Galileo* missions.

His background in astronomy and astrophysics (University of Chicago) and his strong interest in the origin of life on Earth and elsewhere in the universe led him to combine scientific fields such as biology, chemistry, and astrophysics. He popularized Exobiology with talent and wrote many popular science bestsellers. Above all, he was very famous for cowriting and presenting in the 1980s the TV series *Cosmos*: *A Personal Voyage*, which was broadcasted all over the world.

Sagan promoted ► SETI (Search for Extraterrestrial Intelligence) thanks to his fine talent as writer (*Cosmic Connection*: *An Extraterrestrial Perspective*, 1973) and to the universal messages he added on the *Pioneer* and *Voyager* space probes launched in the 1970s and planned to leave the solar system. He was the author of the novel *Contact* (1985), a story dealing with SETI, which became the basis for the film "*Contact*" (1997), starring actress Jodie Foster (1962-).

His scientific career was also brilliant. He became full Professor at Cornell University in 1971, where he directed the Laboratory for Planetary Studies. He published many renowned papers about the high surface temperatures of Venus, the seasonal changes on Mars, or the reddish haze of Titan (and its *tholins*, a word that he invented). His contributions to Martian exploration (*Viking* experiments) consolidated the field of Exobiology. Editor in Chief of the International Journal *Icarus* during 12 years, he was also the cofounder and first president of the

M. Gargaud et al. (eds.), *Encyclopedia of Astrobiology*,
DOI 10.1007/978-3-662-44185-5

Planetary Society in 1980. He received many awards throughout his career and could be seen as a forerunner in lots of topics, thanks to his hypotheses which were confirmed many times.

See Also

- ▶ Galileo Galilei
- ▶ SETI
- ▶ Valles Marineris
- ▶ Viking
- ▶ Voyager, Spacecraft

Sagduction

Nicholas Arndt
ISTerre, Université Grenoble Alpes, France

Definition

This term refers to the return of crustal material into the ▶ mantle in downward-moving diapirs (large teardrop-shaped masses of ductile material) composed of dense metavolcanic and metasedimentary rock. The hypothesis has two sources. First, some authors attribute the dome-and-basin structure of Archean granite-greenstone belts (examples are observed in the ▶ Pilbara Craton, Western Australia) to vertical tectonics involving upward- and downward-directed diapirs. Second, some authors believe that ▶ plate tectonics could not have operated on a hot early Earth and that thus another mechanism must have operated to recycle oceanic crust back into the mantle.

See Also

- ▶ Archean Tectonics
- ▶ Pilbara Craton
- ▶ Plate Tectonics
- ▶ Subduction

Salt Tolerance

- ▶ Halotolerance

Salt-Loving Organisms

- ▶ Halophile

Sample Receiving Facility

Catharine A. Conley
NASA Headquarters, Washington, DC, USA

Definition

For planetary protection, the Sample Receiving Facility is a high-containment facility for samples returned from another planetary body that might contain extraterrestrial organisms and is the location in which sample canisters are open and samples are identified and sorted. Then a fraction of the samples is submitted to the Biohazard Assessment Protocol either in this facility or in other adapted and dedicated facilities while the remaining part is safely stored.

See Also

- ▶ Biological Safety Level
- ▶ Planetary Protection Category
- ▶ Quarantine

Sanukitoid

Hervé Martin
Laboratoire Magmas et Volcans, Université Blaise Pascal, OPGC, CNRS, IRD, Clermont-Ferrand, France

Keywords

Archean-Proterozoic transition; Continental crust; Mantle metasomatism

Synonyms

High-magnesium granodiorite

Definition

Sanukitoids are intermediate to felsic igneous rocks which possess both modern crust characteristics (i.e., richness in K) and Archean TTG features (i.e., fractionated rare-earth element patterns). Most of them were emplaced between 2.7 and 2.3 Ga on Earth.

Overview

Sanukitoids, also called *high-magnesium granodiorites*, were first described by Shirey and Hanson (1984). They consist in a complete magmatic series, from diorite to granite, the most common facies consisting in monzodiorites and monzogranites. Typically they are rich in both K-feldspar phenocrysts and mafic minerals such as biotite and hornblende with sometimes subordinate amounts of clinopyroxene.

Sanukitoid can occur as plutons of all sizes, with a broad range of crustal emplacement levels and degrees of heterogeneity: sanukitoids in the Central Pilbara Craton, Western Australia (Smithies and Champion 1999), form small (<1 km), homogeneous stocks of shallow-emplaced magmas; sanukitoids of South India (Closepet Granite; Moyen et al. 2001) form a huge intrusive body that is about 400 km long and 20 km wide and is rooted in the lower granulitic crust.

From the chemical point of view, these rocks possess both modern characteristics (i.e., richness in K) and Archean TTG features (i.e., fractionated rare-earth element patterns). In other words, their composition is intermediate between that of Archean TTG and that of the modern continental crust.

Melting experiments and petrogenetic geochemical modeling show that sanukitoids may have formed by either (1) melting of mantle peridotite previously transformed (metasomatized) by felsic melts having a TTG composition or (2) by reaction between TTG melts and mantle peridotite (assimilation; Martin et al. 2009).

The transitional character of sanukitoids is not only compositional but also chronologic, since most of them were emplaced between 2.7 and 2.3 Ga, at the Archean-Proterozoic boundary, the period when the Earth geodynamics changed from archaic to modern style. Indeed, then, the source of juvenile continental crust changed from basalt melting, producing TTG to fusion of peridotites, resulting in calc-alkaline magmas; the tectonic regime changed from horizontal + vertical in the Archean to only horizontal in Paleoproterozoic. All these fundamental evolutions, as well as the disappearance of komatiites after 2.5 Ga, result in the progressive cooling of our planet.

See Also

- ▶ Archean Eon
- ▶ Trondhjemite
- ▶ TTG

References and Further Reading

Martin H, Moyen J-F, Rapp R (2009) The sanukitoid series: magmatism at the Archaean-Proterozoic transition. Earth Environ Sci Trans R Soc Edinb 100:15–33

Moyen J-F, Martin H, Jayananda M (2001) Multi-element geochemical modelling of crust-mantle interactions during late-Archaean crustal growth: the Closepet granite (South India). Precambrian Res 112:87–105

Shirey SB, Hanson GN (1984) Mantle derived Archaean monzodiorites and trachyandesites. Nature 310:222–224

Smithies RH, Champion DC (1999) High-Mg diorite from the Archaean Pilbara Craton; anorogenic magmas derived from a subduction-modified mantle. Geol Surv West Austr Annu Rev 1998–1999:45–59

Sarcosine

Kensei Kobayashi
Yokohama National University, Tokiwadai, Hodogayaku, Yokohama, Japan

Synonyms

2-(Methylamino) acetic acid; *N*-Methylglycine

Definition

Sarcosine is a ▶ nonprotein amino acid and a structural isomer of alanine. While alanine is chiral, sarcosine is achiral since it does not have an asymmetric carbon atom. Its molecular structure is CH_3NHCH_2COOH, and its molecular weight is 89.093. Though sarcosine is not a protein ▶ amino acid, it is a biogenic amino acid and is widely distributed in organisms. It is widely distributed in foods such as egg yolks, meats, and vegetables. Since it has no amino group ($-NH_2$) but an imino group (-NH-), it requires special care in amino acid analysis, since sensitive amino acid detection often requires derivatization of the amino group. It is one of the most abundant amino acids in prebiotic chemistry. Sarcosine was found in Miller's spark discharge products and also in extracts from carbonaceous chondrites such as the Murchison meteorite.

See Also

▶ Amino Acid
▶ Nonprotein Amino Acids

Satellite or Moon

Ralf Jaumann
German Aerospace Center (DLR), Institute of Planetary Research, Berlin, Germany

Definition

The term satellite refers to a natural object that orbits another (larger) body or to an artificial object placed into orbit by human action. Thus, ▶ planets that orbit a star may also be considered natural satellites. However, the basic definition of a natural satellite is a celestial body that orbits a planet or a small body and is classically also called a moon. The sizes of natural satellites in our ▶ Solar System range from 5,268 km for the Jovian moon ▶ Ganymede to objects of less than 1 km in diameter. Among the objects classified as natural satellites are 172 objects that orbit planets, 169 of which are in the outer Solar System. Eight satellites orbit ▶ dwarf planets. A significant number of satellites are known to orbit asteroids (186) and trans-Neptunian objects (TNOs) (84).

See Also

▶ Callisto
▶ Deimos
▶ Dwarf Planet
▶ Enceladus
▶ Europa
▶ Ganymede
▶ Io
▶ Miranda
▶ Moon, The
▶ Planet
▶ Phobos
▶ Rhea
▶ Small Solar System Body
▶ System Solar Formation, Chronology of
▶ Titan
▶ TNO
▶ Triton

Saturn

Therese Encrenaz
LESIA, Observatoire de Paris - Section de Meudon, Meudon, France

Keywords

Giant planets

Definition

Saturn is, after ▶ Jupiter, the second of the Solar System's ▶ giant planets, by order of mass, size,

and heliocentric distance. Its mean distance to the Sun is 9.5 AU. Its diameter is 120,530 km or 9.45 times the Earth's diameter and its mass amounts to 95 terrestrial masses. Its density is 0.69 g/cm^3, such that Saturn is the least dense Solar System planet. The difference of density between Jupiter (1.3 g/cm^3) and Saturn can be explained by the stronger compression factor that acts on Jupiter, due to the fact that the latter is more than three times as massive. Basically, Jupiter and Saturn have the same chemical composition, dominated by the protosolar gas (mostly hydrogen and helium), which collapsed on their rocky core at the time of the planets' formation; they are called the gas giants. In contrast, the two other giant planets, Uranus and Neptune, which accreted a minor fraction of protosolar gas around their rocky cores, are called the ice giants.

Overview

Early Exploration

As for Jupiter, the astronomical observation of Saturn started at the beginning of the seventeenth century, when ▶ Galileo Galilei turned his first refractor to the Moon, planets, and stars. Galileo soon noticed that Saturn's shape was slowly changing, but he was not able to explain this phenomenon. The answer, the changing orientation of Saturn's rings with respect to the Earth, was provided by Christiaan ▶ Huygens in 1659 who proposed that a flat equatorial ring surrounded the planet. In 1675 Giovanni Domenico ▶ Cassini discovered the Cassini division in the rings, and, one century later in 1787, Pierre-Simon de Laplace, on the basis of dynamical studies, concluded that Saturn was surrounded by a large number of narrow rings.

In 1676, Cassini discovered the equatorial belt of Saturn. In 1787, William Herschel measured the flattening of the planet and, 3 years later, the planet's rotation period. With a period of 10.6 h, Saturn, as Jupiter, is a fast-rotating object. The average angular diameter of Saturn is 16 arcs.

The Space Exploration

The space exploration of Saturn started with the Pioneer 11 encounter. Launched in 1973 by NASA, Pioneer 11 used the gravity assistance of a ▶ Jupiter flyby to encounter Saturn in 1979. In addition to a camera, UV, and IR photometers, its instruments were specially designed for the study of both the planets and the interplanetary magnetic field. Pioneer 11 sent back amazing images of Saturn's rings, discovered two new satellites and a new ring, and explored Saturn's ▶ magnetosphere.

Only 1 year after Pioneer's discoveries, Saturn's flyby by the Voyager 1 spacecraft brought even more spectacular results. The Voyager mission, composed of two identical spacecraft, was designed to explore the four giant planets by successive flybys during 1979 and 1989. Saturn was approached in 1980 by Voyager 1, which passed close to Titan, and in 1981 by Voyager 2, which continued its way to Uranus and Neptune. Voyager 1 measured the atmospheric composition of Saturn, tracked its atmospheric spots, measured its zonal winds, and detected a high level of auroral activity.

Since the Voyager era, Saturn was continuously monitored by ground-based telescopes and by the Hubble Space Observatory. The next milestone was the ambitious Cassini-Huygens mission, jointly led by NASA and the European Space Agency (ESA), and devoted to the exploration of the Saturnian system. Launched in 1997, the Cassini orbiter approached Saturn in 2004. On January 14, 2005, the Huygens probe successfully landed on ▶ Titan's surface, sending the first images of that satellite's surface. Since 1995, the Cassini orbiter has been exploring Saturn and its rings and satellites, bringing an impressive number of results and discoveries, including the rings' fine structure, ▶ cryovolcanism on ▶ Enceladus, and lakes on Titan. The Cassini mission has been extended until 2017 (Fig. 1).

Dynamical Structure

Like Jupiter, Saturn's disk shows a zone and belt structure, ascribed to a convective, Hadley-type circulation of a fast-rotating body. The zones are

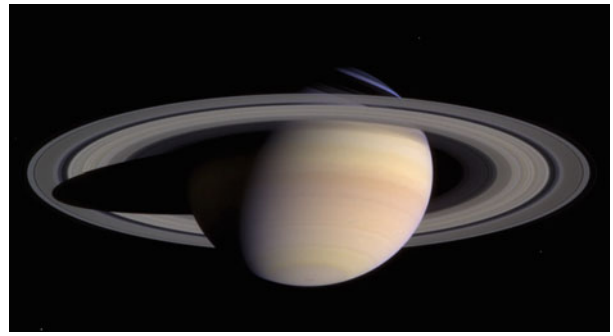

Saturn, Fig. 1 Saturn and its ring system, as observed by the Cassini orbiter (© NASA)

associated with ascending cloudy regions, while the belts are dry subsiding regions. The cloud structures on Saturn appear less contrasted than on Jupiter. The more uniform yellowish color of Saturn is explained by thicker ammonia clouds, resulting from the lower surface temperature of this planet. In spite of this apparent uniformity, Saturn exhibits a strong dynamical activity. At the South Pole, Cassini visible and near-infrared images have shown a hurricane with a giant eye, sharing some similarities with terrestrial hurricanes. In contrast, the northern hemisphere displays a hexagonal feature, already observed on the Voyager images, that encircles the North Pole at a latitude of 77N. It is similar to the Earth's polar vortex, except that it possesses six branches instead of being circular. This feature is the signature of a long-lived, complex system of convective cells that extend deep in the planet's ▶ troposphere. The mechanism that drives these huge cyclonic features is still not understood.

In December 2010, a huge storm appeared in the Northern hemisphere at a latitude of 32N. It rapidly extended over longitudes to form a large band of white clouds, monitored by the Cassini spacecraft. Such phenomena have appeared in the past in the northern hemisphere for over a century, with a mean period of 28.5 years (subject to significant fluctuations), and seem to occur during summer solstice when insolation is maximum. The Cassini instruments recorded a strong atmospheric heating, suggesting a massive atmospheric upwelling.

Atmospheric Composition and Structure

The thermal structure of Saturn is very similar to the Jovian one, with a ▶ troposphere, a tropopause, and a ▶ stratosphere. The tropopause is located at a pressure level of 100 mbar, as in the case of the other giant planets. Because of its large heliocentric distance, its temperature (80 K) is lower than at the Jovian tropopause. Below the tropopause, as in the case of Jupiter, the troposphere extends downward with an ▶ adiabatic gradient. Above the tropopause in the stratosphere, temperature increases with altitude. The heating takes place at higher altitudes than on Jupiter, which implies different heating mechanisms.

The cloud structure of Saturn is also similar to the Jovian one, but it appears at higher pressure due to the colder environment. Thermochemical models predict an NH_3 cloud at about 1.5 bar, an NH_4SH cloud at 4 bars, and an H_2O cloud at about 10 bars. Only, the thick ammonia cloud deck is observed; the other clouds are too deep to be observable. In the stratosphere, a haze is observed, probably due to hydrocarbon condensates.

Similar to Jupiter, Saturn's atmosphere is dominated by hydrogen and helium. At the time of the Voyager encounter (1980), a very low helium abundance was inferred from infrared and radio-occultation data. This result was interpreted in terms of helium condensation inside a liquid hydrogen ocean in the interior of the planet: helium droplets sinking and falling toward the center would lead to the depletion of the helium gas in the outer atmosphere; in addition, it would release some internal energy, as also observed by Voyager (see below: Internal

Structure). However, in 2000 Voyager data were reanalyzed, leading to a greater helium abundance, in better agreement with the Jupiter value. In both cases, the helium abundance is lower than the protosolar value, such that helium condensation within the interior of the planets might be responsible for this depletion and also account partly for the internal energy source.

As a result of the planet's strong dynamical activity, the tropospheric abundance of PH_3 (▶ Phosphine) in Saturn is higher than in Jupiter; indeed, PH_3 is a disequilibrium species that is not expected to be observable according to thermochemical equilibrium models. Its presence in the planets' spectra is believed to be the signature of convective motions, particularly strong in the case of Saturn. As in Jupiter, many hydrocarbons are found in Saturn's stratosphere, resulting from methane photodissociation. Oxygen species (H_2O, CO_2) have also been detected by the Infrared Space Observatory (ISO), and water has been recently monitored with Herschel, as in the other giant planets and Titan. The oxygen species are believed to come from an external source, either local (Saturn's rings and satellites) or interplanetary (comets). In the case of Saturn, which has a very massive ring system, the local source might be dominant.

As Saturn has not yet been explored by an entry probe, we have little information about the abundances of heavy elements. Still, a C/H ratio = 9 can be inferred from the CH_4 abundance, which is consistent with the value expected from a model assuming that the giant planets formed from an icy core of about 10–15 terrestrial masses.

Internal Structure

Saturn's ▶ interior structure can be probed indirectly from the measurements of its basic parameters (mass, radius, density) and its gravitational moments. Additional information is deduced from its composition and its internal heat source. The Voyager IRIS infrared spectrometer measured the planet's emission over the total infrared range and led to the conclusion that the internal energy of Saturn is 1.78 times the absorbed solar energy, that is, slightly greater than in the case of Jupiter.

The structure of Saturn, as predicted by theoretical models, is similar to Jupiter's, with a central core of ices and rocks, surrounded by an ocean of metallic hydrogen and a layer of molecular hydrogen, mixed with helium. The central pressure could be about 50 Mbar with a central temperature of ~12,000 K. As mentioned above, the origin of Saturn's internal energy could partly result from the condensation of helium in the metallic ocean. Another plausible origin is the adiabatic cooling of the planet that slowly releases the energy accumulated during its accretion phase.

The Magnetosphere of Saturn

Saturn's ▶ magnetosphere was unknown prior to the planet's space exploration by Pioneer 11 in 1979, then by Voyagers 1 and 2 in 1980 and 1981. Since 1995, Saturn's environment is being monitored in depth by the Cassini orbiter.

Saturn's magnetic field is almost aligned with the planet's rotation axis. As in the case of Jupiter, the fast rotation of the planet induces a corotation of the plasma and the same general magnetospheric structure. However, Saturn's magnetosphere is coupled to specific sources: ▶ Titan, as a provider of H+ and N+ ions, the neutral torus of hydrogen and nitrogen, the icy satellites, the rings, and the ionosphere.

Auroral phenomena appear at fixed locations at high northern and southern latitudes. In the radio range, Voyager discovered the Saturn Kilometric Radiation (SKR), which is auroral and nonthermal, similar to the Auroral Kilometric radiation (AKR) on Earth.

Measuring the radio emission of giant planets is important for determining precisely the rotation period of the planet's interior. From Voyager measurements, Saturn's rotation period was found to be 10 h 39 min 24 s. However, subsequent measurements by the Ulysses probe and more recently by Cassini have shown that this period has increased by more than 6 min. Recently it has been shown that the rotation period is actually modulated by the solar wind: the dynamical pressure of the solar wind induces

changes in the speed of the solar wind as it interacts with Saturn's magnetic field and thus induces a slight change in the measured radio emission.

See Also

- ▶ Cassini-Huygens Space Mission
- ▶ Enceladus
- ▶ Giant Planets
- ▶ Hadley Cells
- ▶ Jupiter
- ▶ Interior Structure, Planetary
- ▶ Phosphine
- ▶ Pioneer Spacecraft
- ▶ Radiative Processes
- ▶ Titan
- ▶ Voyager, Spacecraft

References and Further Reading

Baines KH et al (2009) Saturn north polar cyclone and hexagon at depth revealed by Cassini/VIMS. Planet Space Sci 57:1671–1681

Drossart P (2001) Saturn. In: Murdin P (ed) Encyclopedia of astronomy and astrophysics. Institute of Physics, Bristol

Gehrels T, Matthews M (1984) Saturn. University of Arizona Press, Tucson

Godfrey DA (1988) A hexagonal structure around Saturn's north pole. Icarus 76:335–356

Zarka P, Lamy L, Cecconi B, Prangé R, Rucker HO (2007) Solar wind modulation of Saturn's radio clock. Nature 450:265–267

Scale Height

Lisa Kaltenegger
Cornell University, Ithaca, NY, USA

Definition

A scale height H is the distance over which a quantity decreases by a factor of e (the base of natural logarithms). For planetary atmospheres, it is the vertical distance upwards over which the pressure of the atmosphere decreases by a factor of 1/e. For an isothermal atmosphere,

$$H = kT/\mu g$$

where k is the Boltzmann constant (1.38×10^{-23} J K^{-1}), T the mean planetary temperature in Kelvin, μ the mean molecular weight of the planetary atmosphere (kg), and g the acceleration due to gravity (ms^{-2}). H in a planetary atmosphere is highest for high temperatures and small μ. Assuming absorption features in an atmosphere are proportional to the scale height, they are largest for hot atmospheres with low mean molecular weight (e.g., made out of hydrogen and helium); they have already been detected in transmission spectroscopy for hot extrasolar giant planets.

See Also

- ▶ Exoplanets, Modeling Giant Planet's Atmospheres

References and Further Reading

Yung YL, Demore WB (1999) Photochemistry of planetary atmospheres. Oxford University Press, New York

Scale-Free Networks

Tom Lenaerts
Département d'Informatique, Université Libre de Bruxelles, Brussels, Belgium

Keywords

Complex network; Power law; Scale free; Small world

Synonyms

Power-law networks

Definition

Networks or graphs are called scale free when their degree distribution, i.e., the distribution of the number of nodes that have a particular degree, decays like a power law (Dorogotsev and Mendes 2003). Researchers have observed that a lot of real-world networks like the Internet or social interaction networks have a topology that comes close to this kind of network.

Overview

The relevance of scale-free networks to represent real-world networks was underlined by the work of Barabási and Albert in 1999 (Barabási and Albert 1999), in which they examined the structure of a number of large networks like the Internet and the coauthorship network between scientists. They showed that these networks follow a power-law distribution, meaning that $P(k)$, which is the probability that a particular vertex in the networks has k interactions, decays as $P(k) \sim k^{-\gamma}$. For instance, the value for γ for the Internet is approximately 2.1 and $\gamma \approx 3$ for the coauthorship network. In addition, they explained the origin of these networks through a simple growth mechanism called the preferential attachment rule. This rule specifies that networks grow by adding new vertices and that these vertices connect not with randomly selected vertices but with popular vertices, meaning here the vertices that already have a high degree. Artificially growing a network in this way produces a network with a power-law degree distribution. This observation was crucial, since prior to their work people mostly assumed that most real-world networks were simply random (small-world) networks (Watts and Strogatz 1998), where the degree distribution corresponds to a Poisson distribution. In the early years after this seminal work, scale-free topologies were discovered in a wide variety of domains, ranging from signaling and metabolic networks to food webs, over different social networks. Yet, it was also observed that a wider variety of heterogeneous topologies exist (Amaral et al. 2000). For instance, Stanley and colleagues observed that the tail of the degree distribution of a movie-actor network decays faster than a power-law network (broad-scale) and that the neuronal network of the worm *Caenorhabditis elegans* decays even faster than a network (single scale). To explain the growth of the other classes of networks, they extended the growth mechanism with a vertex-dependent aging (or cost) factor. This factor takes into account that there is a limit to how long a vertex can keep receiving new links, which is obviously the case in the movie-actor network. Thus when aging is slow (fast), the scale-free network will turn into a broad-scale (single-scale) network. The research on scale-free networks was immensely popularized by the book *Linked: The New Science of Networks* (Barabási 2002).

See Also

- ▶ Bioinformatics
- ▶ Biological Networks
- ▶ Cell
- ▶ Evolution, Biological
- ▶ Metabolism
- ▶ Protein

References and Further Reading

Amaral LAN, Scala A, Barthélémy M, Stanley HE (2000) Classes of small-world networks. Proc Natl Acad Sci U S A 97(21):11149–11152

Barabási A-L (2002) Linked: the new science of networks. Basic Books

Barabási A-L, Albert R (1999) Emergence of scaling in random networks. Science 286:509–512

Dorogotsev S, Mendes J (2003) Evolution of networks: from biological nets to the Internet and WWW. Oxford University Press, Oxford

Watts DJ, Strogatz SH (1998) Collective dynamics of 'small-world' networks. Nature 393:440–442

Scattering

William M. Irvine
University of Massachusetts, Amherst, MA, USA

Definition

Scattering is a process in which a photon, or a particle, interacts with an atom, molecule, or particle and emerges in a different direction without, or with only a slight, difference in energy. In the interstellar medium, radiative scattering plus absorption by dust grains (in which the photon's energy is converted into heat and possibly lower energy radiation) combine to produce extinction. In planetary atmospheres, scattering by molecules and cloud particles plays an important role in the diffuse reflection and transmission of radiation.

See Also

- ▶ Absorption Cross Section
- ▶ Extinction, Interstellar or Atmospheric

Search for Extraterrestrial Intelligence

- ▶ SETI

Seasonal Dark Flows

- ▶ Slope Lineae, Recurrent

Secondary Eclipse

- ▶ Eclipse

Secular Dynamics

Rory Barnes
Astronomy Department, University of Washington, Seattle, WA, USA

Definition

Secular dynamics refers to the gravitational interactions and subsequent evolution of orbits among multiple bodies around a central mass. The semimajor axes of secularly interacting bodies remain constant, but other orbital parameters such as eccentricities, longitudes of pericenter, inclinations, and longitudes of ascending node oscillate with time. For low eccentricities and inclinations, motion in the plane is decoupled from motion out of the plane (see also "▶ Kozai mechanism"), that is, the eccentricities and inclinations will oscillate on different timescales, called the secular periods.

See Also

- ▶ Kozai Mechanism
- ▶ Mean Motion Resonance
- ▶ Orbit

Secular Resonance

Rory Barnes
Astronomy Department, University of Washington, Seattle, WA, USA

Definition

In planetary dynamics, secular resonance is the commensurability of two or more apsidal or nodal precessional frequencies. When multiple planets (more than two) are in a system, their mutual gravitational perturbations cause the shapes and relative orientations of their orbits to change with time (see "▶ Secular Dynamics").

In some cases, the ratios of the frequencies can be close to the ratio of small integers (a commensurability). In these cases, repetitive forces can drive larger or faster oscillations than if the commensurability was not present. This term should not be confused with apsidal libration, which only means the lines of apse are librating.

See Also

- ▶ Apsidal Angle
- ▶ Libration
- ▶ Orbit
- ▶ Precession
- ▶ Secular Dynamics

Sedimentary Rock

Nicholas Arndt
ISTerre, Université Grenoble Alpes, France

Definition

A sedimentary rock is a lithified deposit of detrital particles such as clay, silt, sand, or gravel; of (bio-)chemical precipitates (including ▶ evaporites) and of organic material.

Detrital (or clastic) sedimentary rocks consist of preexisting solid particles that are eroded somewhere, transported (by gravity alone, wind, water, or ice) and deposited. The main detrital ▶ minerals are feldspar, ▶ quartz, and clay minerals, all of which are stable at low-temperature aqueous conditions; due to the comparative greater resistance of quartz, however, quartz is more common than feldspar. Many minerals common in the continental crust do not (or only rarely) survive the exogenic processes of weathering, erosion, transport, and diagenesis. Thus, many clastic sedimentary rocks are largely made of only few minerals. Accessory minerals are therefore of great interest because they can deliver specific information on provenance, climate and transport.

In chemical sediments, water-soluble minerals such as calcite ($CaCO_3$), halite (NaCl), and gypsum ($CaSO_4$ 2 (H_2O)) dominate although many other evaporitic minerals are known. More rarely, sedimentary rocks are dominated by iron oxides such as ▶ hematite (in ▶ banded iron formations) or phosphates.

Carbonates (and perhaps banded-iron formation) are almost always biologically mediated. Since the late Ediacaran, specialized cells in metazoans precipitate calcite and aragonite from ambient water, forming calcareous endo- or exoskeletons in the shape of shells, tests, spicules and many other forms. In ▶ stromatolites and other microbialites, photosynthetic activity increases the alkalinity in the near-cell environment, triggering the nucleation of aragonite or calcite.

Organic sediments include coal and bituminous shales.

Most sedimentary rocks are characterized by a large inventory of sedimentary structures, including a variety of bedforms from deposition by highly variable agents under varying conditions. In addition, diagenesis and bioturbation modify greatly the structure and texture of sediments.

See Also

- ▶ Banded Iron Formation
- ▶ Evaporite
- ▶ Metasediments
- ▶ Mineral
- ▶ Quartz
- ▶ Silicate

Sedna

Therese Encrenaz
LESIA, Observatoire de Paris - Section de Meudon, Meudon, France

Definition

The ▶ trans-Neptunian object (90377) Sedna was discovered in November 2003 by Michael

Brown, Chadwick Trujillo, and David Rabinowitz. Its orbit is very elliptical, with a perihelion at 76 AU and an ▶ aphelion at 975 AU. Its orbital period is about 11,000 years. Its diameter is estimated between 1,200 and 1,600 km and its albedo is about 0.16. It is of a dark red color with little methane or water ice, which suggests the presence of hydrocarbon deposits (or ▶ tholins) on its surface. Sedna has been classified as a "detached" ▶ trans-Neptunian object, which have also been called "extended-scattered" objects or "distant detached objects" (DDO), or as a member of the inner ▶ Oort Cloud.

See Also

- ▶ Kuiper Belt
- ▶ Tholins
- ▶ Trans-Neptunian Object

3-Selanyl-2-Aminopropanoic Acid

- ▶ Selenocysteine

Selection

Susanna Manrubia
Systems Biology Program, Centro Nacional de Biotecnología (CSIC), Madrid, Spain

Definition

In biology, selection refers to the preferential survival and reproduction of organisms in response to particular phenotypic traits. Limited environmental resources and a growth of populations above its capacity promote competition among organisms and lead to ▶ natural selection. Natural selection acts at many different levels, from genes and genomic elements to populations. Darwin introduced sexual selection as a preference of females for attractive males: colorful bodies, long feathers, or big horns are instinctually evaluated as a measure of their competence to breed healthy progeny. Humans perform artificial selection to improve desired qualities in a plant or animal. In vitro evolution is a particular form of artificial selection focused on molecular phenotypes. Though selection acts on the ▶ phenotype, only heritable traits (coded in the ▶ genotype) can be selected.

See Also

- ▶ Darwin's Conception of the Origins of Life
- ▶ Evolution, Biological
- ▶ Evolution, In Vitro
- ▶ Genotype
- ▶ Natural Selection
- ▶ Phenotype

Selenocysteine

Henderson James (Jim) Cleaves II
Earth–Life Science Institute (ELSI), Tokyo Institute of Technology, Meguro–ku, Tokyo, Japan
Institute for Advanced Study, Princeton, NJ, USA
Blue Marble Space Institute of Science, Washington, DC, USA
Center for Chemical Evolution, Georgia Institute of Technology, Atlanta, GA, USA

Synonyms

3-Selanyl-2-Aminopropanoic Acid

Definition

Selenocysteine is a rare biological ▶ amino acid found in several enzymes. Its structure is similar to cysteine, but it has a selenium atom replacing the usual sulfur atom, thus forming a selenol group. Selenocysteine is a stronger acid and has a higher reduction potential than ▶ cysteine. These properties make it optimal for incorporation in proteins involved in antioxidant activity.

Selenocysteine is not directly coded for in the genetic code; rather, it is encoded by a UGA ▶ codon, which is normally a stop codon. The UGA codon is made to encode selenocysteine by the presence of a SECIS (SElenoCysteine Insertion Sequence) element in the coding mRNA. The SECIS element is defined by characteristic nucleotide sequences and secondary structure base-pairing patterns. In bacteria, the SECIS element is located immediately following the UGA codon in the reading frame for the selenoprotein. In archaea and eukaryotes, the SECIS element is in the 3′ untranslated region of the mRNA and can direct multiple UGA codons to encode selenocysteine residues. Unlike the other coded amino acids, no free pool of selenocysteine exists in the cell. Its high reactivity would incur damage to cells. Instead, cells store selenium in the form of the less reactive selenide (H_2Se). Selenocysteine is biosynthesized in situ on a specialized tRNA. In these days, selenocysteine is sometimes included in additional protein amino acids together with pyrrolysine.

See Also

- ▶ Amino Acid
- ▶ Codon
- ▶ Cysteine
- ▶ Nonprotein Amino Acids
- ▶ Proteins, Secondary Structure

Selenology

Ralf Jaumann
German Aerospace Center (DLR), Institute of Planetary Research, Berlin, Germany

Synonyms

Lunar geology

Definition

Selenology (Greek, *Selene*, "Moon," and *logos* "speech, science") is the science of the ▶ Moon. It comprises the study of the structure, composition, physical properties, dynamics, origin, and evolution of the Moon, as well as the processes that formed and shaped the Moon. The term selenology is not frequently used because scientifically and methodologically it is synonymous to "lunar geology." Thus, the latter is commonly used instead of the term "selenology."

See Also

- ▶ Areology
- ▶ Cratering Chronology
- ▶ Geological Time Scale, History of
- ▶ Moon, The
- ▶ Satellite or Moon
- ▶ Stratigraphy

Self-Assembly

Roderich Groß
Department of Automatic Control & Systems Engineering, The University of Sheffield, Sheffield, UK

Keywords

Computation; Formation; Pattern; Structure

Synonyms

Self-organization

Definition

Self-assembly is the process by which preexisting components (separate or distinct parts of a

disordered structure) autonomously organize into patterns or structures without external intervention.

Overview

Self-assembly processes are responsible for the generation of much of the order in nature (Philp and Stoddart 1996; Whitesides and Grzybowski 2002). They involve components at different scales, such as molecules, cells, and organisms. The characteristics of the components control how they interact with each other and thus the patterns and structures that emerge. The components must be mobile, being either externally propelled or self-propelled. In many self-assembly systems, the components selectively bind to, or selectively disband from, each other. Such selective binding regulates, for instance, the replication of genetic information in the assembly of the DNA double helix. Self-assembly processes are either static or dynamic. In static self-assembly, the systems of components do not dissipate energy and reach an ordered state at global or local equilibrium. An example of static self-assembly is molecular crystallization. In dynamic self-assembly, the systems of components dissipate energy in order to form and maintain patterns or structures far from equilibrium. An example of dynamic self-assembly is cell sorting in embryos. In general, dynamic self-assembly systems tend to be more complex than static self-assembly systems. Typically, the components' behaviors (e.g., their binding preferences) are not static but change in response to interactions with other components or the environment. For biological systems, the characteristics of their components undergo evolution as the patterns and structures resulting from the interactions among components are selected for specific functions (Caspar 1966; Sendova-Franks and Franks 1999; Anderson et al. 2002).

At present, researchers are working toward a more unifying theory of self-assembly and a profound understanding of its elementary functions and limits. One such attempt is to view the products of self-assembly systems as computations, and vice versa. For example, it was found that systems based on DNA tiles that implement such algorithmic self-assembly can perform Turing-universal computation.

Until now, self-assembly has most widely been applied in the synthesis and fabrication of products from molecular components. However, increasingly, the potential of self-assembly processes with mesoscopic to macroscopic components is recognized (Whitesides and Boncheva 2002; Groß and Dorigo 2008). At these scales, the characteristics of the components can be precisely controlled and the self-assembly processes can be easily monitored. Potential applications include crystal synthesis with nanometer- to centimeter-scale components, fabrication of electrically or optically functional devices, and autonomous robots with adaptive body plans and functionalities.

See Also

- ▶ Molecular Recognition
- ▶ Self-Assembly, Biological
- ▶ Self-Replication

References and Further Reading

Anderson C, Theraulaz G, Deneubourg J-L (2002) Self-assemblages in insect societies. Insect Soc 49:99–110

Caspar DLD (1966) Design principles in organized biological structures. In: Wolstenholme GEW, O'Connor M (eds) Principles of biomolecular organization. John Wiley & Sons, pp 7–39

Groß R, Dorigo M (2008) Self-assembly at the macroscopic scale. Proc IEEE 96:1490–1508

Philp D, Stoddart JF (1996) Self-assembly in natural and unnatural systems. Angew Chem Int Ed 35:1154–1196

Sendova-Franks AB, Franks NR (1999) Self-assembly, self-organization and division of labour. Philos Trans R Soc B 354:1395–1405

Whitesides GM, Boncheva M (2002) Beyond molecules: self-assembly of mesoscopic and macroscopic components. Proc Natl Acad Sci U S A 99:4769–4774

Whitesides GM, Grzybowski B (2002) Self-assembly at all scales. Science 295:2418–2421

Self-Assembly, Biological

David Deamer
Department of Chemistry, University of California, Santa Cruz, Santa Cruz, CA, USA

Keywords

Hydrogen bonds; Hydrophobic effect; Lipid bilayer; Secondary and tertiary protein structures

Synonyms

Self-organization

Definition

Self-assembly is the process by which certain kinds of molecules in solution are able to associate into larger, more complex structures stabilized by hydrogen bonding and other generally non-covalent interactions.

Overview

The four forces that stabilize the structures of biomolecules are covalent bonds, hydrogen bonds, electrostatic interactions, and the hydrophobic effect. The synthesis of covalent bonds requires a significant expenditure of energy and is not usually associated with self-assembly processes, which are low energy reactions that occur spontaneously without a direct input of metabolic energy. An example of self-assembly is the formation of secondary and tertiary structure of proteins, in which hydrogen bonding is essential. For instance, when peptide chains are synthesized by ribosomes, portions of the growing strand form hydrogen-bonded alpha helices and planar structures called beta sheets. These structures arise spontaneously and are dominant features of most proteins. Another fundamental biological structure stabilized by hydrogen bonds is the ▶ double helix of DNA, in which adenine is paired with thymine with two ▶ hydrogen bonds, and guanine paired with cytosine with three hydrogen bonds. These are now referred to as Watson-Crick base pairs and more generally as complementary base pairing. If a DNA double helix is separated into single strands, for instance, by heating, upon cooling the two strands reassemble into the original double-helix structure.

A self-assembly process also produces lipid bilayers, the structural barriers composing all cell membranes. The primary contribution to bilayer assembly and stability is the hydrophobic effect that arises from the interaction of hydrocarbon chains with water. If a hydrocarbon chain is inserted into an aqueous bulk phase, the water molecules form orderly cage-like structures around the chain, which decreases the overall entropy of the system. However, if the hydrocarbon chains leave the surrounding water and associate into lipid bilayers, the orderly water-cage structures disperse and entropy of the system increases. The entropy-driven hydrophobic effect also contributes to the folding of protein chains into stable tertiary structures, in which nonpolar amino acids tend to reside in the protein molecule interior, with polar and ionic amino acids lining the surface.

Molecular assemblies stabilized by hydrogen bonding and the hydrophobic effect likely contributed to the increasing complexity of prebiotic structures required for the origin of cellular life.

See Also

- ▶ Amphiphile
- ▶ Denaturation
- ▶ Double Helix
- ▶ Hydrogen Bond
- ▶ Lipid Bilayer
- ▶ Micelle
- ▶ Self-Assembly

References and Further Reading

Whitesides GM, Boncheva M (2002) Self-assembly of mesoscopic and macroscopic components. Proc Natl Acad Sci U S A 99:4769–4774

Self-Duplication

▶ Self-Replication

Self-Organization

▶ Self-Assembly
▶ Self-Assembly, Biological

Self-Producing Network

▶ Autopoiesis

Self-Replication

Raphaël Plasson
Department of Earth and Planetary Science, Harvard University, Cambridge, MA, USA

Keywords

Autocatalysis; Evolution

Synonyms

Reproduction; Self-duplication; Self-reproduction

Definition

Self-replication is the property for a system to build a functional and independent copy of itself.

Overview

Self-replication is a general concept that applies to systems of different nature (physical or theoretical) and of different scale (microscopic or macroscopic). It relies on the existence of an internal mechanism for the duplication of the full system. This implies the ability for the duplication mechanism to make a copy of itself. The replicated system becomes a fully functional entity, separated from the parent system, possessing the same properties. Namely, it must be able to replicate itself again. A minimal self-replicative system can be reduced to this sole function, in which case it can do nothing but generate copies of itself – whose function, thus, will be to generate more copies. More complex systems can perform additional functions. In this case, the replicative system must be able to reproduce not only itself but also all the additional mechanisms, so that the replicate can behave similarly to its parent.

Different levels of self-replication can be identified, depending on their accuracy. There can be very strict self-replication systems, producing a copy that is identical to the parent. This is, for example, the case of template ▶ autocatalysis, where a molecule is able to directly catalyze the formation of an identical molecule (Plasson et al. 2011). More tolerant self-replicating systems allow the possibility of imperfect duplication. This is typically the case for biological systems based on ▶ nucleic acid replication, where point ▶ mutations are possible, slightly modifying the outcome. Such "general autocatalysis" (Muller 1922) is necessary for the evolution of the system (Vasas et al. 2010). An example of a minimalistic evolvable self-replicative system is the ▶ prion, an infectious protein that is able to communicate its conformation to normal proteins, which in turn become infectious (Li et al. 2010). In the case of macroscopic systems, the replicate cannot be strictly identical to the parent – molecule wise – but only similar to it. Such imperfect self-replication can be referred to as reproduction, which is typical of all living beings (Sipper 1998). In this case, the replicate globally possesses the same properties and characteristics as the parent, but is compositionally slightly different.

Key Research Findings

Self-Replication in Life

The self-replication of living organisms is based on genetic ▶ replication. Each individual is a complex system, able to perform a large set of actions, among which is the ability to produce offspring. The mechanisms for the replication exist at several levels, but all of them are ultimately coded in DNA, bearing all the genetic information. At the molecular level, proteins enable the replication of the DNA molecules, themselves responsible for the synthesis – among other functions – of the replication proteins. At the cellular level, self-replication occurs by the division of one cell into two distinct ones, each containing the same kind of compounds and structures. At the individual level, self-replication is obtained either by division of the being or – in the case of sexual reproduction – by formation and fusion of gametes, each of which contains all the information and tools necessary for building a fully grown organism. Self-replication can ultimately be found at the level of colonies, where a limited number of individuals can separate from the parent colony to grow a new one. At each level, different accuracy of replication exists: DNA is copied with point mutations, crossover mechanisms generate genetic exchanges between chromosomes, sexual reproduction enables reshuffling of genes, etc. This property is crucial for enabling the key property of life, open-ended evolution, rather than endless duplication of identical objects.

Self-Replication in Artificial Life

Self-replication is one of the most fundamental studied properties of all living beings (Sipper 1998). ▶ Artificial life describes a minimalistic theoretical representation of life, in order to understand its specific properties.

Self-replication by a cellular automaton is the first model to have been developed, initiated in the 1940s by von Neumann (1966). Such a system is composed of several cells that are disposed in a grid that can be of multiple dimensions. All cells can be in different states. A set of rules describes how each cell changes from one state to another after a given time step, depending on their present state and their environment. Some of these systems are prone to self-replication; this is typically the case for Langton's self-replicating loop (Langton 1984). This cellular automaton is based on a two-dimensional space, with eight-state cells. An initial 86-cell structure, disposed as a closed loop, is able to duplicate itself and generate a second identical 86-cell loop. ▶ Cellular automata can possess simple replicative structures, but can be more complex and replicate additional features. For example, the Tempesti self-replicating loop is similar to the Langton loop, as it is able to self-replicate in a similar fashion, but it additionally possesses a program that is automatically activated: once duplicated, the replicated loop is able to write inside itself the same encoded text than the one of its parent (Tempesti 1995).

Some computer programs are also able to self-replicate. In the 1980s, Core Wars, a computer game initially developed by Dewdney (1984), enabled the creation of programs that fight against each other in a computer environment. The purpose of this game is the destruction of the other programs and the domination of the virtual area. Some programs were successfully able to proliferate thanks to their self-replicating abilities. In more recent software, like Tierra (Ray 1994) or Avida (Lenski et al. 2003), the programs are even prone to open-ended evolution. Computer viruses are malicious application of self-replicating programs. Once designed, they are able to make copies of themselves and propagate inside a computer or from one computer to another via the network or physical media. They are, however, unable to evolve without direct intervention by their programmers (Lenski et al. 2003).

Some computer models intend to reproduce systems that are closer to biological systems. The purpose is not only to investigate the property of self-replication per se but to understand the process of self-replication as it is implemented in life (Bersini 2010). The first system described in this spirit is the chemoton of Gánti (1975). This model is a minimalistic chemical representation of a cell that is able to

maintain its activity and to self-replicate. It contains three interconnected autocatalytic cycles: (1) a metabolic subsystem responsible for the building of the other subsystems, (2) an information subsystem responsible for the system's self-replication, and (3) a membrane subsystem encompassing these subsystems and keeping the compounds within one system. These three subsystems are able to grow altogether, until the point where the whole system can divide to give birth to two separated complete systems.

Kinetics of Self-Replication

The self-replication of a system A corresponds formally to a $A \rightarrow 2A$ transformation: starting from one system, two identical or similar systems are obtained. Such a pattern can be referred to as autocatalysis, in analogy with chemical autocatalysis (Muller 1922). Different kinetic behaviors depending on the kinetic *order* of the autocatalytic mechanism can be observed for the evolution of self-replicating systems (Plasson et al. 2011). This results in different efficiency for their ability to compete with other self-replicating systems. Such dynamics are classically studied in population evolution (Nowak 2006). An *order* smaller than one generates a sub-exponential evolution characterized by the coexistence of all competing self-replicating systems ("survival of all"). First-*order* kinetics generates an exponential evolution characterized by the proliferation of the most efficient replicator ("survival of the fittest"). *Orders* larger than one generate hyperbolic evolutions characterized by the proliferation of the system initially present in larger quantity ("survival of the first").

The sub-exponential case, with an order inferior to one, is the least interesting, as it does not lead to a clear selective process. However, real mechanisms that seem to possess first-order kinetics may actually present a lower order. This is often the case for the replication of molecules by template autocatalysis, in which the order falls to one-half on account of the high stability of the dimeric intermediate, which is actually a necessary condition for the selectivity of template replication (Wills et al. 1998).

Future Directions

The elaboration of theoretical self-replicating agents is a way to investigate the possibility for life to emerge from simple chemical systems. Typically, self-replicating programs can spontaneously emerge from an initially random setup. Koza investigated this by letting random programs evolve described by a computationally complete set of functions. He observed a probability of the order of 10^{-6}–10^{-9} for obtaining the emergence of a self-replicative program that is then able to proliferate as soon as it appears (Koza 1994). In that spirit, designing a simple molecular replicator, able to proliferate without external help, would be a good indication of the possibility of the emergence of molecular replicators on the primitive Earth. Simple oligonucleotide (von Kiedrowski 1993) and oligopeptide (Lee et al. 1997) replicators have been successfully described in the literature. However, template replicators imply the formation of stable dimeric intermediates, leading to a parabolic evolution that undermines their ability to replicate efficiently (Wills et al. 1998). More recent work is oriented toward the design of more complete systems (Szostak et al. 2001), in the spirit of Gánti's chemoton (Gánti 1975). These take into account the necessity of energy transfer for efficient metabolism and for a membrane to enclose the system, in addition to the replicating mechanism itself. Ultimately, and beyond the relevance to the ▶ origin of life, complete and autonomous self-replicating machines might be engineered (Freitas and Merkle 2004).

See Also

- ▶ Artificial Life
- ▶ Autocatalysis
- ▶ Automaton, Chemical
- ▶ Cellular Automata
- ▶ Evolution, Molecular
- ▶ Origin of Life
- ▶ Replication (Genetics)

References and Further Reading

Bersini H (2010) Software replica of minimal living processes. Orig Life Evol Biosph 40:121–130
Dewdney AK (1984) Core war. Sci Am 250:15–19
Freitas RA Jr, Merkle RC (2004) Kinematic self-replicating machines. Landes Bioscience/Eurekah. com, Georgetown
Gánti T (1975) Organization of chemical reaction into dividing and metabolizing enzymes units: the Chemoton. Biosystems 7:15–21
Koza JR (1994) Artificial life: spontaneous emergence of self-replicating and evolutionary self-improving computer programs. In: Langton CG (ed) Articial life III. Addison-Wesley, Redwood City, pp 225–262
Langton CG (1984) Self-reproduction in cellular automata. Physica D 10:135–144
Lee DH, Severin K, Yokobayashi Y, Ghadiri MR (1997) Emergence of symbiosis in peptide self-replication through a hypercyclic network. Nature 390:591–594
Lenski RE, Ofria C, Pennock RT, Adami C (2003) The evolutionary origin of complex features. Nature 423:139–144
Li J, Browning S, Mahal SP, Oelschlegel AM, Weissmann C (2010) Darwinian evolution of prions in cell culture. Science 327:869–872
Muller HJ (1922) Variation due to change in the individual gene. Am Nat 56:32–50
Nowak MA (2006) Evolutionary dynamics: exploring the equations of life. Belknap Press/Harvard University Press, Cambridge
Plasson R, Brandenburg A, Jullien L, Bersini H (2011) Autocatalyses: at the root of self-replication. Artif Life 17:219–236
Ray TS (1994) An evolutionary approach to synthetic biology: Zen and the art of creating life. Artif Life 1:179–209
Sipper M (1998) Fifty years of research on self-replication: an overview. Artif Life 4:237–257
Szostak JW, Bartel DP, Luisi PL (2001) Synthesizing life. Nature 409:387–390
Tempesti G (1995) A new self-reproducing cellular automaton capable of construction and computation. Lect Notes Comput Sci 929:555–563
Vasas V, Szathmáry E, Santos M (2010) Lack of evolvability in self-sustaining autocatalytic networks constraints metabolism-first scenarios for the origin of life. Proc Natl Acad Sci U S A 107:1470–1475
von Kiedrowski G (1993) Minimal replicator theory I: parabolic versus exponential growth. Bioorg Chem 3:115–146
von Neumann J (1966) Theory of self-reproducing automata. University of Illinois Press, Urbana (edited and completed by Burks AW)
Wills PR, Kauffman SA, Stadler BMR, Stadler PF (1998) Selection dynamics in autocatalytic systems: templates replicating through binary ligation. Bull Math Biol 60:1073–1098

Self-Replication, Chemical

Alonso Ricardo
Ra Pharmaceuticals, Cambridge, MA, USA

Keywords

Autocatalysis; Cross catalysis; Informational molecule

Definition

Self-replication in astrobiology refers to the ability of a chemical system to make copies of itself without the need for external instructions. The emergence of self-replication is considered to be a necessary step for the origin of ▶ life.

Overview

Self-replication occurs when an informational molecule (such as a ▶ nucleic acid) directs the spontaneous synthesis of a copy of itself. Mechanisms for self-replication can be autocatalytic, where a molecule acts as a template to make a direct copy of itself, or cross-catalytic, where two or more molecules of different informational contents amplify one another. Modern life forms use a complex cross-catalytic mechanism of replication that involves the participation of protein molecules that catalyze the replication of the informational polymer (nucleic acids), which are also involved in the synthesis of the catalysts themselves. Primordial life, however, could have used simpler mechanisms for replication. Nucleic acids are informational polymers that form double-stranded duplexes following the Watson-Crick base pairing rules and have the intrinsic potential to achieve self-replication via either one of the two previously mentioned mechanisms. This property is central to the RNA world hypothesis for the origin of life (Gilbert 1986). Self-replication is not restricted to nucleic acid polymers, and it has been demonstrated to

occur with other types of molecules such as peptides and other nonbiological organic compounds.

Experimental approaches for the study of self-replication were initially focused on RNA template-directed polymerization reactions. This work showed that fully complementary polynucleotide duplexes are accessible starting from a single-stranded RNA ▶ oligomer (template) and energetically activated ribonucleotide monomers. The efficiency of the polymerization chemistry, however, is dependent on the nucleotide composition of the template, and the rates of polymerization are slow and similar to rates of RNA hydrolysis (Orgel 1992). These combined difficulties have prevented the realization of complete replication cycles of RNA.

The first working example of a self-replicating molecule was obtained with a designed system consisting of two modified trinucleotide oligomers that upon ligation yield a product that could act as a template (catalyst) for a ligation reaction that results in the formation of more copies of itself (von Kiedrowski 1986). This demonstration of autocatalytic self-replication indicated the feasibility of such systems but suffered from product inhibition of autocatalysis as a consequence of duplex formation. Improvements on these model systems were later obtained with variations on the chemistry of the building blocks (Zielinski and Orgel 1987). Examples of self-replication using more complex-designed cross-catalytic molecular systems have also been achieved (Sievers and von Kiedrowski 1994). The use of non-nucleoside building blocks in self-replication studies has improved both the efficiency and our understanding of autocatalytic processes (Tjivikua et al. 1990; Terfort and von Kiedrowski 1992). Peptides and supramolecular assemblies of organic molecules represent alternatives to nucleic acid-based self-replication and have interesting implications in astrobiology due to the different nature of their chemistry (Lee et al. 1996). Despite the interest and effort in this area of research, a robust self-replicating system that can undergo Darwinian evolution has not been experimentally obtained. Current efforts toward that goal are mainly focused in chemical replication studies (Schrum et al. 2009) and in vitro evolution experiments (Lincoln and Joyce 2009).

See Also

- ▶ Activated Nucleotide
- ▶ Amplification (Genetics)
- ▶ Biopolymer
- ▶ Emergence of Life
- ▶ Evolution, In Vitro
- ▶ Life
- ▶ Nucleic Acids
- ▶ Oligomer
- ▶ Peptide
- ▶ Protocell
- ▶ Ribonucleoside
- ▶ RNA
- ▶ RNA World
- ▶ Self-Assembly

References and Further Reading

Gilbert W (1986) The RNA world. Nature 319:618
Lee DH, Granja JR, Martinez JA, Severin K, Ghadiri MR (1996) A self-replicating peptide. Nature 382:525
Lincoln TA, Joyce GF (2009) Self-sustained replication of an RNA enzyme. Science 323:1229
Orgel LE (1992) Molecular replication. Nature 358:203
Schrum JP, Ricardo A, Krishnamurty M, Blain JC, Szostak JW (2009) Efficient and rapid template-directed nucleic acid copying using 2′-amino-2′-3′-dideoxyribonucleoside-5′-phosphorimidazolide monomers. J Am Chem Soc 131:14560
Sievers D, von Kiedrowski G (1994) Self-replication of complementary nucleotide-based oligomers. Nature 369:221
Terfort A, von Kiedrowski G (1992) Self-replication by condensation of 3-aminobenzamidines and 2-formylphenoxyacetic acids. Angew Chem Int Ed 31:654
Tjivikua T, Ballester P, Rebek J (1990) A self-replicating system. 112:1249
von Kiedrowski G (1986) A self-replicating hexadeoxynucleotide. Angew Chem Int Ed 25:932
Zielinski WS, Orgel LE (1987) Autocatalytic synthesis of a tetranucleotide analog. Nature 327:346

Self-Reproduction

- ▶ Self-Replication

Self-Shielding

▶ Self-Shielding Effects on Isotope Fractionation

Self-Shielding Effects on Isotope Fractionation

Ko Hashizume
Department of Earth and Space Sciences, Osaka University, Toyonaka, Osaka, Japan

Keywords

Photochemistry; Photodissociation; Mass-independent fractionation

Synonyms

Isotope-selective photolysis; Self-shielding

Definition

The self-shielding effect is a phenomenon expected to occur in a gas medium illuminated by a light source, when a molecule in the gas absorbs light with a particular wavelength that may result in its dissociation. The light of this wavelength is gradually attenuated as it travels through the gas medium, leading to a decreased photodissociation rate of the target molecule. The attenuation rate of the light depends on the abundance of the molecule. When molecules with different combinations of isotopes are photodissociated by different wavelengths, this effect may cause an abundance-dependent isotope fractionation, as opposed to the common mass-dependent fractionation.

Overview

The self-shielding effect may occur when the following conditions are met. (1) Line absorption: The absorption of the photodissociating light occurs only at a narrow range of particular wavelengths. (2) The light with the wavelength of interest reaches to the target molecule, that is, the wavelength is sufficiently intense in the light source and is not shielded by other reasons, for instance, by absorption by other species. Isotope fractionation by the self-shielding effect may occur when the following condition is additionally met. (3) The wavelengths of the photodissociating light for different isotopologues are separated by more than both the above mentioned admitted range and the Doppler width. The fractionation may occur at a certain distance from the edge of the gas medium, determined by the photodissociation cross section and the column density of the isotopologue with the largest abundance.

The self-shielding effect on isotope fractionation was first proposed to occur in a ▶ molecular cloud, possibly irradiated by ultraviolet (UV) light emitted from a nearby young star (Bally and Langer 1982). They discovered that relative abundances among the isotopologues of carbon monoxide show peculiar variations at a certain distance from the edge of the molecular cloud. Comparing the abundances of $^{12}C^{16}O$, $^{13}C^{16}O$, and $^{12}C^{18}O$, after correction for a possible chemical fractionation, they deduced that $^{12}C^{16}O$, the dominantly abundant isotopologue, was enriched about twice as much as the others. They explained this observation by the self-shielding effect associated to the isotope-selective photodissociation of CO molecules that may occur upon line absorption of UV.

The same type of isotope fractionations for carbon monoxide and possibly molecular nitrogen is predicted to have occurred in our solar system, in the early solar nebula or in the ancestral molecular cloud, which could be recorded in planetary solid materials. Note that it is not the isotope composition of the gas species (CO or N_2) that could be recorded among the planetary materials but the composition of the photodissociated products. A viable prediction model must contain a reasonable process to accommodate the isotope record of the products into stable compounds, i.e., cold traps. The cold traps proposed are oxides and

nitrides (Clayton 2002), or water and organics (Yurimoto and Kuramoto 2004; Lyons and Young 2005), depending on the proposed place (temperature) for the self-shielding effect to have occurred.

See Also

- ▶ Fractionation, Mass Independent and Dependent
- ▶ Interstellar Chemical Processes
- ▶ Isotopic Fractionation (Interstellar Medium)
- ▶ Isotopic Fractionation (Planetary Process)
- ▶ Nitrogen Isotopes
- ▶ Optical Depth
- ▶ Oxygen Isotopes
- ▶ Photochemistry
- ▶ Photodissociation Region
- ▶ Protoplanetary Disk, Chemistry

References and Further Reading

Bally J, Langer WD (1982) Isotope-selective photodestruction of carbon-monoxide. Astrophys J 255:143–148

Chakraborty S, Ahmed M, Jackson TL, Thiemens MH (2008) Experimental test of self-shielding in vacuum ultraviolet photodissociation of CO. Science 321:1328–1331, See also comments on this paper

Clayton RN (2002) Self-shielding in the solar nebula. Nature 415:860–861

Kitamura Y, Shimizu M (1983) Oxygen isotopic anomaly and solar nebular photochemistry. Moon Planet 29:199–202

Lyons JR, Young ED (2005) CO self-shielding as the origin of oxygen isotope anomalies in the early solar nebula. Nature 435:317–320

Navon O, Wasserburg GJ (1985) Self-shielding in O_2 – a possible explanation for oxygen isotope anomalies in meteorites? Earth Planet Sci Lett 73:1–16

Visser R, van Dishoeck EF, Black JH (2009) The photodissociation and chemistry of CO isotopologues: applications to interstellar clouds and circumstellar disks. Astron Astrophys 503:323–343

Warin S, Benayoun JJ, Viala YP (1996) Photodissociation and rotational excitation of interstellar CO. Astron Astrophys 308:535–564

Yurimoto H, Kuramoto K (2004) Molecular cloud origin for the oxygen isotope heterogeneity in the solar system. Science 305:1763–1766

Semimajor Axis

Daniel Rouan
LESIA, Observatoire Paris-Site de Meudon, Meudon, France

Synonyms

Half-major axis

Definition

The semimajor axis of an ellipse is one-half of the major axis, that is, of the longest axis. This is one of the basic parameters when describing the ▶ orbit of two bodies in gravitational interaction. It is equivalent to the radius in the case of a circular orbit.

See Also

- ▶ Keplerian Orbits
- ▶ Orbit
- ▶ Semiminor Axis

Semiminor Axis

Daniel Rouan
LESIA, Observatoire Paris-Site de Meudon, Meudon, France

Definition

The semiminor axis of an ellipse is one-half of the minor axis, that is, of the shortest axis.

See Also

- ▶ Half-Major Axis
- ▶ Keplerian Orbits
- ▶ Orbit

Separation

- ▶ Dichotomy, Planetary
- ▶ Fractionation

Sequence

Carlos Briones
Centro de Astrobiología (CSIC/INTA), Consejo Superior de Investigaciones Científicas, Madrid, Spain

Definition

In molecular biology, the term sequence refers to either the order of ▶ nucleotides in a nucleic acid molecule – ▶ DNA or RNA – or the order of ▶ amino acids in a ▶ protein. Different sequencing methods have been developed since the sequence of the first protein was deciphered by F. Sanger in the 1950s and the first sequences of nucleic acids were unveiled in the 1970s by W. Fiers and later by W. Gilbert and by F. Sanger. Knowledge of the nucleic acid or protein sequences is currently required for research on many fields of basic and applied biology.

See Also

- ▶ Amino Acid
- ▶ DNA
- ▶ Genome
- ▶ Nucleotide
- ▶ Protein
- ▶ Proteome, Proteomics
- ▶ RNA
- ▶ Sequence Analysis

Sequence Analysis

Carlos Briones
Centro de Astrobiología (CSIC/INTA), Consejo Superior de Investigaciones Científicas, Madrid, Spain

Definition

In molecular biology, ▶ sequence analysis is the process by which the nucleotide sequence of a nucleic acid, or the amino acid sequence of a ▶ protein, is studied and compared to other sequences. Techniques for sequence analysis include database query, pairwise and multiple sequence alignment, repeated sequence search, mutation screening, and annotation of sequences. In particular, sequence analysis is used to predict the function of newly sequenced genes and proteins through the study of their similarities with other sequences of known function. Bioinformatic tools for sequence analysis are increasingly used in genomics, proteomics, and ▶ phylogeny.

See Also

- ▶ Bioinformatics
- ▶ DNA
- ▶ DNA Sequencing
- ▶ Gene
- ▶ Genome
- ▶ Mutation
- ▶ Phylogeny
- ▶ Protein
- ▶ Proteome, Proteomics
- ▶ RNA
- ▶ Sequence

Sequencing

- ▶ DNA Sequencing

Serine

Kensei Kobayashi
Yokohama National University, Tokiwadai, Hodogayaku, Yokohama, Japan

Definition

Serine is one of the 20 protein amino acids whose chemical structure is $NH_2CH(CH_2OH)COOH$ (Fig. 1). Its three-letter symbol is Ser and one-letter symbol is S. Since serine has a hydroxyl (−OH) group in its side chain, it is classified as a polar amino acid. Its molecular weight is 105.09, and its isoelectric point is 5.68. Serine is present in the active sites of many enzymes such as proteases and is widely distributed in the biosphere. Serine, together with glycine, is a predominant amino acid in the hydrolysate of human fingerprints. In the early analyses of carbonaceous chondrites, serine was one of the most abundant amino acids, but later it was found that most of this amino acid detected was a terrestrial contaminant. In recent amino acid analysis of carbonaceous chondrites, a number of indigenous amino acids were detected, but serine was not common among them. Recently serine was identified in Antarctic carbonaceous chondrites.

See Also

- ▶ Amino Acid
- ▶ Carbonaceous Chondrites, Organic Chemistry of
- ▶ Protein

Serine, Fig. 1 Serine

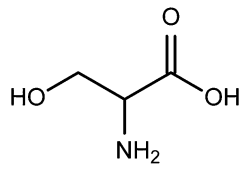

Serpentine

Stephane Guillot
LGCA, Universite de Grenoble, St Martin d'Hères, France

Definition

Serpentine is a hydrous magnesium-iron phyllosilicate having the chemical formula $(Mg, Fe)_6(OH)_nSi_4O_{10}]$. It is greenish, opaque to translucent, light (density of 2.6 g/cm^3), soft (hardness <4) with a greasy luster. All occurrences are microcrystalline and massive in habit, never being found as single crystals. There are three mineral polymorphs: antigorite, chrysotile, and lizardite. Antigorite is stable at high temperatures (400–700 °C) at great depths. Lizardite and chrysotile typically form near the Earth's surface and break down at relatively low temperatures, below 400 °C. Asbestos is a fibrous form of serpentine. Serpentine is the hydrous breakdown product of olivine or – more rarely – orthopyroxene. During hydrolysis of the ferromagnesian minerals contained in ultramafic rocks and the formation of serpentine (serpentinization), large amounts of H_2 gas, CH_4 gas, and alkaline solutions are produced. These products possibly made the sites of active serpentinization (around submarine hydrothermal vents) favorable environments for the development of chemotrophic organisms on the early Earth. It has also been speculated that serpentinization made possible through hydrous alteration of basaltic oceanic crust facilitates subduction. This, in turn, made plate tectonics and crustal segregation by continental growth possible.

See Also

- ▶ Chemoautotroph
- ▶ Chemolithoautotroph
- ▶ Chemolithotroph
- ▶ Fischer-Tropsch-Type Reaction
- ▶ Hydrothermal Environments
- ▶ Hydrothermal Vent Origin of Life Models
- ▶ Serpentinization
- ▶ White Smoker

Serpentinization

Daniele L. Pinti
GEOTOP Research Center for Geochemistry and Geodynamics, Université du Québec à Montréal, Montréal, QC, Canada

Keywords

Carbon isotopes; Chemotrophs; Hydrogen; Hydrothermal vents; Methane; Ultramafic rocks

Definition

Serpentinization is the process of hydrothermal alteration that transforms Fe-Mg-silicates such as ▶ olivine, pyroxene, or amphiboles contained in ▶ ultramafic rocks into serpentine minerals. Much of the uppermost mantle in oceanic setting is altered, as are the cumulus parts of layered intrusions. Serpentine is a soft ductile mineral and its presence in the mantle wedge lubricates the subduction of the oceanic plate. Production of serpentine in the oceanic crust produces hydrothermal fluids and releases gaseous ▶ methane and ▶ hydrogen, as observed along ▶ mid-ocean ridges. The pH of the hydrothermal fluids is generally low but under some conditions, notably at low temperature, may be high enough to be favorable to life.

Overview

The process of serpentinization has received much attention by the astrobiologists for several reasons (Sleep et al. 2004). First, reactions between ferromagnesian minerals (such as Fe-olivine fayalite), hydrothermal water, and carbonic acid can release large amounts of gaseous methane (CH_4) and hydrogen (H_2), following the reactions:

$$\begin{aligned}\text{Fayalite} + \text{water} &\rightarrow \text{magnetite} \\ &+ \text{aqueous silica} + \text{hydrogen}\ 3Fe_2SiO_4 \\ &+ 2H_2O \rightarrow 2Fe_3O_4 + 3SiO_2 + 2H_2\end{aligned} \quad (1)$$

while the liberated silica reacts with forsterite (Mg-olivine) to form serpentine according to

$$3Mg_2SiO_4 + SiO_2 + 4H_2O \rightarrow 2Mg_3Si_2O_5(OH)_4$$

(Barnes and O'Neil, 1969). When CO_2 is present, methane can be formed through the following reaction:

$$\begin{aligned}\text{Olivine} + \text{water} + \text{carbonic acid} &\rightarrow \text{serpentine} \\ &+ \text{magnetite} + \text{methane}(Fe, Mg)2SiO_4 \\ &+ nH_2O + CO_2 \rightarrow Mg_3Si_2O_5(OH)_4 \\ &+ Fe_3O_4 + CH_4\end{aligned}$$

Sites of active serpentinization, that is, around submarine hydrothermal vents where ultramafic rocks react to form serpentine could thus have been favorable environments for chemotrophic organisms (that use reduced species such as H_2 and CH_4 as a source of energy, rather than sunlight) on the early Earth.

Serpentinization could also have been an alternative pathway to produce abiotically complex organics in the Hadean Earth, such as methane, n-alkanes, and potentially simple organic acids and N-bearing compounds. The larger volumes of ultramafic rocks at the surface of the early Earth motivate chemical reactive flow modeling to investigate production of complex organics by serpentinization.

Finally, reduced carbon species (▶ graphite) produced during the early stages of serpentinization of ultramafic rocks show isotopic composition ($\delta^{13}C$ from −15‰ to −50‰) mimicking those of organic compounds (McCollom and Seewald 2006; van Zuilen et al. 2002; Lopez-Garcia et al. 2006). These isotopic compositions overlap with those observed in several putative traces of life in Archean rocks, clearly indicating that the isotopic composition of carbon cannot be used alone for determining the biogenicity of those findings.

See Also

▶ Carbon Isotopes as a Geochemical Tracer
▶ Earth, Formation and Early Evolution

- ▶ Hydrothermal Environments
- ▶ Isotope Biosignatures
- ▶ Mid-Ocean Ridges
- ▶ Olivine
- ▶ Serpentinization (Mars)

References and Further Reading

Barnes I, O'Neil JR (1969) The relationships between fluids in some fresh alpine-type ultramafics and possible serpentinization, Western United States. Geol Soc Bull 80:1947–1960

Lopez-Garcia P, Moreira D, Douzery E, Forterre P, Van Zuilen M, Claeys P, Prieur D (2006) Ancient fossil record and early evolution (ca. 3.8 to 0.5 Ga). Earth Moon Planet 98:247–290

McCollom T, Seewald J (2006) Carbon isotope composition of organic compounds produced by abiotic synthesis under hydrothermal conditions. Earth Planet Sci Lett 243:74–84

Sleep N, Meibom A, Fridriksson T, Coleman R, Bird D (2004) H_2-rich fluids from serpentinization: geochemical and biotic implications. Proc Natl Acad Sci 101:12818–12823

van Zuilen MA, Lepland A, Arrhenius G (2002) Reassessing the evidence for the earliest traces of life. Nature 418:627–630

Serpentinization (Mars)

Vlada Stamenković
Earth, Atmospheric and Planetary Sciences, Massachusetts Institute of Technology (MIT), Cambridge, MA, USA

Keywords

Geochemical reaction; Hydrothermal vents; Mars; Methane of Mars

Definition

Serpentinization is the reaction of ultramafic (high in magnesium and iron) ▶ minerals with ▶ water, occurring especially in olivine ($[(Mg, Fe)_2SiO_4]$) as well as in pyroxenes (mostly $[(Mg, Fe)_2Si_2O_6]$). The reaction occurs below a critical temperature of about 500–700 K (Oze and Sharma 2007) in the crust and upper mantle of Earth and possibly Mars. Below temperatures of 500 K, the reaction rate decreases rapidly (Martin and Fyfe 1970), although the dependence of the reaction rate on temperature is not well quantified. The hydrated minerals that are formed by serpentinization are called ▶ serpentines and contain hydrous magnesium iron phyllosilicates ($[(Mg, Fe)_3Si_2O_5(OH)_4]$), whereas ▶ rocks containing serpentines are called serpentinites.

Overview

Serpentines have been detected on Mars by the CRISM spectrometer on the Mars Reconnaissance Orbiter (MRO) (Ehlmann et al. 2009). Serpentinization has been suggested to explain the yet unconclusive and debated observations of ▶ methane in the Martian atmosphere (Mumma et al. 2009; Zahnle et al. 2011). It is furthermore speculated to potentially create locally habitable conditions for microorganisms, analogous to hydrothermal vent systems like Lost City near the Mid-Atlantic Ridge at the Atlantis massif on ▶ Earth (Kelley et al. 2005). Serpentinization might help to sustain ecological niches by providing heat and ▶ hydrogen to be used by autotrophic organisms. Hydrogen released during serpentinization can react with dissolved ▶ carbon dioxide in a ▶ Fischer-Tropsch-type reaction to produce higher hydrocarbons such as methane, the main nutrient for methanotrophs. But the hydrogen and heat generation rates both depend on the amount of water present, the ambient temperature, and the magnesium number of the reacting mineral. Because of the similar size of magnesium and iron ions, olivine can contain arbitrary magnesium-to-iron ratios, described by the magnesium number x_{Mg} of the reacting mineral $x_{Mg} = \frac{\text{mol(Mg)}}{\text{mol(Mg)+mol(Fe)}}$. Below are the typical olivine end-member serpentinization reaction for fayalite $\left([Fe_2SiO_4], x_{Mg} = 0\right)$ and forsterite $\left([Mg_2SiO_4], x_{Mg} = 1\right)$ at $T_0 = 298\,\text{K}$ and $p_0 = 1$ bar and associated Gibbs energies found by Oze and Sharma (2005):

$$3Fe_2SiO_4 + 2H_2O = 2Fe_3O_4 + 3SiO_2 + 2H_2 \text{ and } \Delta G = 56.3 kJ/mol$$

$$2Mg_2SiO_4 + 3H_2O = Mg_3SiO_5(OH)_4 + MG(OH)_2 \text{ and } \Delta G = -47.4 kJ/mol$$

Hydrogen is only produced when iron is present, resulting in the formation of magnetite [Fe_3O_4] and quartz [SiO_2] for fayalite serpentinization. Further analysis (Oze and Sharma 2007) shows that both, the Gibbs energy and the enthalpy, are negative and minimal at large magnesium contents and become positive for x_{Mg} between 0.25 and 0.5 (depending on temperature), making the reaction thermodynamically not favorable and endothermic (heat consuming). The observed magnesium of Martian olivine is lower than on Earth between $0.3 < x_{Mg} < 0.7$ (Hoefen et al. 2003) but still large enough to provide hydrogen and heat on Mars if enough subsurface water is present.

See Also

- ▶ Carbon Dioxide
- ▶ Crust
- ▶ Earth
- ▶ Fischer-Tropsch-Type Reaction
- ▶ Hydrogen
- ▶ Hydrothermal Environments
- ▶ Hydrothermal Vent Origin of Life Models
- ▶ Mantle
- ▶ Mars
- ▶ Methane
- ▶ Mineral
- ▶ Phyllosilicates, Extraterrestrial
- ▶ Rock
- ▶ Serpentinization
- ▶ Water

References and Further Reading

Ehlmann BL et al (2009) Identification of hydrated silicate minerals on Mars using MRO-CRISM: geologic context near Nili Fossae and implications for aqueous alteration. J Geophys Res E Planets 114(10):E00208

Hoefen TM et al (2003) Discovery of olivine in the Nili Fossae region of Mars. Science 302(5645):627–630

Kelley DS et al (2005) A serpentinite-hosted ecosystem: the lost city hydrothermal field. Science 307:1428

Martin B, Fyfe WS (1970) Some experimental and theoretical observations on the kinetics of hydration reactions with particular reference to serpentinization. Chem Geol 6:185–202

Mumma MJ et al (2009) Strong release of methane on Mars in northern summer 2003. Science 323(5917):1041–1045

Oze C, Sharma M (2005) Have olivine, will gas: serpentinization and the abiogenic production of methane on Mars. Geophys Res Lett 32:L10203

Oze C, Sharma M (2007) Serpentinization and the inorganic synthesis of H_2 in planetary surfaces. Icarus 186:557–561

Zahnle K et al (2011) Is there methane on Mars? Icarus 212:493–503

SETI

David W. Latham
Harvard-Smithsonian Center for Astrophysics, Cambridge, MA, USA

Synonyms

Search for extraterrestrial intelligence

Definition

SETI, the Search for Extraterrestrial Intelligence, is an exploratory science that seeks evidence of life in the universe by looking for some signature of its technology. See ▶ SETI (the SETI Institute) for more details.

Overview

Are there any technical civilizations out there? Do we have the technology to detect their signals? What would be the most efficient way to decipher their messages? The answers to these questions make the foundation of SETI.

Modern attempts to detect extraterrestrial signals date back half a century, to project Ozma in

1960. Early searches focused on the microwave region of the radio spectrum, where there is minimum interference from natural sources in the Galaxy. From those early beginnings, enormous improvements were achieved in the coverage of radio frequencies and area on the sky, but vast regions of search space remained unexplored. With time, new developments in our own technological capabilities suggested alternative strategies for communication, such as nanosecond optical laser pulses aimed very precisely in extremely narrow and efficient beams.

In the 1980s, NASA became involved in an ambitious SETI program with two prongs; an all-sky survey and a targeted search. The search was mainly in the radio domain, until the congress defunded the effort, just a year after Carl Sagan pushed the ceremonial key in 1992 to initiate the search at the Arecibo Observatory in Puerto Rico. Aside from this program, most of the interest in and support for SETI has come from the public, through a wide variety of initiatives. A pioneering effort by SETI@home harnessed the power of millions of underused computers around the world to analyze data acquired serendipitously with the Arecibo telescope. The Planetary Society supported powerful new searches in both the radio and the optical, and papers reporting null results appeared in professional publications such as the prestigious *Astrophysical Journal*. Despite the lack of success to date, SETI continues in two major directions; Research and Development (R&D) and Projects. R&D efforts include the development of new signal processing algorithms, new search technology, and new SETI search strategies that are then incorporated into specific observing projects.

References and Further Reading

Anderson DP et al (2002) SETI@home: an experiment in public-resource computing. Commun ACM 45:56–61

Cocconi G, Morrison P (1959) Searching for interstellar communication. Nature 184:844–846

Garber SJ (1999) Searching for good science: the cancellation of NASA's SETI program. J Br Int Soc 52:3–12

Howard AW et al (2004) Searches for nanosecond optical pulses from nearby solar-type stars. Astrophys J 613:1270–1284

SETI, History of

Florence Raulin-Cerceau
Maître de Conférences, Centre Alexandre Koyré (UMR 8560-CNRS/EHESS/MNHN/CSI)
Muséum National d'Histoire Naturelle, Brunoy, France

History

The history of SETI (Search for Extraterrestrial Intelligence) began with the *1959* Cocconi and Morrison paper published in *Nature*, entitled "Searching for Interstellar Communications", establishing the feasibility of interstellar signaling by radio waves. Their authors, the physicists Giuseppe Cocconi (1914–2008) and Philip Morrison (1915–2005) (Cornell University, USA), suggested that the spectral frequency of 1,420 MHz (or 21-cm emission, corresponding to the famous hyperfine line of neutral hydrogen) could be used as the preferential frequency for communication in the Galaxy. In the mean time, radio astronomers were testing the possibilities afforded by a new generation of devices. In such a context, listening to other star systems in the hope of catching artificially produced signals appeared as an exalting challenge.

Independently, the radio astronomer Frank D. Drake (1930–) (Cornell University, USA) was fascinated by the possibility of communicating with other intelligences in the Galaxy. He became the first to test the Cocconi and Morrison hypothesis, at the National Radio Astronomy Observatory (NRAO) in Green Bank (West Virginia, USA). Drake's project Ozma (named after the fictional Princess Ozma in L. Frank Baum's *Land of Oz*) began in April 1960 when he pointed the 85 ft diameter antenna at two nearby Sun-like stars (Epsilon Eridani and Tau Ceti). Two hundred hours were dedicated to Project Ozma, but, as confirmed by Drake himself, "no signals of extraterrestrial origin

were discovered during these preliminary observations."

The year after, a meeting held at Green Bank established SETI as a scientific discipline. During this event, Drake proposed a formula that came to be best known as the "► Drake equation," which was supposed to provide a framework to estimate the number of technological civilizations capable of communicating in the Galaxy.

Directly linked to this formula, the "► Fermi Paradox" stated that if such extraterrestrial civilizations were existing, they should have mastered space travel and have already undertaken the colonization of the Galaxy (including the Earth). Since there was no evidence of any visit of extraterrestrials to Earth, the (pessimistic and questionable) conclusion was obvious: No other technological civilization could be present in the Galaxy.

No matter what this paradox suggested, concrete SETI programs have been undertaken from the late 1970s up to now (Sentinel, META, BETA, SERENDIP, southern SERENDIP, Phoenix, Optical SETI, Argus, ATA) and successively carried out, in spite of strong difficulties about funds.

See Also

► Drake Equation
► Fermi Paradox

References and Further Reading

Cocconi G, Morrison P (1959) Searching for interstellar communications. Nature 184:844–846
Drake F (1961) Project Ozma. Phys Today 14:40–46

Settlement

► Colonization, Biological

SgrB2

Brett A. McGuire[1], Joanna F. Corby[2], P. Brandon Carroll[1] and Anthony J. Remijan[3]
[1]California Institute of Technology, Pasadena, CA, USA
[2]University of Virginia, Charlottesville, VA, USA
[3]NRAO, Charlottesville, VA, USA

Keywords

Chemistry; Molecules; Interstellar medium; Prebiotic species; Green Bank Telescope; Atacama Large Millimeter Array; Herschel Space Observatory

Definition

Sagittarius B2 (Sgr B2) is an exceptionally massive (3×10^6 $M_\odot$; de Vicente et al. 1996) giant ► molecular cloud located ~130 pc (Reid et al. 2009) from Sgr A* – the Milky Way Galaxy's central supermassive ► black hole – which is at a distance of ~8.5 kpc from Earth (Genzel et al. 2010). Sgr B2 is within the Central Molecular Zone (CMZ) of the Galaxy, a ~300 pc radius region around Sgr A* that exhibits widespread emission from ► complex organic molecules (COMs), with Sgr B2 containing the most complex identified to date. The Sgr B2 cloud is highly heterogeneous and composed of both compact (hot) and extended (cold) molecular material, molecular ► maser regions, and ultracompact continuum sources (Remijan et al. 2014).

History

In terms of its astrobiological relevance, Sgr B2 is the preeminent source for the detection and study of new molecules in the ► interstellar medium (Remijan et al. 2014). The first interstellar detections of polyatomic molecules including ► ammonia (NH_3) and ► water (H_2O) were

toward Sgr B2 (Cheung et al. 1968; Cheung et al. 1969). Since that time, study of the region has resulted in the detection of a number of biologically relevant molecules; many of these detections have been the result of extensive ▶ molecular line surveys which have been conducted toward the region with a wide variety of facilities including the Green Bank Telescope, the Herschel Space Telescope, and the Atacama Large Millimeter Array (▶ ALMA), with nearly continuous frequency coverage from ~5 to 1,900 GHz (see, e.g., Neill et al. 2012 [1–50 GHz], Turner 1989 [70–115 GHz], Nummelin et al. 1998 [218–263 GHz], Neill et al. 2014 [480–1910 GHz]).

Overview

Structure

Sgr B2 has a complex physical structure with cores of star formation embedded in an extended envelope. Molecular, atomic, and ionized gas has been observed in the extended envelope, appearing without obvious spatial separation between the three phases of gas (Goicochea et al. 2003; Jones et al. 2008). Three main cores of star formation have erupted, namely, the North, Main, and South cores. More than 50 HII regions with compact, cometary, and shell shapes have been identified in and close to the cores. All known molecular masing transitions are detected in Sgr B2, with each transition typically detected at multiple positions near the cores of Sgr B2 (Mehringer and Menten 1997; Hoffman et al. 2007). At submillimeter wavelengths, two continuum sources are present in the North core of Sgr B2 (Sgr B2(N)), and a clumpy sub-mm structure is detected in the Main core (Qin et al. 2011). The submillimeter continuum emission is produced by warm dust in environments with high densities. One of the sub-mm peaks corresponds to the position of the co-called Large Molecule Heimat, the preeminent source of molecular line emission.

As the most massive known molecular cloud in the Galaxy, Sgr B2 is accessible only at X-ray and radio to far-infrared wavelengths. Sgr B2 is known to have an unusually high flux of X-ray radiation. As no compact X-ray source is observed in Sgr B2, the X-ray radiation is understood as evidence for highly elevated X-ray emission from Sgr A* 300–400 years ago, making Sgr B2 an X-ray ▶ reflection nebula (Terrier et al. 2010). Like most clouds in the CMZ, the gas exhibits supersonic turbulence and widespread shocks. The cosmic ray ionization rate is observed to be an order of magnitude higher in Sgr B2 than in most Galactic molecular clouds (van der Tak et al. 2006), and observations of Zeeman splitting of the 21cm spin-flip transition of HI indicate a high magnetic field strength (Crutcher et al. 1996). Given these conditions, Sgr B2 is regarded as the only Galactic source with an environment analogous to the central regions of starburst galaxies.

Perhaps because of the unique physical environment in this cloud, Sgr B2 hosts the most diverse molecular chemistry observed anywhere outside of the solar system.

Chemistry

Indeed virtually every complex organic molecule detected outside our solar system has been detected toward Sgr B2, often exclusively toward this source (Menten 2004). This rich chemical complexity is likely the result of the unique physical conditions that produce favorable conditions for both production and detection of a wide range of complex organic molecules. Among the species detected are ▶ amines, ▶ amides, cyanides, saturated and unsaturated molecules, alcohols, ▶ aldehydes, ▶ ethers, ▶ esters, ▶ carboxylic acids, ketones, and epoxides. Of particular interest for astrobiology are the detections of the simplest sugar-related species, ▶ glycolaldehyde (CH_2OHCHO; Hollis et al. 2004), the first interstellar molecule detected with a branched carbon backbone: *iso*-propyl cyanide (C_3H_7CN; Belloche et al. 2014), and acetamide (CH_3CONH_2; Hollis et al. 2006), the largest interstellar molecule to possess a peptide bond. Detections of these and other complex organic species in the cold extended envelope (e.g.,

glycolaldehyde), as well as in compact regions toward the ▶ hot core (e.g., *iso*-propyl cyanide), demonstrate both the spatial and chemical complexity of the region.

See Also

- ▶ ALMA
- ▶ Gas-Grain Chemistry
- ▶ Herschel Mission
- ▶ Interstellar medium
- ▶ Molecular Cloud
- ▶ Molecules in space
- ▶ Radio Astronomy

References and Further Reading

Belloche A, Müller HSP, Menten KM, Schilke P, Comito C (2013) Complex organic molecules in the interstellar medium: IRAM 30 m line survey of sagittarius B2(N) and (M). A&A 559:A47

Belloche A, Garrod RT, Müller HSP, Menten KM (2014) Detection of a branched alkyl molecule in the interstellar medium: iso-propyl cyanide. Science 345:1584–1587

Cheung AC, Rank DM, Townes CH, Thornton DD, Welch WJ (1968) Detection of NH_3 molecules in the interstellar medium by their microwave emission. PRL 21:1701–1705

Cheung AC, Rank DM, Townes CH, Thornton DD, Welch WJ (1969) Detection of water in interstellar regions by its microwave radiation. Nature 221:626–628

Crutcher RM, Roberts DA, Mehringer DM, Troland TH (1996) HI Zeeman measurements of the magnetic field in sagittarius B2. ApJ 462:L79–L82

de Vicente P, Martin-Pintado J, Wilson TL (1996) A hot ring in the SGR B2 molecular cloud. ASPC 102:64–67

Genzel R, Eisenhauer F, Gillessen S (2010) The galactic center massive black hole and nuclear star cluster. Rev Mod Phys 82:3121–3195

Goicochea JR, Rodriquez-Fernandez NJ, Cernicharo J (2003) Extended photoionization and photodissociation in Sgr B2. ANS 324:139–143

Hoffman IA, Goss WM, Palmer P (2007) The formaldehyde masers in Sgr B2: very long baseline array and very large array observations. ApJ 654:971–977

Hollis JM, Jewell PR, Lovas FJ, Remijan AJ (2004) Green bank telescope observations of interstellar glycolaldehyde: low-temperature sugar. ApJ 613:L45

Hollis JM, Lovas FJ, Remijan AJ, Jewell PR, Ilyushin VV, Kleiner I (2006) Detection of acetamide (CH_3CONH_2): the largest interstellar molecule with a peptide bond. ApJ 643:L25–L28

Jones PA, Burton MG, Cunningham MR, Menten KM, Schilke P, Belloche A, Leurini S, Ott J, Walsh AJ (2008) Spectral imaging of the sagittarius B2 region in multiple 3-mm molecular lines with the mopra telescope. MNRAS 386:117–137

Mehringer DM, Menten KM (1997) 44 GHz methanol masers and quasi-thermal emission in sagittarius B2. ApJ 474:346–361

Menten KM (2004) In the dense interstellar medium in galaxies. In: Pfalzner S, Kramer C, Staubmeier C, Heithausen A (eds) Springer proceedings in physics, vol 91. Springer, Berlin/Heidelberg, p 69. ISBN 978-3-642-62348-6

Neill JL, Muckle MT, Zaleski DP, Steber AL, Pate BH, Lattanzi V, Spezzano S, McCarthy MC, Remijan AJ (2012) Laboratory and tentative interstellar detection of *trans*-methyl formate using the publicly available green bank telescope PRIMOS survey. ApJ 755:153

Neill JL, Bergin EA, Lis DC, Schilke P, Crockett NR, Favre C, Emprechtinger M, Comito C, Qin S-L, Anderson DE, Burkhardt AM, Chen J-H, Harris BJ, Lord SD, McGuire BA, McNeill TD, Monje RR, Phillips TG, Steber AL, Vasyunina T, Yu S (2014) *Herschel* observations of extraordinary sources: analysis of the full herschel/HIFI molecular line survey of Sagittarius B2(N). ApJ 789:8

Nummelin A, Bergman P, Hjalmarson Å, Friberg P, Irvine WM, Millar TJ, Ohishi M, Saito S (1998) A three-position spectral line survey of sagittarius B2 between 218 and 263 GHz. I. The observational data. ApJS 117:427–529

Qin SL, Schilke P, Rollfs R, Comito C, Lis DC, Zhang Q (2011) Submillimeter continuum observations of sagittarius B2 at subarcsecond spatial resolution. A&A 530:L9

Reid MJ, Menten KM, Zheng XW, Brunthaler A, Xu Y (2009) A trigonometric parallax of Sgr B2. ApJ 705:1548–1553

Remijan AJ, Snyder LE, McGuire BA, Kuo H-L, Looney LW, Friedel DN, Golubiatnikov GY, Lovas FJ, Ilyushin VV, Alekseev AE, Dyubko SF, McCall BJ, Hollis JM (2014) Observational results of a multi-telescope campaign in search of interstellar urea [$(NH_2)_2CO$]. ApJ 783:77

Terrier R, Ponti G, Bélanger G, Decourchelle A, Tatischeff V, Goldwurm A, Trap G, Morris MR, Warwick R (2010) Fading hard X-ray emission from the galactic center molecular cloud Sgr B2. ApJ 719:143–150

Turner BE (1991) A molecular line survey of Sagittarius B2 and Orion-KL from 70 to 115 GHz. II. Analysis of the data. ApJS 76:617–686

van der Tak FFS, Belloche A, Schilke P, Guesten R, Phillip S, Comito C, Bergman P, Nyman L (2006) APEX mapping of H_3O^+ in the Sgr B2 region. A&A 454:99–102

SH

► Sulfur Hydrides in the Interstellar Medium

SH+

► Sulfur Hydrides in the Interstellar Medium

Shadow Zone

► Oxygen-Minimum Zone

Shale

Nicholas Arndt
ISTerre, Université Grenoble Alpes, France

Synonyms

Latite; Pelite

Definition

Shale is a fine-grained ► sedimentary rock composed mainly of clay minerals (hydrous aluminum phyllosilicates) with minor proportions of quartz, feldspar, calcite, and iron oxides. Because of its small grain size, the constituent particles can settle only in water free of turbulence. This is only the case in nearly standing water bodies. Shale is thus deposited in closed basins, estuaries, lakes, and similar depositional settings protected from currents, waves, and wind and in deep water far from continents. Varieties rich in organic material, called black shales, provide valuable sources of information about the earliest forms of life and serve as petroleum source rocks. Shale is converted by metamorphism into mica schist. The occurrence of shale deposits in planetary surfaces would be a good indicator of the past presence of liquid water on their surfaces.

See Also

► Sedimentary Rock
► Weathering

Shark Bay Microbialites

► Shark Bay, Stromatolites of

Shark Bay Thrombolites

► Shark Bay, Stromatolites of

Shark Bay, Stromatolites of

Abigail Allwood
Jet Propulsion Laboratory, Pasadena, CA, USA

Synonyms

Shark Bay microbialites; Shark Bay thrombolites

Definition

Stromatolites are microbially mediated sedimentary structures. The best-known examples are thriving in the shallow waters of Hamelin Pool at the southern end of Shark Bay in Western Australia. Among the first modern ► stromatolites to be described, the Shark Bay stromatolites provide insights to the biological and physical forces controlling stromatolite growth and are

an important analog to ancient stromatolites. The Shark Bay structures include meter-sized, lithified, dome- and club-shaped structures forming at subtidal to intertidal water depths, as well as millimeter-sized, tufted microbial mats forming in the supratidal zone. The lithified stromatolites consist of very coarsely layered detrital sediment accreted over time through microbial trapping and binding of particles and carbonate precipitation.

See Also

- ▶ Archean Traces of Life
- ▶ Biogenicity
- ▶ Stromatolites

Sheet Silica

- ▶ Phyllosilicates, Extraterrestrial

Shepherding

Sean N. Raymond
Laboratoire d'Astrophysique de Bordeaux, CNRS, Universite de Bordeaux, France

Definition

Shepherding is the process by which a much larger body constrains the motion of many much smaller objects. Thus, a migrating planet can push ▶ protoplanetary disk material inward along with it; in the context of a giant planet migrating toward its central star, ▶ planetesimals and ▶ planetary embryos can be shepherded by the giant planet via resonances and may enable the formation of close-in super-Earth planets. In planetary rings, small shepherding satellites can constrain the motion of ring particles and hence structure the appearance of the rings.

See Also

- ▶ Planetary Migration
- ▶ Saturn

Shergottites

Ana-Catalina Plesa
German Aerospace Center (DLR), Institute of Planetary Research, Berlin, Germany

Keywords

SNC meteorites; Rare earth elements; Cosmic ray exposure age; Noachian; Hesperian; Amazonian

Definition

Shergottites are a subgroup of the SNC meteorites named after the Shergotty meteorite. About 78 % of the Martian meteorites are classified as shergottites.

Overview

The age of all shergottites is still debated since some isotopic systems like Pb-Pb indicate an age between 4.1 and 4.3 Ga, corresponding to the Noachian period (e.g., Bouvier et al. 2009), but all other isotopic systems mark these rocks as young samples with ages between 165 and 475 Ma placing them in the late Amazonian epoch (e.g., Nyquist et al. 2001). A young age of shergottites results in a so-called "age paradox," since young volcanic surfaces from which shergottites might have been ejected by impacts represent only about 20 % of the Martian surface (Tanaka et al. 1988). Craters possibly representing the impact locations from which the shergottites were ejected have been identified on the young terrains in Tharsis and Elysium provinces (e.g., Tornabene et al. 2006). However,

the Mojave crater, formed on a 4.3 Ga old terrain, has been recently found to match the mineralogy of three shergottite samples, i.e. Shergotty, Los Angeles, and QUE94201 (Werner et al. 2014).

The shergottites can be divided into three petrological subgroups (basaltic pricritic and lherzolitic shergottites) depending on their olivine content. Basaltic shergottites are rocks composed of pyroxene and plagioclase but do not contain olivine or chromite. Picritic or olivine-phyric shergottites are catalogued as extrusive pyroxene-plagioclase basalts with olivine megacrysts (large olivine crystals surrounded by finer-grained matrix). The third petrological subgroup is defined by lherzolitic shergottites, which are plutonic ultramafic rocks containing at least 40 % modal olivine. Depending on the ratio LREE/HREE (light rare earth elements/heavy rare earth elements) relative to CI chondrites, one can distinguish between depleted (highly depleted), intermediate (moderately depleted), and enriched (slightly depleted) shergottites. Although there are exceptions, most of the enriched shergottites are basaltic; intermediate samples are lherzolitic, while the picritic shergottites are usually depleted. The depleted shergottites have a LREE/HREE ratio close to 0.12 × CI chondrites, while the enriched samples have a ratio close to 1.0 × CI (Bridges and Warren 2006). These different subtypes of the shergottites are thought to hint at different reservoirs in the Martian mantle.

See Also

- ▶ Crater, Impact
- ▶ Isotopic Fractionation (Planetary Process)
- ▶ Isotopic Ratio
- ▶ Meteorites
- ▶ Meteoritics
- ▶ Shergotty
- ▶ SNC Meteorites

References and Further Reading

Bouvier A, Blichert-Toft J, Albarède F (2009) Martian meteorite chronology and the evolution of the interior of Mars. Earth Planet Sci Lett 280(1–4):285–295

Bridges JC, Warren PH (2006) The SNC meteorites: basaltic igneous processes on Mars. J Geol Soc Lond 163:229–251

Nyquist LE, Bogard DD, Shih C-Y, Greshake A, Stöer D, Eugster O (2001) Ages and geologic histories of Martian meteorites. Chronol Evol Mars 96:105–164

Tanaka KL, Isbell NK, Scott DH, Greeley R, Guest JE (1988) The resurfacing history of Mars: a synthesis of digitized, viking-based geology. Proc Lunar Planet Sci Conf 18:665–678

Tornabene LL, Moersch JE, McSween HY, McEwen AS, Piatek JL, Milam KA, Christensen PR (2006) Identification of large (2–10 km) rayed craters on Mars in THEMIS thermal infrared images: implications for possible Martian meteorite source regions. J Geophys Res 111:E10006

Werner SC, Ody A, Poulet F (2014) The source crater of Martian Shergottite meteorites. Science 343(6177):1343–1346

Shergotty

Ana-Catalina Plesa
German Aerospace Center (DLR), Institute of Planetary Research, Berlin, Germany

Definition

Shergotty is a 5 kg Martian meteorite discovered in 1865 in Shergotty (now Sherghati), India. It also names a subgroup of the SNC meteorites, the shergottites, representing 78 % of the Martian meteorites. Its age has been dated to ca. 165 Ma by most isotopic systems, but according to the Pb-Pb dating, it can be as old as 4.3 Ga. Although shergottite source craters have been identified on young terrains in Tharsis and Elysium provinces, the Mojave crater, formed on a 4.3 Ga old terrain, has been recently found to match the mineralogy of *Shergotty*. Petrologically, *Shergotty* is a basaltic sample (containing pyroxene and plagioclase but no olivine or chromite), enriched in trace elements.

See Also

- ▶ Crater, Impact
- ▶ Isotopic Fractionation (Planetary Process)

- ▶ Isotopic Ratio
- ▶ Meteorites
- ▶ Meteoritics
- ▶ SNC Meteorites

Shield

Nicholas Arndt
ISTerre, Université Grenoble Alpes, France

Definition

Shield, when used as geological term, has two meanings. It refers to the old central nucleus of continents, the typical example being the ▶ Canadian Precambrian Shield or the Aldan Shield of Siberia. A shield is composed mainly of granitoids and high-grade ▶ metamorphic rocks, with ▶ greenstone belts in its upper sections. It is tectonically stable and has typically a low ▶ geothermal gradient and a thick lithosphere; it is flanked by younger fold belts.

A *shield* volcano is a large volcano edifice with shallow-dipping flanks and composed of low-viscosity basaltic lava, such as the Mauna Loa and Mauna Kea volcanoes of Hawaii or Olympus Mons on Mars.

See Also

- ▶ Canadian Precambrian Shield
- ▶ Craton
- ▶ Granite
- ▶ Greenstone Belts
- ▶ Metamorphic Rock
- ▶ Volcano

Shock Devolatilization

- ▶ Impact Degassing

Shock Front

- ▶ Shock Wave
- ▶ Shock, Interstellar

Shock Wave

Henderson James Jim Cleaves II
Earth–Life Science Institute (ELSI), Tokyo Institute of Technology, Meguro–ku, Tokyo, Japan
Institute for Advanced Study, Princeton, NJ, USA
Blue Marble Space Institute of Science, Washington, DC, USA
Center for Chemical Evolution, Georgia Institute of Technology, Atlanta, GA, USA

Synonyms

Shock front

Definition

A shock wave is a type of propagating disturbance. Like other waves, it carries energy and can propagate through a physical medium or, in some cases, in the absence of a material medium, for example, through an electromagnetic field. When an object or disturbance, such as a meteor entering the atmosphere of a planet and its concomitant shock wave, moves faster than its effects can be propagated into the surrounding fluid, fluid near the disturbance cannot change its properties before the disturbance arrives. In a shock wave, the properties of the fluid such as density, pressure, and temperature change almost instantaneously. The energy of a shock wave dissipates relatively quickly with distance.

Many types of shock waves are found in astrophysical environments. Some examples are shock waves accompanying supernovae or blast waves

traveling through the interstellar medium and the bow shock front caused by the Earth's magnetic field colliding with the solar wind.

See Also

- ▶ Comet
- ▶ Meteorites
- ▶ Shock, Interstellar
- ▶ Supernova

Shock, Interstellar

Steven B. Charnley
Solar System Exploration Division, Code 691, Astrochemistry Laboratory, NASA Goddard Space Flight Center, Greenbelt, MD, USA

Synonyms

Shock front; Shock wave

Definition

A shock is a highly nonlinear compression wave in a medium, which may be a fluid or solid, where the wave carries energy and where the physical parameters of the medium change abruptly. Astrophysicists recognize two types of shocks in the ▶ interstellar medium, C type and J type. C-type shocks are supersonic, multi-fluid flow structures occurring in weakly ionized plasma in which the physical variables (density, temperature) undergo a *continuous* change over the scale of the flow. In this case, the speed of the disturbance, the shock speed, is less than that of the magnetosonic speed in the plasma. In contrast, a J-type shock is a supersonic flow structure in which the physical variables (density, temperature) undergo a discontinuous change (*jump*) at the shock front. In this case, the speed of the disturbance, the shock speed, is greater than that of the sound speed in the gas. Interstellar shocks are produced, for example, by the propagation of a ▶ supernova blast wave into the ambient medium.

See Also

- ▶ Interstellar Medium

Shocked Quartz

Philippe Claeys
Earth System Science, Vrije Universiteit Brussel, Brussels, Belgium

Definition

Shocked quartz refers to quartz grains displaying microscopic defects in crystalline structure that were produced by the passage of high-velocity and high-pressure (>5 GPa) shock waves. Shock metamorphism is commonly illustrated in quartz by the presence of fine lamellae of amorphous SiO_2 oriented parallel to two (or more) specific crystallographic planes and called planar deformation features, or PDF. Under extreme pressure, the whole quartz crystal transforms to glass. Shocked quartz is a diagnostic criterion to recognize hypervelocity impacts. Indeed, there are no other natural geological processes (tectonics, volcanism, etc.) capable of producing the required high-pressure dynamic shock waves. Shock features are common in impact crater rocks and in some meteorites. Shock metamorphism is also known in zircon, feldspar, and olivine.

See Also

- ▶ Crater, Impact
- ▶ Impactite

Shooting Star

▶ Meteor

Siderite

Daniele L. Pinti
GEOTOP Research Center for Geochemistry and Geodynamics, Université du Québec à Montréal, Montréal, QC, Canada

Synonyms

Iron carbonate; Iron spar; Spathose iron

Definition

Siderite is a mineral of chemical formula $FeCO_3$ (trigonal crystalline system). It forms mainly in sedimentary and hydrothermal environments and occasionally in igneous pegmatite (pegmatite is an intrusive igneous rock with large, well-developed crystals). Siderite is found in ▶ banded iron formations of different ages, the oldest being at Isua, West Greenland (ca. 3.8 Ga).

The occurrence of siderite is considered an index of intermediate oxidation conditions, compared to that in sulfide-facies (reducing conditions) and ▶ hematite-▶ magnetite facies iron formations (oxidizing conditions). Being a carbonate, siderite is actively sought on planetary surfaces such as ▶ Mars as indirect evidence of the presence of water and mildly oxidizing conditions.

See Also

▶ Banded Iron Formation
▶ Iron
▶ Mars
▶ Ocean, Chemical Evolution of
▶ Oxygenation of the Earth's Atmosphere

Siderophile Elements

Francis Albarède
Ecole Normale Supérieure de Lyon, Lyon, France

Definition

In the Berzelius-Goldschmidt classification, siderophile elements alloy with metallic iron (sideros), most notably in planetary cores. Transition elements such as Ni, Co, Mn, Mo, Au, and the ▶ platinum-group elements (Os, Pd, Pt, Re, Rh, Ru) are highly siderophilic. Under reducing conditions, carbon, silicon, and phosphorus become moderately siderophilic. Likewise, under high pressure, some ▶ lithophile elements tend to fractionate into the core and become siderophilic. The question of which elements behave in this way is hotly debated for K, Pb, and Nb for the implication it has on the evolution of planetary interiors.

See Also

▶ Chalcophile Elements
▶ Lithophile Elements

SiH_4

▶ Silane

Silane

William M. Irvine
University of Massachusetts, Amherst, MA, USA

Synonyms

SiH_4; Silicane; Silicon tetrahydride

Definition

Silane (SiH_4) is the silicon analog of methane (CH_4). The symmetry of its tetrahedral shape, with four equivalent hydrogen atoms, results in a zero electric dipole moment and hence no pure rotational transitions. Silane is a gas under standard laboratory conditions, where it is extremely flammable. Astronomically, silane is observed in the envelopes of some evolved stars by means of infrared transitions at a wavelength of about 11 μm. It is expected by chemical equilibrium arguments to be present in the deep atmospheres of Jupiter and other gas ▶ giant planets (Visscher et al. 2010).

See Also

▶ Stellar Evolution
▶ Thermodynamical Chemical Equilibrium

References and Further Reading

Goldhaber DM, Betz AL (1984) Silane in IRC+10216. Astrophys J 279:L55–L58
Visscher C, Lodders K, Fegley B Jr (2010) Atmospheric chemistry in giant planets, brown dwarfs, and low-mass dwarf stars. III. Iron, magnesium, and silicon. Astrophys J 716:1060–1075

Silicane

▶ Silane

Silicate

▶ Silicate Minerals

Silicate Minerals

José Carlos Gaspar
Institute of Geosciences, University of Brasília, Brasília, DF, Brazil

Keywords

Earth's crust; Earth's mantle; Silica; Silicate classification; Silicate structure; Silicium

Synonyms

Silicate

Definition

Silicate minerals are those minerals that contain $[SiO_4]^{-4}$ as the fundamental unit of their chemistry and structure. Any other chemical element may occur in silicate minerals. $[SiO_4]^{-4}$ is a tetrahedron containing the four oxygen atoms in the apices and the silicium atom in the center. Up to all four oxygen atoms may be shared with other tetrahedrons. The number of shared oxygen atoms and the final space distribution are used to classify the silicate minerals.

Overview

Despite the fact that silicate minerals may accommodate any chemical element in their structures, the most common elements found are Al, Mg, Fe, Ca, Na, and K. Al is a common substitute for Si in the silica tetrahedron. Table 1 shows the classification of silicates, including their basic tetrahedral structure and most common minerals.

The Earth's ▶ crust, upper ▶ mantle, and transition zone are essentially composed of silicate

Silicate Minerals, Table 1 Classification scheme of silicate minerals

Name	Basic Si-tetrahedra structure	Number of shared oxygens	Example of common minerals
Nesosilicates	Independent tetrahedra	0	Olivine
Sorosilicates	2 tetrahedra	1	Epidote
Cyclosilicates	Rings of 3, 6, and 4 tetrahedra	2	Tourmaline
Inosilicates	Single tetrahedra chain	2	Pyroxene
	Double tetrahedra chain	2 or 3	Amphibole
Phyllosilicates	Tetrahedra sheet	3	Mica
Tectosilicates	Tridimensional framework	4	Quartz, feldspar

minerals. The crust is mainly composed of silicate minerals containing mostly Al, Ca, Na, and K, as quartz [SiO_2], feldspar [alkali-feldspar (K, Na)(Al, Si)$_3O_8$, and plagioclase Na($AlSi_3O_8$)-Ca($AlSi_2O_8$)]. Much less abundant but still widespread and important in the Earth's crust are Ca-, Fe-, and Mg-silicates, for example, mica [K_2(Al, Mg, Fe)$_{4-6}$(Al, Si)$_8O_{20}$(OH,F)$_4$], amphibole [(Ca, Na)$_{2-3}$(Mg, Fe, Al, Ti)$_5$(Si, Al,)$_8O_{22}$(OH)$_2$], and pyroxene [(Ca, Na)$_{1-p}$(Mg, Fe)$_{1+p}$(Al, Si)$_2O_6$($0<p<1$)]. Earth's upper mantle and the transition zone are largely composed of the following Ca-, Mg-, Fe-bearing silicate minerals: olivine [(Mg, Fe)$_2SiO_4$], pyroxene (see above), and garnet [(Ca, Mg, Fe)$_3$Al, Fe, Cr, Ti)$_2Si_3O_{12}$]. Chemical elements inside parenthesis in the chemical formulas occupy the same structural site and may vary in proportion one to another in a replacement process. Whenever valences are different, a conjugate elemental substitution occurs to compensate charge imbalance. The chemical element substitutions characterize these minerals as solid solutions. Extreme chemical compositions are called "end members." Each end member has a specific name, as for example "diopside" for the pyroxene end member $CaMgSi_2O_6$.

See Also

- ▶ Crust
- ▶ Mantle
- ▶ Quartz
- ▶ Zircon

References and Further Reading

Deer WA, Howie RA, Zussman J (1997) Rock forming minerals. The Geological Society, London

Hurlbut CS Jr., Klein C (after James D. Dana) (1993) Manual of mineralogy, 21st edn. Wiley, New York

Reviews of Mineralogy and Geochemistry, Mineralogical Society of America

Siliciclastic Microbialites

▶ Microbially Induced Sedimentary Structures

Silicon Isotopes

Luc André[1] and Damien Cardinal[2]

[1]Department of Earth Sciences, Royal Museum of Central Africa, Tervuren, Belgium

[2]LOCEAN, Université Pierre & Marie Curie, Paris, France

Keywords

Archean cherts; Bulk silicate earth; Early life; Meteorites; Siliceous organisms; Weathering

Definition

Silicon (Si) is an element present in all natural environments, including the biosphere. It has three stable isotopes of mass 28, 29, and 30, respectively. Its isotopic composition is

expressed in the delta notation $\delta^{30}Si$ ($^{30}Si/^{28}Si$) and $\delta^{29}Si$ ($^{29}Si/^{28}Si$) in per mil units normalized to a standard reference (see "▶ Delta, Isotopic"). The $\delta^{30}Si$ and $\delta^{29}Si$ vary in the solar system by up to 10 ‰ and 5 ‰, respectively. These isotopic changes in Earth and extraterrestrial materials are used to constrain diverse processes such as the origin of the ▶ solar system, core-mantle segregation, the appearance of life on the early Earth, the temperatures of the early oceans, the weathering of silicate rocks, or the role of siliceous organisms in C-Si cycles.

Overview

The potential role of silica (SiO_2) in the emergence of life has been often questioned, especially because SiO_2-rich deposits (cherts) host the oldest putative evidence for life. Others have wondered about the biological essentiality of silicon for life (Exley 2009). The main biologically reactive Si form is its most common dissolved form, silicic acid $Si(OH)_4$, which is massively present in natural waters. Most biological compartments may have been therefore visited by silicic acid since organisms rarely exclude it. This was likely the case for primitive forms of life because of the extensive Si mobilization at the surface of the early Earth caused by intense weathering. However, the potential role, if any, of silicon in these early biogeochemical cycles was probably complex because it certainly involved numerous Si reservoirs and processes: primary and secondary silicates, adsorption on nonsilicates, biogenic silica, and aqueous $Si(OH)_4$. These multiple Si components have been shown to bear contrasted Si isotopic signatures, which may in turn potentially trace the various vectors involved in the early biogeochemical cycles. This is one way by which Si isotopes represent a timely tool in the quest for the earliest archives of life.

Silicon has three stable isotopes: ^{28}Si, ^{29}Si, and ^{30}Si with respective abundances of 92.23 %, 4.67 %, and 3.1 %. ^{28}Si is a primary nucleus that exists owing to the nuclear oxygen-burning processes within stars whose initial compositions are hydrogen and helium rich, the two left elements from the Big Bang. Secondary nuclei ^{29}Si and ^{30}Si derive from ^{28}Si by neutron capture or by conversion of $^{25,26}Mg$ to $^{29,30}Si$. Because they require initial carbon and oxygen in the stars, the yield of ^{29}Si and ^{30}Si production increases with time in the universe as the interstellar gas becomes increasingly enriched in C and O.

The Si isotopic variations in natural samples are expressed in the delta notation per mil units (‰): $\delta^{x}Si = 1{,}000 \times [(^{x}Si/^{28}Si)_{sample}/(^{x}Si/^{28}Si)_{reference} - 1]$, where x refers to the atomic mass number 29 or 30. The large Si isotopic changes (>100‰) observed in presolar grain are commonly referred to as the solar abundances (e.g., $\delta^{30}Si_{Sol}$). The Earth, Moon, and meteorite abundances, with much smaller isotopic range of variations (<10‰), are normalized relative to a quartz standard, most often the NBS28 reference material (e.g., $\delta^{30}Si_{NBS28}$).

Si isotopes fractionate following laws that could be dependent on their mass differences (isotopic changes about twice larger for $\delta^{30}Si$ than for $\delta^{29}Si$) or not. Actually, stellar nucleosynthesis is the sole known process by which Si isotopes are fractionated along non-mass-dependent laws. Samples whose isotopic composition derives from a mass-dependent isotopic effect will fit two near-superimposed straight lines on a three-isotope graph according to the equilibrium ($\delta^{29}Si = 0.518 \times \delta^{30}Si$) or kinetic ($\delta^{29}Si = 0.509 \times \delta^{30}Si$) conditions of fractionation. All solar system and terrestrial materials follow these "solar-terrestrial" lines because both mechanisms cannot be distinguished within the current analytic capabilities.

Basic Methodology

Four analytic methods are available to measure Si isotopes. Two are adapted for bulk sample determination (gas source isotope ratio mass spectrometry (IRMS) and multicollector inductively coupled plasma mass spectrometry (MC-ICP-MS)) while two are dedicated for *in situ* micromeasurements (secondary ion mass spectrometry (SIMS) and laser ablation

MC-ICP-MS). Precise determinations have been gradually carried out by Si fluorination in combination with gas source IRMS (De La Rocha et al. 1996). Despite its accuracy and precision, this technique is not widely used because of its long and potentially hazardous procedures (making use of F_2 gas). The recently developed MC-ICP-MS methodology (e.g., Cardinal et al. 2003) is less contamination prone, quicker, and safer with similar or better precision and accuracy as shown by an interlaboratory comparison exercise ($2\sigma_M < \pm 0.15‰$, Reynolds et al. 2007). This methodology has been extended for *in situ* measurements using UV femtosecond laser ablation systems coupled to MC-ICP-MS (Chmeleff et al. 2008).

Key Research Findings

Significant silicon isotopic variations have been detected in eight major groups of samples, spreading different time periods, from presolar events to the modern biogeochemical Si cycle. All these isotopic fractionations were used to get new insights into the processes from which they derived.

The major group of silicon carbide (*SiC*) *grains* preserved in the most primitive meteorites defines a nonsolar-terrestrial trend line within the three-isotope diagram, showing larger $\delta^{29}Si$ changes compared to $\delta^{30}Si$ (slope of 4/3) (Nittler et al. 2005). Their extrasolar isotopic composition suggests that they condensed outside the solar system in dense winds leaving the surface of a presolar carbon-rich asymptotic giant branch star.

Si isotopes in high-temperature meteoritic calcium-aluminum-rich inclusions (*CAIs*) trace a process of partial Si evaporation-condensation at an early stage of the solar nebula evolution. Their $\delta^{29}Si$-$\delta^{30}Si$ plot defines a good correlation line with a mass-dependent slope of 0.5 with $-3.5‰ < \delta^{30}Si_{NBS28} < +5‰$. This line includes the mean Solar System composition ($\delta^{30}Si_{NBS28} = -0.5‰$) showing that the CAIs are fractionated products of the solar nebula. The lighter isotopes are preferentially lost during sublimation of the solid or evaporation from a liquid phase (Richter et al. 2009). So the CAIs enriched in heavy Si isotopes are likely residues of rapid Si evaporation while they were molten (~1–70 days, Shahar and Young 2007). In contrast, those depleted in heavy isotopes may represent lasting-years condensates from a gas phase containing previously evaporated light Si.

The bulk meteoritic compositions were found to be homogeneous for ordinary (O) and carbonaceous (C) chondrites, at about $\delta^{30}Si_{NBS28} = -0.48 \pm 0.10‰$ (Georg et al. 2007; Armytage et al. 2011; Savage and Moynier 2013), in good agreement with the solar wind values. In contrast, the enstatite (E) chondrites were shown to bear lighter isotopic signatures at $\delta^{30}Si_{NBS28} = -0.59‰$ and $-0.77‰$, for low-Fe and High-Fe E-chondrites, respectively. Their lighter Si isotopic compositions are most likely due to the presence of light Si in the kamacites (Savage and Moynier 2013).

The ▶ *bulk silicate Earth* (*BSE*) *composition* was deduced from mantle-derived peridotitic and basaltic rocks at $\delta^{30}Si_{NBS28} = -0.29 \pm 0.08‰$ (Georg et al. 2007; Fitoussi et al. 2009; Savage et al. 2010). The small but resolvable difference ($\Delta^{30}Si \sim +0.2‰$) between the BSE and the 0 and C chondrites demonstrates that the BSE is nonchondritic with respect to Si isotopes. This is interpreted as resulting from a Si isotope fractionation due to the incorporation of a significant proportion of Si (2–9 wt%) along with metals into the Earth's core during its segregation (Georg et al. 2007; Fitoussi et al. 2009; Armytage et al. 2011). Besides the significant Si isotopic offset between the E chondrites and the BSE precludes the E chondrites to represent a significant proportion of the material that accreted to form the proto-Earth (Savage and Moynier 2013).

Loess samples, which are a good proxy to the *bulk upper continental crust* (*UCC*) composition, define a narrow range of Si isotopic composition ($\delta^{30}Si_{NBS28} = -0.22 \pm 0.07‰$, Savage et al. 2013), identical to average granite and felsic rock compositions ($\delta^{30}Si_{NBS28} = -0.23 \pm 0.15‰$, Savage et al. 2012). The slightly heavier isotopic signature of the UCC ($\Delta^{30}Si \sim +0.1‰$) relative to the BSE results of

two balanced processes: (1) the magnitude of isotopic fractionation ($\Delta^{30}Si \sim +0.2‰$) observed between the mafic minerals and the felsic melts during the magmatic differentiation and partial melting processes, (2) the lighter signatures generated by the weathering processes which are transferred to the secular sedimentary mass.

The numerous Archean ▶ cherts display a very large range of Si isotopic signatures ($-2.5‰ < \delta^{30}Si_{NBS28} < +2.5‰$), with an apparent secular increase from 3.8 to 2.5 Ga (André et al. 2006; Robert and Chaussidon 2006). This secular change can be interpreted either as a gradual decrease of the oceanic temperature (Robert and Chaussidon 2006) or a progressive change in the Si source (Van den Boorn et al. 2010), from dominant pristine hydrothermal fluid in the early Archean ($\delta^{30}Si_{NBS28} \approx -0.3‰$) to pure seawater precipitations in the late Archean $\delta^{30}Si_{NBS28} \gg 0‰$).

Weathering conditions generate mass-dependent fractionation of Si isotopes with more negative values of $\delta^{30}Si$ in secondary soil minerals by direct Si incorporation into clays (Opfergelt et al. 2010) or Si adsorption onto Fe oxides (Delstanche et al. 2009) and heavier values in the percolating soil water compared to the original mineral Si source. Clays become isotopically lighter with the increase of soil weathering (Opfergelt et al. 2010).

Siliceous organisms, such as diatoms and sponges, along with amorphous silica stored in plants (phytoliths) have been well documented as an important pool of light silicon relative to their ambient fresh or marine waters. Combined with clay formation and silicification, they contribute to generate heavy Si isotopic compositions within most compartments of the modern hydrosphere ($+0.3‰ < \delta^{30}Si_{NBS28} < +4.7‰$).

Future Directions

The probability exists that a long-term record of continental weathering might be preserved in $\delta^{30}Si$ from fine-grained sediments. Considering the resistance of Si isotopes to postemplacement metamorphic redistributions (André et al. 2006), these $\delta^{30}Si$ archives could be useful in solving the debate about the strength of soil weathering during the Archean. A better estimation of biogenic versus inorganic silica fractionation factors relative to dissolved silicic acid would also be a potential progress toward a more accurate constraint on the processes involved in the Si cycle. At a longer term, if the $\delta^{29}Si$-$\delta^{30}Si$ analytic precision might be significantly improved ($<\pm 0.02‰$), Si isotopes might be used to discriminate between kinetic and equilibrium isotopic fractionations. Such a progress would be essential to distinguish kinetically controlled biogenic Si incorporation from temperature-controlled equilibrated Si partitioning between minerals with or without fluid phases. This is another way by which Si isotopes might be a helpful tracer in exploring the rise of life.

See Also

- ▶ Archean Traces of Life
- ▶ Isotope Biosignatures
- ▶ CAIs
- ▶ Chert
- ▶ Ocean, Chemical Evolution of

References and Further Reading

André L, Cardinal D, Alleman LY, Moorbath S (2006) Silicon isotopes in 3.8 Ga West Greenland rocks as clues to the Eoarchaean supracrustal Si cycle. Earth Planet Sci Lett 245:162–173

Armytage RMG, Georg RB, Savage PS, Williams HM, Halliday AN (2011) Silicon isotopes in meteorites and planetary core formation. Geochim Cosmochim Acta 75:3362–3676

Cardinal D, Alleman LY, de Jong J, Ziegler K, André L (2003) Isotopic composition of silicon measured by multicollector plasma source mass spectrometry in dry plasma mode. J Anal Atom Spectrom 18:213–218

Chmeleff J, Horn I, Steinhoefel G, von Blanckenburg F (2008) In situ determination of precise stable Si isotope ratios by UV-femtosecond laser ablation high-resolution multi-collector ICP-MS. Chem Geol 249:155–166

De La Rocha CL, Brzezinski MA, DeNiro MJ (1996) Purification, recovery and laser-driven fluorination of silicon from dissolved and particulate silica for the measurement of natural stable isotope abundances. Anal Chem 68:3746–3750
Delstanche S, Opfergelt S, Cardinal D, Elsass F, André L, Delvaux B (2009) Silicon isotopic fractionation during adsorption of aqueous monosilicic acid onto iron oxide. Geochim Cosmochim Acta 73:923–934
Exley C (2009) Darwin, natural selection and the biological essentiality of aluminium and silicon. Trends Biochem Sci 34:589–593
Fitoussi C, Bourdon B, Kleine T, Oberli F, Reynolds BC (2009) Si isotope systematics of meteorites and terrestrial peridotites: implications for Mg/Si fractionation in the solar nebula and for Si in the Earth's core. Earth Planet Sci Lett 287:77–85
Georg RB, Halliday AN, Schauble EA, Reynolds BC (2007) Silicon in the Earth's core. Nature 447:1102–1106
Molini-Velsko C, Mayeda TK, Clayton RN (1986) Isotopic composition of silicon in meteorites. Geochim Cosmochim Acta 50:2719–2726
Nittler LR, Gallino R, Lugaro M, Straniero O, Dominguez I, Zinner E (2005) Si and C isotopes in Presolar silicon carbide grains from AGB stars. Nucl Phys A 758:348–351
Opfergelt S, Cardinal D, André L, Delvigne C, Bremond L, Delvaux B (2010) Variations of δ^{30}Si and Ge/Si with weathering and biogenic input in tropical basaltic ash soils under monoculture. Geochim Cosmochim Acta 74:225–240
Reynolds BC, Aggarwal J, André L, Baxter D, Beucher C, Brzezinski MA, Engström E, Georg RB, Land M, Leng MJ, Opfergelt S, Rodushkin I, Sloane HJ, Van den Boorn SHJM, Vroon PZ, Cardinal D (2007) An inter-laboratory comparison of Si isotope reference materials. J Anal Atom Spectrom 22:561–568
Richter FM, Dauphas N, Teng F-Z (2009) Non-traditional fractionation of non-traditional isotopes: evaporation, chemical diffusion and Soret diffusion. Chem Geol 258:92–103
Robert F, Chaussidon M (2006) A palaeotemperature curve for the Precambrian oceans based on silicon isotopes in cherts. Nature 443:969–972
Savage PS, Moynier F (2013) Silicon isotopic variation in enstatite meteorites: clues to their origin and Earth-forming material. Earth Planet Sci Lett 361:487–496
Savage PS, Georg RB, Armytage RMG, Williams HM, Halliday AN (2010) Silicon isotope homogeneity in the mantle. Earth Planet Sci Lett 295:139–146
Savage PS, Georg RB, Williams HM, Turner S, Halliday AN (2012) The isotopic composition of granites. Geochim Cosmochim Acta 92:184–202
Savage PS, Georg RB, Williams HM, Halliday AN (2013) The silicon isotope composition of the upper continental crust. Geochim Cosmochim Acta 109:384–399
Shahar A, Young ED (2007) Astrophysics of CAI formation as revealed by silicon isotope La-ICP-MS of an igneous CAI. Earth Planet Sci Lett 257:497–510
Van den Boorn SHJM, van Bergen MJ, Vroon PZ, de Vries ST, Nijman W (2010) Silicon isotope and trace element constraints on the origin of 3.5 Ga cherts: implications for Early Archaean marine environments. Geochim Cosmochim Acta 74:1077–1103

Silicon Monosulfide

William M. Irvine
University of Massachusetts, Amherst, MA, USA

Synonyms

SiS

Definition

Radio astronomers have found that the diatomic molecule SiS, containing silicon and sulfur, is quite abundant in the gas phase in the envelope expelled by the evolved star IRC + 10216, and it has also been identified in warm gas in star-forming regions of our Galaxy. In the stellar envelope, some seven rare isotopic variants have been detected, involving ^{29}Si, ^{30}Si, ^{34}S, ^{33}S, and ^{36}S, as well as the principal isotopes ^{28}Si and ^{32}S. The abundance of SiS relative to SiO in warmer molecular clouds seems to be roughly in the ratio of the cosmic abundance of sulfur relative to oxygen.

See Also

- Hot Core
- Isotope
- Molecular Cloud
- Molecules in Space
- Silicon Monoxide
- Stellar Evolution

References and Further Reading

Morris M, Gilmore W, Palmer P, Turner BE, Zuckerman B (1975) Detection of interstellar SiS and a study of the IRC + 10216 molecular envelope. Astrophys J 199:L47–L51
Ziurys LM (1991) SiS in outflow regions – more high-temperature silicon chemistry. Astrophys J 379:260–266

Silicon Monoxide

William M. Irvine
University of Massachusetts, Amherst, MA, USA

Synonyms

SiO

Definition

This diatomic molecule is the simplest oxide of silicon. Silicon monoxide, SiO, has been detected in the gas phase in both interstellar molecular clouds and in the envelopes of evolved stars. In addition to the principal isotopic species, $^{28}Si^{16}O$, the rarer forms $^{29}Si^{16}O$ and $^{30}Si^{16}O$ are also observed. Maser emission is frequently observed from various transitions of SiO. Not surprisingly, SiO is not detected in cold, dark interstellar clouds or in the diffuse ▶ interstellar medium, where the silicon is thought to be primarily in the ▶ interstellar dust grains. However, it is detected in the shocks associated to molecular outflows emanating from newly formed stars.

History

Interstellar SiO was first detected in 1974 by L. Snyder and D. Buhl at millimeter wavelengths. The maser emission from stellar envelopes is often strong enough to provide useful sources for evaluating the pointing accuracy of radio telescopes.

See Also

- ▶ Interstellar Dust
- ▶ Interstellar Medium
- ▶ Maser
- ▶ Molecular Cloud
- ▶ Molecules in Space

References and Further Reading

Snyder LE, Buhl D (1974) Detection of possible maser emission near 3.48 millimeters from an unidentified molecular species in orion. Astrophys J Lett 189: L31–L33
Ziurys LM, Friberg P, Irvine WM (1989) Interstellar SiO as a tracer of high-temperature chemistry. Astrophys J 343:201–207

Silicon Nitride

William M. Irvine
University of Massachusetts, Amherst, MA, USA

Synonyms

SiN

Definition

The diatomic radical SiN is referred to by astronomers as silicon nitride, although that nomenclature is used by chemists for Si_3N_4, which is a solid at room temperature and which has been found in ▶ meteorites. Gas phase SiN has been detected by radio astronomers in both the envelopes expelled by evolved stars and in the ▶ molecular clouds toward the center of our Milky Way galaxy. It has been suggested that the SiN in the ▶ interstellar medium is produced by gas phase chemistry after silicon has been released from ▶ interstellar dust grains by ▶ sputtering in shocks.

See Also

- ▶ Interstellar Dust
- ▶ Interstellar Medium
- ▶ Molecular Cloud
- ▶ Molecules in Space
- ▶ Sputtering

References

Schilke P, Leurini S, Menten KM, Alcolea J (2003) Interstellar SiN. Astron Astrophys 412:L15–L18
Turner BE (1992) Detection of SiN in IRC+10216. Astrophys J 388:L35–L38

Silicon Tetrahydride

- ▶ Silane

SIM

David W. Latham
Harvard-Smithsonian Center for Astrophysics, Cambridge, MA, USA

Synonyms

Space interferometry mission

Definition

SIM is a proposed NASA mission to fly an interferometer in space, primarily to discover and characterize planets as small as the Earth in the habitable zones of solar-type stars but also to address several problems in astrophysics that require very accurate astrometry. SIM has two modes of operation. In the wide-angle mode, it uses a grid of astrometric standard stars to achieve all-sky astrometry that is accurate up to 4 μ-arcsec. In the narrow-angle mode, it can measure relative positions with a precision of 1 μ-arcsec or better. The main application for the narrow-angle mode is the search for planets like the Earth around nearby stars.

History

SIM has a long history dating back more than 20 years. Originally it was conceived as an astrometric mission for doing astrophysics. With the discovery of the first exoplanets, the emphasis was shifted to the search for habitable planets like the Earth. ▶ Interferometry from space requires an instrument with many moving parts and a capability for metrology at the picometer level. Years of development at the Jet Propulsion Laboratory in Pasadena succeeded in demonstrating that the required technology was feasible. However, the cost of proceeding with SIM was beyond the resources available to NASA for astrophysics, if undertaken in parallel with the *James Webb Space Telescope* (*JWST*), and the decision was made to proceed with *JWST* first. In the meantime, ESA's GAIA mission is proceeding toward a launch in 2012. GAIA will have poorer astrometric performance but will monitor one billion stars and thus should serve as an excellent pathfinder for SIM (although the main objective of GAIA is not exoplanet detection, but high-precision parallaxes and proper motions of stars, as a follow-up of ▶ Hipparcos). The cost of the original SIM design has escalated as the understanding of the technology has improved, and recent efforts have been aimed at a smaller scaled-down version of the mission called SIM Lite, whose funding has not been approved by NASA.

See Also

- ▶ Astrometric Planets
- ▶ Exoplanets, Discovery
- ▶ Gaia Hypothesis
- ▶ Habitable Zone
- ▶ Hipparcos
- ▶ Interferometry
- ▶ James Webb Space Telescope

Simple Sugar

► Monosaccharide

SiN

► Silicon Nitride

SiO

► Silicon Monoxide

SIRTF

► Spitzer Space Telescope

SiS

► Silicon Monosulfide

Skumanich Law

Steven W. Stahler
Department of Astronomy, University of California, Berkeley, CA, USA

Definition

An empirical relationship, discovered by Andrew Skumanich in 1972, between the rotation rate of a star and its age is referred to as the Skumanich Law. The equatorial speed of a star at its equator falls as the inverse square root of the star's age, for ages between 100 Myr and 10 Gyr. This law has only been established for solar-type objects, i.e., main-sequence stars of spectral type G. Along with the rotation rate, the surface activity of such stars, such as their X-ray emission, also declines in a similar manner. This activity arises ultimately from the star's surface magnetic field. Slowing of the rotation rate occurs because solar-type stars also emit winds. Such magnetized outflows carry off angular momentum.

See Also

► Rotational Velocity
► Stellar Winds

Slope Lineae, Recurrent

Alessandro Airo
Institut für Geologische Wissenschaften Tektonik und Sedimentäre Geologie, Freie Universität Berlin, Fachbereich Geowissenschaften, Berlin, Germany

Synonyms

Recurring slope lineae; Seasonal dark flows; Warm season flows

Definition

Recurring slope lineae (RSL) are seasonal dark markings on steep slopes (25–40°) that appear and progressively grow throughout the warm season and subsequently fade in the cold season (McEwen et al. 2011). RSL generally originate at rocky bedrock outcrops on slopes and are frequently associated with small channels. RSL have been found between 50 and 30°S latitude on slopes facing the equator and reaching surface temperatures during summer of up to 300 K. At these temperatures, liquid brines could develop close to the surface and percolate downhill through the subsurface pore space resulting in dark surficial "water tracks" that are know from

Antarctic environments (Levy 2012). However, the origin of these seasonal features on Mars remains debated.

See Also

- ▶ Dark Streaks (Mars)
- ▶ Gullies
- ▶ Slope Streaks (Mars)

References and Further Reading

Levy J (2012) Hydrological characteristics of recurrent slope lineae on Mars: evidence for liquid flow through regolith and comparisons with Antarctic terrestrial analogs. Icarus 219:1–4

McEwen AS, Ojha L, Dundas CM, Mattson SS, Byrne S, Wray JJ, Cull SC, Murchie SL, Thomas N, Gulick VC (2011) Seasonal flows on warm Martian slopes. Science 333:740–743

Slope Streaks (Mars)

Alessandro Airo
Institut für Geologische Wissenschaften Tektonik und Sedimentäre Geologie, Freie Universität Berlin, Fachbereich Geowissenschaften, Berlin, Germany

Definition

Slope streaks are dark features extending usually a few hundred meters downslope in a fan-shaped fashion and are prevalent in equatorial, high-albedo, dust-covered regions on Mars. They were first identified on images taken by the Viking Orbiters in 1977 and more than two decades later the appearance of new slope streaks was discovered (Edgett et al. 2000). New slope streaks appear to form sporadically and independent of the season (Schorghofer and King 2011). Various mechanisms of their formation have been proposed, ranging from dry dust avalanches (Sullivan et al. 2001) to wet mass wasting (Kreslavsky and Head 2009).

See Also

- ▶ Dark Streaks (Mars)
- ▶ Slope Lineae, Recurrent

References and Further Reading

Edgett KS, Malin MC, Sullivan RJ, Thomas P, Veverka J (2000) Dynamic Mars: new dark slope streaks observed on annual and decadal time scales. Lunar Planet. Sci. Conf. XXXI Abstract #1058

Kreslavsky MA, Head JW (2009) Slope streaks on Mars: a new "wet" mechanism. Icarus 201:517–527

Schorghofer N, King CM (2011) Sporadic formation of slope streaks on Mars. Icarus 216:159–168

Sullivan R, Thomas P, Veverka J (2001) Mass movement slope streaks imaged by the Mars Orbiter Camera. J Geophys Res 106(E10):23607–23633

Slushball Earth

- ▶ Snowball Earth

Small Solar System Body

Tilman Spohn
Deutsches Zentrum für Luft- und Raumfahrt (DLR), Institut für Planetenforschung, Berlin, Germany

Synonyms

Minor planet

Definition

According to IAU (International Astronomical Union) resolutions five and six (Resolution_GA26-5-6), all objects that are neither a satellite, a ▶ planet, nor a ▶ dwarf planet are to be considered a small solar system body (SSSB). This definition covers most of the ▶ asteroids, ▶ near-Earth objects (NEO),

▶ comets, ▶ trans-Neptunian objects (TNO) or ▶ Kuiper belt objects (KBO), and other small bodies. Small bodies are bare objects without stable atmospheres. Some of the icy small bodies (in particular the comets and the distant asteroids named Centaurs) have transient atmospheres when they come sufficiently close to the Sun. The temporary atmospheres are caused by sublimation of ices heated by the solar radiation. The term "small solar system body" replaces the term "minor planet" which has been very often used as a synonym for asteroid but does not exist as an official term anymore.

See Also

- ▶ Asteroid
- ▶ Centaurs (Asteroids)
- ▶ Comet
- ▶ Dwarf Planet
- ▶ Kuiper Belt
- ▶ Near-Earth Objects
- ▶ Planet
- ▶ Satellite or Moon
- ▶ Trans-Neptunian Object

SNC Meteorites

Frank Sohl and Tilman Spohn
Deutsches Zentrum für Luft- und Raumfahrt (DLR), Institut für Planetenforschung, Berlin, Germany

Synonyms

Martian meteorites

Definition

The SNC ▶ meteorites are a group of petrologically similar ▶ achondrites named after the locations where examples of these meteorites were first found – **S**hergotty (India), **N**akhla (Egypt), and **C**hassigny (France). Subgroups are the shergottites, nakhlites, and chassignites. The term SNC meteorites is sometimes restricted to the shergottites, nakhlites, and chassignites but many times includes meteorites from other findings as well. SNC meteorites are basalts, and most of them are much younger than other meteorites – with an apparent age of 1.3 Ga or younger. Together, these findings suggest that the meteorite parent body was a planetary size object. The only undisputed example of an old SNC meteorite is ▶ ALH 84001 – found in the Allan Hills, Antarctica, in 1984 – which is 4.1 Ga old (Bouvier et al. 2009). Most researchers accept that SNC meteorites were part of the regolith layer of ▶ Mars, as their composition is similar to that of the Martian regolith analyzed by space probes. Gas inclusions found in some SNC meteorites resemble the Martian atmosphere in isotopic composition. It is believed that these ▶ igneous rocks probably reached escape velocity (5.4 km/s) when a body impacted Mars and thus could leave its gravity field. Later, some of these ▶ rocks got captured by *Earth's* gravity field and ended up as meteorites on Earth' surface.

See Also

- ▶ Achondrite
- ▶ ALH 84001
- ▶ Basalt
- ▶ Earth
- ▶ Igneous Rock
- ▶ Mars
- ▶ Meteorites
- ▶ Rock

References and Further Reading

Bouvier A, Blichert-Toft J, Albarede F (2009) Martian meteorite chronology. Earth Planet Sci Lett 280:285–295

Snow Line

Avi M. Mandell
NASA Goddard Space Flight Center, Greenbelt, MD, USA

Synonyms

Frost line; Ice line

Definition

The snow line is the radial position within a ▶ protoplanetary disk where the conditions in the disk allow the existence of water ice. It implies in particular that the temperature is low enough and, equally important, that water (vapor or ice) is present in the same region. The snow line marks the transition between the inner region of the disk where water exists in the gaseous phase and the outer region of the disk where water condenses into solid ice particles. The position of the snow line changes with time and with the viscous dissipation assumed for the disk. In the ▶ solar nebula and other protoplanetary disks, this position is of great importance for understanding the formation and evolution of both giant and ▶ terrestrial planets, due to the role of water as both a major constituent of the solid material in the disk and as the primary liquid medium on planetary surfaces and within planetary interiors.

Overview

The temperature structure of a protoplanetary disk is determined by both the accretion history of the disk as it forms from the stellar birth cloud and accretes onto the central star and the ongoing radiative heating from the central star itself. Viscous heating caused by accretion is mostly constrained to the midplane of the disk, so the radial temperature structure is primarily driven by heating from the central star and decreases from the inner disk to the outer disk. The inner regions of the disk can be heated by the central star to more than 5,000 K, while the outer regions of the disk beyond 50 AU can have gas and grain temperatures as low as 10 K, based on studies of comets in our own Solar System.

This substantial range in temperature encompasses the sublimation temperatures for many chemical species within the protoplanetary disk, leading to "condensation fronts" where a specific chemical constituent transitions from the gaseous phase to the solid phase. Refractory materials such as silicates have very high condensation temperatures and condense out in the inner disk, while volatile materials such as water and methane condense out at larger distances from the central star. The condensation temperature for water in a low-pressure environment such as a protoplanetary disk is ~150 K; early models of the minimum-mass solar nebula suggested that this transition temperature would occur at 2.7 AU in our own Solar System, but since then the location and evolution of the snow line has been a topic of debate (see below).

The location of the snow line during the formation of planets in a circumstellar disk is important for several reasons. First, H_2O is thought to comprise at least half of the available solid material in a protoplanetary disk, based on thermochemical models of the solar nebula. Therefore, the density of solid material beyond the snow line will be much greater than the density of solid material within the snow line, leading to faster growth of planets and larger planetary cores beyond the snow line. This enhancement has been invoked to explain the fact that all the giant planets in our Solar System orbit beyond 5 AU – the larger planetary cores beyond the snow line were able to reach the critical mass for runaway gas accretion, while smaller planetary cores within the snow line never accreted significant gaseous atmospheres.

The location of the snow line is also important for constraining the source and abundance of water on the terrestrial planets, particularly Earth. If all the source material for the terrestrial planets formed within the snow line where the water content of planetesimals would be very

low, there should be very little water on the surfaces or in the interiors of planets in the inner system. We clearly know of only one planet with a significant water fraction today (Earth), the Moon is essentially dry, and there may have been significant amounts of water on both Venus and Mars at the time of their formation; the origin of the water on Earth and the potential for water-rich terrestrial planets in other planetary systems are therefore an active area of research (see below).

Key Research Findings

The location of the snow line during the formation of the Solar System, and by extension other planetary systems, is an area of active research. Hayashi (1981) first calculated the location of the snow line in the minimum-mass solar nebula to be at 2.7 AU; however, the calculation was only an energy balance between the solar radiation absorbed and re-emitted from a ▶ blackbody absorber. Since then our knowledge of the various heating and cooling processes in the solar nebula has advanced significantly, improving our ability to determine the temperature structure of the disk over time. Calculations by Sasselov and Lecar (2000) and Lecar et al. (2006) incorporated more recent models of protoplanetary disk structure and included heating from accretion and solar radiation and variations in condensation temperature with gas density. They found that for a minimum-mass solar nebula with low levels of accretion similar to observed protoplanetary disks, the snow line would lie between 1.6 and 1.8 AU; however, increasing the mass, the accretion rate, or the opacity of grains in the disk could move the snow line out as far as 3.5 AU.

The role of the snow line in aiding the formation of giant planets is also still under debate. The obvious increase in planet mass beyond 5 AU naturally correlates with the enhancement of solid material beyond the snow line, but this increased mass has been thought to be insufficient to overcome the long dynamical timescales for accretion in the outer Solar System; estimated timescales for unaided core accretion in the giant planet region were 10^7–10^8 years, much longer than the lifetime of gas in the solar nebula. Beginning with Stevenson and Lunine (1988), who postulated that water vapor in the disk would be redistributed to the snow line by eddy diffusion and lead to core formation at the condensation front, various researchers have invoked processes that could lead to a buildup of material at or near the snow line and lead to rapid core formation. Recent hydrodynamic simulations of giant ▶ planet formation with a more accurate treatment of the role of the expanding planetary atmosphere seem to suggest that no additional mechanism is necessary (Lissauer et al. 2009), but this does not rule out other enhancement processes.

The other active area of research relating to the snow line concerns the delivery of water and other volatile material to the terrestrial planets. If the snow line was located beyond the orbit of Mars, as would be expected based on models and the water content of asteroids in the asteroid belt, then the bulk of the material that formed the terrestrial planets should have been very water poor. However, we know that the Earth has a water mass fraction of ~0.1 %, and there is evidence of significant past water flow on the surface of Mars over geologic timescales. Researchers have debated whether the Earth's water was delivered primarily by comets from the Jupiter-Saturn region (e.g., Delsemme 2000) or by hydrated asteroids from the outer asteroid belt (e.g., Morbidelli et al. 2000), relying primarily on comparisons between the deuterium-to-hydrogen ratio (D/H) for Earth's water and that of different classes of Solar System bodies. More recent simulations of the final stages of the accretion of terrestrial planets have shown that water-rich asteroid-type planetesimals from 2 to 3 AU are naturally incorporated into terrestrial planets during the late stages of formation (Raymond et al. 2007; Bond et al. 2010).

See Also

▶ Core Accretion, Model for Giant Planet Formation

- ▶ Planet Formation
- ▶ Protoplanetary Disk
- ▶ Solar Nebula
- ▶ Water, Delivery to Earth

References and Further Reading

Bond JC, Lauretta DS, O'Brien DP (2010) Making the earth: combining dynamics and chemistry in the solar system. Icarus 205:321

Delsemme AH (2000) 1999 Kuiper prize lecture cometary origin of the biosphere. Icarus 146:313

Hayashi C (1981) Structure of the solar nebula, growth and decay of magnetic fields and effects of magnetic and turbulent viscosities on the nebula. Prog Theor Phys Suppl 70:35

Lecar M et al (2006) On the location of the snow line in a protoplanetary disk. Astrophys J 640:1115

Lissauer JJ et al (2009) Models of Jupiter's growth incorporating thermal and hydrodynamic constraints. Icarus 199:338

Morbidelli A et al (2000) Source regions and time scales for the delivery of water to earth. Meteorit Planet Sci 35:1309

Raymond SN, Quinn T, Lunine JI (2007) High-resolution simulations of the final assembly of earth-like planets. 2. Water delivery and planetary habitability. Astrobiology 7:66

Sasselov DD, Lecar M (2000) On the snow line in dusty protoplanetary disks. Astrophys J 528:995

Stevenson DJ, Lunine JI (1988) Rapid formation of Jupiter by diffuse redistribution of water vapor in the solar nebula. Icarus 75:146

Snowball Earth

Paul Hoffman
Department of Earth & Planetary Sciences, Harvard University, Cambridge, MA, USA

Keywords

Albedo; Atmospheric oxygenation; CO_2 hysteresis; Energy balance models; Fe-Mn ore deposits; Greenhouse effect; Ice grounding line; Ice sheet; Paleomagnetism; Radiative forcing; Geochemical carbon cycle; Silicate-weathering feedback; Volcanic-metamorphic outgassing; Multicellular animals

Synonyms

Hard snowball; Ice-albedo instability; Makganyene glaciation; Marinoan glaciation; Pan-glacial; Runaway ice-albedo feedback; Slushball Earth; Sturtian glaciation; White Earth

Definition

"Snowball Earth" refers to the planet's appearance from space during parts of the Neoproterozoic and Paleoproterozoic eras, when geological evidence suggests that most continental areas and arguably the entire ocean were covered by dynamic ice sheets, limiting air-sea gas exchange to cracks at ice grounding lines and shallow-water hydrothermal vents. *Slushball Earth* refers to an alternative scenario in which ice sheets existed on all ▶ continents, but the tropical ocean was largely ice-free. *Pan-glacial* is a term used when the extent of marine ice is unstipulated. *White Earth* is a prior synonym of snowball Earth referring to a model outcome thought never to have actually existed.

History

That dynamic ice sheets covered northern Europe and North America in the geologically recent past was first inferred in the 1820s, debated fiercely in the 1840s, and accepted widely in the 1860s. It was the first clear indication that climate change was bidirectional: previously it had been thought to be monotonic due to secular dimming of the Sun. The peri-North Atlantic ice sheets were Quaternary in age (less than 2.6 Ma), but geological evidence of far more ancient ice sheets was soon uncovered (Fig. 1). By the 1900s, it was firmly established that Paleozoic ice sheets had episodically waxed and waned over South Polar ▶ Gondwana (the South America-Africa-Arabia-India-Antarctica-Australia supercontinent). Late Precambrian (now Neoproterozoic) ice sheets proved to have been even more widespread: by the 1960s, their telltale signs were documented on virtually every continent. By the 1990s,

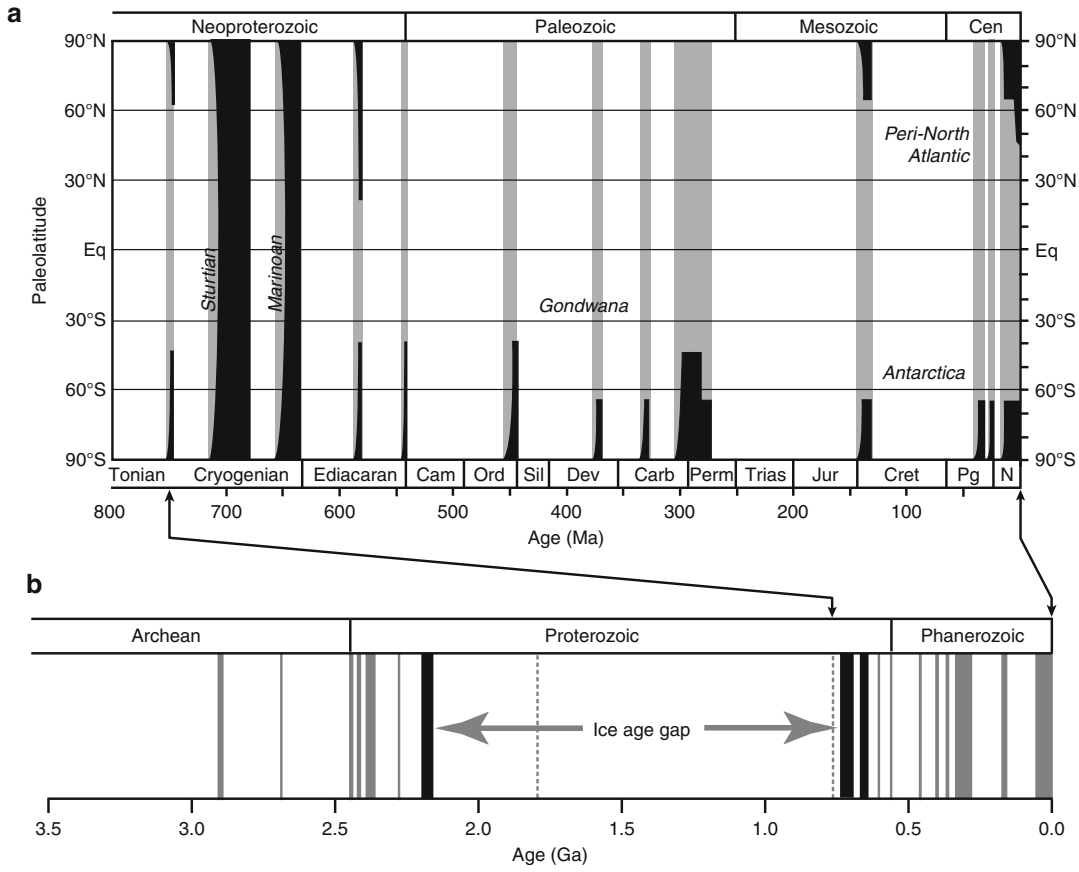

Snowball Earth, Fig. 1 (**a**) Equatorward extent of grounded ice sheets (*black*) on Earth from 800 Ma to present, defining "glacial" (*gray*) and "non-glacial" (*white*) periods. (**b**) "Non-glacial" (*white*), "glacial" (*gray*), and "pan-glacial" (*black*) periods from 3.5 Ga to present. Note ice age gap from ~2.22 to 0.72 Ga, when evidence for glaciation (*dashed bars*) is local and uncertain

combined sedimentological and paleomagnetic data demonstrated that ice sheets had flowed into the ocean close to the paleo-equator (Evans 2000). The occurrence of ice sheets at sea level in the tropics (Fig. 2) trumps uncertainties over correlation: if the warmest areas were glaciated, colder regions must have been frozen as well. The only escape from this logic – a reverse climatic gradient due to extreme (≥53°) orbital ▶ obliquity – is untenable because the zonal ranges of other climatic indicators such as ▶ carbonates (warm) and ▶ evaporites (dry) did not change significantly.

Ice-▶ albedo feedback was conceived in the 1860s as an amplifier of orbitally induced ice-sheet growth and decay. In the 1920s, it was incorporated into a theory of bistable climate states, consistent with geological observations: "non-glacial" when no ice sheets existed and "glacial" when ice sheets existed permanently in polar regions and periodically in midlatitudes (Fig. 1). In the 1960s, a third stable climate state emerged from simple energy balance models developed to describe zonal mean surface temperatures as a function of solar radiative forcing. With a surprisingly modest negative forcing (a few percent), surface temperatures fell below freezing everywhere due to runaway ice-albedo feedback. The resulting "white Earth" is very stable because greatly increased radiative forcing is required to overcome the high planetary albedo (Fig. 3). These findings stimulated the nascent

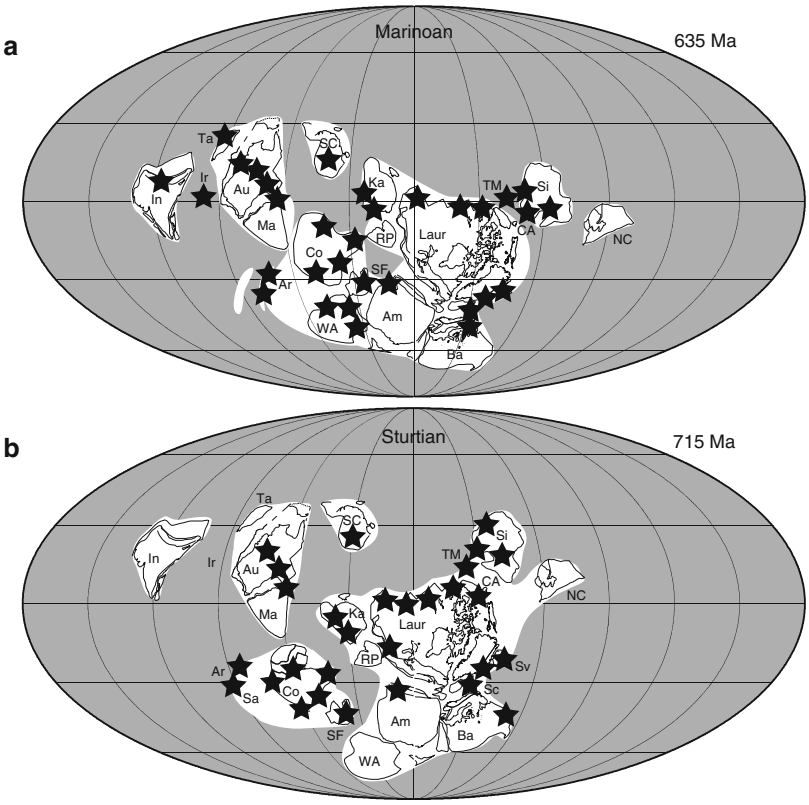

Snowball Earth, Fig. 2 Distribution of glacigenic deposits (*black stars*) of (**a**) Marinoan and (**b**) Sturtian age on paleogeographic maps for 635 and 715 Ma, respectively (Hoffman and Li 2009). Maps were compiled using paleomagnetic and tectonic constraints, but not paleoclimatic data

science of climate modeling because they were assumed to expose an erroneous formulation of the climate response. If solar luminosity had risen by nearly 30 % since 4.5 Ga, Earth's surface should have been frozen for most of its history (it was not) and should still be ice covered today because of planetary albedo. This proved to be an insurmountable problem for physical models because its solution was chemical in nature.

In 1981, three planetary scientists proposed that the temperature dependence of silicate weathering (which consumes atmospheric CO_2) provides a negative climatic feedback through which CO_2 concentration self-adjusts toward whatever level leads to a balance between the sources and sinks of CO_2 (Walker et al. 1981). They credited silicate-weathering feedback for the maintenance of a habitable climate, but they understood that it could not prevent runaway ► glaciation under all circumstances because its operation is ponderously slow (Myrs) compared to albedo feedback (months). They pointed out that a white Earth disaster would not be permanent because surface temperatures would be too low to scrub CO_2 from the atmosphere in rain, but too high for unlimited sequestering of CO_2 as dry ice. Volcanic-► metamorphic emissions would drive atmospheric CO_2 concentrations ever higher until ► greenhouse radiative forcing reached the critical point for deglaciation. If white Earth disasters were self-terminating, their occurrence in the geological past could not be ruled out a priori.

The concept of self-reversing ice-albedo instability was first applied to Neoproterozoic glaciation by Kirschvink (1992), who coined the term "snowball Earth," and to Paleoproterozoic glaciation by Evans et al. (1997). Both interpretations rested on paleomagnetic-sedimentary evidence that ice sheets reached sea level in low paleolatitudes. The occurrence of large

sedimentary Fe and Mn ore deposits within glacial marine sequences of both ages was taken as indicating deep-ocean anoxia due to marine ice covers (Hoffman and Schrag 2002).

Overview

Paleomagnetic and sedimentological studies demonstrate that dynamic ice sheets existed simultaneously on virtually every continent during two discrete Neoproterozoic glaciations (Fig. 2). The younger (Marinoan) glaciation lasted for up to 20 Myrs and terminated at 635 Ma; the older (Sturtian) glaciation began at 717 Ma and lasted for up to 55 Myrs (Condon et al. 2005; Macdonald et al. 2010). Other Neoproterozoic glaciations occurred at 582 Ma (Gaskiers) and perhaps around 745 Ma (Bayisi and Kaigas), but, like Phanerozoic glaciations, they appear to have been regional in extent (Fig. 1).

Three discrete Paleoproterozoic glaciations are recognized in North America, two in South Africa, and one each in northern Finland and Western Australia. The younger South African glaciation (Makganyene) occurred in a very low paleolatitude, $11 \pm 5^{\circ}$ (Evans et al. 1997). With a maximum age of 2.22 Ga, it is younger than the three North American glaciations and postdates the appearance of $>10^{-5}$ PAL O_2 in the atmosphere by as much as 220 Ma. Its termination was accompanied by sedimentary Fe_2O_3 and MnO_2 ore deposits, the latter the largest on Earth (Kirschvink et al. 2000).

Deep-sea sedimentary records are virtually nonexistent because ▶ Proterozoic oceanic crust was recycled. Consensus is lacking as to whether the tropical ocean was ice covered during pan-glacial episodes ("snowball" scenario) or ice-free ("slushball" scenario). Fe-Mn ore deposition and evidence for extreme CO_2 concentration support the snowball scenario; apparent continuity of a poor fossil record supports the more benign slushball scenario. The stability of the slushball scenario is questionable (Bendtsen 2002).

Basic Methodology

There are two approaches to the study of snowball Earth phenomena, empirical geology and numerical modeling. The first attempts to determine the extent, dynamics, development, and duration of the glacial ice covers; the circumstances of glacial onsets and terminations; and their impacts on the ocean, atmosphere, biosphere, and biogeochemical cycling. The extent of glaciation is mapped using the same sedimentological criteria as for vanished Quaternary ice sheets, developed through comparative sedimentology with active ice margins. Ice-sheet dynamics are inferred from regional patterns of erosion and deposition. The most precise and reliable dating method utilizes U-Pb isotope systematics of volcanic zircon ($ZrSiO_4$), subjected to CA-ID-TIMS (chemical abrasion isotope-dilution thermal ionization mass spectrometry). Because glacial advance reworks the record of earlier advances, surviving glacial deposits represent the end of a glacial interval. Hysteresis in CO_2 (Fig. 3) implies that snowball glaciations began cold and dry and ended warm and wet. Consequently, existing sedimentary records disappoint those seeking to test the predicted extreme condition. An assortment of geochemical and isotopic proxies contributes to an emerging history of Neoproterozoic seawater. Given limitations on preservation, changes in Neoproterozoic marine life are chronicled by micro- and molecular paleontology, but reworking is an ever-present danger, particularly if primary productivity was greatly reduced by ice cover.

Numerical models are used to characterize aspects of the snowball Earth scenario for critical comparison with geological observations. In a comprehensive general circulation model (GCM), the atmosphere, oceans, ice sheets, and sea glaciers (see below) would be dynamically coupled (with appropriately reduced solar luminosity and faster spin, relative to present), but no such fully coupled model has yet been achieved. Because the tropics are critical in the initiation and termination of a snowball Earth, the diurnal cycle is amplified, and the seasonal and orbital cycles muted relative to models of Quaternary ice

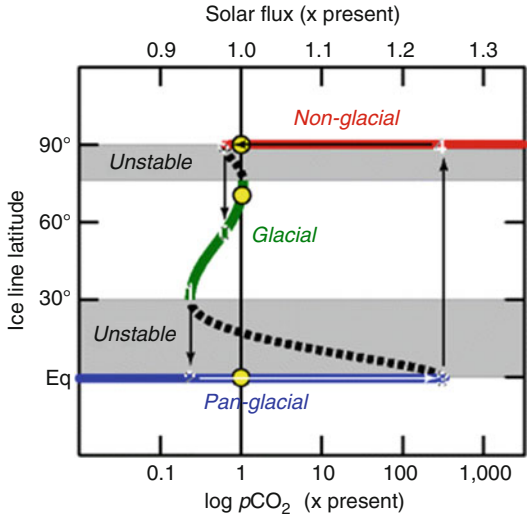

Snowball Earth, Fig. 3 Ice line latitude as a function of solar flux and equivalent CO_2 radiative forcing, showing three stable branches (non-glacial, glacial, and pan-glacial), unstable regions (*gray*), and possible stable climates under present conditions (*open circles*), as depicted in simple energy balance climate models. CO_2 hysteresis loop (*thin arrows*) associated with a snowball Earth cycle: (0–1) negative radiative forcing drives ice line equatorward to the ice-albedo instability around 30° latitude; (1–2) with no additional forcing, ice line advances catastrophically to the equator; (2–3) in the near absence of silicate weathering, pCO_2 (buffered by submarine carbonate dissolution) slowly rises over millions of years to the critical point for deglaciation; (3–4) millennial-scale deglaciation, driven by ice-albedo and greenhouse gas feedbacks; (4–5) drawdown of CO_2 by silicate weathering on a million-year e-unfolding time due to hyperreactive glacial debris including rock "flour"; (5–0) polar ice sheets develop stochastically without additional radiative forcing

sheets. The thickness of equatorial sea ice and the critical radiative forcing at termination have received particular attention (Pollard and Kasting 2005; Pierrehumbert 2005). Simplified GCMs coupled to the geochemical carbon cycle have investigated the climatic responses to supercontinental fragmentation and stochastic flood basalt weathering (Donnadieu et al. 2004).

Key Research Findings

The snowball Earth concept was first questioned on the grounds that dynamic ice sheets could not be sustained after the oceans froze over in the absence of a hydrologic cycle. Coupled climate models, however, indicate that ice sheets would continue to grow until they reached dynamic steady state after a few hundred thousand years, driven by sublimation of tropical sea ice (Donnadieu et al. 2003; Pollard and Kasting 2004).

A second question concerned the evolutionary survival of phototrophic primary producers and extant clades of eukaryotic algae known to have evolved before 720 Ma. The planetary albedo of a snowball Earth would drive surface temperatures below freezing everywhere, and the global mean thickness of marine ice, set by the geothermal heat flux, would cause the ice to flow under its weight from the extratropics where it was thicker toward the equator where it was thinnest. Equatorward flowage would be dynamically maintained by sublimation and basal melting in the tropics and condensation and basal freezing in the extratropics. The aptly named "sea glacier" had meteoric and marine ice components, and simple models suggest that maximum flow velocities were comparable with mountain glaciers (Warren et al. 2002; Goodman and Pierrehumbert 2003). Although it may be physically possible to keep equatorial ice thin enough for significant sub-ice phototropism (Pollard and Kasting 2005), a more robust refugium may have existed within crack systems along grounding lines where ice sheets peripherally lost their moorings and were swept into the sea glacier.

A key test for the snowball Earth scenario is greatly elevated CO_2, which, augmented by other forcings, is required for deglaciation (Pierrehumbert 2005). Extreme pCO_2 has been inferred from boron and carbon isotopes in Marinoan syndeglacial carbonates and from ^{18}O-^{17}O-^{16}O ratios in Marinoan glacial and syndeglacial sulfates (Bao et al. 2008).

The oldest molecular biomarker (24-isopropylcholestane) and microfossils (diapause eggs and embryos) attributed to multicellular animals come, respectively, from within Marinoan glacial deposits in Oman (Love et al. 2009) and ~3 Myr after the

same glacial termination in South China (Yin et al. 2007). Population genetic modeling suggests that strong kin selection and protective isolation from "cheaters" engendered by a snowball Earth would favor cellular "altruism," promoting multicellularity in animals (Boyle et al. 2007).

Applications

Snowball Earth was a dynamic planet, alien to Earth as we know it, but one whose geological archives can be directly examined, at little expense, close to home. It was a dramatic manifestation of interaction between a positive climatic feedback due to ice-albedo and a negative feedback due to silicate weathering, the former operating on a timescale of months and the latter over millions of years (Walker et al. 1981). Snowball deglaciations caused transient hyper-greenhouse warming (stage 4–5 in Fig. 3). Snowball Earth presents a testable demonstration of the power of the atmospheric "greenhouse" effect. These features make it a captivating vehicle for learning and teaching.

Future Directions

A "wish list" of directions in which progress is needed includes: (1) detailed temporal relations between both Paleo- and Neoproterozoic pan-glacial episodes and the history of atmospheric oxygenation; (2) temporal relations between those same episodes and the early evolution of ▶ cyanobacteria and multicellular animals, respectively; and (3) the significance of the 1.47-billion-year gap in the record of ice sheets between ~2.22 and ~0.75 Ga (Fig. 1), when there is scarcely any geological evidence for glaciation anywhere on Earth. The records of many ice sheets older than 2.2 Ga, the oldest at 2.9 Ga, show that the middle Proterozoic ice age gap does not simply reflect the imperfection of the geological record.

See Also

- ▶ Cyanobacteria
- ▶ Glaciation
- ▶ Gondwana
- ▶ Great Oxygenation Event
- ▶ Mass Extinctions
- ▶ Ocean, Chemical Evolution of
- ▶ Oxygenation of the Earth's Atmosphere
- ▶ Proterozoic Eon

References and Further Reading

Bao H, Lyons JR, Zhou C (2008) Triple oxygen isotope evidence for elevated CO2 levels after a Neoproterozoic glaciation. Nature 452:504–506

Bendtsen J (2002) Climate sensitivity to changes in solar insolation in a simple coupled climate model. Clim Dyn 18:595–609

Boyle RA, Lenton TM, Williams HTP (2007) Neoproterozoic 'snowball Earth' glaciations and the evolution of altruism. Geobiology 5:337–349

Condon D, Zhu M, Bowring SA, Wang W, Yang A, Jin Y (2005) U-Pb ages from the neoproterozoic doushantuo formation, China. Science 308:95–98

Donnadieu Y, Fluteau F, Ramstein G, Ritz C, Besse J (2003) Is there a conflict between the Neoproterozoic glacial deposits and the snowball Earth interpretation: an improved understanding with numerical modeling. Earth Planet Sci Lett 208:101–112

Donnadieu Y, Goddéris Y, Ramstein G, Nédélec A, Meert J (2004) A 'snowball Earth' climate triggered by continental break-up through changes in runoff. Nature 428:303–306

Evans DAD (2000) Stratigraphic, geochronological, and paleomagnetic constraints upon the Neoproterozoic climatic paradox. Am J Sci 300:347–433

Evans DAD, Beukes NJ, Kirschvink JL (1997) - Low-latitude glaciation in the Palaeoproterozoic era. Nature 386:262–266

Goodman J, Pierrehumbert RT (2003) Glacial flow of floating marine ice in snowball Earth. J Geophys Res 108:3308. doi:10.1029/2002JC001471

Hoffman PF, Li ZX (2009) A palaeogeographic context for Neoproterozoic glaciation. Palaeogeogr Palaeoclimatol Palaeoecol 277:158–172

Hoffman PF, Schrag DP (2002) The snowball Earth hypothesis: testing the limits of global change. Terra Nova 14:129–155

Kirschvink JL (1992) Late proterozoic low-latitude glaciation: the snowball Earth. In: Schopf JW, Klein C (eds)

The Proterozoic biosphere. Cambridge University Press, Cambridge, pp 51–52
Kirschvink JL, Gaidos EJ, Bertani LE, Beukes NJ, Gutsmer J, Maepa LN, Steinberger RE (2000) Paleoproterozoic snowball Earth: extreme climatic and geochemical global change and its biological consequences. Proc Natl Acad Sci U S A 97:1400–1405
Love GD, Grosjean E, Stalvies C, Fike DA, Grotzinger JP, Bradley AS, Kelly AE, Bhatia M, Meredith W, Snape CE, Bowring SA, Condon DJ, Summons RE (2009) Fossil steroids record the appearance of demospongiae during the cryogenian period. Nature 457:718–722
Macdonald FA, Schmidtz MD, Crowley JL, Roots CF, Jones DS, Maloof AC, Strauss JV, Cohen PA, Johnston DT, Schrag DP (2010) Calibrating the cryogenian. Science 327:1241–1243
Pierrehumbert RT (2005) Climate dynamics of a hard snowball Earth. J Geophys Res 110, D01111. doi:10.1029/2004JD005162
Pollard D, Kasting JF (2004) Climate-ice sheet simulations of neoproterozoic glaciation before and after collapse to snowball Earth. In: Jenkins GS, McMenamin MAS, McKay CP, Sohl L (eds) The extreme proterozoic: geology, geochemistry, and climate, vol 146, Geophysical monograph. American Geophysical Union, Washington, pp 91–105
Pollard D, Kasting JF (2005) Snowball Earth: a thin-ice solution with flowing glaciers. J Geophys Res 110, C07010. doi:10.1029/2004JC002525
Walker JCG, Hays PB, Kasting JF (1981) A negative feedback mechanism for the long-term stabilization of Earth's surface temperature. J Geophys Res 86(C10):9776–9782
Warren SG, Brandt R, Grenfell TC, McKay CP (2002) Snowball Earth: ice thickness on the tropical ocean. J Geophys Res 107:3167
Yin L, Zhu M, Knoll AH, Yuan X, Zhang J, Hu J (2007) Doushantuo embryos preserved inside diapause egg cysts. Nature 446:661–663

SO

► Sulfur Monoxide

Soda

► Natron

Soda Lakes

Daniele L. Pinti
GEOTOP Research Center for Geochemistry and Geodynamics, Université du Québec à Montréal, Montréal, QC, Canada

Keywords

Alkaline environments; Extreme environments; Natron; Rift Valley lakes; Thermonatrite

Synonyms

Alkaline lakes; Hypersaline lakes

Definition

Soda lakes are alkali lakes rich in dissolved sodium salts, especially sodium carbonate, sodium chloride, and sodium sulfate. Soda lakes are the most stable alkaline environments on Earth with pH values above 11.5. They form in arid and semiarid areas of tropical and subtropical deserts of North America, continental Asia, and East African Rift Valley. Despite the extreme caustic conditions, soda lakes are the most productive aquatic environments on Earth. Microbial communities are studied in soda lakes as a possible analogue for ancient life on Earth, while soda lake chemistry is studied as an alternative model for the early ocean chemical evolution.

Overview

As the name indicates, soda lakes are characterized by the occurrence of large deposits of sodium in the form of carbonates such as ► trona ($Na_3H(CO_3)_2 \cdot 2H_2O$), ► natron ($Na_2CO_3 \cdot 10H_2O$), ► thermonatrite ($Na_2CO_3 \cdot H_2O$), halite (NaCl) and thenardite (Na_2SO_4). They are also very

S

alkaline with pH never below 10.5, with the highest values of pH = 12 recorded at Magadi Lake, Kenya. These particular conditions derive from a peculiar mixture of geographical, geological, and climatic features. Soda lakes are formed in very arid environments, often in depressions located above sea level and formed by continental rifting and with few or no freshwater inflow. Soda lakes occur worldwide but occur predominantly in the desert environments of Western North America (Soda Lake, Mojave Desert), inland Asia (North Tibet, Mongolia, Siberia), and the East African Rift Valley (Magadi and Natron Lakes, Kenya). The geology of the surrounding rocks, particularly the presence of rocks much depleted in Ca^{2+} and Mg^{2+} ions, plays a key role in the development of alkalinity. In most lacustrine environments, water rapidly becomes saturated with respect to Ca^{2+}, resulting in the precipitation of calcite ($CaCO_3$), magnesite ($MgCO_3$), and dolomite ($MgCa(CO_3)_2$) and preventing alkalinity. If the CO_3^{2-} concentration exceeds that of Mg^{2+} and Ca^{2+}, alkalinity increases, and rock-available Na precipitates as halite and sodium carbonate. These ▶ extreme environments are studied in astrobiology for three main reasons. Though living in caustic waters, a prolific ▶ prokaryote life developed in soda lakes, because of the high luminosity, high temperatures, and large supply of nutrients (CO_2). Grant (2006) listed more than 60 species of living prokaryotes among ▶ cyanobacteria, ▶ archaea (▶ methanogens, thermophiles, and halobacteria), sulfur oxidizers, and anoxygenic phototrophs. The possible occurrence of similar soda lake habitats on Mars in the past (Kempe and Kazmierczak 1997) makes these prokaryote communities an analogue for ancient life on Mars. Studying the chemistry of these lakes is also important because it has been proposed that ancient oceans were alkaline and not acidic, as a consequence of ▶ weathering of the basaltic protocrust of the Earth where Na^+ ions dominated over Ca^{2+} (Kempe and Degens 1985). Finally, the alkaline Lake Magadi, Kenya, contains chert deposits (Magadi chert), which are likely formed inorganically from sodium silicate precursors (magadiite $NaSi_7O_{13}(OH)_3 \cdot 3H_2O$ and/or kenyaite $NaSi_{11}O_{20.5}(OH)_4 \cdot 3H_2O$). They have been often cited as modern analogues for inorganic-produced Precambrian ▶ cherts found in iron formations (Schubel and Bruce 1990).

See Also

- ▶ Archaea
- ▶ Banded Iron Formation
- ▶ Chert
- ▶ Cyanobacteria
- ▶ Evaporite
- ▶ Extreme Environment
- ▶ Ocean, Chemical Evolution of
- ▶ Oceans, Origin of
- ▶ Thermonatrite

References and Further Reading

Grant WD (2006) Alkaline environments and biodiversity. In: Gerday C, Glansdorff NE (eds) Extremophilies (Encyclopedia of Life Support Systems (EOLSS)). Developed under the Auspices of the UNESCO. Eolss Publishers, Oxford

Kempe S, Degens ET (1985) An early soda ocean? Chem Geol 53:95–108

Kempe S, Kazmierczak J (1997) A terrestrial model for an alkaline martian hydrosphere. Planet Space Sci 45:1493–1495

Schubel KA, Bruce M (1990) Petrography and diagenesis of cherts from Lake Magadi, Kenya. J Sed Res 60:761–776

Sol

Tilman Spohn
Deutsches Zentrum für Luft- und Raumfahrt (DLR), Institut für Planetenforschung, Berlin, Germany

Definition

A sol is a solar day on another ▶ planet or other body orbiting the sun. It is the time between two successive returns of the ▶ Sun to the same local meridian.

See Also

► Planet
► Sun (and Young Sun)

Solar Constant

Daniel Rouan
LESIA, Observatoire Paris-Site de Meudon, Meudon, France

Synonyms

Total solar irradiance; TSI

Definition

The solar constant is the amount of total solar electromagnetic power that crosses a unit area perpendicular to the rays, at the mean distance from the Sun to the Earth. Its average value is 1,367.7 W m^{-2}. Despite its name, the solar constant is not exactly a constant and its fluctuations, most accurately measured since 1978, are of the order of one part in a thousand and are correlated with the 11-year cycle of the solar activity. They are also correlated with climate variations; however, they are too weak by a factor 3–6 to explain the temperature variations on Earth. A planet-dependent solar constant has also been defined in the case of other solar system planets such as Mars.

Solar Luminosity

Daniel Rouan
LESIA, Observatoire Paris-Site de Meudon, Meudon, France

Definition

The solar luminosity is defined as the total power emitted by the Sun in the form of electromagnetic radiation. The currently accepted value is 3.839×10^{26} W. This is the most common unit used to express the luminosities of other stars or bigger objects such as galaxies or clusters of galaxies. Note that the Sun is a weakly variable star, with its luminosity fluctuating periodically by about a part in a thousand over the 11-year solar (sunspot) cycle.

See Also

► Bolometric Magnitude

Solar Mass

Daniel Rouan
LESIA, Observatoire Paris-Site de Meudon, Meudon, France

Definition

The solar mass is defined as the total mass of the Sun. The currently accepted value is 1.99×10^{30} kg. This is the unit commonly used to express the mass of huge astrophysical objects: stars, galaxies, black holes, dark matter.

Solar Nebula

Avi M. Mandell
NASA Goddard Space Flight Center, Greenbelt, MD, USA

Definition

The solar nebula is the original ► protoplanetary disk from which the Solar System formed. The solar nebula itself formed from a pre-stellar cloud during the collapse phase of the Sun's formation. The solar nebula had an initial composition

similar to that of the outer layers of the present Sun and had a minimum mass sufficient to form the current planets. The latter model nebula is known as the "minimum-mass solar nebula" (MMSN), which is estimated by adding enough light elements to the masses of all the planets to bring them to solar composition.

See Also

- ▶ Planet Formation
- ▶ Protoplanetary Disk
- ▶ Protoplanetary Disk, Chemistry
- ▶ Protosolar Nebula, Minimum Mass
- ▶ System Solar Formation, Chronology of

Solar Neighborhood

Leticia Carigi
Instituto de Astronomía, Universidad Nacional Autónoma de México, México, DF, Mexico

Keywords

Milky Way; Stellar populations

Synonyms

Solar vicinity

Definition

The solar neighborhood is the space associated with a cylinder centered at the Sun and perpendicular to the ▶ Milky Way disk. This solar cylinder is located at ∼8 kpc from the galactic center, with a radius of 1 kpc. Hence, the solar vicinity includes diverse physical entities that belong to the galactic disk and halo, such as planets; stars of different masses, ages, and evolutionary stages; ▶ interstellar medium; and HII regions, among others.

Overview

The solar neighborhood contains mostly baryonic matter (stars and gas); the amount of dark matter is negligible inside it. The total mass surface density is roughly 50 $M_{\odot}$ pc^2, of which the stars take 80 % and 20 % is in gaseous material.

The solar cylinder contains two main structures: first, a *disk component* where approximately 95 % of the total mass is found in Population I stars embedded in metal-rich gas. They are located between 1.5 kpc above and below the central plane of the disk, and secondly, a *halo component* formed by the older Population II stars and no gas.

The first component (*disk*) in turn shows two subcomponents: (1) a thin disk of 300 pc formed by interstellar gas with 1.5 times the solar ▶ metallicity ($Z_{\odot}$) and a young stellar population with an average age of 5 Gyr and a average metal content of 0.8 $Z_{\odot}$. (2) A thick disk of ∼1,000 pc thickness and formed by an older stellar population with an average age of 10 Gyr and a metallicity of 0.2 $Z_{\odot}$. The stellar mass of the thick disk is ∼10 % of the mass in the thin disk.

The solar neighborhood stars show an age-metallicity relation, such that low age correlates with high metallicity. That relation has been basic to understanding the chemical evolution of galaxies. However, this relation presents a spread in ages for a fixed value of Z. The main cause for this is not clear yet.

Those stars show another important evolutionary relation, involving α/Fe versus Fe/H, where α represents an alpha chemical element (e.g., O, Mg, Si, S, Ca, and Ti). This relation has led to elucidating several questions, such as the chemical contribution in time by massive stars (the main producers of α elements) and by thermonuclear supernovae (the main producers of Fe), the star formation efficiency, and the different scenarios for galactic formation. The thick disk stars, just like the stars of the galactic bulge, exhibit

overabundances of α elements, compared to the thin disk stars with the same Fe abundance.

The solar neighborhood is the astronomical laboratory for studying the properties of the ▶ stellar populations and of the interstellar medium.

Due to the current methods for exoplanet detection, most of the extrasolar planets have been found in stars at distances from the Sun closer than 0.5 kpc, that is, in the disk component of the solar vicinity.

There are other definitions of the solar neighborhood in the literature, for instance, (1) the region within 0.2 pc, where the planets, minor bodies, and the Oort cloud of the solar system are; (2) the region up to 100 pc from the Sun, where the closest stars are; and (3) the region up to 20 Mpc from the Milky Way, where the galaxies of the local cluster are.

See Also

- ▶ Metallicity
- ▶ Milky Way
- ▶ Stellar Population

References and Further Reading

Carigi L, Peimbert M (2011) HII regions and protosolar abundances in galactic chemical evolution. Revista Dexicance de Astronomía y Astrofísica 47:139–158

Matteucci F (2001) The chemical evolution of the galaxy. Kluwer Academic, New York

Pagel BEJ (2009) Nucleosynthesis and chemical evolution of galaxies. Cambridge University Press, Cambridge

Sparke L, Gallagher J (2007) Galaxies in the universe: an introduction. Cambridge University Press, Cambridge

The Extrasolar Planets Encyclopaedia. http://exoplanet.eu/

Solar Particle Events

M. A. Shea
Air Force Research Laboratory (Emeritus), Bedford, MA, USA

Keywords

Solar activity; Solar composition; Solar cosmic rays; Solar cycle; Solar protons

Synonyms

SPE

Definition

Ions and electrons that are accelerated by major solar activity and propagate through the interplanetary medium.

History

Major high energy events were first detected by ground-based detectors in 1942. Routine measurements of lower energy protons by spacecraft instrumentation commenced in 1965.

Overview

Solar particle events occur when activity on the Sun such as a solar flare and/or a coronal mass ejection accelerates and releases particles into the interplanetary medium. The actual process of solar particle acceleration is still under debate although it is most likely some type of shock acceleration process.

The frequency of solar particle events is correlated with the solar activity cycle although there is a large variance in the distribution. Major solar particle events consist primarily of sizable fluxes of energetic electrons and energetic protons with a small and variable flux of heavier elements. Protons are the most abundant ions. While most solar protons have energies less than 100 MeV, energies greater than 25 GeV have been identified. The flux and spectrum of solar particle events are not well correlated with solar activity parameters. Typical spectral slopes of solar particle events have values of −3, with a large variation between events. Simple power laws or exponentials are generally not adequate to depict spectra over many orders of magnitude.

There are two general types of solar particle events frequently delineated by the duration of

Solar Particle Events, Table 1 Normalized "average" solar particle composition

Charge	Species	Normalized abundance
Z = 1	Protons	1.0
Z = 2	Alpha particles	$1.5 \times 10^{-2} \pm 50\ \%$
Z = 6	Carbon	1.3×10^{-4}
Z = 7	Nitrogen	3.7×10^{-5}
Z = 8	Oxygen	2.4×10^{-4}
Z = 26	Iron	3.4×10^{-5}

the associated solar X-ray emission. Solar particle events associated with solar flare impulsive X-ray events are generally small events detectable only over a limited range of heliolongitudes from the solar active region site. The elements in these events have an ionization state that is consistent with a ten million Kelvin plasma source. Solar particle events associated with fast coronal mass ejections are much larger events and can be detected over a range of heliolongitudes often in excess of 180°. As the coronal mass ejection driven shock moves outward from the sun through the interplanetary medium, additional acceleration of the ambient particle flux occurs, and this is often observed as a particle increase as the fast interplanetary shock moves past an observation position. These larger events with a proton flux that can exceed 100 particles $cm^{-2}\ s^{-1}\ ster^{-1}$ with energies >10 MeV have an elemental composition and charge state of the accelerated ions similar to that of the one million Kelvin solar corona. Table 1 gives the normalized "average" composition of these large events.

See Also

- ▶ Cosmic Rays in the Heliosphere
- ▶ Radiation Biology
- ▶ Space Environment
- ▶ Stellar Winds

References and Further Reading

Reames DV (1999) Particle acceleration at the Sun and in the heliosphere. Space Sci Rev 90:413–491
Reames DV (2004) Solar energetic particle variations. Adv Space Res 34:381–390
Townsend LW, Badhwar GD, Blakely EA, Braby LA, Cucinotta FA, Curtis SB, Fry RJM, Land CE, Smart DF (2006) Information needed to make radiation protection recommendations for space missions beyond low-Earth orbit, NCRP report no. 153. National Council on Radiation Protection and Measurements, Bethesda

Solar Radius

Daniel Rouan
LESIA, Observatoire Paris-Site de Meudon, Meudon, France

Definition

The solar radius is defined as the mean radius of the Sun. The currently accepted value is 6.955×10^8 m. This is the unit most frequently used to express the radius of other stars. Note that the Sun is very slightly oblate because of its rotation, by about 10 ppm.

Solar System

Tilman Spohn
Deutsches Zentrum für Luft- und Raumfahrt (DLR), Institut für Planetenforschung, Berlin, Germany

Definition

The solar system may be defined as a system including all celestial objects which are subject to the gravitational field of the Sun. According to this definition, the solar system extends over a distance of about 2 light-years, or 0.65 pc, or about 120,000 AU. The most distant frontier that we know is the ▶ Oort cloud, a spherical shell that extends beyond about 40,000 AU from the Sun, and is a reservoir for nonperiodic ▶ comets. The solar system contains two main regions, the inner solar system between the Sun and the main asteroidal belt and the outer solar

system beyond this limit. The inner solar system contains the ▶ terrestrial planets and their satellites and several families of ▶ asteroids. The outer solar system contains the ▶ giant planets and their systems, distant asteroids (▶ Centaurs), and ▶ trans-Neptunian objects. Most comets reside in the outer solar system but some enter the inner solar system as they approach the Sun.

The solar wind is a flow of plasma emitted by the solar corona that fills the heliosphere and extends up to the heliopause, the frontier where the pressure from the solar wind equals the interstellar pressure. The heliopause has been detected by the ▶ Voyager 1 spacecraft at a distance of about 120 AU from the Sun.

See Also

- ▶ Asteroid
- ▶ Centaurs (Asteroids)
- ▶ Comets, History of
- ▶ Oort Cloud
- ▶ Solar System, Inner
- ▶ Solar System, Outer
- ▶ Trans-Neptunian Object

Solar System, Inner

François Forget[1] and Tilman Spohn[2]
[1]Institut Pierre Simon Laplace, Laboratoire de Météorologie Dynamique, UMR 8539, Université Paris 6, Paris, France
[2]Deutsches Zentrum für Luft- und Raumfahrt (DLR), Institut für Planetenforschung, Berlin, Germany

Definition

The inner solar system is the region of the solar system that stretches between the Sun and the asteroid belt. It contains the ▶ terrestrial planets ▶ Mercury, ▶ Venus, ▶ Earth, and ▶ Mars (in order of distance to the Sun), as well as the Earth's ▶ Moon and ▶ Phobos and ▶ Deimos, which orbit Mars. In addition, the inner solar system is home to an unknown number of small bodies, ▶ asteroids, and comet nuclei. Furthermore, the inner solar system contains the ▶ habitable zone of our solar system.

See Also

- ▶ Asteroid
- ▶ Asteroid Belt, Main
- ▶ Comet (Nucleus)
- ▶ Deimos
- ▶ Earth
- ▶ Habitable Zone
- ▶ Mars
- ▶ Mercury
- ▶ Moon, The
- ▶ Phobos
- ▶ Sun (and Young Sun)
- ▶ Terrestrial Planet
- ▶ Venus

Solar System, Outer

William M. Irvine
University of Massachusetts, Amherst, MA, USA

Definition

The informal phrase "outer Solar System" normally refers to the region of the ▶ giant planets and beyond, corresponding to distances from the Sun $\geq$5 AU. The outer Solar System thus also includes almost all ▶ comets during most of their orbital periods, as well as centaurs and objects in the ▶ Kuiper Belt and ▶ Oort Cloud. As a result of the low temperatures in this region, solid objects contain a much higher percentage of volatiles such as water and other ices than the rocky objects closer to the Sun.

See Also

- ▶ Centaurs (Asteroids)
- ▶ Comet
- ▶ Giant Planets
- ▶ Kuiper Belt
- ▶ Oort Cloud
- ▶ Snow Line

Solar UV Radiation, Biological Effects

Gerda Horneck
DLR German Aerospace Center, Institute of Aerospace Medicine, Radiation Biology, Köln, Germany

Keywords

Early Earth; Solar extraterrestrial UV radiation; Space experiments; Stratospheric ozone layer; Survival

Synonyms

Solar UV rays

Definition

Solar ▶ UV radiation is the ultraviolet (UV) component of the solar extraterrestrial electromagnetic radiation that amounts to about 7 % of the whole spectrum. Space experiments have shown that UVC (200–280 nm) is mainly responsible for the high lethality of extraterrestrial solar radiation to microorganisms exposed to it. Due to absorption by stratospheric ozone, only UV at wavelengths longer than 290 nm reaches the surface of the Earth. Several effects on human health and the integrity of ▶ ecosystems are caused by this UV range. In the Archean, before the buildup of the stratospheric ozone layer, UV at wavelengths shorter than 290 nm would have reached the Earth's surface with the associated severe biological consequences.

Overview

The ultraviolet (UV) component of the extraterrestrial ▶ electromagnetic spectrum of our Sun can be divided into three spectral ranges: UVC (200–280 nm) contributing 0.5 %, UVB (280–320 nm) contributing 1.5 %, and UVA (320–400 nm) contributing 6.3 % to the whole solar electromagnetic spectrum, respectively. Although the UVC and UVB regions make up only 2 % of the entire solar extraterrestrial irradiance, they are mainly responsible for the high lethality of extraterrestrial solar radiation to microorganisms exposed to it. This is due to the high absorption of those wavelengths by DNA, the decisive target within that UV range for inactivation and mutation induction. Experiments in space, such as on board of Apollo, Spacelab, LDEF, Foton, MIR, and ▶ EURECA, as well as at space simulation facilities on ground, have shown that extraterrestrial solar UV radiation is biologically a thousand times more efficient than UV at the surface of the Earth and kills 99 % of bacterial spores within a few seconds. In addition, a synergistic effect was observed in spores of *Bacillus subtilis* that were simultaneously exposed to solar UV radiation and space vacuum (Nicholson et al. 2000; Horneck et al. 2010).

Solar UV radiation undergoes absorption and scattering as it passes through the Earth's atmosphere, with the absorption by ozone being the most important process. As a result, no UV radiation at wavelengths shorter than 290 nm reaches the surface of the Earth. Several deleterious effects of sunlight on human health and ecosystem integrity are due to the Sun's UV emission that does reach the surface of the Earth. In addition, concern of an increase in solar UVB radiation has arisen in view of a gradual reduction in stratospheric ozone concentration, as already visualized by the ozone hole during austral spring. In humans, mainly the skin, the eye, and the immune system are influenced by increased UVB radiation; at the ecosystem level, most important effects are expected

on aquatic ecosystems as marine primary producers (Diffey 1991; Häder 1997; Horneck and Baumstark-Khan 2002; Björn 2008). Without the stratospheric ▶ ozone layer, as assumed to be the case for the Archean, UVC and UVB would have reached the Earth's surface with biologically effective doses three orders of magnitude higher than today (Cockell and Horneck 2001). A similar high biological effectiveness is assumed for UV at the surface of ▶ Mars, which is bombarded with solar UV radiation of wavelengths longer than 200 nm (Cockell et al. 2000; Patel et al. 2004).

Solar UV radiation and its biological effects are important factors for considering the following astrobiological questions:

- How did solar UV radiation affect chemical evolution and biological evolution on the early Earth?
- How does solar UV radiation influence the habitability of other planets, for example, the surface of Mars?
- What is the impact of solar UV radiation on viable interplanetary transport of life by natural or anthropogenic processes?

See Also

- ▶ Aerobiology
- ▶ Apollo Mission
- ▶ Archean Traces of Life
- ▶ Biological Efficacy
- ▶ DNA Damage
- ▶ Ecosystem
- ▶ Electromagnetic Spectrum
- ▶ EURECA
- ▶ Exposure Facilities
- ▶ Lithopanspermia
- ▶ Mars
- ▶ Ozone Layer
- ▶ Panspermia
- ▶ Photobiology
- ▶ Planetary Protection
- ▶ Space Environment
- ▶ Spore
- ▶ UV Radiation
- ▶ UV Radiation Dose

References and Further Reading

Björn LO (ed) (2008) Photobiology – the science of life and light, 2nd edn. Springer, New York

Cockell CS, Horneck G (2001) The history of the UV radiation climate of the Earth – theoretical and space-based observations. Photochem Photobiol 73:447–451

Cockell CS, Catling DC, Davis WL, Snook K, Kepner RL, Lee P, McKay CP (2000) The ultraviolet environment of Mars: biological implications past, present, and future. Icarus 146:343–359

Diffey BL (1991) Solar ultraviolet radiation effects on biological systems. Phys Med Biol 36:299–328

Häder DP (ed) (1997) The effects of ozone depletion on aquatic ecosystems. Academic, San Diego

Horneck G, Baumstark-Khan C (eds) (2002) Astrobiology, the quest for the conditions of life. Springer, Berlin

Horneck G, Klaus DM, Mancinelli RL (2010) Space microbiology. Microbiol Mol Biol Rev 74:121–156

Nicholson WL, Munakata N, Horneck G, Melosh HJ, Setlow P (2000) Resistance of *Bacillus* endospores to extreme terrestrial and extraterrestrial environments. Microbiol Mol Biol Rev 64:548–572

Patel MR, Bérces A, Kerékgyárto T, Gy R, Lammer H, Zarnecki JC (2004) Annual solar UV exposure and biological effective dose rates on the Martian surface. Adv Space Res 33:1247–1252

Solar UV Rays

▶ Solar UV Radiation, Biological Effects

Solar Vicinity

▶ Solar Neighborhood

Solid-State Greenhouse Effect

François Forget
Institut Pierre Simon Laplace, Laboratoire de Météorologie Dynamique, UMR 8539, Université Paris 6, Paris, France

Definition

A quasispecies is a distribution of ▶ mutant genomes centered around one dominant or master

sequence. Quasispecies theory was developed by M. Eigen as a general model to understand the dynamics of the first replicative molecules in the context of the origin of information and the early evolution of life (Eigen 1971). Although they were initially conceived as steady-state distributions of infinite size in equilibrium, quasispecies dynamics – characterized by a continuous process of mutant generation, competition, and selection – have also provided an interpretation of the great adaptive potential of RNA viruses (Domingo and Holland 1997). Indeed, experimental evidence has shown that, due to their error-prone replication, different current biological entities behave as quasispecies: ▶ viroids, RNA viruses, and DNA viruses that use RNA as an intermediate molecule during their replicative cycle. The response of the evolving viral quasispecies to selective pressures, e.g., immune response of the infected host or antiviral treatment, is influenced by the ensemble of mutants that compose the population (Lauring and Andino 2010).

See Also

- ▶ Error Rate
- ▶ Evolution, Molecular
- ▶ Hypercycle
- ▶ Mutant
- ▶ Origin of Life
- ▶ RNA
- ▶ RNA World
- ▶ Viroid
- ▶ Virus

References and Further Reading

Domingo E, Holland JJ (1997) RNA virus mutations and fitness for survival. Annu Rev Microbiol 51:151–178

Eigen M (1971) Self-organization of matter and evolution of biological macromolecules. Naturwissenschaften 58:465–523

Lauring AS, Andino R (2010) Quasispecies theory and the behaviour of RNA viruses. PLoS Pathog 6: e1001005

Solidus

Henderson James (Jim) Cleaves II
Earth–Life Science Institute (ELSI), Tokyo Institute of Technology, Meguro–ku, Tokyo, Japan
Institute for Advanced Study, Princeton, NJ, USA
Blue Marble Space Institute of Science, Washington, DC, USA
Center for Chemical Evolution, Georgia Institute of Technology, Atlanta, GA, USA

Definition

In chemistry and geology, a solidus is the set of temperatures below which a substance is completely solid or crystallized. The solidus defines the temperature at which a substance begins to melt, but not necessarily when the substance is completely melted. A solidus may be contrasted with a ▶ liquidus. The solidus and liquidus may not be the same in all cases. When a difference exists between the solidus and liquidus temperatures, then in the intervening region, the system consists of a mixture of solid and liquid phases. In eutectic systems, solidus and liquidus temperatures are the same: the mixture melts completely at the eutectic point.

See Also

- ▶ Liquidus

South Indian Shield

- ▶ Dharwar Craton

Space Biology

Ruth Hemmersbach
German Aerospace Center (DLR), Institute of Aerospace Medicine, Cologne, Germany

Synonyms

Space Life Sciences

Definition

The ▶ space environment is characterized by an intense radiation field of solar and galactic origin and by high vacuum, extreme temperatures, and – induced by orbital space flight – reduced gravity (▶ microgravity) conditions. Thus, the interdisciplinary field of space biology includes all basic disciplines in ▶ Life Sciences by investigating the impact of space environmental factors on all organizational levels (from subcellular to organismal) of living matter.

History

The beginnings of the discipline "space biology" may be set with the start of orbital flights that means ballistic flights (1948–1957) and early orbital missions (1957–1961) with animals, followed in 1961 by human flights. This opened a new experimental field by enabling the investigation of the influence of the space environment (mainly microgravity and radiation) on living systems.

See Also

- ▶ Astrobiology
- ▶ Cosmic Rays in the Heliosphere
- ▶ Gravitational Biology
- ▶ International Space Station
- ▶ Life
- ▶ Microgravity
- ▶ Radiation Biology
- ▶ Solar UV Radiation, Biological Effects
- ▶ Space Environment
- ▶ Space Vacuum Effects

Space Environment

Gerda Horneck
DLR German Aerospace Center, Institute of Aerospace Medicine, Radiation Biology, Köln, Germany

Keywords

Galactic cosmic radiation; Solar extraterrestrial UV radiation; Space radiation; Space vacuum; Temperature in space

Definition

Space environment is the large void which occupies the (relatively) empty areas of the universe outside the atmosphere or surface of any planet or other celestial body. It is a vacuum that contains a low density of particles, as well as electromagnetic radiation, magnetic fields, and neutrinos. Based on our own perspective from planet Earth, the space environment is defined as the area beyond the atmosphere of the Earth. It is also considered as a branch of astronautics that addresses conditions of space that might affect the operations of spacecraft, the health of astronauts, and any other living being during space flight.

Overview

The space environment is characterized by a high vacuum, an intense radiation of galactic and solar origin, and extreme temperatures (Table 1).

Space Environment, Table 1 Parameters of interplanetary space and in low Earth orbit (LEO)

Space parameter	Interplanetary space	Low Earth orbit
Space vacuum		
Pressure (Pa)	10^{-14}	10^{-7}–10^{-4}
Residual gas (part/cm^3)	1 H	10^4–10^5 H
		10^4–10^6 He
		10^3–10^6 N
		10^3–10^7 O
Solar electromagnetic radiation		
Irradiance (W/m^2)	Different values[a]	1,370[b]
Spectral range (nm)	Continuum from 0.01 (X-rays) to 10^6 (IR)	Continuum from 0.01 (X-rays) to 10^6 (IR)
Cosmic ionizing radiation		
Dose (▶ Gy/a)	≤0.1[c]	0.1–10,000[d]
Temperature (*K*)	>4[a]	Wide range (153–393)[e]
Microgravity (*g*)	$<10^{-6}$	10^{-3}–10^{-6}

[a]Depending on orientation and distance to the Sun
[b]Above the Earth atmosphere
[c]Depending on shielding, highest values at mass shielding of 0.15 g/cm^2
[d]Depending on altitude, orbit, and shielding, highest values at high altitudes, during frequent passages through the SAA of the radiation belts and through the polar horns, and shield of 0.15 g/cm^2
[e]Depending on orientation to the Sun and albedo of the body

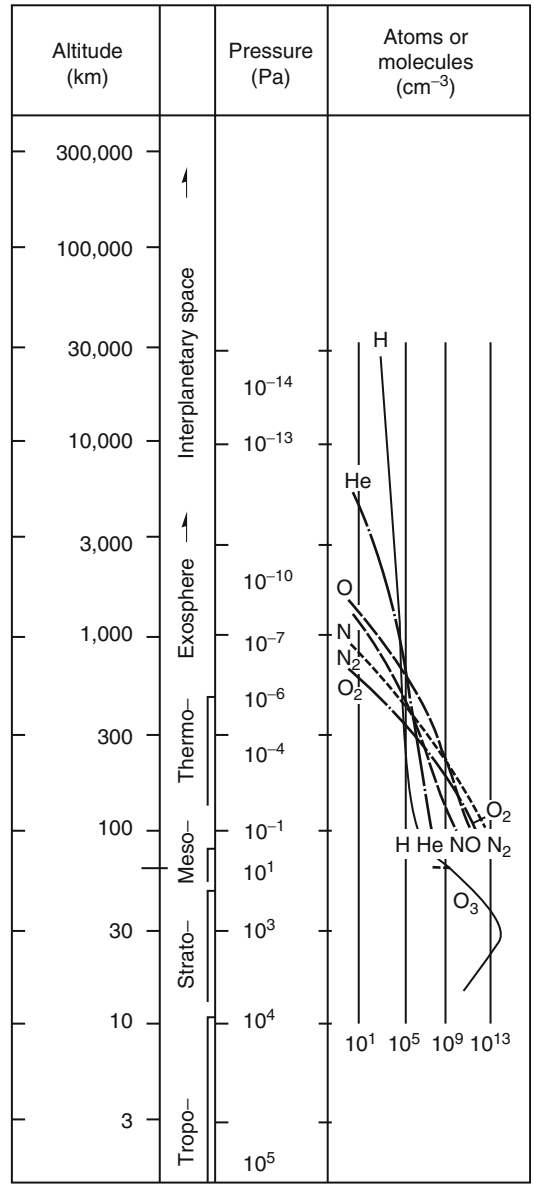

Space Environment, Fig. 1 Altitude profile of the Earth's atmospheric components and pressure

Space Vacuum

In interplanetary space, vacuum reaches pressures down to 10^{-14} Pa. Within the vicinity of a body, the pressure may significantly increase due to outgassing. In a low Earth orbit of an altitude below 450 km, which is the average altitude of the ▶ International Space Station, pressure reaches 10^{-7}–10^{-4} Pa. The major constituents of this environment are hydrogen, molecular oxygen, and molecular nitrogen as well as highly reactive oxygen and nitrogen atoms. In the vicinity of a spacecraft, the pressure further increases, depending on the degree of outgassing of the spacecraft itself. In the Space Shuttle cargo bay, a pressure of 3×10^{-5} Pa was measured.

There is no definite boundary between the atmosphere of the Earth and outer space. With increasing altitude, the atmosphere becomes thinner and eventually fades away into space (Fig. 1). The Kàrmàn line, at an altitude of 100 km, is often regarded as the "official" boundary for space human flights between the Earth's atmosphere and space.

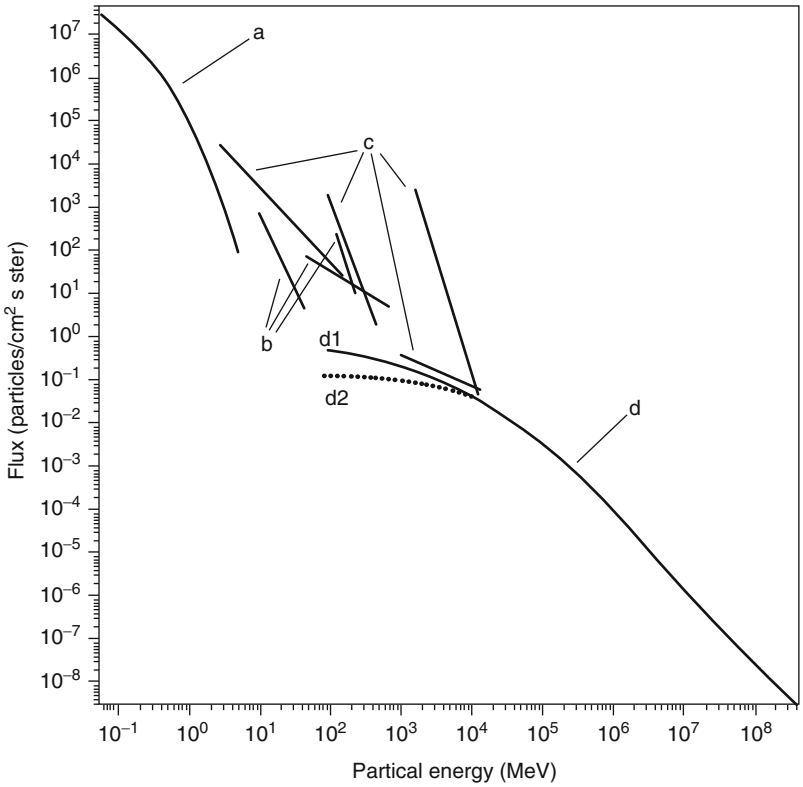

Space Environment, Fig. 2 The energy spectra of the components of the radiation field in space in the vicinity of the Earth: (*a*) electrons (belts); (*b*) protons (belts); (*c*) solar particle events; (*d*) heavy ions of galactic cosmic radiation; (*d1*) during solar minimum; (*d2*) during solar maximum

Space Radiation

The planets, moons, and small bodies in our solar system are continuously bombarded by charged particles coming from sources outside our solar system and from the Sun. The radiation field in interplanetary space is composed primarily of two types of radiation: galactic cosmic radiation (GCR) and solar cosmic radiation (SCR). GCR originates outside the solar system in cataclysmic astronomical events, and the particles are accelerated by supernova shock waves. They are composed of energetic particles, i.e., nuclei with all their orbital electrons stripped off, and have traveled for several million years through the galaxy before entering the solar system. GCR covers a broad spectrum of energy and mass values (Fig. 2). About 98 % are atomic nuclei and 2 % electrons and positrons. The nuclear component consists of about 87 % protons, about 12 % α-particles (He nuclei), and about 1 % nuclei of an atomic mass $Z > 2$, the so-called ▶ HZE particles. When these charged particles enter the solar system, they interact with the outbound streaming of the solar wind and its embedded interplanetary magnetic field which varies with the solar activity. In interplanetary space, the annual ▶ radiation dose amounts to $\leq$0.1 Gy depending on mass shielding with the highest dose at 0.15 g/cm^2 shielding due to built-up radiation (Table 1). With increasing solar activity, the interplanetary magnetic field increases, resulting in a decrease of the intensity of GCR of low energies. Hence, the GCR fluxes vary with the solar cycle and differ by a factor of approximately three between solar minimum and solar maximum with a peak level during minimum solar activity and the lowest level during solar maximum activity.

SCR consists of the low-energy solar wind particles that flow constantly from the Sun and the so-called ▶ solar particle events (SPEs) that originate from magnetically disturbed regions of the Sun and sporadically emit bursts of charged particles with high energies (up to several GeV). These events are composed primarily of protons and electrons with a minor component (5–10 %)

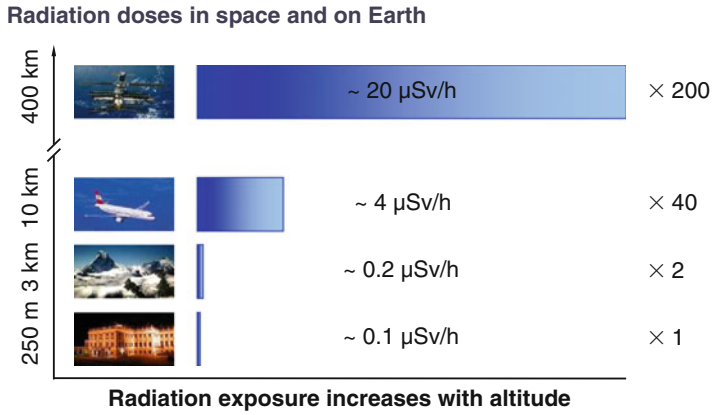

Space Environment, Fig. 3 Increase of the environmental radiation dose with altitude of the Earth

of α-particles and an even smaller component (1 %) of heavy ions. SPEs develop rapidly and generally last for no more than a few hours at energies >100 MeV and up to a few days at low MeV energies.

In low Earth orbit (LEO), which reaches up to an altitude of 450 km, the Earth's magnetic field provides a latitude dependent shielding against GCR and SPE particles, so they are primarily experienced in high-inclination orbits. In LEO, the radiation field includes an additional component: the radiation belts, the so-called Van Allen belts (Fig. 2). These Van Allen belts in the vicinity of the Earth are a result of the interaction of GCR and SCR with the Earth's magnetic field and atmosphere. They consist of two radiation belts that are comprised of electrons and protons as well as some heavier particles trapped in closed orbits by the Earth's magnetic field. The main production process for the inner belt particles is the decay of neutrons produced in cosmic particle interactions with the atmosphere. The outer belt consists mainly of trapped electrons and low-energy protons. In each zone, the charged particles spiral around the geomagnetic field lines and are reflected back between the magnetic poles that act as mirrors. Electrons reach energies of up to 7 MeV and protons up to about 200 MeV (Fig. 2). Of special importance for LEO missions is the so-called South Atlantic Anomaly (SAA), a region over the coast of Brazil, where the radiation belt reaches as low as 200 km above the Earth's surface. This behavior is due to an 11° offset of the Earth's magnetic dipole axis from its rotation axis and a 500 km displacement toward the Western Pacific, with corresponding significantly reduced field strength values. The inner fringes of the inner radiation belt come down to the altitude of LEO, which results in a thousand times higher proton flux than in other parts of the orbit. Almost all radiation received in LEO is due to passages through the SAA. This complex radiation field experienced in outer space cannot be simulated by any ground-based facility. The ▶ radiation doses in low Earth orbit and on Earth-Moon transfer have been measured since the beginnings of space flight activities (Swenberg et al. 1993; Reitz et al. 2009). Figure 3 reflects the increase of the space radiation dose with altitude of the Earth. At the surface of the Earth, the atmosphere provides a shielding of 1,000 g/cm^2.

▶ Mars has currently no planetary magnetic field and therefore also no radiation belts. The only radiation shielding is due to the Martian atmosphere, the thickness of which varies with surface altitude from 16 to 8 g/cm^2. Higher altitudes are less shielded; low altitudes such as Hellas Planitia are more shielded. Dose rates range from 200 to 300 mSv/year. The ▶ radiation doses expected during Earth-Mars transfer have been measured during the 2001 NASA Mars Odyssey mission (Zeitlin et al. 2004).

Jupiter has a strong global magnetic field. The Galilean satellites Io, ▶ Europa, Ganymede, and Callisto are embedded within Jupiter's

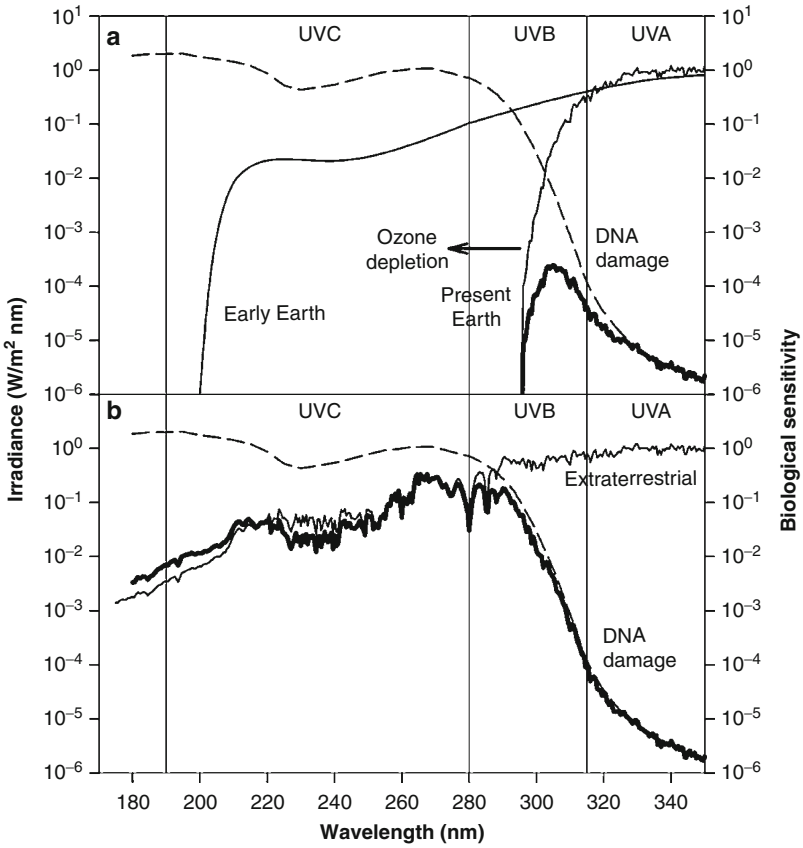

Space Environment, Fig. 4 Solar terrestrial (**a**) and extraterrestrial (**b**) UV irradiance spectra, action spectrum for DNA damage as example for the biological sensitivity (*dashed line*) and biological effectiveness spectra (*bold line*) for present terrestrial and for extraterrestrial conditions (Modified from Horneck et al. 2010)

magnetosphere, and Io is known as a source of ions and neutral particles. Jupiter's inner radiation belt is analogue to the Earth's Van Allen belts, but about 10,000 times more intense. Europa is therefore continually bombarded by magnetically trapped ionizing radiation reaching an electron dose rate at its surface of several gray per minute (Baumstark-Khan and Facius 2002).

Solar Electromagnetic Radiation

The spectrum of solar electromagnetic radiation spans over several orders of magnitude, from short wavelength X-rays at 0.01 nm to radio frequencies at mm wavelengths. At the average distance of the Earth (1 AU), solar irradiance amounts to 1,370 W/m^2, which is the ▶ solar constant. Of this radiation, 45 % is attributed to the infrared fraction, 48 % to the visible fraction, and 7 % to the ultraviolet range. The extraterrestrial solar spectral UV irradiance has been measured during several space missions, such as Spacelab 1 and ▶ EURECA (Labs et al. 1987).

On its way through the Earth atmosphere, solar electromagnetic radiation is modified by scattering and absorption processes. Numerous lines of isotopic and geologic evidence suggest that the Archean atmosphere was essentially anoxic. As a result, the amount of ozone in the stratosphere, if any, would have been insufficient to affect the surface UV radiation environment. Thus, UV radiation at wavelengths >200 nm would have penetrated to the Earth's surface with its associated biological consequences (Cockell and Horneck 2001). It took more than 2 billion years, until about 2.2 billion years ago, when as a consequence of oxygenic photosynthesis, the Earth's atmosphere was subject to rapid oxidation, and hence a stratospheric ▶ ozone layer was photochemically formed. This UV screen allowed life to colonize the surface of the

Earth. Today, the stratospheric ozone layer effectively absorbs UV radiation at wavelengths shorter than 290 nm (Fig. 4).

For Mars, the solar constant is only 43 % of that for Earth. However, the very low concentrations of oxygen in its atmosphere prevent the formation of a stable UV-absorbing planetwide ozone layer. The energy-rich short wavelengths of solar UV radiation penetrate the Martian atmosphere and lead to high surface fluxes of UV radiation with wavelengths longer than 200 nm in contrast to the conditions on Earth, where only wavelengths longer than 290 nm reach the surface. Therefore, the biologically effective dose rate of UV irradiation on the surface of Mars is up to three orders of magnitude higher than on the surface of the Earth (Cockell et al. 2000; Patel et al. 2002, 2004). The actual UV irradiance at a certain location on the surface of Mars varies depending on factors like dust cover, season, local time, and altitude (Patel et al. 2003).

Temperature of Bodies in Space

The temperature of a body in interplanetary space depends on its position and distance to the Sun and also on its albedo, surface, size, and mass. It is determined by the absorption and emission of energy. In Earth orbit, the energy sources are the solar radiation (1,370 W/m^2), the effects of Earth's albedo (480 W/m^2), and terrestrial thermal radiation (230 W/m^2). In Earth orbit, the temperature of a body can reach extreme values. In different space exposure experiments, the samples were subjected to temperatures in the range of 243–318 K (Horneck 1998; Rabbow et al. 2009).

See Also

- ▶ Aerobiology
- ▶ Albedo
- ▶ Cosmic Ray in the Galaxy
- ▶ Cosmic Rays in the Heliosphere
- ▶ Desiccation
- ▶ Earth's Atmosphere, Origin and Evolution of
- ▶ Environment
- ▶ EURECA
- ▶ Europa
- ▶ Extreme Ultraviolet Light
- ▶ Giant Planets
- ▶ HZE Particle
- ▶ International Space Station
- ▶ Mars
- ▶ Mars Odyssey
- ▶ Ozone Layer
- ▶ Photochemistry, Atmospheric
- ▶ Radiation Biology
- ▶ Radiation Dose
- ▶ Solar Constant
- ▶ Solar Particle Events
- ▶ Solar UV Radiation, Biological Effects
- ▶ Space Vacuum Effects
- ▶ Space Weathering
- ▶ Supernova
- ▶ UV Climate
- ▶ UV Radiation
- ▶ UV Radiation, Biological Effects
- ▶ UV Radiation Dose
- ▶ Wavelength

References and Further Reading

Baumstark-Khan C, Facius R (2002) Life under conditions of ionizing radiation. In: Horneck G, Baumstark-Khan C (eds) Astrobiology – the quest for the conditions of life. Springer, Berlin, pp 261–284

Cockell CS, Horneck G (2001) The history of the UV radiation climate of the Earth – theoretical and space-based observations. Photochem Photobiol 73:447–451

Cockell CS, Catling DC, Davis WL, Snook K, Kepner RL, Lee P, McKay CP (2000) The ultraviolet environment of Mars: biological implications past, present, and future. Icarus 146:343–359

Horneck G (1998) Exobiological experiments in Earth orbit. Adv Space Res 22:317–326

Horneck G, Klaus DM, Mancinelli RL (2010) Space microbiology. Microbiol Mol Biol Rev 74:121–156

Labs D, Neckel H, Simon PC, Thullier G (1987) Ultraviolet solar irradiance measurement from 200 to 358 nm during Spacelab 1 mission. Sol Phys 107:208–219

Patel MR, Zarnecki JC, Catling DC (2002) Ultraviolet radiation on the surface of Mars and the Beagle 2 UV sensor. Planet Space Sci 50:915–927

Patel MR, Bérces A, Kolb C, Lammer H, Rettberg P, Zarnecki JC, Selsis F (2003) Seasonal and diurnal variations in Martian surface ultraviolet irradiation: biological and chemical implications for the Martian regolith. Int J Astrobiol 2:21–34

Patel MR, Bérces A, Kerékgyárto T, Rontó GY, Lammer H, Zarnecki JC (2004) Annual solar UV

exposure and biological effective dose rates on the Martian surface. Adv Space Res 33:1247–1252
Rabbow E, Horneck G, Rettberg P, Schott J-U, Panitz C, L'Afflitto A, von Heise-Rotenburg R, Willnecker R, Baglioni P, Hatton J, Dettmann J, Demets R, Reitz G (2009) EXPOSE, an astrobiological exposure facility on the International Space Station – from proposal to flight. Orig Life Evol Biosph 39:581–598
Reitz G, Berger T, Bilski P, Facius R, Hajek M, Petrov V, Puchalska M, Zhou D, Bossler J, Akatov Y, Shurshakov V, Olko P, Ptaszkiewicz M, Bergmann R, Fugger M, Vana N, Beaujean R, Burmeister S, Bartlett D, Hager L, Pálfalvi J, Szabó J, O'Sullivan D, Kitamura H, Uchihori Y, Yasuda N, Nagamatsu A, Tawara H, Benton E, Gaza R, McKeever S, Sawakuchi G, Yukihara E, Cucinotta F, Semones E, Zapp N, Miller J, Dettmann J (2009) Astronaut's organ doses inferred from measurements in a human phantom outside the International Space Station. Radiat Res 171:225–235
Smart DF, Shea MG (1997) Solar radiation. Encycl Appl Phys 18:339–429
Swenberg CE, Horneck G, Stassinopoulos EG (eds) (1993) Biological effects and physics of solar and galactic cosmic radiation, part A and B, NATO ASI series A: life sciences, vol 243A and B. Plenum, New York
Zeitlin C, Cleghorn T, Cucinotta F, Saganti P, Andersen V, Lee K, Pinsky L, Atwell W, Turner R, Badhwar G (2004) Overview of the Martian radiation environment experiment. Adv Space Res 33:2204–2210

Space Infrared Telescope Facility

► Spitzer Space Telescope

Space Interferometry Mission

► SIM

Space Life Sciences

► Space Biology

Space Vacuum Effects

Gerda Horneck
DLR German Aerospace Center, Institute of Aerospace Medicine, Radiation Biology, Köln, Germany

Definition

The vacuum of interplanetary space reaches pressures down to 10^{-14} Pa. Within the vicinity of a body, the pressure significantly increases due to outgassing (e.g., in low Earth orbit, pressure reaches 10^{-6}–10^{-4} Pa). Pressures below the vapor pressure of a certain material cause vaporization of atoms or molecules from the material's surface. In addition to water, sealants, lubricants, and adhesives are the main substances that outgas from spacecraft. However, even metals and glasses can release gases from cracks and impurities. For biological samples in space, vacuum dehydration is the main process affecting their integrity.

See Also

► Desiccation
► Space Biology
► Space Environment

Space Weathering

Harald Hoffmann
DLR, Institute of Planetary Research, Berlin, Germany

Keywords

Cosmic rays; Exospheres; Micrometeorite impacts; Optical alteration; Solar wind; Sputtering

Definition

Space weathering describes all the effects caused by the interaction between the surface of an airless planetary body and the space environment.

Overview

The term space weathering summarizes alteration processes on an atmosphereless planetary surface due to the interaction of the surface material or regolith with the ▶ space environment. As the direct contact layer between the planetary body and space, the surface is permanently reworked and physically and/or chemically modified by micrometeorite impacts, galactic and solar cosmic rays, solar irradiation, and the solar wind. These weathering processes may strongly affect the optical properties of the surface material and have to be taken into account in the analysis of remotely sensed observations.

The planetary surface is pulverized and turned over by a continuous micrometeorite bombardment. Depending on the kinetic energy involved, micrometeorite impacts may result in the melting of material and the formation of glass-welded aggregates (agglutinates), known as a major constituent of the lunar regolith, as well as glass splashes on single grains. Impact-related vaporization and sputtering due to the interaction with highly energetic particles can generate thin rims on individual grains. The reduction of iron in silicates like olivine or pyroxene can result in the formation of metallic nanophase (single-domain) iron within these rims or glassy materials. Collisions with cosmic rays and the solar wind can also form tracks and result in the implantation of particles like ▶ hydrogen, helium, and other rare gases. Space weathering processes result in the maturation of a planetary regolith over time until a steady-state equilibrium is reached and as long as fresh material is not excavated by a large impact.

Optical alterations due to space weathering of terrestrial planetary surfaces are mainly associated with the formation of single-domain iron and of glassy material. The spectral signature becomes darker, diagnostic absorption features weaker, and the spectral curvature redder. Similar effects have been reported not only for the ▶ Moon but also for ▶ Mercury, the Martian ▶ satellites, and some ▶ asteroids. Pulverization and gas implantation are more effective for determining the spectral characteristics of icy satellites.

Space weathering processes are also responsible for the formation of the tenuous atmospheres (exospheres) found around, e.g., the Moon or Mercury, which consist mainly of Na^+ and K^+ ions.

See Also

- ▶ Asteroid
- ▶ Cosmic Ray in the Galaxy
- ▶ Crater, Impact
- ▶ Hydrogen
- ▶ Mercury
- ▶ Moon, The
- ▶ Regolith, Planetary
- ▶ Satellite or Moon
- ▶ Space Environment

References and Further Reading

Chapman CR (2004) Space weathering of asteroid surfaces. Ann Rev Earth Planet Sci 32:539–567. doi:10.1146/annurev.earth.32.101802.120453

Hapke B (2001) Space weathering from mercury to the asteroid belt. J Geophys Res 106(E5):10039–10073. doi:10.1029/2000JE001338

Lucey P, Korotev RL, Gillis JJ, Taylor LA, Lawrence D, Campbell BA, Elphic R, Feldman B, Hood LL, Hunten D, Mendillo M, Noble S, Papike JJ, Reedy RC, Lawson S, Prettyman T, Gasnault O, Maurice S (2006) Understanding the lunar surface and space-moon interactions. Rev Mineral Geochem 60:83–219

Pieters CM, Fischer EM, Rode O, Basu A (1993) Optical effects of space weathering: the role of the finest fraction. J Geophys Res 98(E11):20817–20824. doi:10.1029/93JE02467

Spall

► Spallation Zone

Spallation

► Spallation Zone

Spallation Reaction

Nikos Prantzos
Institut d'Astrophysique de Paris, Paris, France

Definition

Spallation reactions are ► nuclear reactions where a high-energy projectile (usually a proton, neutron, or alpha particle) fragments a heavy nucleus, removing one or more nucleons from it and producing lighter nuclei. Such reactions occur during the propagation of cosmic rays in the galaxy's ► interstellar medium. Spallation of abundant CNO nuclei is the main nucleosynthesis mechanism producing the light and fragile nuclides of Li, Be, and B, which are destroyed by thermonuclear reactions in stars (notice that ^{7}Li is also produced in the Big Bang and in stars, while some ^{11}B is, perhaps, produced through neutrino-induced nucleosynthesis). The abundance of particular spallation products on the surface of a meteorite provides a means of measuring the duration of its exposure to cosmic rays.

See Also

► Cosmic Rays in the Heliosphere
► Interstellar Medium
► Nuclear Reaction
► Nucleosynthesis, Neutrino

Spallation Zone

H. Jay Melosh
Departments of Earth, Atmospheric and Planetary Sciences, Physics and Aerospace Engineering, Purdue University, West Lafayette, IN, USA

Keywords

High-speed ejection; Lithopanspermia; Meteorite impact

Synonyms

Cavitation zone; Interference zone; Spall; Spallation

Definition

Spallation zones are regions adjacent to the free surface of a solid where the reflection of a strong incident stress wave induces tensile stresses and ejects material at high speed. The tensile stresses add to the compressive stresses in the incident wave and partially cancel its compression, leading to high-speed ejection of lightly compressed ("shocked") material.

History

Spallation of the surface following impingement of a strong shock wave was first observed in association with underground nuclear explosions. During the 1980s, accumulated evidence indicated that the SNC suite of ► meteorites originated on a large planet, probably ► Mars. Their launch raised the conundrum of how intact rocks could be ejected at high enough speed to escape from Mars (a minimum of 5 km/s) and yet escape melting or vaporization. Melosh (1984) first suggested that spallation could provide the answer. Furthermore, Melosh (1988) suggested

that the launch conditions might be gentle enough that microbes could survive interplanetary transfer inside the ejected rocks. This suggestion renewed modern interest in the ▶ panspermia idea.

Overview

The process of "spallation" is responsible for the high-speed ejection of rocks (often denoted "spalls" when produced by this process) from the surface of a planet near the site of a meteorite impact. While the ejection speed of the rocks may suggest that large compressive pressures are required by the Hugoniot equations that express the conservation of mass, momentum, and energy across a sharp shock front, the presence of a free surface drastically reduces the pressure in the incident wave near the surface (boundary conditions require that the normal stress on the free surface itself is exactly zero). This zone in which the reflected tensile wave adds destructively to the incident compressive wave is sometimes described as an "interference zone." In a liquid, the same process produces an opaque "cavitation zone" that forms on the surface near underwater explosions. Away from the free surface, pressures rise rapidly to the level required by the Hugoniot equations. The distance over which this rise occurs is comparable to the diameter of the projectile but also depends on the distance from the impact site.

The existence of a spallation zone explains how nearly intact rocks can be ejected from the surfaces of such bodies as Mars (escape velocity 5 km/s) and the Moon (escape velocity 2.4 km/s), whose large escape velocities would normally imply that escaping material is melted or vaporized (Melosh 1984, 1985). Such rocks are the progenitors of the many dozens of meteorites that are now known to originate on Mars or the Moon, some of which show little sign of the forces that ejected them (Head et al. 2002). Antarctic meteorite ▶ ALH 84001 not only shows no sign of shock damage upon launch but, between its formation on Mars and its recovery on the Earth, did not experience temperatures greater than about 40 °C (Weiss et al. 2000). The spallation process has now been observed in the ejecta of large impact craters on Earth, in laboratory experiments, and in very high-resolution numerical simulations of impact.

The process of spallation allows viable microbes or microbial spores to survive launch from the surface of a planet into interplanetary space (Stöffler et al. 2007; Horneck et al. 2008; Fajardo-Cavazos et al. 2009). It may thus initiate interplanetary exchange of living organisms between planets in our solar system (Mileikowsky et al. 2000), although interstellar exchange seems very unlikely (Melosh 2003; Valtonen et al. 2009). This process of meteorite exchange between planets has variously been called panspermia or ▶ lithopanspermia.

See Also

- ▶ ALH 84001
- ▶ Crater, Impact
- ▶ Lithopanspermia
- ▶ Mars
- ▶ Meteorites
- ▶ Moon, The
- ▶ Panspermia
- ▶ SNC Meteorites

References and Further Reading

Fajardo-Cavazos P, Langenhorst F, Melosh HJ, Nicholson WL (2009) Bacterial spores in granite survive hypervelocity launch by spallation: implications for lithopanspermia. Astrobiology 9:647–657

Head JN, Melosh HJ, Ivanov BA (2002) Martian meteorite launch: high-speed ejecta from small craters. Science 298:1752–1756

Horneck G, Stöffler D, Ott S, Hornemann U, Cockell CS, Moeller R, Meyer C, de Vera J-P, Fritz J, Schade S, Artemieva NA (2008) Microbial rock inhabitants survive impact and ejection from host planet: first phase of lithopanspermia experimentally tested. Astrobiology 8:17–44

Melosh HJ (1984) Impact ejection, spallation, and the origin of meteorites. Icarus 59:234–260

Melosh HJ (1985) Ejection of rock fragments from planetary bodies. Geology 13:144–148

Melosh HJ (1988) The rocky road to panspermia. Nature 332:687–688
Melosh HJ (2003) Exchange of meteorites (and life?) between stellar systems. Astrobiology 3:207–215
Mileikowsky C, Cucinotta F, Wilson JW, Gladman B, Horneck G, Lindegren L, Melosh J, Rickman H, Valtonen M, Zheng JQ (2000) Natural transfer of viable microbes in space, Part 1: from Mars to Earth and Earth to Mars. Icarus 145:391–427
Stöffler D, Horneck G, Ott S, Hornemann U, Cockell CS, Moeller R, Meyer C, de Vera J-P, Fritz J, Artemieva NA (2007) Experimental evidence for the potential impact ejection of viable microorganisms from Mars and Mars-like planets. Icarus 186:585–588
Valtonen M, Nurmi P, Zheng J-Q, Cucinotta FA, Wilson JW, Horneck G, Lindegren L, Melosh J, Rickman H, Mileikowsky C (2009) Natural transfer of viable microbes in space from planets in the extra-solar systems to a planet in our solar system and vice-versa. Astrophys J 690:210–215
Weiss BP, Kirschvink JL, Baudenbacher FJ, Vali H, Peters NT, Macdonald FA, Wikswo JP (2000) A low temperature transfer of ALH84001 from Mars to Earth. Science 290:791–795

Spark Discharge

Jeffrey Bada
Scripps Institution of Oceanography, La Jolla, CA, USA

Keywords

Cavendish; Electrodes; Miller

Synonyms

Electric discharge

Definition

A spark discharge is an electrical discharge between two electrodes that is used to simulate atmospheric lightning and coronal discharges. It occurs when the electric field strength between the two electrodes exceeds a certain threshold value in volts per cm. This leads to a momentary increase in the concentration of ions between the two points, temporarily allowing the gases between the electrodes to serve as an electrical conductor.

Overview

Henry Cavendish did one of the first spark discharge chemistry experiments in the late eighteenth century. His investigations were designed to study aspects of atmospheric chemistry and showed that the action of a spark discharge in air resulted in the production of nitrous acid (Cavendish 1788). In Stanley Miller's classic 1953 experiment, a spark discharge acting on a mixture of hydrogen, methane, ammonia, and water produced HCN, aldehydes, and ketones, which in turn reacted by the Strecker reaction to form ▶ amino acids.

See Also

▶ Amino Acid
▶ Atmosphere, Organic Synthesis
▶ Corona Discharge
▶ Electric Discharge
▶ Miller, Stanley
▶ Strecker Synthesis

References and Further Reading

Cavendish H (1788) On the conversion of a mixture of dephlogisticated and phlogisticated air into nitrous acid, by the electric spark. Philos Trans R Soc Lond 78:261–276
Miller SL (1953) A production of amino acids under possible primitive earth conditions. Science 117:528–529

Spathose Iron

▶ Siderite

SPE

► Solar Particle Events

Special Region (Mars)

Catharine A. Conley
NASA Headquarters, Washington, DC, USA

Definition

Special regions are locations on Mars that could be hospitable for Earth life or be a habitat for Martian life. Currently, special regions are defined using the parameters of temperature and water activity. The specification as of 2010 is a location where the temperature reaches above −25 °C and the water activity is above 0.5 (relative humidity above 50 %).

According with the planetary protection policy edited by the COSPAR, these special regions define a new category (Category IVc) of Martian mission. For those missions which investigate Martian special regions, even if they do not include life detection experiments, all of the requirements applicable to the a mission aiming at the surface of Mars (Category IVa) apply, along with the following requirements:

- Case 1. If the landing site is within the special region, the entire landed system is restricted to a surface bioburden level of ≤30* spores.
- Case 2. If the special region is accessed though horizontal or vertical mobility, either the entire landed system is restricted to a surface bioburden level of ≤30* spores, or the subsystems which directly contact the special region shall be sterilized to these levels, and a method of preventing their recontamination prior to accessing the special region shall be provided.

If an off-nominal condition (such as a hard landing) would cause a high probability of inadvertent biological contamination of the special region by the spacecraft, the entire landed system must be sterilized to a surface bioburden level of ≤30* spores and a total (surface, mated, and encapsulated) bioburden level of ≤30 + (2 × 105)* spores.

*This figure takes into account the occurrence of hardy organisms with respect to the sterilization modality. This specification assumes attainment of Category IVa surface cleanliness, followed by at least a four order-of-magnitude reduction in viable organisms. Verification of bioburden level is based on pre-sterilization bioburden assessment and knowledge of reduction factor of the sterilization modality.

References and Further Reading

https://cosparhq.cnes.fr/sites/default/files/pppolicy.pdf
http://mepag.jpl.nasa.gov/reports/MEPAG_SR-SAG_final1.pdf
http://www.nap.edu/catalog.php?record_id=11381

Species

Ramon Rosselló-Móra
IMEDEA (CSIC-UIB), Esporles, Mallorca, Balearic Islands, Spain

Keywords

Pattern of recurrence; Taxonomic category; Unit of biodiversity

Synonyms

Lowest taxonomic category

Definition

In biology, species is the basic rank (category) supporting the taxonomic hierarchy that attempts

to embrace all of the biological diversity present in the biosphere.

Overview

Aristotle first enunciated the idea of species about 2,400 years ago (fourth century before Christ). Linnaeus, in the eighteenth century, consolidated its use within a scientific framework and initiated the modern binomial classification. Since then, it has been used to identify each of the different biological units that can be observed in nature. As Jody Hey states, "species are categories motivated by recurrent observations about the world, and as humans are great observers of patterns of recurrence they devise categories as a response." However, such patterns of recurrence are necessarily different for different kinds of organisms that exhibit distinct levels of morphological and/or physiological complexity. The idea of what a species may be depends on the type of organisms under study and the ability of the taxonomists to identify the phenotypic, genetic, and ecological singularities that make a unit different from its closest relatives. For organisms exhibiting complex morphologies such as plants and animals, the circumscription of the unit is mainly based on simple, easily recognizable, observable traits requiring no experimentation on living specimens. However, for morphologically simpler organisms such as prokaryotes and some microscopic eukaryotes, simple ocular examination is insufficient. In such taxonomies, there is a need to experiment with living specimens in the laboratory in order to retrieve enough genetic and phenotypic information to establish the taxa boundaries.

Over the years, philosophers and taxonomists have insistently tried to formulate the essence of what this biological unit could be. However, the search for a universal concept that describes the basic taxonomic rank soon became the focus of strong debates. Hitherto, more than 25 different concepts have been formulated. The most widely known is the "biological species concept" (BSC) by Ernst Mayr who understood "species as groups of actually or potentially interbreeding natural populations which are reproductively isolated from other such groups." However, while this concept works for most animals, it is not applicable to the vast majority of the biological entities that do not reproduce sexually. Among the different concepts formulated, scientists debate between the use of those of high theoretical load (such as "evolutionary" (ESC) or "cohesive" (CSC) species concepts, both considered synonyms) and those that can be considered theory-free (such as the "phenetic" (PhSC) or the "polythetic" (PtSC) species concepts, both considered synonyms). The former formulates that species is "an entity composed of organisms which maintains its identity from other such entities through time and over space, and which has its own independent evolutionary fate and historical tendencies"; the latter is formulated as "a similarity concept based on statistically co-varying characteristics which are not necessarily universal among the members of the taxa." The success of the PhSC or PtSC is mainly based on the achievement of as many independent characters as possible. However, neither concept is well accepted. The ESC or CSC is very difficult to apply, and the PhSC or PtSC lacks a theoretical background.

Each discipline in biology creates its own classification and especially tailors its species circumscriptions in a manner that best fits the patterns of recurrence that they observe. Either we admit that biological diversity is so vast and evolutionary constraints are so varied among different biological lines of descent that a variety of species concepts are necessary to accurately capture the complexity of variation patterns in nature (pluralistic view) or if we want to achieve a universal concept that takes into account all biological diversity (monistic view), we have to admit that the concept of species may lack applicability and may not be operative.

As a final remark, we can consider species as each of the recurrence patterns that humans observe in nature, each of them having a different evolutionary fate. The ability to recognize species depends on the biological complexity of the organisms under observation and the technological capacities available to recognize their unique

properties. The final circumscription of a species will depend on the scientists' abilities to recognize genetic and/or phenotypic complexities.

See Also

- ▶ Darwin's Conception of the Origins of Life
- ▶ Evolution, Biological
- ▶ Phylogeny
- ▶ Taxonomy

References and Further Reading

Claridge MF, Dawah HA, Wilson MR (1997) Species: the units of biodiversity. Chapman & Hall, London

Ereshefsky M (1992) The units of evolution, essays on the nature of species. In: A bradford book. MIT Press, Cambridge. http://people.ucalgary.ca/~ereshefs/

Ereshefsky M (1994) Some problems with the Linnaean hierarchy. Philos Sci 61:186–205

Ereshefsky M (1998) Species pluralism and anti-realism. Philos Sci 65:103–120

Hey J (2001) Genes, categories and species. Oxford University Press, New York

Hull DL (1970) Contemporary systematic philosophies. Annu Rev Ecol Syst 1:19–54

Mishler BD, Donoghue MJ (1982) Species concepts: a case for pluralism. Syst Zool 31:491–503

Rosselló-Mora R, Amann R (2001) The species concept for prokaryotes. FEMS Microbiol Rev 25:39–67

Sokal PH, Sneath RR (1973) Numerical taxonomy. W. H. Freeman, San Francisco

Species (Prokaryote)

Antonio Ventosa and Cristina Sanchez-Porro
Department of Microbiology and Parasitology, Faculty of Pharmacy, University of Sevilla, Sevilla, Spain

Keywords

Classification; DNA-DNA hybridization; Phylogeny; Taxonomy

Definition

A ▶ species is a category that circumscribes a (preferably) genomically coherent group of individual isolates/strains sharing a high degree of similarity in (many) independent features, comparatively tested under highly standardized conditions (Rosselló-Mora and Amann 2001).

Overview

Species is the basic unit and most important taxonomic rank in prokaryote classification, represented by a group of microorganisms that have a genotypic relationship and coherent phenotypic features. The concept of species in prokaryotes is quite complex, since it is based on the premises of the species adopted for higher organisms, which are differentiated by the inability of reproduction among the organisms. However, this concept cannot be applied to prokaryotes, able to exchange genetic material easily among different species. Besides, morphologically they are not so diverse, and thus the relative morphologic simplicity of most prokaryotic microorganisms implies that morphology is, in general, of little importance in contrast with the classification of higher organisms. A species is represented by a type strain, a designated strain that is used as a reference specimen as a permanent example of the species.

Currently, the definition of species in prokaryotes is based on the determination of the DNA-DNA hybridization values and ΔT_m. It is generally accepted that strains with approximately 70 % or greater DNA-DNA relatedness and with 5 °C or less ΔT_m should be considered as members of the same species (Wayne et al. 1987). However, certain drawbacks with respect to reproducibility, workability, and rigid application of DNA-DNA hybridization have been reported (Stackebrandt et al. 2002). Therefore, the current prokaryote species delimitation is based on a polyphasic approach which includes phenotypic, genotypic, chemotaxonomic, and phylogenetic features. Phenotypic characteristics should agree with DNA-DNA hybridization

values, and it is recommended that a distinct genospecies that cannot be differentiated from another genospecies on the basis of any known phenotypic property not be named until they can be differentiated by some phenotypic properties.

New methods and techniques have been proposed to supplement or supplant DNA-DNA reassociation. Perhaps, the most extensively used is the 16S rRNA gene sequence analysis, a molecular marker to establish relationships among nucleotide sequences in the definition of prokaryotic species. It has been demonstrated that strains sharing 16S rRNA gene similarities below 97 % can be considered as a different genospecies (Stackebrandt and Goebel 1994). However, comparative studies clearly reveal the limitations of the sequence analysis of this highly conserved gene in the determination of relationships at the strain level for which DNA-DNA reassociation experiments still constitute the superior method. To overcome these limitations, multilocus sequence analysis (MLSA) based on conservative protein-coding genes, called housekeeping genes, has been developed for its applicability to genomically circumscribe the taxon species and differentiating it from neighboring species. Such genes should be at diverse chromosomal loci and widely distributed among taxa.

A more recent approach that advances the species definition for prokaryotes is the determination of the average nucleotide identity (ANI) of the shared genes between two strains. It has been estimated that ANI values of approximately 94 % corresponded to the traditional 70 % DNA-DNA reassociation standard of the current species definition (Konstantinidis and Tiedje 2005).

See Also

► Species

References and Further Reading

Bapteste E, Boucher Y, Leigh J, Doolittle WF (2004) Phylogenetic reconstruction and lateral gene transfer. Trends Microbiol 12:406–411

Brenner DJ, Staley JT, Krieg NR (2005) Classification of prokaryotic organisms and the concept of bacterial speciation. In: Brenner DJ, Krieg NR, Staley JT (eds) Bergey's manual of systematic bacteriology, vol 2, 2nd edn, The Proteobacteria, Part A. Springer, New York, pp 27–32

Gevers D, Cohan FM, Lwrence JG, Spratt G, Coenye T, Feil EJ, Stackebrandt E, Van de Peer Y, Vandamme P, Thompson FL, Swings J (2005) Re-evaluating prokaryotic species. Nat Rev Microbiol 3:733–739

Konstantinidis KT, Tiedje JM (2005) Genomic insights that advance the species definition for prokaryotes. Proc Natl Acad Sci U S A 102:2567–2572

Richter M, Rosselló-Móra R (2009) Shifting the genomic gold standard for the prokaryotic species definition. Proc Natl Acad Sci U S A 106:19126–19131

Rosselló-Mora R, Amann R (2001) The species concept for prokaryotes. FEMS Microbiol Rev 25:39–67

Stackebrandt E, Goebel BM (1994) Taxonomic note: a place for DNA-DNA reassociation and 16 S rRNA sequence analysis in the present species definition in bacteriology. Int J Syst Bacteriol 44:846–849

Stackebrandt E, Frederiksen W, Garrity GM, Griment PAD, Kämpfer P, Maiden MCJ, Nesme X, Rosselló-Mora R, Swings J, Trüper HG, Vauterin L, Ward AC, Whitman WB (2002) Report of the ad hoc committee for the re-evaluation of the species definition in bacteriology. Int J Syst Evol Microbiol 52:1043–1047

Tindall BJ, Rosselló-Mora R, Busse H-J, Ludwig W, Kämpfer P (2010) Notes on the characterization of prokaryote strains for taxonomic purposes. Int J Syst Evol Microbiol 60:249–266

Vandamme P, Pot B, Gillis M, de Vos P, Kersters K, Swings J (1996) Polyphasic taxonomy, a consensus approach to bacterial systematics. Microbiol Rev 60:407–438

Wayne LG, Brenner DJ, Colwell RR, Grimont PAD, Kandler O, Krichevsky MI, Moore LH, Moore WEC, Murray RGE, Stackebrandt E, Starr MP, Truper HG (1987) Report of the ad hoc committee on reconciliation of approaches to bacterial systematics. Int J Syst Bacteriol 37:463–464

S

Specific Activity

Dionysis Foustoukos
Geophysical Laboratory, Carnegie Institution of Washington, Washington, DC, USA

Definition

Specific activity is a measure of the reactivity of a compound per unit mass under specific

physicochemical conditions. For example, the specific activity of an enzyme, used to assess enzyme purity, is defined as the amount of substrate converted through enzymatic processes per unit of time and mass of the total protein (e.g., μmol min^{-1} mg^{-1}). For a system containing a specific number of radionuclides, specific activity describes the number of decay events per unit time per mass or, equivalently, the product of the number of nuclides by the decay constant (Becquerel or counts per second).

See Also

- ▶ Enzyme
- ▶ Radioactivity

Spectral Analysis

- ▶ Spectroscopy

Spectral Classification of Embedded Stars

Philippe André
Laboratoire AIM, IRFU/Service d'Astrophysique, CEA Saclay, Gif-sur-Yvette, France

Keywords

Circumstellar disk; Infrared excess; Pre-main-sequence stars; Protostars; Spectral energy distributions; Star formation; Submillimeter; Young stellar objects

Synonyms

Evolutionary sequence of young stellar objects

Definition

Young stars and their protostellar precursors are referred to as "young stellar objects" (YSOs) (Strom 1972), by astronomers since they are often deeply embedded in circumstellar dust and invisible at optical wavelengths. While most of them cannot be placed in the Hertzsprung-Russell diagram, YSOs can be organized along an empirical evolutionary sequence based on the shape of their spectral energy distributions (SEDs) from near-infrared to submillimeter wavelengths. Four broad classes of YSOs are distinguished (Class 0 → Class I → Class II → Class III) as the peak of the SED shifts from the submillimeter to the optical domain.

History

With the development of near-▶ infrared astronomy in the 1970s, many YSOs heavily obscured by dust at optical wavelengths were discovered in nearby star-forming clouds (e.g., Strom 1972). In the 1980s, the launch of the infrared satellite *IRAS* and the advent of near-infrared detectors allowed extensive surveys for embedded YSOs to be carried out and nearly complete spectral distributions of radiated energy to be constructed. Lada and Wilking (1984) and Lada (1987) proposed to divide the observed YSOs into three distinct morphological classes (I–III), depending on the slope $\alpha_{IR} = d\log(\lambda F_\lambda)/d\log\lambda$ of their near-infrared to far-infrared spectral energy distributions (energy flux λF_λ vs. wavelength λ). Adams et al. (1987) suggested that this infrared classification scheme could be interpreted in terms of an evolutionary sequence. With the development of millimeter and submillimeter observations, a fourth class (Class 0) was then added to accommodate the discovery of YSOs so deeply embedded that they radiate large amounts of far-infrared and submillimeter emission relative to their total luminosities (André et al. 1993).

Overview

Classification of Spectral Energy Distributions

It is convenient to describe the spectral evolutionary classification of YSOs (cf. Fig. 1) by going backward in time, starting from objects detected in the near-infrared and ending with objects only (or mostly) visible at far-infrared and submillimeter wavelengths. In the near-/mid-infrared, three broad classes of YSOs can be distinguished based on the index $\alpha_{IR} = d\log(\lambda F_\lambda)/d\log\lambda$ of the spectral energy distributions (SEDs) between ~2.2 and ~10–25 μm (Lada 1987). Class III sources have $\alpha_{IR} < -1.5$ and display reddened starlike or blackbody-like energy distributions. Class II sources have $-1.5 < \alpha_{IR} < 0$, reflecting the presence of significant near-▶ infrared excess emission superposed on a typical stellar blackbody. Class I sources have $\alpha_{IR} > 0$ and thus rising SEDs toward long wavelengths, implying a huge excess of far-infrared emission compared to that expected from a stellar photosphere. When optically visible, Class III and Class II objects correspond to pre-main-sequence stars ("weak" and "classical" T Tauri stars, respectively). The SEDs of Class I sources are successfully modeled in the framework of the "classical" theory of isolated protostars (e.g., Adams et al. 1987), in agreement with the view that a substantial fraction of their luminosity arises from accretion of circumstellar material (e.g., Greene and Lada 1996). Using millimeter and submillimeter observations, younger protostars, corresponding to a fourth class of YSOs (Class 0), have been identified. Class 0 objects, whose SEDs peak longward of 100 μm in the submillimeter domain, are very weak and often even undetected at near- and mid-infrared wavelengths shortward of 25 μm. These objects are characterized by high ratios of submillimeter to bolometric luminosity ($L_{submm}/L_{bol} > 1$ %) and overall SEDs resembling 15–30 K blackbodies (André et al. 1993). The full sequence of SEDs from Class 0 to Class III objects is in fact quasi-continuous and may be conveniently parameterized by a single parameter, the average or "bolometric" temperature (T_{bol}), defined as the temperature of a blackbody having the same mean frequency as the observed YSO SED (Myers et al. 1998).

Circumstellar Evolution

YSOs are composite objects made up of a growing central star, a circumstellar disk, a circumstellar envelope, and a bipolar outflow. The SED classification described above primarily tracks the evolution of the circumstellar components. The strong submillimeter emission of Class 0 sources relative to their total luminosity indicates that the circumstellar envelope is the dominant component at the Class 0 stage, with a mass that exceeds the mass of the central stellar object ($M_{env} \gg M_*$; André et al. 2000). Class 0 objects are thus excellent candidates for being very young accreting protostars in which a hydrostatic protostellar embryo has formed within a dense cloud core but not yet accreted the majority of its final mass. They represent a pivotal evolutionary stage in the path leading from interstellar cloud matter to solar systems like our own. Class I objects are still associated with dense molecular gas and derive their large infrared excesses from the presence of both a disk and a circumstellar envelope (Adams et al. 1987). Mapping at millimeter wavelengths confirms the presence of a significant envelope at the Class I stage but shows that this envelope is no longer very massive and often only a remnant of the parent prestellar core ($M_{env} < M_*$; André and Montmerle 1994). Class II and Class III objects lack a dense circumstellar envelope component and are only surrounded by a circumstellar disk (optically thick and optically thin at $\lambda < 10$ μm, respectively). While the disk is still massive enough to be protoplanetary in nature at the Class II stage ($M_{disk} \sim 0.01$ M on average; Beckwith et al. 1990), it has evolved to an optically thin debris disk by the Class III stage.

Bipolar Outflows and Gravitational Infall

Class 0 sources are associated with powerful, highly collimated bipolar outflows (Bontemps et al. 1996; Bachiller 1996), which provide indirect evidence of the presence of a central protostar and distinguish Class 0 YSOs from prestellar cores, i.e., starless dense fragments within molecular clouds.

As a whole Class 0 objects drive much more powerful outflows than Class I sources of

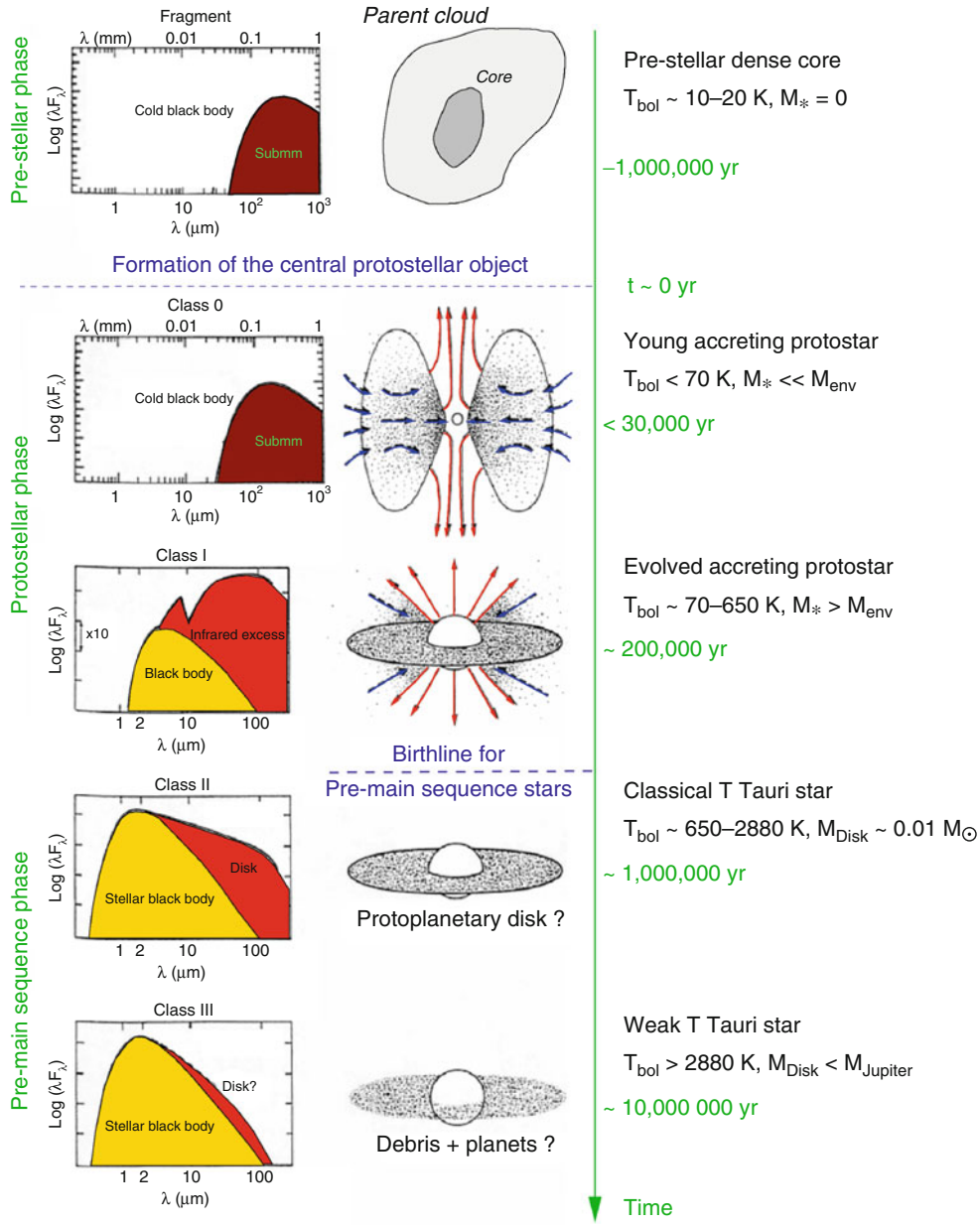

Spectral Classification of Embedded Stars, Fig. 1 Empirical sequence for the formation and circumstellar evolution of a single star from a prestellar cloud core to a Class III young stellar object, based on the shape of the spectral energy distribution (*left*), the bolometric temperature, and the mass of circumstellar (envelope + disk) material indicated on the *right* (From Lada (1987), André et al. (1993, 2000), and Myers et al. (1998))

comparable bolometric luminosities (Bontemps et al. 1996). Furthermore, the ▶ bipolar flows from Class 0 objects are much better collimated than those from Class I (and Class II) sources.

Class 0 protostars were the first YSOs for which convincing spectroscopic signatures of gravitational infall motions could be obtained, confirming their protostellar nature (see Evans

1999 for a review). While some infall is still present at the Class I stage, the outflow is so broad in Class I sources that there often appears to be little transfer of mass to the inner 2,000 AU radius region around these objects.

Although the accretion/ejection phenomenon is believed to be episodic, the observed outflow and infall properties are suggestive of a global decline in the mass accretion rate onto the central protostar from $\sim 10^{-6} - 10^{-5} M_{\odot}$/year at the Class 0 stage to $\sim 10^{-7} - 10^{-6} M_{\odot}$/year at the Class I stage. Despite substantial scatter, a general decline in mass accretion rate as a function of age is similarly observed among T Tauri stars from $\sim 10^{-7} M_{\odot}$/year for the youngest Class II objects to less than $\sim 10^{-9} M_{\odot}$/year for Class III sources (e.g., Hartmann 1998).

Time Evolution and Approximate Timescales

To summarize, combining observations at near-infrared to millimeter wavelengths makes it possible to distinguish two classes of protostars (Class 0 and Class I) and two classes of pre-main-sequence stars (Class II and Class III), which are interpreted as an evolutionary sequence (Class 0 → Class I → Class II → Class III). Statistical arguments based on the numbers of sources observed in the various classes suggest that the corresponding lifetimes run from ~1–5 × 10^4 years for Class 0 protostars to ~1–5 × 10^7 years for Class III young stars, increasing by roughly a factor of ~10 from one evolutionary stage to the next (e.g., André and Montmerle 1994; Greene et al. 1994; Evans et al. 2009). These lifetimes also provide very rough estimates of the typical ages of YSOs according to their SED class. This is only true in a statistical average sense, however, since the above-described classification corresponds to an evolutionary sequence only for the circumstellar material and is not directly related to the evolution of the underlying stellar objects. For instance, when placed in the Hertzsprung-Russell diagram, a significant fraction of weak T Tauri stars (Class III objects) appears to be not older than, but coeval with, Class II objects (e.g., Stahler and Walter 1993). These relatively young Class III objects may have dissipated their circumstellar disks and infalling envelopes particularly early, as a result of, e.g., unusually strong fossil magnetic fields and/or the tidal effects of a close companion. To some extent, therefore, the circumstellar evolution of YSOs is decoupled from their purely stellar evolution.

Basic Methodology

The practical diagnostics that one uses to order YSOs and cloud cores along the evolutionary sequence sketched in Fig. 1 are the infrared spectral index α_{IR} or shape of the infrared SED (Lada 1987), the "bolometric" temperature T_{bol} of a source (Myers et al. 1998), and the mass of circumstellar (envelope + disk) material (e.g., André and Montmerle 1994). Independently of the details of any protostellar theory, and in a statistical sense at least, one expects young stellar objects to become warmer and to be surrounded by progressively smaller amounts of circumstellar material as they evolve. Accordingly, the peak of the SED moves from the submillimeter for prestellar cores and (cold, deeply embedded) Class 0 protostars, to the far-IR for Class I protostars, to the near-IR and the optical for pre-main-sequence stars (Class II and Class III sources) (see Fig. 1). In the case of embedded protostars, the decrease of circumstellar mass with time results from the progressive dissipation of the protostellar envelope through accretion and outflow. For instance, in all self-similar isothermal models of collapse, including the classical Shu et al. (1987) model, the mass enclosed within a given radius R of the infalling envelope scales approximately as $M_{env}(r < R) \propto t^{-1//2}$ with time.

Future Directions

While ground-based near-IR surveys, coupled with infrared and X-ray observations from space with the *IRAS*, *ISO*, *Spitzer*, *XMM-Newton*, and *Chandra* satellites, have provided a fairly complete census of YSOs from Class I to Class III in nearby clouds, no such census exists yet for Class 0 protostars and cold prestellar cores. Only about 30 Class 0 protostars are known to date and only

four in the nearest clouds ($d < 150$ pc) (cf. André et al. 2000). Consequently, the ages and lifetimes of prestellar cores and Class 0 objects are very uncertain compared to those of pre-main-sequence stars and remain a matter of lively debate in the star formation community (e.g., Ward-Thompson et al. 2007; Evans et al. 2009). Wide-field imaging at far-infrared and submillimeter wavelengths (70–500 μm) with the *Herschel* Space Observatory, successfully launched by ESA in May 2009, will soon remedy this unsatisfactory situation by providing complete samples of prestellar cores and Class 0 protostars in nearby Galactic molecular clouds. The first results of *Herschel* are extremely promising and suggest that more than 5,000 prestellar cores and more than 500 Class 0 protostars will be identified by the end of the space mission (see Astronomy and Astrophysics Vol. 518, special feature on *Herschel*).

See Also

- Bipolar Flow
- Birthline
- Debris Disk
- Dense Core
- Fragmentation of Interstellar Clouds
- Hertzsprung-Russell Diagram
- Infrared Astronomy
- Infrared Excess
- Pre-Main-Sequence Star
- Protoplanetary Disk
- Protostars
- Protostellar Envelope
- Star Formation, Observations
- Star Formation, Theory
- T Tauri Star

References and Further Reading

Adams FC, Lada CJ, Shu FH (1987) Spectral evolution of young stellar objects. Astrophys J 312:788–806

André P, Montmerle T (1994) From T Tauri stars to protostars: circumstellar material and young stellar objects in the ρ Ophiuchi cloud. Astrophys J 420:837–862

André P, Ward-Thompson D, Barsony M (1993) Submillimeter continuum observations of rho ophiuchi A: the candidate protostar VLA1623 and prestellar clumps. Astrophys J 406:122–141

André P, Ward-Thompson D, Barsony M (2000) From pre-stellar cores to protostars: the initial conditions of star formation. In: Mannings V, Boss A, Russell S (eds) Protostars and planets IV. University Arizona Press, Tucson, pp 59–96

Bachiller R (1996) Bipolar molecular outflows from young stars and protostars. Annu Rev Astron Astrophys 34:111–154

Beckwith SVW, Sargent AI, Chini RS, Guesten R (1990) A survey for circumstellar disks around young stellar objects. Astron J 99:924–945

Bontemps S, André P, Terebey S, Cabrit S (1996) Evolution of outflow activity around low-mass embedded young stellar objects. Astron Astrophys 311:858–872

Evans NJ (1999) Physical conditions in regions of star formation. Annu Rev Astron Astrophys 37:311–362

Evans NJ et al (2009) The spitzer c2d legacy results: star-formation rates and efficiencies; evolution and lifetimes. Astrophys J Suppl 181:321–350

Greene TP, Lada CJ (1996) Near-infrared spectra and the evolutionary status of young stellar objects: results of a 1.1–2.4 4 μm mu;m survey. Astron J 112:2184–2221

Greene TP, Wilking BA, André P, Young ET, Lada CJ (1994) Further mid-infrared study of the rho Ophiuchi cloud young stellar population: luminosities and masses of pre-main-sequence stars. Astrophys J 434:614–626

Hartmann L (1998) Accretion processes in star formation. Cambridge University Press, New York

Lada CJ (1987) Star formation – from OB associations to protostars. In: Peimbert M, Jugaku J (eds) Star forming regions (IAU Symposium 115). Reidel, Dordrecht, pp 1–17

Lada CJ, Wilking BA (1984) The nature of the embedded population in the Rho Ophiuchi dark cloud – mid-infrared observations. Astrophys J 287:610–621

Myers PC, Adams FC, Chen H, Schaff E (1998) Evolution of the bolometric temperature and luminosity of young stellar objects. Astrophys J 492:703–726

Shu FH, Adams FC, Lizano S (1987) Star formation in molecular clouds – observation and theory. Annu Rev Astron Astrophys 25:23–81

Stahler SW, Palla F (2005) The formation of stars. Wiley Interscience, New York. ISBN 3-527-40559-3

Stahler SW, Walter FM (1993) Pre-main sequence evolution and the birth population. In: Levy EH, Lunine JI (eds) Protostars and planets III. University of Arizona Press, Tucson, pp 405–428

Strom SE (1972) Optical and infrared observations of young stellar objects – an informal review. Publ Astron Soc Pac 84:745–756
Ward-Thompson D, André P, Crutcher R, Johnstone D, Onishi T, Wilson C (2007) An observational perspective of low mass dense cores: evolution toward the initial mass function. In: Reipurth B et al (eds) Protostars and planets V. University of Arizona Press, Tucson, pp 33–46

Spectral Line

Daniel Rouan
LESIA, Observatoire Paris-Site de Meudon, Meudon, France

Definition

A spectral line is a deficiency or excess of radiation at a precise wavelength in the spectrum of a source because of a quantum effect (transition between two energy states) in an atom, molecule, ion or functional group (in the case of a solid) present in the source. The terminology originated with the slit spectrometers used by physical scientists to display a spectrum. Each spectral line is very specific to a given species, so that it can be used to identify the chemical composition of the object emitting or transmitting the light analyzed with a ▶ spectrometer. Comparing the intensities of different spectral lines provides information on physical conditions such as temperature and density. The displacement of spectral lines under the Doppler Effect allows astronomers to derive the velocity of the emitter (or absorber).

See Also

- ▶ Doppler Shift
- ▶ Electromagnetic Spectrum
- ▶ Spectrometer
- ▶ Spectroscopy

Spectral Survey

▶ Molecular Line Survey

Spectral Type

Sylvia Ekström
Observatoire Astronomique de l'Université de Genève, Faculté des Sciences, Université de Genève, Versoix, Switzerland

Definition

Stars are classified based on the ionization state of their atmosphere and thus on their surface temperature. From hottest to coolest, the classification goes as O, B, A, F, G, K, and M (with the mnemonic "Oh Be A Fine Girl/Guy, Kiss Me"):

Type	Temperature	Main lines
O	≥30,000 K	He II, C III, N III, O III, Si IV
B	10,000–30,000 K	He I, Mg II, Si II
A	7,500–10,000 K	H, Mg II, Fe II, Si II
F	6,000–7,500 K	H, Fe I, Cr I, Ca II
G	5,200–6,000 K	Fe I, Ca II, CH
K	3,700–5,200 K	Fe I, Si I, Mn I, TiO
M	≤3,700 K	TiO, VO, molecular

Each category has ten subdivisions numbered from 0 (hottest) to 9. The spectral type is usually complemented by the *luminosity class*, labeled in roman numbers from I (supergiants) to V (main sequence dwarfs); that is, stars of the same effective temperature may have differing luminosities, depending on their mass and evolutionary state.

The Sun has a spectral class G2V.

History

Historically, spectral types were assigned alphabetically primarily in an order reflecting the decreasing strength of hydrogen absorption lines

in their spectra. Only later was it realized that the different spectral types resulted from differing surface temperatures.

See Also

- ▶ Hertzsprung-Russell Diagram
- ▶ Stellar Evolution

Spectral Veiling of Young Stars

Steven W. Stahler
Department of Astronomy, University of California, Berkeley, CA, USA

Definition

Stellar spectra exhibit sharp absorption lines superposed on a smooth, background flux. The pattern of lines reveals both the chemical elements present in the stars' surface layers and the temperature of this material. In classical ▶ T Tauri stars, pre-main-sequence objects of solar mass and below, the absorption lines are partially filled in. This is referred to as veiling and is thought to represent emission from shocks created as material crashes onto the stellar surface. The degree of spectral veiling correlates with the amount of ▶ infrared excess, which arises from heated dust grains in circumstellar disks. Indeed, the infall creating spectral veiling is thought to arise largely from such disks. Both features are absent in weak-lined T Tauri stars.

See Also

- ▶ Gravitational Collapse, Stellar
- ▶ Infrared Excess
- ▶ Pre-Main-Sequence Star
- ▶ Spectral Line
- ▶ T Tauri Star

Spectrofluorometry

- ▶ Fluorometry

Spectrometer

Daniel Rouan
LESIA, Observatoire Paris-Site de Meudon, Meudon, France

Definition

A spectrometer is an instrument used by scientists to decompose the radiation either emitted by a source or transmitted by a region or substance of interest, so as to measure the intensity as a function of the wavelength in a way that can be recorded. In the visible, it may be based on a prism or a grating; in the infrared, it can be a Fourier transform technique which is used, and in the radio domain, it is generally an autocorrelator. It produces a spectrum (plural spectra) which is an accurate record of the intensity versus the wavelength.

See Also

- ▶ Mass Spectrometry
- ▶ Spectral Line
- ▶ Spectroscopy

Spectroscopic Orbit

David W. Latham
Harvard-Smithsonian Center for Astrophysics, Cambridge, MA, USA

Definition

When two stars orbit each other and the orbital motion is detected spectroscopically from the

changes in the Doppler shifts (also known as Doppler velocimetry), the system is traditionally called a spectroscopic binary. Accordingly, the orbital solution based on the observed changes in radial velocities of the two stars is called a spectroscopic orbit. When the companion is a planet, only the spectrum of the host star is detected. In this case, the planet and star revolve around their center of mass. Although the orbit of the primary star around the center of mass is smaller than that of the planet, it is still called a spectroscopic orbit. The five parameters that define a single-lined spectroscopic orbit are the orbital ▶ period P, the ▶ eccentricity of the elliptical orbit e, the velocity of the center of mass γ, the amplitude of the orbital velocity projected along the line of sight K, the orientation on the sky of the long axis of the ellipse ω, and the time of ▶ periastron passage T. When the orbit is circular, $e = 0$ and ω is not defined, so the time of maximum velocity away from the observer is used instead of T.

Radial velocities do not provide enough information to determine the orbital inclination, but do provide some information about the masses:

$$M_{\mathrm{B}} \sin(i) = (M_{\mathrm{A}} + M_{\mathrm{B}})^{2/3} f^{2/3}$$

Where f is the mass function and is given by

$$f = 1.036 \times 10^{7} K_{\mathrm{A}} P (1 - e)^{3/2},$$

M_{A} and M_{B} are the masses of the primary and secondary in solar masses, i is the orbital inclination (90° for an edge-on orbit), K_{A} is the observed semi-amplitude of the orbital velocity of the primary in km/s, P is the orbital period in days, and e is the orbital eccentricity. If the orbital inclination can be determined through other observations, then the sin(i) ambiguity can be removed. In a binary star, when the spectrum of the secondary star is also detected, the orbital amplitude of both stars can be determined, and thus the mass ratio $q = M_{\mathrm{B}}/M_{\mathrm{A}} = K_{\mathrm{A}}/K_{\mathrm{B}}$ can be obtained.

See Also

- ▶ Doppler Shift
- ▶ Eccentricity
- ▶ Inclination (Astronomy)
- ▶ Periastron
- ▶ Period
- ▶ Radial Velocity
- ▶ Radial-Velocity Planets

Spectroscopy

Daniel Rouan
LESIA, Observatoire Paris-Site de Meudon, Meudon, France

Keywords

Spectra; Spectral lines; Spectrograph; Spectrometer; Spectrum

Synonyms

Spectral analysis

Definition

Spectroscopy is the technique used to measure the intensity of electromagnetic radiation as a function of either wavelength or frequency. Spectroscopy is an important tool to derive the physical and chemical properties of astronomical objects as well as their velocity. The study of spectral features from atoms, ions, and molecules is of particular importance to give access to abundances, temperature, pressure, magnetic field, radial velocity, etc. The term spectroscopy is also applied in other fields, for example, to the measurement of the abundances by mass of chemical species in a sample (see Mass Spectroscopy).

Overview

Light brings a wealth of information, which a blind person misses badly every day. Generally, we think of this information primarily in the form of images of the world around us that light carries to our retina or to the electronic retinas of our cameras. In astronomy, imaging is often the first phase of discovery to derive morphology, shape, size, and displacement. From the planets to the discovery of giant structures or filaments in the Universe, images have played a major role in astronomy. Light carries yet another crucial piece of information, perhaps richer than the image, its energy. A celestial object indeed registers in the light it emits a footprint, often very accurate, of its composition, its energy state, and its dynamics. On one hand, physical processes will produce photons following a well-defined energy distribution, depending on the physical conditions like temperature or elementary composition of the source (gas of electrons, atoms of different chemical species), and, on the other hand, internal or global movements of this source often subtly alter this distribution.

Whatever is the description of light, photons, or electromagnetic waves, its energy content is perfectly defined. A photon, the particle of light, is described by two parameters only: its energy E and its state of polarization. Energy is the most important parameter because it will drive all the basic properties of the photon-matter interactions. This energy is unchanged as long as the photon is *alive*, that is to say, is not absorbed. If we now consider an electromagnetic wave, the other complementary way to describe light, it carries power in the form of waves progressing very rapidly: at the speed of light of course! Two wave crests are separated at a given moment by a characteristic length, called wavelength, and always denoted by the symbol λ. E and λ are related to the simple law $E = hc/\lambda$, where c is the speed of light and h is a physical constant introduced by Max Planck. The wavelength is a quantity which results in a clearly discernible property that our brain can perceive in visible light, which is the color. For instance, dark red corresponds to a wavelength of 750 nm, typically two times larger than the wavelength of blue light.

Most generally the resulting emission of a given phenomenon is the superposition of several waves at different wavelengths, in fact a continuum. If in music the superposition of wavelengths makes the richness of the sound, in contrast, for the astrophysicist, the wealth comes from the separation into the basic components of the light. This separation or decomposition is essential to analyze the predominance of one portion of the wavelength domain or another or for seeking for *spectral lines* which are reinforcements (known as emission lines) or gaps at a particular wavelength (absorption lines). This information bears the mark of processes that gave birth to the light or have influenced it later and which allow the astrophysicist to go much further in the physical understanding of phenomena than is allowed by the image alone. Spectroscopy is the science of analyzing the light into its components, and it is customary to say that astrophysics, to distinguish it from conventional astronomy, was born in the middle of the nineteenth century with the advent of spectroscopy. It is always amazing to realize the extraordinary richness of the spectroscopic information. It actually gives access to a wide variety of physical quantities: the velocity of an object or even the velocity distribution of its components (for instance, in a galaxy); the composition of the matter it is made of, atoms or molecules; the state of this matter (ionized, atomic, molecular, solid, gaseous); the temperature, density, or pressure of the gas; the intensity and direction of the magnetic field, etc. These quantities are then used by the astrophysicist to constrain physical models describing the objects and their interactions. Predictions are then proposed that new spectroscopic measurements will confirm or deny in a continuously repeated cycle.

Basic Methodology

Spectrographs. Spectroscopy uses dedicated instruments to decompose the light in order to produce a spectrum, i.e., a measure of the light

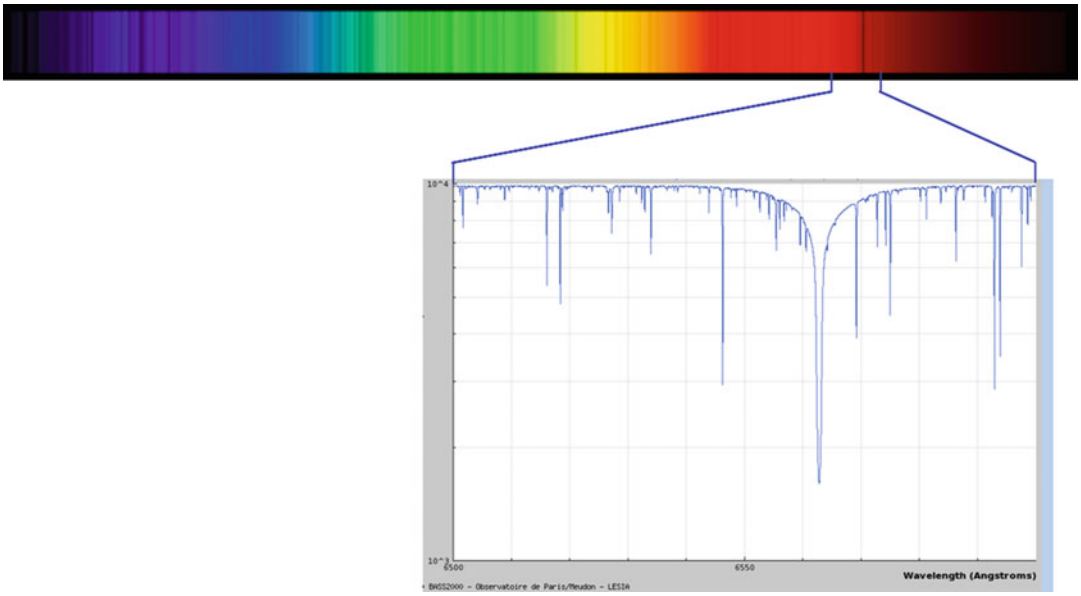

Spectroscopy, Fig. 1 The visible spectrum of the Sun presented in two forms. *Top*: as it appears in a spectroscope, that is to say, as a bright band showing the colors of the rainbow and streaked with many lines more or less dark; *bottom*: a plot giving the accurate information of the intensity versus wavelength in a narrow region. Note the significant depression in the spectrum at 656.6 nm: it corresponds to an absorption due to hydrogen (Doc: BASS 2000)

intensity as a function of wavelength. Figure 1 illustrates a spectrum of sunlight in two forms: the colorful one that the eye sees in the spectroscope and the more quantitative one as a plot of light intensity as a function of wavelength. The instrument that makes this decomposition is a spectrograph or a ▶ spectrometer; however, for the purist, the later term refers rather to an instrument that provides a direct and accurate calibration of the wavelength.

The prism spectrograph. The first spectrographs exploited the variation with wavelength of the optical index of materials to produce differential deviation of the light according to its color (its wavelength) when refracted by a prism. Figure 2 shows the basic elements of a prism spectrograph. Issued from a point source, whose extension is limited by a slit, a parallel beam is formed thanks to the first lens – the collimator; the beam falls then on the prism at a specific angle of incidence – and the second lens

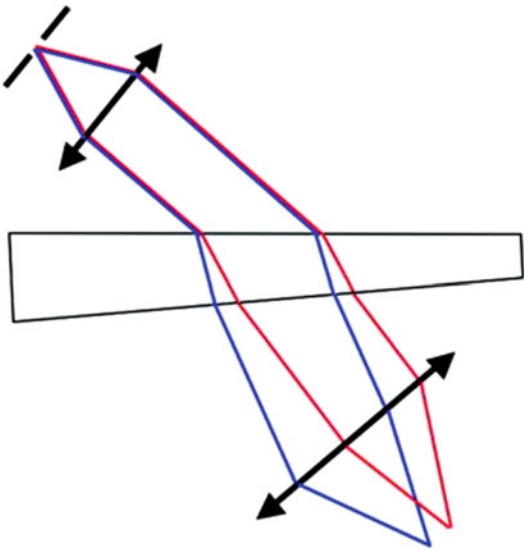

Spectroscopy, Fig. 2 The principle of a prism spectrograph: it includes a slit, a collimator (*double-headed arrow*), the prism, a camera lens (a *second double arrow*), and a detector on which the spectrum is formed

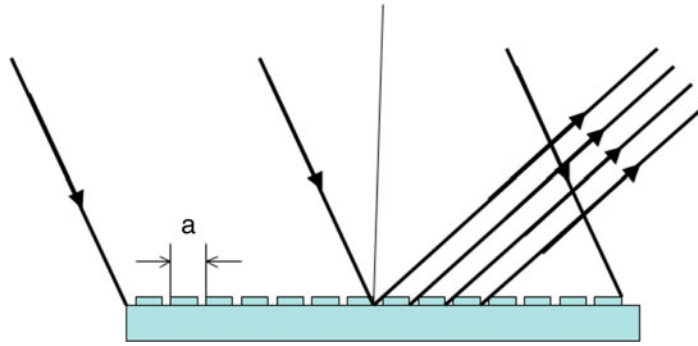

Spectroscopy, Fig. 3 The principle of the diffraction grating. Each groove engraved on the surface of the grating diffracts light in all directions. In a given direction, there is a single wavelength for which all the waves from the different grooves are constructive. In the same direction but at a different wavelength, the waves are incoherent and destroy each other

after the prism, the camera, reforms a series of distinct images of the source, each one at a given wavelength.

Among the disadvantages of the prism is the size it must have when one wishes to achieve a high resolution. Producing glass blocks of large volume, while guaranteeing a very good homogeneity of their optical properties, becomes a challenge. The absorption in the glass is another limitation. The prism spectrograph has been supplanted gradually by the grating spectrograph.

The grating spectrograph. The grating spectrograph uses the principle of light interference that stems directly from the wave nature of light. A grating is a reflective surface which has been engraved with a series of fine parallel grooves separated by very small distances, a few micrometers to a few tens of micrometers. If a beam of light falls on the surface, then each slot, because it is very small, will spread the light in all directions (the ▶ diffraction phenomenon). In a given direction, there is a unique wavelength for which the wavelets emitted by all the grooves are in phase and will therefore add, as shown in Fig. 3. In a direction somewhat different, waves at that wavelength are somehow out of synchronization, and, as there is a very large number of them, they cancel each other. A given direction is thus associated with a single wavelength whose intensity is preserved, while at all other wavelengths, the destructive phenomenon is extremely effective. Eventually, we obtain the desired effect: each wavelength is isolated in a given direction.

In practice, for a good separation of wavelengths, one looks for a large number of lines per unit length (about 40–200), a result obtained thanks to a very precise machine equipped with diamond tools. In addition, the grating is used at large angles of incidence of the beam on the grating. Significant progress has been made with the introduction of the *échelette* grating, so named because of the particular stair shape of the grooves: the facets that behave like small mirrors can better focus the light in the direction where the spectral analysis has to be done.

From the viewpoint of its implementation in a spectrograph, the grating is used in a manner quite similar to that of the prism: it is placed in the parallel beam issued from a collimator and a camera objective reforms the image of the entrance slit on the detector, the slit being oriented parallel to the lines of the grating. Figure 4 illustrates this configuration.

Fourier transform spectrograph. Fourier transform spectroscopy is a clever use of the interference of light to derive the spectrum. The intensity of a beam containing all the different wavelengths of the studied light, but each with a different weighting, is measured by a unique detector. The weighting is due to interferences in a Michelson interferometer, an optical instrument that allows some wavelengths to pass through but blocks partially or totally others.

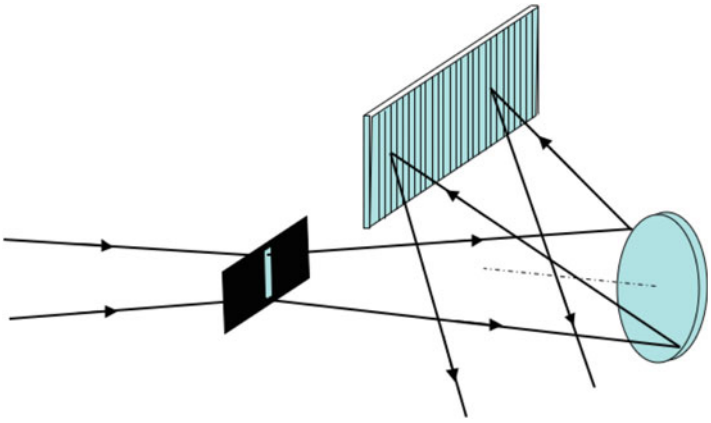

Spectroscopy, Fig. 4 Arrangement of the entrance slit, of collimator (here a spherical mirror), and of the grating in a grating spectrograph

By moving one of the mirrors of the interferometer, the interference structure and thus the weighting is changed, so that repeating the process many times produces as many data points as there are distinct wavelengths. However, this is not yet a spectrum, each measurement being a linear combination of different intensities of the various wavelengths. Inverting the set of data to produce the spectrum is done with a computer, thanks to a rather simple algorithm called the Fourier transform. One advantage of the Fourier transform spectrograph is the capability to reach very high resolving power. It is becoming a widespread laboratory instrument to measure molecular or atomic spectra.

Performances of a spectrograph. Since the goal of a spectrograph is to separate the wavelengths, its main characteristic is its resolution or resolving power $R = \lambda/\Delta\lambda$, defined as the ratio of the central wavelength to the smallest difference in wavelength $\Delta\lambda$ between two *colors* that can be distinguished unambiguously. $\Delta\lambda$ is called the spectral resolution element. Figure 5 illustrates how the information becomes more accurate when the resolving power increases and thus the spectral resolution element becomes smaller. For a grating, one may show that the maximum resolving power is directly given by the ratio of the length of the grating to the wavelength. A large grating is thus required to reach a large resolving power.

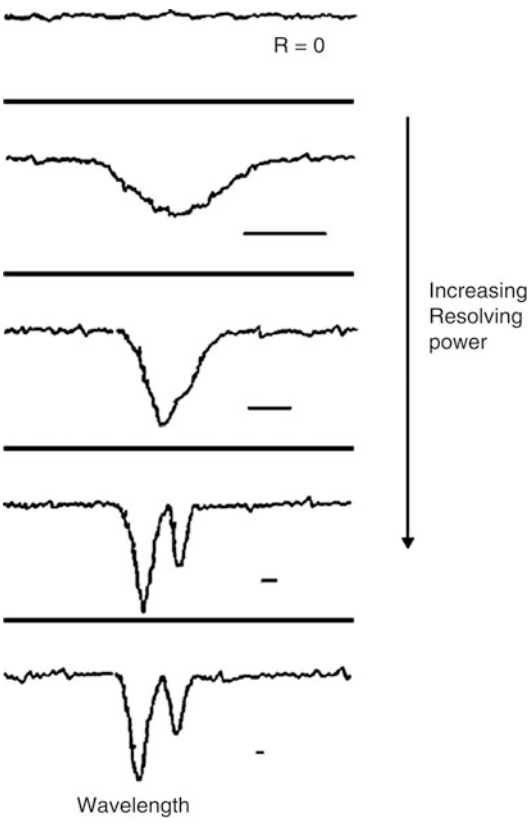

Spectroscopy, Fig. 5 Observation of a spectral feature in a spectrum (a *double line* in absorption) when the resolving power increases: from a mere depression, one passes to the separation into two distinct components. The spectral resolution element is indicated by the *horizontal line* segment to the right of each curve

The resolution of a spectrograph varies according to the goal to be achieved: for the spectroscopy of faint distant galaxies, a resolution of $R = 2{,}000$ is well suited. In contrast, in spectroscopy of a bright source like the Sun, where extremely fine physical effects can be looked for, resolving powers of several hundreds of thousands are common. In ▶ radio astronomy, heterodyne techniques can provide even much higher resolution.

A second element of performance is the wavelength range that a spectrograph is able to analyze at once. The size of the detectors often limits the spectral range. Note that the prism has the advantage over the grating in having a spectral range that is bounded solely by the transmission of the glass, while the grating is limited in principle to an octave or less if very high spectral resolution is the goal. However, a clever combination of optics can overcome this limitation and provides simultaneously broad spectral range and high resolution. The trick is to use a second grating or a prism of modest resolving power to disperse the light in a direction perpendicular to the primary dispersion, so that the spectrum is divided into bands that can cover the surface of a CCD detector with no overlap. This setup, called a cross-dispersed spectrograph, is more and more popular in astronomy, and, in particular, it is the choice instrument for the detection of exoplanets through ▶ radial velocity measurements.

Among other factors to judge the quality of a spectrograph is its transmission: for instance, it should not lose 95 % of the photons reaching the telescope because of too many optical elements.

Key Research Findings

Recent developments in spectroscopic techniques have aimed at responding to new needs of the astronomer. Among them two have particularly emerged: linking imaging and spectroscopy and simultaneous spectroscopy of a large number of objects (we do not discuss here developments in ▶ radio astronomy or very short wavelength astronomy).

Spectroscopy of extended objects: *integral field spectroscopy*. Conventional spectrographs are well adapted to stellar physics, which studies essentially spatially unresolved objects. However, when one deals with extended objects such as planets, galaxies, or some nebulae (HII regions, planetary nebulae), the access to spectral information anywhere on the object is required to understand the physics that governs the different parts (e.g., the temperature) or to measure the relative velocities, etc. A conventional spectrograph does not allow it, its entrance slit limiting the field of view.

Different ideas have been proposed to obtain what is called an integral field spectrograph that can simultaneously obtain spectra from all points of the field or at least from a significant number of cells covering the object.

One idea is to divide the field of view into small cells with an array of microlenses, each of which will form a small bright spot at its focus. Each point feeds one optical fiber among a few tens of fibers arranged in a compact bundle. The light is then carried by each fiber to the entrance slit of a spectrograph where the output fibers are aligned along the slit. This configuration is well suited to simple objects that do not require many pixels. When this is not the case, then other solutions have been proposed. A variant of the previous configuration that uses an array of microlenses is to collimate the light at the focus of each microlens on a diffraction grating (actually a grism, a particular type of grating deposited on a prism and whose advantage is that the central wavelength is not deviated) that will give a spectrum of each micro-point source. All spectra are formed on a CCD array with a trick: the dispersive grating is rotated by a small angle with respect to the pattern of microlenses, so that no overlap occurs, as illustrated below (Fig. 6).

Multi-object spectroscopy. The need to conduct simultaneous spectroscopy of many objects in the same field has emerged with the advent of large surveys in the late 1990s.

Two concepts have been successfully developed: One is based on the use of a bundle of several tens of optical fibers and the other one

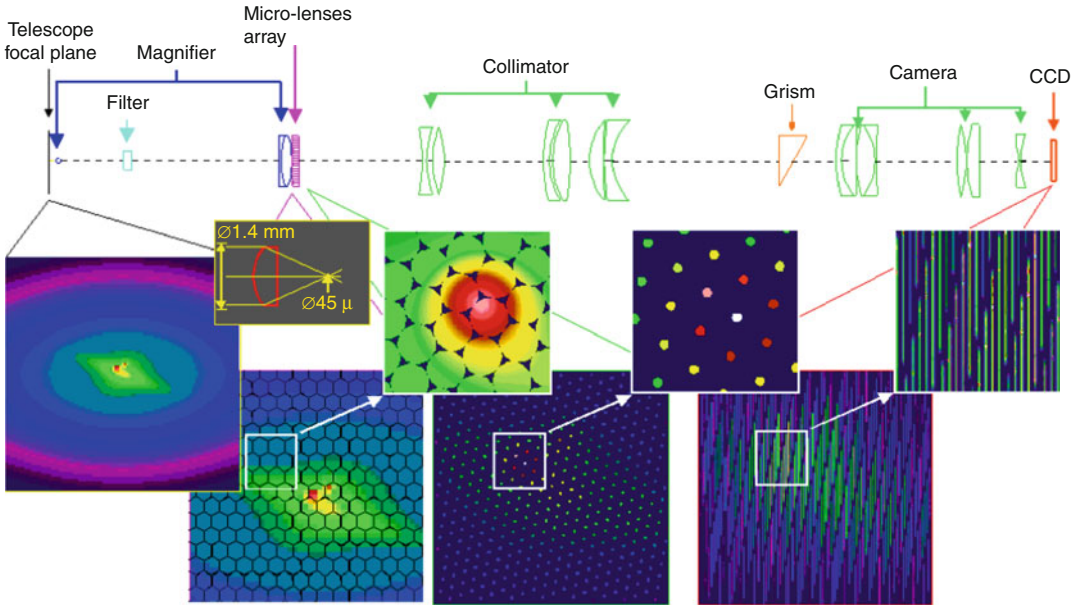

Spectroscopy, Fig. 6 The concept of an integral field spectrograph designed by George Courtès. It forms simultaneously the spectra of different regions of an object whose image has been divided into smaller areas by an array of microlenses. Note that the dispersion is provided by a grism whose direction of dispersion is slightly rotated relative to the pattern of microlenses so as to avoid overlapping spectra of nearby regions

on the use of a slit mask. In the first case, the head of each fiber is positioned very precisely in the field of the telescope, at the location, previously measured, of the object. This positioning is performed by robotic arms or by fixing each fiber head on a large metal plate thanks to a magnet. The plate is then placed at the focus of the telescope by a robotic system. The other end of each fiber is placed on the entrance slit of a standard spectrograph that can accommodate a large number of them and produces all spectra simultaneously.

In the second configuration, a mask punched with small slits at the locations of objects whose spectrum is wished is put in place at the focus of the telescope. An optical system, a grism, can then decompose the light from each of the mini-slits to form as many spectra as there are selected objects. One has to choose carefully the slit positions so that the spectra do not overlap and cover almost entirely the surface of a CCD array of large size. The punching of the masks is done by machining a thin metal plate with a power laser, after a picture was first taken from the field and then analyzed, and the objects selected by the astronomer to finally produce a code that controls the movements of the laser. The plates of planned observations are then inserted into a set of "drawers" to be set up rapidly with a great accuracy.

See Also

- ▶ Continuum
- ▶ Line Profile
- ▶ Linewidth
- ▶ Spectral Line
- ▶ Spectrometer

References and Further Reading

Allington-Smith J (2007) Integral field spectroscopy for panoramic telescopes. Rev Mex Astron Astrofís (Serie de Conferencias) 28:17

Content R (1997) New design for integral field spectroscopy with 8-m telescopes. Proc SPIE 2871:1295

Courtès G (1982) An integral field spectrograph (IFS) for large telescopes. In: Humphries CM

(ed) Instrumentation for astronomy with large optical telescopes, vol 92, ASSL. Reidel, Dordrecht, p 123
Lena P, Rouan D, Lebrun F, Mignard F, Pelat D (2012) Observational astrophysics. Astronomy and astrophysics library. Springer, Berlin
Liller W (1970) High dispersion stellar spectroscopy with an echelle grating. Appl Opt 9(10):2332
Monnet GJ (2009) Astronomical spectroscopy in the last four decades: survival of the fittest. Exp Astron 25:91
Vanderriest C (1980) A fiber-optics dissector for spectroscopy of nebulosities around quasars and similar objects. Publ Astron Soc Pac 92:858

Spectroscopy, History of

Stéphane Le Gars
Centre François Viète, Université de Nantes, Nantes, France

Keywords

Astronomy; Chemistry; Physics; Gustav Kirchhoff; Robert Bunsen

Definition

Establishing, at the end of the seventeenth century, that sunlight consisted of colors which were refracted differently by prisms, Isaac Newton (1643–1727) laid the foundation of physical optics. It was only at the beginning of the nineteenth century that major experimental innovations allowed the discovery of dark lines in the solar spectrum. Kirchhoff and Bunsen's works published in 1859 gave an explanation of these lines and made the spectral analysis (soon called ► spectroscopy) a powerful tool in the fields of astronomy, physics, and chemistry.

Overview

Spectroscopy is the study of luminous spectra, i.e., the analysis of the intensity of radiation as a function of wavelength (color, for visible wavelengths). For the Greek philosophers, such as Xenophanes (c.570–460 BCE), Aristotle (384–322 BCE), or Epicurus (341–270 BCE), the colors observed in the rainbow were only a dimming of the solar light after going through an aqueous medium denser than the air. At the beginning of the seventeenth century, Kepler took an interest in prisms, but only described the colored rays he observed at the exit of the prism, putting forward a "sensual axiom" to justify the coloration of refracted rays. In 1672, in his *Traité d'Optique* published in 1704, Newton proposed a real color theory. Newton quantified refraction for the first time, characterizing each color by a number. Indeed, Newton showed that the colors obtained with the help of the prism are homogeneous and really form the solar light.

In the eighteenth century, the Swiss mathematician Leonhard Euler (1707–1783) adhered to a wave conception of light and gave another meaning to the number connected to each color: He identified it with the wavelength in a given medium. But later on, it was on an experimental level that the study of spectra progressed. Using a slit in front of a prism, British William Hyde Wollaston (1766–1828) discovered in 1802 five dark lines in the solar spectrum; in 1815, the German optician Joseph von Fraunhofer (1787–1826) detected 576 of them by joining an astronomical reflector to the slit-prism system. The nature of these dark lines was identified by the German scientists Gustav Robert Kirchhoff (1824–1887) and Robert Wilhelm Eberhard von Bunsen (1811–1899): They arise from the absorption of light by a medium set in front of the light source. Moreover, under defined conditions of excitation, an object can only emit the radiations it is capable of absorbing. This law, called "Kirchhoff's," allowed chemical analysis by the study of emission and absorption spectra. The Kirchhoff and Bunsen discoveries sharply affected the scientific world: e.g., spectroscopy ruined with the ideas of Auguste Comte (1798–1857) about the impossibility of a chemical and physical study of the astronomical objects and permitted the development of astrophysics.

See Also

- ▶ Spectral Line
- ▶ Spectrometer
- ▶ Spectroscopy

References and Further Reading

Bennet JA (1984) The spectroscope first decade. Bull Sci Instrum Soc 4:3–6
Fajl J (1985) The creation of a Victorian myth: the historiography of spectroscopy. Hist Sci 23:1–24
Gingerich O (1981) Astronomical scrapbook, unlocking the chemical secrets of the cosmos. Sky and telescope, July 13–15
Mac Gucken W (1970) Nineteenth century spectroscopy, development of the understanding of spectra 1802–1897. Johns Hopkins Press, Baltimore
Saillard M (1983) Notes sur l'histoire de la spectroscopie. Bull Union Phys 655:1157
Saillard M (1988) Histoire de la Spectroscopie, De la théorie de la lumière et des couleurs de I. Newton (1672) à la découverte de l'effet Zeeman (1897). Cah d'Hist Philos Sci N 26
Salet G (1888) Traité Elémentaire de Spectroscopie. Masson, Paris
Salet P (1909) Spectroscopie Astronomique. Doin et fils, Paris
Schellen H (1872) Spectrum analysis in its application to terrestrial substances. Longmans, Londres
Urbain G (1911) Introduction à l'étude de la spectrochimie. Hermann, Paris

Spheroplast

- ▶ Protoplast

Spherules

Nadja Drabon
Stanford University, Stanford, CA, USA

Keywords

Meteorite impact; Microtektite; Microkrystite

Synonyms

Distal impact ejecta; Microkrystite; Microtektite

Definition

Spherules are distal deposits of meteorite impacts. They are spherical droplets that can form in two ways: as silicate splash particles of ejected impact melt and as condensates from the rock-vapor plume. Glassy spherules that do not contain any crystallites are called microtektites (Glass 1990). These often contain vesicles and are commonly originated as melt spherules. Crystal-bearing spherules, in contrast, are typical to have originated from vapor condensates and are termed microkrystites (Glass and Bohor 1988). Spherules can be less than a hundred micrometers to a few millimeters in diameter. Spherules may be deposited globally or in *strewn fields* which radiate from the crater.

Overview

Spherule beds are sedimentary layers that are composed entirely of spherules or, if reworked, may contain detrital material. Pure spherule beds can be up to a few decimeters thick. The impact-related origin can be recognized by geochemical anomalies that indicate extraterrestrial components, such as abnormally high concentrations of platinum group elements, especially iridium, and extraterrestrial chromium isotope signatures (Shukolyukov and Lugmair 1998, 2000), and by the presence of shocked minerals.

Spherules were first discovered by Bill Glass in 1967 in the Australasian microtektite layer which is the largest Cenozoic strewn field. Since then, spherules have been widely used to identify meteorite impacts in the Earth's and the moon's history (Chao et al. 1970). In contrast to regionally to potentially globally distributed spherule beds, craters are local features and thus more vulnerable to be entirely obliterated by erosion or tectonic processes. To date, 31 spherule layers have been identified. The Archean spherule

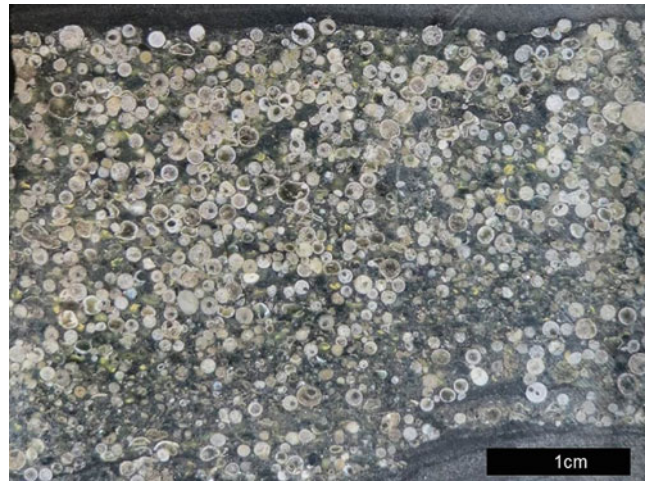

Spherules,
Fig. 1 Paleoarchean spherules of the Barberton greenstone belt, South Africa

layers in South Africa and Australia are the oldest evidence of impacts (Fig. 1) (Lowe and Byerly 1986; Lowe et al. 2003) and were formed by the largest impactors identified to date on Earth. Their bolides are thought to have been 20 km to over 100 km in diameter (Lowe et al. 1989; Melosh and Vickery 1991; Kyte et al. 1992; Shukolyukov et al. 2000). Impacts of this size had a profound effect on the environment and early life (e.g., Sleep et al. 1989; Toon et al. 1997; Naumov 2005; Pierazzo and Artemieva 2012; Kring 2003; Abramov and Mojzsis 2009). They include local effects, such as fireballs and shock waves. Large impacts may have had global effects, such as global darkening by dust loading of the atmosphere and global climate change. Because physical changes are relatively short lived and local, the most important biologic effects result from impact-induced environmental changes. These may cause the collapse of the food chain or the destruction of geochemical gradients. Yet, impacts may also be beneficial for life on a molecular to evolutionary scale (Cockell and Bland 2005). They are thought to potentially have carried life to Earth (→ *Panspermia*) or shock-synthesized the organic building blocks necessary for life during the impact. Impacts also create new habitats such as crater lakes, hydrothermal systems, and shock-weakened rocks and can empty ecological niches to subsequently allow other species to radiate.

See Also

► Panspermia

References and Further Reading

Abramov O, Mojzsis SJ (2009) Microbial habitability of the Hadean Earth during the late heavy bombardment. Nature, 459(7245):419–422

Chao ECT, Boreman JA, Minkin JA, James OB, Desborough JA (1970) Lunar glasses of impact origin: physical and chemical characteristics and geologic implications. J Geophys Res 75(35):7445–7479

Cockell CS, Bland PA (2005) The evolutionary and ecological benefits of asteroid and comet impacts. Trends Ecol Evol 20(4):175–179

Cockell CS, Lee P, Osinski G, Horneck G, Broady P (2002) Impact-induced microbial endolithic habitats. Meteorit Planet Sci 37(10):1287–1298

Glass BP (1990) Tektites and microtektites: key facts and inferences. Tectonophysics 171(1):393–404

Glass BP, Burns CA (1988) Microkrystites-A new term for impact-produced glassy spherules containing primary crystallites. In Lunar and Planetary Science Conference Proceedings 18:455–458

Glass BP, Simonson BM (2012) Distal Impact Ejecta Layers: A Record of Large Impacts in Sedimentary Deposits. Springer Science & Business Media

Kring DA (2003) Environmental consequences of impact cratering events as a function of ambient conditions on Earth. Astrobiology 3(1):133–152

Kyte FT, Shukolyukov A, Lugmair GW, Lowe DR, Byerly GR (2003) Early Archean spherule beds: Chromium isotopes confirm origin through multiple impacts of projectiles of carbonaceous chondrite type. Geology 31(3):283–286

Kyte FT, Zhou L, Lowe DR (1992) Noble metal abundances in an Early Archean impact deposit. Geochimica et Cosmochimica Acta 56(3):1365–1372
Lowe DR, Byerly GR (1986) Early Archean silicate spherules of probable impact origin, South Africa and Western Australia. Geology 14(1):83–86
Lowe DR, Byerly GR, Asaro F,Kyte F J (1989) Geological and geochemical record of 3400-million-year-old terrestrial meteorite impacts. Science 245(4921): 959–962
Lowe DR, Byerly GR, Kyte FT, Shukolyukov A, Asaro F, Krull A (2003) Spherule beds 3.47–3.24 billion years old in the Barberton Greenstone Belt, South Africa: a record of large meteorite impacts and their influence on early crustal and biological evolution. Astrobiology 3(1):7–48
Melosh HJ, Vickery AM (1991) Melt droplet formation in energetic impact events. Nature 350:494–497.
Mojzsis S, Abramov O (2009) Microbial habitability of the Hadean Earth during the late heavy bombardment. Nature 459:419–422
Pierazzo E, Artemieva N (2012) Local and global environmental effects of impacts on earth. Elements 8(1):55–60
Sleep NS, Zahnle K, Kasting JF, Morowitz H (1989) Annihilation of ecosystems by large asteroid impacts on the early Earth. Nature 342:139–142
Shukolyukov A, Lugmair G (1998) Isotopic evidence for the Cretaceous-Tertiary impactor and its type. Science 282(5390):927–930
Shukolyukov A, Kyte FT, Lugmair GW, Lowe DR, Byerly GR (2000) The oldest impact deposits on Earth—First confirmation of an extraterrestrial component. Impacts and the early Earth:99-115. Springer Berlin Heidelberg
Shukolyukov A, Lugmair GW (2001) Extraterrestrial matter on Earth: Evidence from the Cr isotopes. In Catastrophic events and mass extinctions: Impacts and beyond 1:3041
Toon OB, Zahnle K, Morrison D, Turco RP, Covey C (1997) Environmental perturbations caused by the impacts of asteroids and comets. Rev Geophys 35(1):41–78

Spin-Polarized Electron Beam

► Polarized Electron

Spitzer Space Telescope

Michel Viso
CNES/DSP/SME, Vétérinaire/DVM, Astro/Exobiology, Paris Cedex 1, France

Keywords

Dust clouds; Exoplanet; Planetary disks; Star formation

Synonyms

SIRTF; Space infrared telescope facility; SST

Definition

The Spitzer Space Telescope is the fourth of the Great Observatories that ► NASA has sent in orbit for astronomy. This three-axis stabilized pointing and scanning telescope with a spectral range from 3 to 180 μm has an 85-cm mirror made of beryllium and cooled by liquid helium (360 l at launch). The 950-kg satellite was placed on a heliocentric orbit on August 25, 2003, by a Delta II rocket launched from Cape Canaveral. Thanks to its unusual heliocentric orbit, it has continued observations with the Infrared Array Camera using only the 3.6 and 4.5 μm channels even after the cryogen was exhausted. This warm mission mode began on May 15, 2009 (Fig. 1).

History

As early as 1979, the US National Academy of Sciences was recommending a Shuttle Infrared Telescope Facility (SIRTF). The proposed 1-m telescope was supposed to operate from the Shuttle cargo bay during orbiting missions. With Shuttle weekly flights able to last up to several weeks, the telescope would be refurbished and refilled with cryogen on the ground, and focal plane instruments could be changed frequently. It appeared in 1985, after the STS-51F flight and tests of the first Shuttle-based Infrared Telescope (IRT), that the Shuttle environment would not be suitable for the IR observations. The planned observatory then changed the first word of its denomination from Shuttle to Space, still keeping the acronym SIRTF. The experience and data gained from the Infrared Astronomical Satellite (IRAS; 1983) as well the later success of the European Infrared Space Observatory (ISO, 1995–1998) led to several remodelings of the SIRTF project. During the following years, the budgetary pressure imposed a dramatic downsizing from an ambitious 5,700-kg space

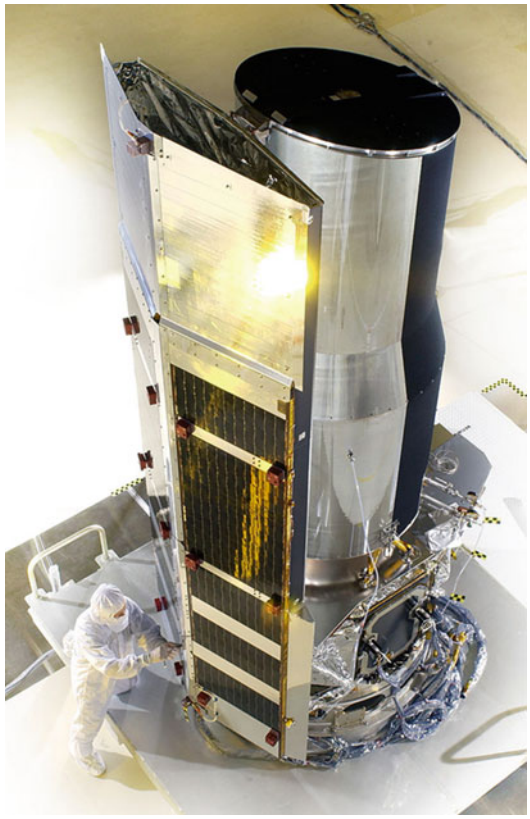

Spitzer Space Telescope, Fig. 1 NASA Spitzer Telescope (http://www.cosmosportal.org/view/article/140793/ last accessed 31 July 2014)

platform to the actual 950 kg. Technical improvements saved most of the scientific objectives and performances.

Overview

The Spitzer Space Telescope is a three-axis stabilized pointing and scanning telescope with a spectral range from 3 to 180 μm. The primary 85-cm mirror is made of beryllium and the instruments are cooled by liquid helium (360 litens at launch). The 950-kg telescope was placed on a heliocentric orbit on August 25, 2003, by a Delta II rocket launched from Cape Canaveral. In this orbit, the spacecraft is trailing the Earth around the Sun, drifting away and "losing" around 15 million kilometers per year. This orbit permits excellent, uninterrupted viewing of a large portion of the sky without the need for Earth-avoidance maneuvers. In addition, the absence of heat input from the Earth provides a stable thermal environment. This allows innovative passive cooling of the exterior of the telescope to reach a low temperature via radiative cooling. The telescope was launched "warm" and then cooled in space for 45 days. Overall, these innovations drastically reduced the total mass of helium needed. This orbit also simplifies telescope pointing, but does require the Deep Space Network for communications. The 1-m-diameter transmitting antenna is used twice each day to transmit 12 h of stored science data.

Spitzer's science payload consists of three cryogenically cooled instruments, which together offer observational capabilities stretching from the near to the far infrared. The Infrared Array Camera (IRAC) provides images at 3.6, 4.5, 5.8, and 8.0 μm, with two adjacent fields of view. One field of view images simultaneously at 3.6 and 5.8 μm and the other at 4.5 and 8.0 μm via dichroic beam splitters. The Infrared Spectrograph (IRS) performs both low- and high-resolution spectroscopy. Low-resolution, long-slit spectra can be obtained from 5.2 to 38.0 μm. High-resolution spectra in Echelle mode can be obtained from 9.9 to 37.2 μm. The spectrograph consists of four modules. One of the modules incorporates a peak-up function that can be used in locating and positioning sources on any of the four spectrometer slits. The Multiband Imaging Photometer for Spitzer (MIPS) is designed to provide photometry and superresolution imaging, as well as efficient mapping capabilities, in three wavelength bands centered near 24, 70, and 160 μm.

The cryogenic mission was planned for 2.5 years and lasted actually around 5.5 years. Since May 15, 2009, after the exhausting of the liquid helium, Spitzer is on a warm mission. In this mode, only the IRAC channels at 3.6 and 4.5 μm are usable. During the cryogenic phase, the focal temperature was stabilized around 15 K, and it has been raised to 30 K during the warm phase.

The "warm" Spitzer surveys about 700 near-Earth objects, cataloguing their individual characteristics. Such a survey is helping to gather

more accurate estimates of asteroids' compositions and sizes.

The Spitzer Space Telescope is a NASA mission managed by the Jet Propulsion Laboratory. The science and data archiving as well as the selection of observation times is managed by Spitzer Science Centre, located on the campus of the California Institute of Technology and part of NASA's Infrared Processing and Analysis Centre.

Key Research Findings

Spitzer gathered a tremendous amount of data, ranging from the early universe up to extrasolar planets, including the discovery of ▶ fullerenes (in 2010).

With the capability of detecting stars behind dusty interstellar clouds, Spitzer snapped the first portraits of stars as they form (Fig. 2). At the same time, it was used to study dying stars, giving

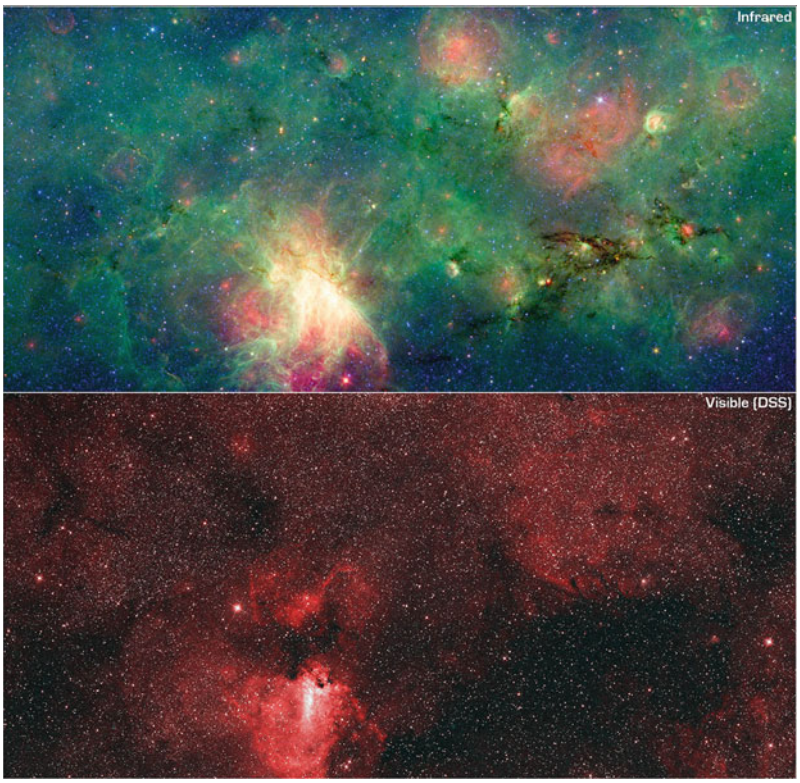

Spitzer Space Telescope, Fig. 2 A dragon-shaped cloud of dust seems to fly out from a bright explosion in this infrared light image taken by the Spitzer Space Telescope (*top*), a feature that is entirely cloaked in shadow when viewed in visible part of the spectrum (*bottom*). The infrared image has revealed that this dark cloud, called M17 SWex, is forming stars at a very high rate. The remnants of an older burst of star formation blew a type of bubble to the left, in the region called M17 EB. The visible-light view of the area clearly shows the bright M17 nebula, as well as the glowing hot gas filling the "bubble" to its left. However, the M17 SWex "dragon" is hidden within dust clouds that are opaque to visible light. It takes an infrared view to catch the light from these shrouded regions and reveal the earliest stages of star formation. The *top* image is a three-color composite that shows infrared observations from two Spitzer instruments. The *bottom* visible-light image is a composite of visible-light data from the Digitized Sky Survey (DSS) from the UK Schmidt Telescope. The image combines two observations that represent the *blue* and *red* light from the region (Image Credit NASA/JPL-Caltech/M. Povich (Penn State Univ.))

some insight into the possible origin of the dust filling up our Universe.

Spitzer telescope was also used to study the ultraluminous infrared galaxies (ULIRGs) emitting more than 90 % of their light in the infrared. These galaxies are primarily found in the distant Universe. This large amount of infrared light could come from extreme star formation, an active central supermassive black hole, or both: three hypotheses that Spitzer could help to sort out.

Several "active galactic nuclei" (AGN) have been unveiled which were hidden from X-ray telescopes by large, massive, and dense dust clouds.

Spitzer has discovered thousands of brown dwarves and found some evidence that some of these failed stars may perhaps have planets. The large amount of such brown dwarves could also explain why galaxies are heavier than they look. Part of the "dark matter," but not part of the exotic undefined matter, could be represented by these dwarves that do not produce optical light and are too faint to be detected from Earth.

Some discoveries are opening wide possibilities for astrobiology, such as that terrestrial planets form around many, if not most, of the nearby Sun-like stars in our Galaxy, as well as around dead stars or stars as young as 1 Ma old.

Spitzer was the first telescope to directly detect light from planets outside of our Solar System, allowing "extrasolar" planets to be directly studied and compared. The planet's glow is extracted from the measurement of the total infrared light collected from both the star and the planet and then measuring the infrared light coming from just the star while the planet dips behind it as part of its regular orbit (see ▶ Transiting Planets). In this way, Spitzer identified a planetary hot spot on a hot Jupiter (Fig. 3).

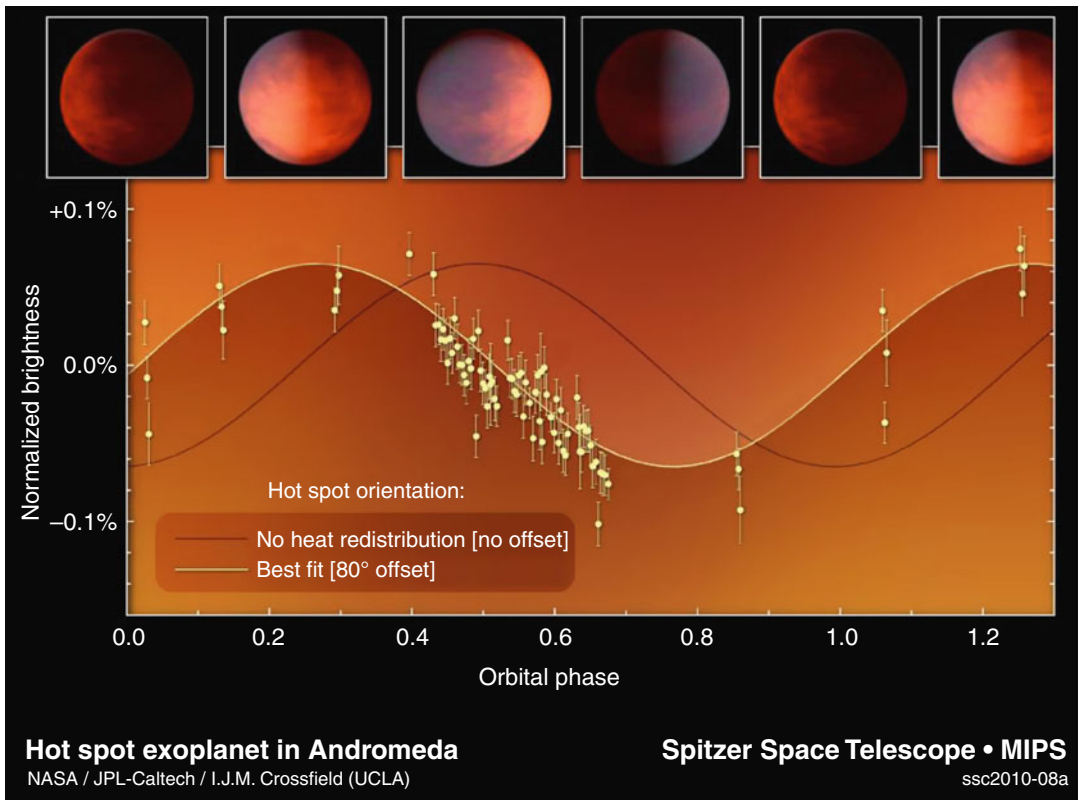

Spitzer Space Telescope, Fig. 3 This plot shows that hot spot on Upsilon Andromedae B. The *black line* shows what the light curve would look like if the hot spot were in the middle of the sun-facing side of the planet. The *yellow line* is the best fit with actual observations, demonstrating an offset of the hot spot by 80° (Image credit: NASA/JPL-Caltech/UCLA)

See Also

- ▶ Herschel Mission
- ▶ IRAS
- ▶ ISO
- ▶ JWST
- ▶ Transiting Planets

Splicing

Carlos Briones
Centro de Astrobiología (CSIC/INTA), Consejo Superior de Investigaciones Científicas, Madrid, Spain

Synonyms

RNA splicing

Definition

In genetics and molecular biology, splicing is the process by which the transcribed RNA – also known as pre-messenger RNA – is modified to produce messenger RNA ready to be translated into proteins by the ribosomes. In eukaryotes, splicing takes place within the nucleus, after or concurrently with transcription. During splicing, introns – intervening, noncoding sequences present in split genes – are removed and degraded, and exons, protein-coding sequences, are covalently joined. This stepwise process is usually catalyzed by ribonucleoprotein complexes called spliceosomes. In turn, autocatalytic splicing is produced when certain introns are able to splice themselves out of the messenger RNA. Thus, the first ribozyme discovered was a self-splicing intron present in the precursor of the large subunit ribosomal RNA of the ciliate protozoan *Tetrahymena thermophila*.

See Also

- ▶ Exon
- ▶ Gene
- ▶ Gene Expression
- ▶ Genetics
- ▶ Intron
- ▶ Ribozyme
- ▶ RNA
- ▶ Transcription
- ▶ Translation

Split

- ▶ Dichotomy, Planetary

Spontaneous Generation, History of

Stéphane Tirard
Centre François Viète d'Histoire des Sciences et des Techniques EA 1161, Faculté des Sciences et des Techniques de Nantes, Nantes, France

Keywords

Animalcules; Origins of life

Definition

Spontaneous generations have a very long history from antiquity to the nineteenth century. From the seventeenth century, there have been three successive and important experimental approaches to this problem. From the debate between Louis Pasteur (1822–1895) and Félix Archimède Pouchet (1800–1872), the scientific community has been broadly rejecting the spontaneous generations.

Overview

The idea of spontaneous generations consists in the possibility of the formation of the living being from inert matter. This idea is extremely ancient and comes from antiquity. For example, the Greek philosopher Aristotle (384–322 BCE) claimed that spontaneous generations existed in nature. From the seventeenth century, there have been three successive and important experimental approaches of this problem.

In 1668, the Italian naturalist Francesco Redi (1626–1697) published the results of his experiments on the possible spontaneous generation of flies. He accurately showed that the larvae of flies never developed in bottles containing meat if the former were closed by gauze. Indeed, in this case, female flies were not able to lay on meat. Therefore, Redi's results argued against the spontaneous generation of insects and visible animals.

However, the discussion carried on during the eighteenth century. For example, the French naturalist Buffon (1707–1788) claimed that spontaneous generations formed each species at the beginning of life on Earth and that spontaneous generations of animalcules occurred in nature. Consequently, according to him, after the cooling of the primitive Earth, the origin of life was the fact of spontaneous generations.

During the eighteenth century, an important scientific debate about the spontaneous generations took place. It notably opposed Joseph Needham (1713–1781) and Lazzaro Spallanzani (1729–1799). The former claimed that in his experiments he had proven the spontaneous generations of animalcules. Indeed, he had placed hot sheep juice in closed bottles and maintained them on warm ash during several minutes to purify them. A few days later, microscopic animalcules had appeared. But Spallanzani did not accept these results. He repeated the experiments, heating and closing the bottles differently, and animalcules never developed. Arguing about their results, Needham, who was an excellent microscopist, very close to Buffon, claimed that Spallanzani had destroyed the vital force because of too much heating.

The debate was not limited to a circle of naturalists and strongly interested philosophers: Denis Diderot (1713–1784) supported the spontaneous generation theory, whereas Voltaire did not.

At the beginning of the nineteenth century, the discussion about the possible existence of spontaneous generations was far from being closed. For example, the French naturalist Lamarck took a significant interest in spontaneous generations in his theory on the transformation of species.

The debate between Pouchet and Pasteur is the main and final episode of the history of this biological problem. As a supporter of spontaneous generations, Pouchet published several papers and a book on heterogenesis at the end of the 1850s. Then, in 1860, the Academy of Sciences of Paris created a contest about the experimental proofs of spontaneous generation. At the time, the debate between Pouchet and Pasteur was very active and they discussed their own protocols and experimental results. In his experiments, Pasteur showed that microorganisms appeared in sterilized solutions containing organic mixture, only if there was a contamination from the environment. In his conclusions, Pasteur firmly asserted that he had proved the inexistence of spontaneous generations. Pasteur's position on the spontaneous generations was linked to his conception of life. Indeed, according to him, the molecular dissymmetry in living beings could be the proof of an impassable frontier between inert and living bodies.

In 1862, the Academy of Sciences of Paris favored Pasteur, and from this date, the scientific community has been broadly rejecting the spontaneous generations.

See Also

- ▶ Buffon's Conception of Origins of Life
- ▶ Lamarck's Conception of Origins of Life
- ▶ Life

References and Further Reading

Farley J (1977) Spontaneous generation from Descartes to Oparin, 2nd edn. Johns Hopkins University Press, Baltimore

Spore

Wayne L. Nicholson[1,2] and Ralf Moeller[3]
[1]Space Life Sciences Laboratory, University of Florida, Merritt Island, FL, USA
[2]Space Life Sciences Laboratory, Kennedy Space Center, University of Florida, Gainesville, FL, USA
[3]German Aerospace Center (DLR), Institute of Aerospace Medicine, Cologne, Germany

Keywords

Bacillus; *Clostridium*; Endospore

Definition

A small, usually single-celled asexual reproductive body produced by many nonflowering plants, ▶ fungi, protozoans, and ▶ bacteria that is capable of developing into a new individual without sexual fusion.

History

For information on the early history of microbiology, including the discovery of the bacterial spore, the reader is directed to Brock (1999) and de Kruif (1926). A short history of early milestones in *Bacillus* spore research can be found in Nicholson (2004).

Overview

This entry will concentrate on bacterial spores, upon which the most information has been gathered. When faced with nutrient starvation, bacteria of several genera, most notably *Bacillus* and *Clostridium*, possess the ability to differentiate from actively growing cells into dormant resting structures called ▶ endospores, or spores. In the context of astrobiology, bacterial spores are important organisms to study for a number of reasons.

First, bacterial spores can persist in the environment for at least millennia and are arguably the longest-lived organisms known (reviewed in Nicholson 2004). Spores are globally distributed and are found in ▶ extreme environments around the world. The underlying mechanisms of why spores exhibit such incredible hardiness have been the subject of intense study for the past half-century. Spores are highly resistant to being killed by a large range of physical parameters such as extremes of temperature, radiation, or pressure, as well as by various chemical disinfectants. Some of the various mechanisms of spore resistance are quite well understood at the molecular level, such as resistance to ultraviolet radiation (reviewed in Nicholson et al. 2000, 2005; Setlow 2006). However, the molecular details of spore resistance to other lethal treatments, such as heat, pressure, or certain chemicals, are not as well understood and are the subjects of current research.

Second, because of their notorious resistance and longevity, spores have been studied as possible candidates for natural transfer of life between the planets. This theory, variously dubbed "▶ panspermia," "▶ lithopanspermia," or "transpermia," postulates that viable microorganisms, residing within meteors ejected from a planet's surface by large impacts, could survive a trip through space to another planet (reviewed in Nicholson et al. 2000; Nicholson 2009). Spores have been shown to inhabit the interiors of near-surface igneous rocks such as ▶ granite and ▶ basalt (the most likely candidates for launch by impact) and have been experimentally demonstrated to survive the rigors of impact-mediated launch, transfer through space, high-speed atmospheric entry, and landing (reviewed in Fajardo-Cavazos et al. 2007; Nicholson 2009).

Third, spores are important in the field of ▶ planetary protection. By international convention, spacecraft sent on life-detection missions to other planets must meet rigorous criteria for

disinfection, to avoid the risk of contaminating the target planet with Earth microbes (Rummel 2001; reviewed in Nicholson et al. 2009). To comply with planetary protection requirements, robotic landers and rovers are assembled in ultraclean rooms inside Spacecraft Assembly Facilities (SAFs). Interestingly, precisely because of their environmental ubiquity and resistance to killing by chemical and physical disinfection procedures, bacterial spores are common isolates from the ultraclean rooms in which spacecraft are assembled and indeed from the spacecraft themselves (Venkateswaran et al. 2001, reviewed in Nicholson et al. 2009). In fact, the most resistant spore discovered to date, *Bacillus pumilus* strain SAFR-032, was isolated from a SAF (Link et al. 2004). Therefore, it appears that ultraclean SAFs act as extreme environments which select for ▶ survival of only the hardiest microbes, such as spores – and these are exactly the types of organisms best able to survive the journey through space (Link et al. 2004; Crawford 2005). For these reasons, spores pose a particular risk of contaminating spacecraft sent on life-detection missions to destinations such as ▶ Mars, Jupiter's moon ▶ Europa, or Enceladus (Nicholson et al. 2009).

Future Directions

Unlike rocks transferred between planets by chance impacts, spacecrafts are (i) designed to be launched and landed gently, (ii) highly protected from space exposure during transit, and (iii) launched on trajectories with short transit times. Therefore, spores contaminating spacecraft would have a relatively high probability to survive a voyage between Earth and, say, Mars. However, in order for such "forward contamination" to be ecologically relevant, an organism transferred into a new extraterrestrial environment must be able not only to survive, but to grow and proliferate in that environment. Recent research has been conducted to understand the ability of bacterial spores to survive, germinate, and grow in extraterrestrial environments such as the surface or near-subsurface of Mars. To date, it has been found that the surface environment of Mars – characterized by intense UV and ionizing radiation, extreme cold, a CO_2-dominated low-pressure atmosphere, and a lack of liquid water and organic nutrients – poses a formidable barrier to survival and proliferation of spore-forming bacteria and of microbes in general (Fajardo-Cavazos et al. 2008; Nicholson and Schuerger 2005; Schuerger and Nicholson 2006; Tauscher et al. 2006).

See Also

- ▶ Bioburden
- ▶ BIOPAN
- ▶ Colonization, Biological
- ▶ Endospore
- ▶ EXPOSE
- ▶ Exposure Facilities
- ▶ Extremophiles
- ▶ Fungi
- ▶ Granite
- ▶ Lithopanspermia
- ▶ Long Duration Exposure Facility
- ▶ Planetary Protection
- ▶ Radiation Biology
- ▶ Sterilization
- ▶ STONE
- ▶ UV Radiation, Biological Effects

References and Further Reading

Brock TD (1999) Milestones in microbiology. ASM Press, Washington, DC

Crawford RL (2005) Microbial diversity and its relationship to planetary protection. Appl Environ Microbiol 71:4163–4168

de Kruif P (1926) Microbe hunters. Harcourt Brace Jovanovich, New York

Fajardo-Cavazos P, Schuerger AC, Nicholson WL (2007) Testing interplanetary transfer of bacteria by natural impact phenomena and human spaceflight activities. Acta Astronaut 60:534–540

Fajardo-Cavazos P, Schuerger AC, Nicholson WL (2008) Persistence of biomarker ATP and ATP-generating capability in bacterial cells and spores contaminating spacecraft materials under Earth and simulated Mars environments. Appl Environ Microbiol 74:5159–5167

Link L, Sawyer J, Venkateswaran K, Nicholson WL (2004) Extreme spore UV resistance of *Bacillus pumilus* isolates obtained from an ultra-clean Spacecraft Assembly Facility. Microb Ecol 47:159–163

Nicholson WL (2004) Ubiquity, longevity, and ecological roles of *Bacillus* spores. In: Rizza E, Henriques AO, Cutting SM (eds) Bacterial spore formers: probiotics and emerging applications. Horizon Bioscience Press, Wymondham, pp 1–15
Nicholson WL (2009) Ancient micronauts: interplanetary transport of endolithic microbes by cosmic impacts. Trends Microbiol 17:243–250
Nicholson WL, Schuerger AC (2005) Survival and germinability of *Bacillus subtilis* spores after incubation at Mars atmospheric pressure: implications for planetary protection and lithopanspermia. Astrobiology 5:536–544
Nicholson WL, Munakata N, Horneck G, Melosh HJ, Setlow P (2000) Resistance of bacterial endospores to extreme terrestrial and extraterrestrial environments. Microbiol Mol Biol Rev 64:548–572
Nicholson WL, Schuerger AC, Setlow P (2005) The solar UV environment and bacterial spore UV resistance: considerations for Earth-to-Mars transport by natural processes and human spaceflight. Mutat Res 571:249–264
Nicholson WL, Schuerger AC, Race MS (2009) Migrating microbes and planetary protection. Trends Microbiol 17:389–392
Rummel JD (2001) Planetary exploration in the time of astrobiology: protecting against biological contamination. Proc Natl Acad Sci U S A 98:2128–2131
Schuerger AC, Nicholson WL (2006) Interactive effects of hypobaria, low temperature, and CO_2 atmosphere inhibit the growth of mesophilic *Bacillus* spp. under simulated Martian conditions. Icarus 185:143–152
Setlow P (2006) Spores of *Bacillus subtilis*: their resistance to and killing by radiation, heat and chemicals. J Appl Microbiol 101:514–525
Tauscher C, Schuerger AC, Nicholson WL (2006) Survival and germinability of *Bacillus subtilis* spores exposed to simulated Mars solar radiation: implications for life detection and planetary protection. Astrobiology 6:592–605
Venkateswaran K, Satomi M, Chung S, Kern R, Koukol R, Basic C, White D (2001) Molecular microbial diversity of a spacecraft assembly facility. Syst Appl Microbiol 24:311–320

Sporicide

Catharine A. Conley
NASA Headquarters, Washington, DC, USA

Definition

A sporicide is a compound that kills microbial spores.

See Also

► Spore

Sporogenesis

► Sporulation

Sporulation

Gerda Horneck
DLR German Aerospace Center, Institute of Aerospace Medicine, Radiation Biology, Köln, Germany

Synonyms

Sporogenesis

Definition

Sporulation is a differentiation process of bacteria and fungi by which a vegetative cell becomes converted into a dormant structure. Bacteria of the genus *Bacillus* and *Clostridium* form ► endospores, i.e., spores inside the cell at the end of their growth period when nutrients become limited. During the different stages of the sporulation cycle, different proteins are synthesized. Sporulation includes the following subsequent steps: structural changes of DNA, septum formation, separation of ► spore DNA, synthesis of a prespore, engulfment, forespore formation, cortex formation, deposition of spore coats, spore maturation, lyses of the sporangium, and release of the spore. The released spore is more resistant to environmental stressing conditions than the vegetative mother cell.

See Also

- ▶ Endospore
- ▶ Spore

SPR

- ▶ Surface Plasmon Resonance

S-Process

Nikos Prantzos
Institut d'Astrophysique de Paris, Paris, France

Definition

The s-process is one of the two main nucleosynthesis processes forming nuclei heavier than those of the iron peak. Neutron captures are slower than beta-decays (hence the s, for *slow*), keeping the flow of matter on the nuclear stability valley. The s-process occurs during helium fusion in stars, neutrons being released through $^{13}C(\alpha, n)$ or $^{22}Ne(\alpha, n)$, on timescales of 10^4 years. The latter reaction operates in the cores of massive stars and produces the light s-nuclei (with mass number $A < 90$, like Sr), while the former operates during shell He burning in ▶ asymptotic giant branch (AGB) stars and produces the heavier s-nuclei (up to ^{208}Pb).

See Also

- ▶ Asymptotic Giant Branch Star
- ▶ Nucleosynthesis, Stellar
- ▶ R-Process
- ▶ Stellar Evolution

Sputtering

William M. Irvine
University of Massachusetts, Amherst, MA, USA

Definition

Sputtering is the process in which a solid surface, as of an ▶ interstellar dust grain, is eroded by the impact of atoms or ions from the gas phase. Chemical sputtering occurs when the impacting particle has relatively low kinetic energy, chemical bonds are formed between it and the surface, and desorption of a newly formed molecule incorporating surface atoms occurs. Physical sputtering occurs when the impacting particle simply knocks surface atoms into the gas; this process can involve either thermal motion for high temperature gas or nonthermal impact if a solid particle and the gas have high relative velocities. Sputtering of interstellar grains commonly occurs in shocks.

See Also

- ▶ Interstellar Dust
- ▶ Molecular Desorption
- ▶ Shock, Interstellar

Square Kilometre Array

Jeff Wagg, Jimi Green, Tyler Bourke,
Robert Braun, Phil Diamond, William Garnier
and Mathieu Isidro
Square Kilometre Array Organisation,
Macclesfield, Cheshire, UK

Keywords

Radio; Astronomy; Instrumentation

Definition

The Square Kilometre Array (SKA) will be the largest radio telescope in the world for observations at centimeter and meter wavelengths. It is an international project involving about 20 countries in the design effort, coordinated by the SKA Organisation. The SKA is planned to be built in two phases, with the first consisting of three radio interferometers located at two sites, one in Western Australia and one in South Africa. The second phase is intended to deliver ten times the capability of the first phase. The SKA will deliver transformational science in a number of astronomy and physics fields and produce data at a rate ten times the 2013 global Internet traffic.

History

The original concept that would later evolve into the SKA began formulating in the late 1980s and was led by a group from the Netherlands. This idea was discussed with members of the UK astronomy community in 1990 at the 10th anniversary meeting of the Very Large Array, and in 1993 the International Union of Radio Science (URSI) established the Large Telescope Working Group to develop the scientific goals and technical specifications for a next-generation radio observatory. In 1997, eight institutions from six countries (Australia, Canada, China, India, the Netherlands, and the USA) signed a memorandum of agreement to cooperate in a technology study. The number of countries increased to 11 during 1999 for the creation of the International Square Kilometre Array Steering Committee (ISSC). In 2007, an international SKA Project Office was established in the UK. The Square Kilometre Array Organisation (SKAO) was then established in 2011 as a nonprofit company in the UK to formalize relationships between the international partners and to centralize the leadership of the project. In 2012 it was agreed that phase 1 of the SKA should be built on two sites in Western Australia and South Africa, both chosen for their remarkable radio quietness. The SKAO is located at the Jodrell Bank Observatory in Manchester, UK. As of October 2014, members of the SKA Organisation are Australia, Canada, China, Germany, India, Italy, New Zealand, South Africa, Sweden, the Netherlands, and the UK.

Overview

Phase 1 of the SKA (SKA1) is being designed by 11 engineering consortia (with global representation) and coordination from the SKAO. Construction is expected to begin in 2017–2018, with early science observations in 2020. The baseline design of SKA1 incorporates a low-frequency aperture array (SKA1-LOW), a mid-frequency antenna array (SKA1-MID), and a phased array feed-equipped antenna array (SKA1-SURVEY). During SKA1 operations, Western Australia will host both SKA1-LOW and SKA1-SURVEY. SKA1-MID will operate in the Karoo desert of South Africa. The SKA1 telescopes will take advantage of the existing infrastructure at the two sites. There are three SKA precursors: MeerKAT, located in South Africa, and the Australian SKA Pathfinder (ASKAP) and the Murchison Widefield Array (MWA), both located in Western Australia. The infrastructure of MeerKAT will be combined with SKA1-MID, while the infrastructure of ASKAP will be incorporated into SKA1-SURVEY.

Phase 2 of the SKA (SKA2) is planned to provide ten times the capability of SKA1, by expanding significantly the number of SKA1 elements and by incorporating other technologies such as very wide band antenna feeds and higher-frequency aperture arrays.

There is a broad spectrum of science goals that will be addressed by the SKA. In phase 1, headline science includes testing general relativity in the strong field regime through surveys and timing of pulsars in the Milky Way and studying the reionization history of the Universe through measurements of brightness temperature fluctuations in 21 cm atomic hydrogen during the Epoch of Reionization and Cosmic Dawn. The SKA will investigate radio emission from objects within our own galaxy and others. The astrobiology

science goals include the detection of prebiotic molecules in our own galaxy, the imaging of cm size dust grains in protoplanetary disks, and the search for extraterrestrial intelligence (SETI).

See Also

- ▶ Long Wavelength Astronomy
- ▶ Protoplanetary Disk
- ▶ Pulsar
- ▶ Radio Astronomy
- ▶ SETI

References and Further Reading

Carilli C, Rawlings S (eds) (2004) Science with the Square Kilometre Array. New Astronomy Reviews, vol 48. Elsevier

SRB

- ▶ Sulfate Reducers

SSB

Michel Viso
CNES/DSP/SME, Vétérinaire/DVM, Astro/Exobiology, Paris Cedex 1, France

Definition

The Space Studies Board is a unit of the US National Research Council. The original charter of the Space Science Board was established in June 1958. The Space Science Board became in 1989 the Space Studies Board (SSB) and provided expert external and independent scientific and programmatic advice on a continuous basis from NASA's inception until the present. Today, the SSB is providing an independent, authoritative forum for information and advice on all aspects of space science and applications. The SSB also serves as the US National Committee for the Committee on Space Research (COSPAR) of the International Council for Science.

The Board is composed of prominent scientists, engineers, industrialists, scholars, and policy experts in space research appointed for 2-year staggered terms. The Board itself does not conduct studies, but it oversees advisory studies and program assessments conducted by ad hoc study committees formed in response to a request from a sponsor. It publishes the reports of such studies. Decadal surveys are a major outcome from the SSB, providing strategic direction to NASA and other agencies on the top priorities over the next 10 years in astronomy and astrophysics, solar system exploration, solar and space physics, and Earth science.

Concerning astrobiology, the SSB issued numerous reports beyond the decadal surveys about ▶ Mars exploration, ▶ planetary protection, and mission categorization. Special focus was given to the ▶ Mars Sample Return mission.

References and Further Reading

http://sites.nationalacademies.org/SSB/index.html

SS-Bond

- ▶ Disulfide Bond

SST

- ▶ Spitzer Space Telescope

Stable Isotopes

Vincent Busigny
Institut de Physique du Globe de Paris, Paris, France

Keywords

Isotopes; Isotope fractionation; Fractionation factor; Stable isotopes; Nontraditional

Definition

The term isotope defines the various forms of a chemical element, characterized by the same number of protons but different numbers of neutrons in their nucleus. Isotopes share the same atomic number and location in the periodic table, but have distinct atomic weights. Two types of isotopes can be distinguished: radioactive or stable. Stable isotopes of a single element have roughly identical properties due to similar electronic configuration and atomic size, but their mass differences induce variations in terms of bound energy and chemical reactivity. In a specific process, stable isotopes are thus fractionated according to either equilibrium or kinetic reactions.

History

Stable isotope geochemistry was born around 1945, and its first application was dedicated to geothermometry (Urey 1947). Experimental applications were initiated by McCrea (1950) and illustrated by the early work of Urey et al. (1951) on ambient paleotemperatures of the Upper Cretaceous in the northern hemisphere, measuring oxygen isotopes in carbonates. Since then the development of stable isotope geochemistry has been rapid and exponential, with applications to all kinds of geological and extraterrestrial environments.

Overview

Stable isotopes in natural environments have been identified for 81 elements, from hydrogen to lead. Contrasting with radioactive isotopes, which are mostly used for dating or deciphering mixing processes, stable isotopes can be applied to trace any type of physicochemical reaction such as diffusion, dissolution/precipitation, oxidation/reduction, acid/base exchange, evaporation/condensation, or adsorption. Stable isotopes can be useful to distinguish biotic from abiotic signatures recorded in ancient terrestrial rocks or meteorites. For extensive reviews on stable isotopes and their use in geochemistry, the reader should refer to textbooks such as Criss (1999) and Hoefs (2004).

Stable isotopes are presently classified as either "traditional" or "nontraditional." Traditional stable isotopes refer to isotopic tracers developed since the earliest works in the 1950s and include systems such as C, O, H, N, or S. A common feature of these traditional stable isotopes is the analytical method based largely on gaseous Isotope Ratio Mass Spectrometry (IRMS). For instance, C and N isotope compositions are measured on the molecules CO_2 and N_2, respectively. Nontraditional stable isotopes refer to isotopic systems developed more recently (since the 1990s) and include heavy metals such as Fe, Cu, Zn, Cr, Se, and Mo and alkali or alkaline earth metals such as Li, Mg, and Ca. These elements are usually separated from sample matrix using aqueous chemistry and chromatographic methods. Isotope analyses are performed either on solid using thermoionization mass spectrometry (TIMS) or aqueous solution using multicollector inductively coupled plasma mass spectrometry (MC-ICPMS). It is likely that nontraditional stable isotopes may become traditional in the next few decades, and this term may need to be revised. Recent reviews on traditional and nontraditional stable isotopes have been published in volumes of Reviews in Mineralogy and Geochemistry (Valey and Cole 2001; Johnson et al. 2004).

Basic Methodology

Stable isotope compositions are generally reported in δ notation, which is a deviation of an isotopic ratio relative to the same ratio in a standard, and can be written as

$$\delta^i E = \left(\frac{R^{i/j}_{spl} - R^{i/j}_{std}}{R^{i/j}_{std}} \right) \times 10^3$$

where R is the ratio of the two stable isotopes i and j of element E, spl is the sample of interest,

and *std* is the standard reference material. The δ unit is expressed in parts per thousand or "per mil," noted ‰. The ratio *i/j* usually corresponds to heavy over light isotopes so that positive δ *v*alue indicates that the sample is enriched in heavy isotope relative to the standard (and vice versa). A careful examination of the standard material is thus crucial when considering δ values. For traditional stable isotopes, the standards are well established. For instance, carbon stable isotope composition (ratio $^{13}C/^{12}C$) is always expressed as $\delta^{13}C$ relative to the fossil marine carbonate standard (PDB), while the standard for hydrogen isotope composition (D/H ratio) is Standard Mean Ocean Water (SMOW). In contrast, for recent "nontraditional" stable isotopes, data from the literature are sometimes reported relative to various standards (e.g., igneous rock or IRMM-014 synthetic metal for Fe isotope composition, see Craddock and Dauphas (2010)).

Isotope fractionations between species or phases can be determined experimentally or predicted from theoretical calculation (e.g., Richet et al. 1977). The isotopic fractionation factor associated to an isotope exchange reaction between two species *A* and *B* is defined as:

$$\alpha_{A-B} = \frac{R_A^{i/j}}{R_B^{i/j}}$$

and can be expressed in terms of δ values as

$$\alpha_{A-B} = \frac{1,000 + \delta^i E_A}{1,000 + \delta^i E_B}$$

The isotope fractionation between two species *A* and *B* represents the difference between their isotope compositions and can be related to the fractionation factor using the following formulae (e.g., Criss 1999):

$$\Delta_{A-B} = \delta^i E_A - \delta^i E_B \approx 1,000.\ ln\alpha_{A-B}$$

Applications

Stable Isotopes in Astrobiology

The main questions in astrobiology concern the origin and evolution of life on Earth and whether life may have risen elsewhere in the Solar System and on extrasolar planets. Stable isotopes are powerful tools for tracing microbial processes and the origin of biomolecules in various geological and extraterrestrial systems. Applications range from direct analyses of organic components to identification of biominerals, formed through biological-induced (extracellular) or biological-controlled (intracellular) pathways. One of the key observations is that traditional stable isotope systems such as C, H, N, O, and S all represent the basic components of life. This was recognized very early in studies of stable isotope geochemistry, so that these systems were rapidly used for searching for life signatures in the geological record. The most famous system is probably C isotopes, and one of its well-known applications can be summarized as follows. Inorganic carbon assimilation by autotrophic organisms is based on various carboxylation pathways with specific kinetic isotope fractionations, favoring light isotope assimilation. Organic carbon is thus ^{12}C enriched relative to the source of inorganic carbon (DIC: dissolved inorganic carbon), with an isotopic fractionation $\Delta^{13}C_{DIC\text{-}Corg}$ generally between −20 ‰ and −30 ‰ (see review in Thomazo et al. 2009). In contrast, carbonate precipitation from dissolved inorganic carbon roughly records the composition of the source (i.e., the equilibrium isotope fractionation is ~1 ‰). The difference of isotope compositions between carbonate and organic carbon coexisting within a single rock sample can thus be used to determine if organic carbon is related to biological activity or not and eventually define the C assimilation pathway. This feature was recognized in the 1970s and has been used to infer the existence of life on Earth as early as 3.8 Ga ago (Schidlowski 1988). The virtue of stable isotopes

for life identification is that even though a rock experienced strong modifications of structure and mineralogy due to metamorphism, the primary isotope signature may be preserved.

A Reliable Biosignature?

An important limit on the application of stable isotopes as tracers of life is that abiotic processes may mimic isotope fractionations usually ascribed to biogenic origin. For instance, several experimental studies demonstrated that the production of organic carbon through abiotic pathways such as ▶ Fischer-Tropsch-Type Reaction generates C isotope compositions similar to those expected for biological pathways. Thus the question of the origin of ▶ methane on Mars and Titan (which has been suggested to derive from bacterial methanogenesis or abiotic ▶ serpentinization process) will probably not be solved from C isotopes alone. One possibility to explore further may be the simultaneous measurement of C and H isotopes in methane and other types of hydrocarbons (Sherwood Lollar et al. 2002).

Sulfur isotope composition recorded in ancient sedimentary sulfides may represent one of the most reliable isotopic biomarkers, with no abiotic counterpart. Indeed, bacterial sulfate reduction (BSR) produces a strong kinetic isotope fractionation, favoring the light S isotopes in the hydrogen sulfide product by ~45 ‰ in terms of $^{34}S/^{32}S$ ratio (see the pioneer work by Harisson and Thode 1958). When aqueous Fe^{2+} is present, hydrogen sulfide immediately precipitates as FeS and is then transformed into pyrite (FeS_2). Watanabe et al. (2009) showed experimentally that abiotic thermochemical sulfate reduction produces hydrogen sulfide either enriched or depleted in light S isotopes, with a range of $\Delta^{34}S_{SO4\text{-}H2S}$ from −20 ‰ to +5 ‰. The record of very negative $\delta^{34}S$ values in pyrite thus remains an unchallenged tracer of bacterial sulfate-reduction activity. The main drawback of this method is that the expression of the isotope fractionation depends strongly on the size of the sulfate reservoir. At low sulfate concentrations, the uptake and reduction of sulfate by microorganisms does not result in significant discrimination between sulfur isotopes and, therefore, does not produce significant fractionations. In contrast, at high sulfate concentration, large isotope fractionation can be efficiently transferred to sedimentary sulfides. Based on this interpretation, the long-term evolution of the sulfur isotope record on terrestrial sediments has been interpreted to reflect the response of sulfate-reducing bacteria to changes in oceanic sulfate concentrations (Canfield et al. 2000).

Future Directions

The identification of biological activity from a single isotope system is limited by the possibility of producing similar isotope fractionation from abiotic reactions. Unequivocal evidence for life will require the combination of several isotope tracers (C and H in methane, S and Fe in iron sulfides, Fe and O in iron oxides, Ca, Mg, Fe, C, and O in carbonates. . .). Additionally, a coupling with other methods such as mineralogy (shape, size, crystallinity) or chemistry (e.g., purity) will put further constraints on potential biological origin as exemplified by multidisciplinary study of the Martian meteorite ▶ ALH 84001 (McKay et al. 1996). A promising field, which grows with improvement of the analytical precision on stable isotope measurements, is the analysis of multiple-isotope systems for elements that possess three or more isotopes (e.g., O, S). Once calibrated, application of these systems may provide useful tools for distinguishing biological from abiotic pathways (Farquhar et al. 2003).

See Also

- ▶ Carbon Isotopes as a Geochemical Tracer
- ▶ Fischer-Tropsch Effects on Isotopic Fractionation
- ▶ Fractionation, Mass Independent and Dependent
- ▶ Iron Isotopes
- ▶ Isotopic Exchange Reaction

- ▶ Isotopic Fractionation (Interstellar Medium)
- ▶ Isotopic Ratio
- ▶ Nitrogen Isotopes
- ▶ Oxygen Isotopes
- ▶ Silicon Isotopes
- ▶ Sulfur Isotopes
- ▶ Transition Metals and Their Isotopes

References and Further Reading

Canfield DE, Habicht KS, Thamdrup B (2000) The Archean sulfur cycle and the early history of atmospheric oxygen. Science 288:658–661

Craddock PR, Dauphas N (2010) Iron isotopic compositions of geological reference materials and chondrites. Geostand Geoanal Res 35:101–123

Criss RE (1999) Principles of stable isotope distribution. Oxford Univ Press, New York

Farquhar J, Johnston DT, Wing WA, Habitch KS, Canfield DE, Airieau S, Thiemens MH (2003) Multiple sulphur isotopic interpretations of biosynthetic pathways: implications for biological signatures in the sulphur isotope record. Geobiology 1:27–36

Harrison AG, Thode HG (1958) Mechanism of the bacterial reduction of sulphate from isotope fractionation studies. Trans Faraday Soc 54:84–92

Hoefs J (2004) Stable isotope geochemistry, 5th edn. Springer, Berlin

Johnson CM, Beard BL, Albarede F (eds) (2004) Geochemistry of non-traditional stable isotopes. Rev Mineral Geochem 55:454

McCrea JM (1950) On the isotopic chemistry of carbonates and a paleotemperature scale. J Chem Phys 18:849–857

McKay DS, Gibson EK Jr, Thomas-Keprta KL, Vali H, Romanek CS, Clemet SJ, Chillier XDF, Maechling CR, Zare RN (1996) Search for past life on Mars: possible relic biogenic activity in Martian meteorite ALH84001. Science 273:924–930

Richet P, Bottinga Y, Javoy M (1977) A review of hydrogen, carbon, nitrogen, oxygen, sulphur and chlorine stable isotope fractionation among gaseous molecules. Ann Rev Earth Planet Sci 5:65–110

Schidlowski M (1988) A 3800-million-year isotopic record of life from carbon in sedimentary rocks. Nature 333:313–318

Sherwood Lollar B, Westgate T, Ward J, Slater GF, Lacrampe-Couloume G (2002) Abiogenic formation of alkanes in the Earth's crust as a minor source for global hydrocarbon reservoirs. Nature 416:522–524

Thomazo C, Pinti DL, Busigny V, Ader M, Hashizume K, Philippot P (2009) Biological activity and the Earth's surface evolution: insights from carbon, sulfur, nitrogen and iron stable isotopes in the rock record. C R Palevol 8:665–678

Urey HC (1947) The thermodynamic properties of isotopic substance. J Chem Soc 2:562–581

Urey HC, Lowenstam HA, Epstein S, McKinney CR (1951) Measurement of paleotemperatures and temperatures of the Upper Cretaceous of England, Denmark, and the southeastern United States. Bull Geol Soc Am 62:399–416

Valley JW, Cole DR (eds) (2001) Stable isotope geochemistry. Rev Mineral Geochem 43:531

Watanabe Y, Farquhar J, Ohmoto H (2009) Anomalous fractionations of sulfur isotopes during thermochemical sulfate reduction. Science 324:370–373

Stagnant Lid Convection

Doris Breuer
German Aerospace Center (DLR), Institute of Planetary Research, Berlin, Germany

Definition

Stagnant lid convection is a form of convection that occurs in a material with strongly temperature dependent viscosity for a viscosity contrast larger than about 10^4. It is characterized by an upper stagnant layer – the stagnant lid – that forms on top of the convecting layer. Heat in the stagnant lid is transported mainly by heat conduction. Stagnant lid convection is typical of ▶ mantles of the ▶ terrestrial planets, ▶ Mercury, ▶ Mars and ▶ Venus and large rocky satellites such as the Moon. Stagnant lid convection may also occur in the ice layers of the icy satellites of the outer ▶ Solar System. Stagnant lid planets are usually also one-plate ▶ planets. Their tectonic style differs substantially from planets with mobile lid convection or ▶ plate tectonics like Earth. Here, the near-surface layers take part in the convective flow and are recycled with the interior.

See Also

- ▶ Interior Structure, Planetary
- ▶ Mantle
- ▶ Mars
- ▶ Mercury

- ▶ Moon, The
- ▶ Planet
- ▶ Plate Tectonics
- ▶ Satellite or Moon
- ▶ Solar System, Inner
- ▶ Terrestrial Planet
- ▶ Venus

Star

Patrick Eggenberger[1] and Sylvia Ekström[2]
[1]Geneva Observatory, University of Geneva, Geneva, Switzerland
[2]Observatoire Astronomique de l'Université de Genève, Faculté des Sciences, Université de Genève, Versoix, Switzerland

Keywords

Hydrostatic equilibrium; Nuclear reactions; Nucleosynthesis

Definition

Stars are spheres of plasma in hydrostatic equilibrium, where the inward force of gravity is balanced by the outward gas pressure. The energy source for the gas is partly gravitational, but mostly nuclear, resulting from thermonuclear fusion reactions in the hot stellar interior. Stars form by contraction of a portion of a molecular cloud.

Overview

Stars are spheres of gas that can most of the time be considered as in hydrostatic and radiative equilibrium. They form during the contraction of cold molecular clouds. In the process of star formation, a part of the original matter of the cloud may form a disk around the star, and in such a disk planets could be built.

At the center of the collapsing cloud, the temperature rises until it is sufficient for nuclear reactions to take place; thus, a new star is born. Through these reactions, new chemical elements are synthesized (nucleosynthesis) accompanied by a production of energy. The energy release sustains the star against its own gravity. Successive fusion phases can be identified in the course of the evolution of stars: deuterium and lithium at the very beginning of the evolution and then hydrogen (Main sequence). Stars more massive than 0.5 $M_{\odot}$ go on with a phase of helium fusion ("burning") and the ones more massive than 8–9 $M_{\odot}$ enter the advanced phases: carbon burning, neon photodisintegration, oxygen, and eventually silicon burning.

The way stars end their evolution depends on their initial mass: below 8–9 $M_{\odot}$, they experience a strong wind evaporating their external layers and they end as white dwarfs surrounded sometimes by a planetary nebula. Above 9 $M_{\odot}$, stars end their evolution in the explosion of a ▶ supernova. The remnant may be a neutron star or a black hole, depending on the mass of the iron core at the time of the collapse.

Stars are the source of all the heavy elements in the Universe. The products of nucleosynthesis that occurs in their core are spread in the interstellar medium by the winds or the supernova explosion, contributing to the general chemical enrichment of galaxies.

See Also

- ▶ Asteroseismology
- ▶ High-Mass Star
- ▶ Low Mass Star
- ▶ Main Sequence, Star
- ▶ Protoplanetary Disk
- ▶ Protostars
- ▶ Star Formation, Observations
- ▶ Stellar Evolution
- ▶ Supernova

Star Counts

William M. Irvine
University of Massachusetts, Amherst, MA, USA

Definition

Counting the number of stars per unit area on the sky, when compared to the equivalent "star count" in an adjacent region of the sky, can illustrate the presence of extinction by ▶ interstellar dust.

See Also

▶ Extinction, Interstellar or Atmospheric
▶ Interstellar Dust

Star Dust

Sun Kwok
Faculty of Science, The University of Hong Kong, Hong Kong, China

Keywords

Infrared spectroscopy; Evolved stars; Stellar winds

Synonyms

Circumstellar grains

History

The fact that stars can manufacture solid-state particles in large quantities (stardust) was first recognized through the discovery of infrared excess in the spectra of evolved stars. Infrared spectrophotometric observations in the late 1960s have revealed that stars in the ▶ asymptotic giant branch (AGB) of evolution show excess emission above the stellar photospheric continuum emission (Woolf and Ney 1969). This excess is interpreted as the result of thermal emission by micron-size solid particles (grains) heated by the stellar radiation. These solid particles absorb visible light from the star and reemit the energy in the infrared.

Overview

Stardust also manifests itself through the absorption of starlight. Circumstellar dust can cause very large extinction in the visible. In extreme cases, the entire photospheric output of a star is converted to dust emission, making the star itself extremely faint or even invisible in optical light (Volk et al. 1992). The most well-known examples of such stars are IRC+10216 and AFGL 3068, which are very bright in the infrared but very faint in the visible.

In terms of chemical composition, stardust can be either oxygen rich or carbon rich. The most common kinds of oxygen-rich solid particles are amorphous silicates, which manifest themselves through their Si–O stretching mode at 9.7 μm and the Si–O–Si bending mode at 18 μm. In the *Infrared Astronomical Satellite* (▶ *IRAS*) low-resolution spectrometer (LRS) all-sky survey, over 4,000 oxygen-rich AGB stars were found (Fig. 1). The most common kind of carbon-rich stardust is silicon carbide, which is detected in over 700 carbon-rich AGB stars (Kwok et al. 1997).

In addition to amorphous silicates and silicon carbide, silicate minerals (olivines and pyroxenes) as well as several refractory oxides are also made in the circumstellar envelopes of AGB stars. A broad feature centered around 13 μm, first discovered by the IRAS LRS, could be due to corundum (α-Al_2O_3, which has a feature at 12.7 μm), glass (amorphous SiO_2, 12.3 μm), spinel ($Mg_2Al_2O_4$, 12.95 μm), or rutile (TiO_2, 13.4 μm). An emission feature at 19.5 μm

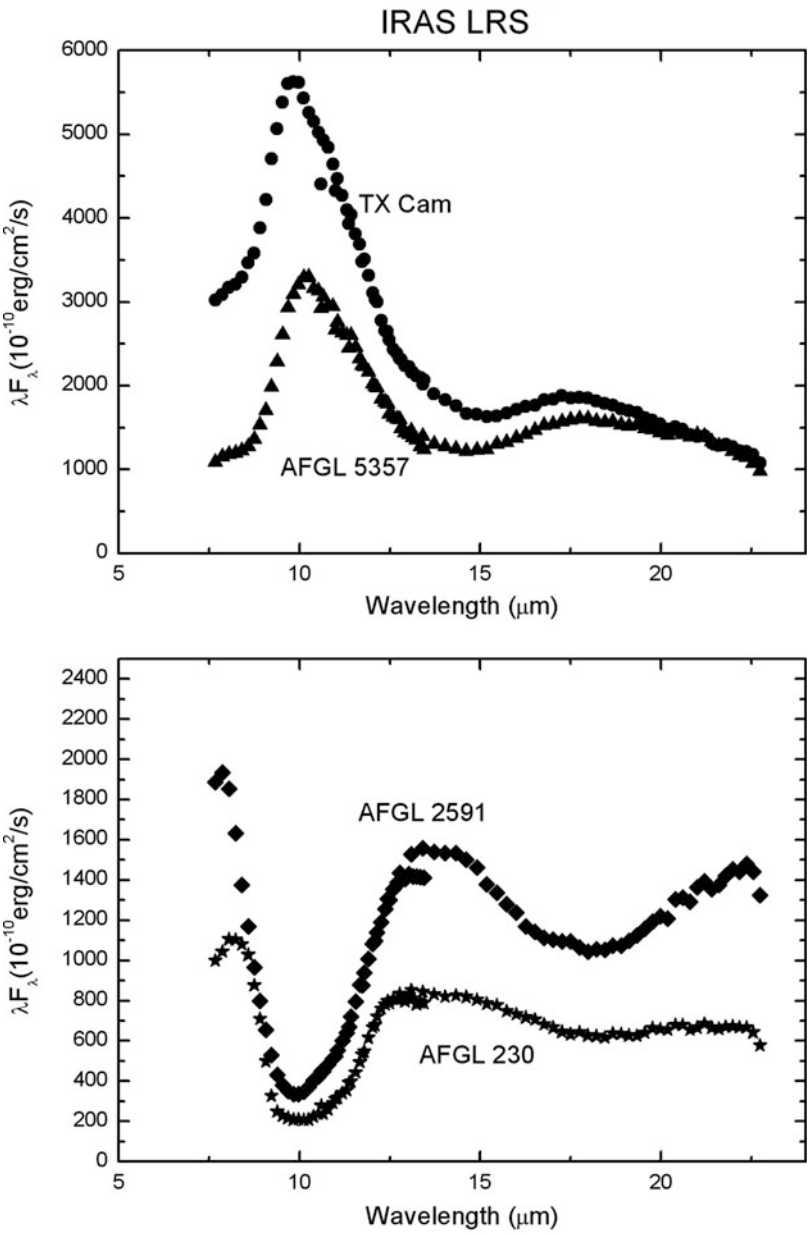

Star Dust, Fig. 1 Infrared spectra of amorphous silicates. The 9.7 and 18 μm features of silicates can be seen both in emission (*top panel*) and in self-absorption (*bottom panel*). Data obtained from the low-resolution spectrometer observations from the ▶ *Infrared Astronomical Satellite*

observed by ▶ *ISO* has been attributed to a mixture of Mg-Fe-oxides (e.g., $Mg_{0.1}Fe_{0.9}O$) (Posch et al. 1999, 2002). The detection of minerals in stellar environments has led to the establishment of the field of astromineralogy (Henning 2003).

Stardust of organic composition has also been found in carbon-rich ▶ planetary nebulae. Organic stardust has not been detected in AGB stars, suggesting that these particles are synthesized in the post-AGB phase of evolution, after the synthesis of gas phase molecules such as acetylene and benzene (Kwok 2004).

Stardust can also be found in the vicinity of young stars, Wolf-Rayet stars, planetary nebulae, ▶ novae, and ▶ supernovae. The disc shape of the dust-emitting region around young stars is suggested to be the precursor of the nebula out of which planets form.

The exact mechanism of stardust formation is not known. It is usually assumed that these solid particles are the result of ▶ nucleation through collision of gas-phase molecules. When the particles are far enough from the stellar surface such that the radiation temperature of the particles has fallen below the condensation temperature of the solid, it will condense spontaneously, similar to soot formation in a flame. Spectral monitoring of novae has shown that novae change from a gaseous free-free spectrum to a dust thermal emission spectrum over periods as short as a few days, suggesting that dust can condense in novae ejecta very quickly (Ney and Hatfield 1978).

Stardust is generally believed to be the source of solid-state particles found in the interstellar medium (▶ interstellar grains). Through radiative and physical processes, the morphology and/or chemical composition of stardust may be modified in the interstellar medium. Most interestingly, various presolar grains (SiC, diamonds, corundum, silicates) of stellar origin have been found in meteorites, suggesting that we actually can hold stardust in our hands (Zinner 1998). The presence of stardust in the solar system provides evidence that stardust is sturdy enough to survive its journey through the ▶ interstellar medium.

See Also

- ▶ Asymptotic Giant Branch Star
- ▶ Interstellar Dust
- ▶ Meteorites
- ▶ Nova
- ▶ Nucleation of Dust Grains
- ▶ Organic Dust, Synthesis by Stars
- ▶ Stellar Winds
- ▶ Supernova

References and Further Reading

Henning TK (ed) (2003) Astromineralogy. Springer, Berlin
Kwok S (2004) The synthesis of organic and inorganic compounds in evolved stars. Nature 430:985–991
Kwok S, Volk K, Bidelman WP (1997) Classification and identification of IRAS sources with low-resolution spectra. Astrophys J Suppl 112:557–584
Ney EP, Hatfield BF (1978) The isothermal dust condensation of Nova Vulpeculae 1976. Astrophys J 219: L111–L115
Posch T, Kerschbaum F, Mutschke H, Fabian D, Dorschner J, Hron J (1999) On the origin of the 13 13 μm mu;m feature. A study of ISO-SWS spectra of oxygen-rich AGB stars. Astron Astrophys 352:609–618
Posch T, Kerschbaum F, Mutschke H, Dorschner J, Jäger C (2002) On the origin of the 19.5 5 μm mu;m feature. Identifying circumstellar Mg-Fe-oxides. Astron Astrophys 393:L7–L10
Volk K, Kwok S, Langill PP (1992) Candidates for extreme carbon stars. Astrophys J 391:285–294
Woolf NJ, Ney EP (1969) Circumstellar infrared emission from cool stars. Astrophys J 155:L181–L184
Zinner E (1998) Stellar nucleosynthesis and the isotopic composition of presolar grains from primitive meteorites. Ann Rev Earth Planet Sci 26:147–188

Star Formation, Observations

Gopal Narayanan
Five College Radio Astronomy Observatory,
University of Massachusetts, Amherst, MA, USA

Keywords

Gravitational collapse; Molecular clouds; Interstellar medium; Spectral energy distribution

Definition

Star formation is the process by which dense portions of interstellar ▶ molecular clouds collapse into small regions that become hot enough at the center to initiate the process of nuclear fusion, thereby creating a star. Observations of star formation require all wavelengths from radio to X-ray and help elucidate the processes underlying the birth of both low-mass and high-mass stars.

History

It is worth reviewing a little bit of the history behind the realization that star formation is an

ongoing process in our Galaxy. By the middle of the twentieth century, the theory of stellar structure and evolution had already demonstrated that the hottest stars (OB stars) consume their nuclear fuel at such a prodigious rate that they can live for only a short fraction of the lifetime of our Galaxy. So the very fact of their continued existence was proof that star formation has occurred in the present epoch of galactic history. In addition, in the 1940s the Armenian astronomer Viktor Ambartsumian showed that OB stars are in associations (see "▶ OB Association") whose internal motions would cause them to be disrupted on timescales in agreement with the nuclear ages of the individual stars in the association (that is, on times much less than the age of the Galaxy), again providing direct observational evidence that star formation is still ongoing in our Galaxy. The last piece of the puzzle was provided by the discovery of the ▶ interstellar medium (ISM) of gas and dust in the early part of the twentieth century. Observations of the interstellar medium established that the clouds of interstellar material (giant molecular clouds) had roughly stellar chemical composition, but were much more massive than individual stars or stellar associations. The presence of the ISM showed that the raw material needed to make stars was relatively abundant in the Galaxy.

For much of the last 50 years, direct observations of the star formation process, and subsequent development of a good theory, have been hampered severely by the fact that the earliest phases of star formation occur in dark clouds which have an extremely large amount of extinction toward them, rendering them optically opaque. Fortunately, over the past 30 years, significant advances in infrared to millimeter wavelength technologies have spurred progress in a new generation of telescopes and associated instrumentation that allows the detailed study of even these deeply embedded stages of star formation.

Overview

The theory of ▶ stellar evolution, which has been very successful in explaining the life history and the deaths of stars, has nevertheless been unable to explain how stars form. It is likely that the inherent complexity of the physical processes behind star formation is the main reason for this inability of the theory. Knowledge of the physical mechanisms that govern the formation of stars within molecular clouds is crucial, as it has a wide-ranging impact on a variety of other fields of astronomy. Thus, understanding star formation is necessary to form a clear picture of galactic evolution from the Big Bang to the current time in cosmic history. The development of a theory of star formation is also important for the study of origins of planetary systems, which in turn has implications for biology outside the solar system (see "▶ Protostars").

The fact that star formation has been an ongoing and continuous process that extends from the early universe into the present epoch is an important property of the universe that facilitates the observational study of star formation. Because of this important property, the physical processes of various stages of star formation can be investigated by observational methods.

Giant Molecular Clouds and Dense Cores: The Nurseries of New Stars

We know from observations that the dark bands that one can see crossing the Milky Way in the night-time sky are made up of many interstellar dark clouds which contain gas and tiny opaque dust grains that effectively absorb and scatter starlight (see "▶ Interstellar Dust"). These dark clouds are the sites of star and planet formation in the Galaxy. The first millimeter-wavelength observations in the 1970s showed that these dark clouds are predominantly molecular in composition (see "▶ Molecular Cloud") and with a temperature of 10–15 K are some of the coldest objects in the universe. The observations that were performed were molecular line surveys of carbon monoxide, CO. While cold molecular hydrogen has no detectable emission spectrum, CO is the next most abundant molecular species after H_2 in these regions and is easily detected at millimeter wavelengths. CO observations show that the molecular mass of the Galaxy is about two billion solar masses and that this mass is

concentrated tightly in the flattened galactic disk and is dominated by giant molecular clouds (GMCs). The physical properties of GMCs are reviewed exhaustively in many papers (see, e.g., Evans 1999). With sizes ranging from 20 to 100 pc, and masses ranging from 10^4 to 10^6 $M_\odot$ (solar masses), these objects are the largest structures in the Milky Way and rival ▶ globular clusters for sheer mass. The mean densities of GMCs are 50–100 molecules cm^{-3} which, given their cold temperatures, implies that they are gravitationally bound, if not stable entities. Measurements of molecular line widths indicate cloud velocity dispersions of 2–3 kms^{-1}. Given that the cloud sound speed $c_S \sim 0.2$ kms^{-1}, the velocity fields of these objects are highly supersonic. These supersonic motions are not for the most part due to any systematic motions such as collapse or expansion, but appear to be turbulent in nature. For example, the relation between molecular line width and cloud size is similar to that expected for incompressible turbulent flows (Larson 1981). The lifetime of typical GMCs is an area of considerable controversy, with estimates ranging from an order of the free-fall time of the GMC (a few million years) to as much as 100 million years. Clearly it is important to have a better constraint on the ages of these complexes to understand the evolution of such clouds into stars.

Within GMCs, there are identifiable discrete entities with higher densities. These are referred to as dense cores and have typical mean densities of 10^4 molecules cm^{-3}, with central densities reaching up to 10^6 cm^{-3}. The fraction of GMC mass in these dense cores is typically 1–10 %, with the most evolved GMCs having higher percentages. The masses of these dense cores vary from 1 to 1,000 $M_\odot$. The frequency distribution of the masses tends to follow a power law, such that most of the mass in dense molecular gas is located in M $\geq$100 $M_\odot$ cores. The velocity dispersions of dense cores tend to be supersonic, with the low-mass cores tending to have smaller dispersions, which in some cases become subsonic. Higher-mass cores tend to be warmer and more turbulent.

Knowledge of the content and distribution of ▶ protostars and young stellar objects (YSOs) within the GMCs or any molecular cloud is important for understanding how the process of star formation proceeds within it. Since protostars are often buried deep within the clouds, they tend to be invisible optically. However, the opacity of dust is an order of magnitude smaller in these sites at longer wavelengths compared to optical wavelengths. The younger or less evolved the star is, the more heavily obscured it typically is, and for such objects far-infrared and submillimeter observations are required to study them.

The ▶ Infrared Astronomical Satellite (IRAS) in the early 1980s produced the first sensitive surveys in the mid- to far-infrared emission of GMCs. By the end of that same decade, near-infrared imaging detectors mounted on ground-based telescopes added complementary data. In the late 1980s and 1990s, the IRAS observations were followed up with targeted millimeter and submillimeter observations of star-forming regions. In the current generation, a large number of ground-based near-infrared surveys combined with space telescope observations such as Hubble Space Telescope, Spitzer Space Telescope, and Herschel Telescope are being used to study dense cores. All these competing but complementary surveys revealed that (1) stars form in dense molecular gas ($\geq 10^4$ H_2 molecules cm^{-3}), (2) most stars form in embedded clusters, and (3) the overall efficiency of star formation in GMCs is quite low (1–3 % or less). The low global star formation efficiency is rather significant. This indicates that the bulk of the molecular mass in GMCs does not participate in the star formation process and exists in a semi-stable configuration. In this sense, the problem of star formation shifts from finding what makes the bulk of the material collapse to finding what holds up the bulk of the material against global collapse (see Shu et al. 1987). Molecular emission line and extinction surveys do find that a small fraction of molecular gas is at high density, and, not surprisingly, the efficiency of star formation in dense gas is much higher (10–20 %) compared to the efficiency in the entire GMC. The highest efficiencies are found in the most massive

cores that form embedded clusters (e.g., Lada 1992).

From Dense Cores to Stars

The initial conditions and the earliest stages of star formation in dense cores are still areas of active study for observers and theorists. In active star-forming clouds such as those in Orion and Taurus, a large fraction of dense molecular cores harbor stars, while in clouds with a low level of star formation, 75 % of the dense cores are starless (Lee and Myers 1999). Starless cores offer a unique opportunity to constrain the initial conditions of star formation. Submillimeter observations of the dust emission from starless cores show that these cores have densities that are not strong functions of cloud radius, unlike cores with stars. It is also interesting to note that the measured emission linewidths of starless cores are consistent with purely thermal internal motions and do not show any evidence of turbulent broadening. This may indicate that dense cores form initially from turbulent cores, but evolve by dissipating the internal turbulence before forming stars.

At least in isolated, low-mass dense cores, the formation of stars from dense cores is now well understood and backed with a wealth of observations and a good theoretical underpinning (see Shu et al. 1987). The theoretical process can be described as follows: Before being incorporated into a forming star, the molecular material within the collapsing dense core must increase in density by 20 orders of magnitude and decrease in size by 7 orders of magnitude relative to its initial state. Because the dust in the material is optically thin, internal energy and heat generated by collapse is radiated away, thereby maintaining the same temperature in the core. The collapse thus proceeds in an isothermal, dynamical manner, with the inner layers becoming denser and collapsing faster than the outer layers which are left behind. Eventually the inner layers become dense enough to become optically thick to their own radiation, resulting in the formation of a quasi-static stellar core surrounded by an infalling envelope.

In the last two decades of the twentieth century, evidence of this so-called pure infall stage was sought by many astronomers. The search for unique collapse signatures in dense cores with and without stars has been carried out by way of spectroscopic observations of molecular species that trace high density (like HCO^+, CS, and N_2H^+). But surprisingly, the first YSOs studied with molecular spectroscopy showed evidence for expansion signatures rather than collapse signatures. In fact, it was discovered that most if not all protostellar objects have vigorous bipolar outflows that are predominantly molecular and extend sometime to parsec scales from the driving source (see Snell et al. 1980 for the discovery of molecular outflows). It is now understood that outflows originate from YSOs due to angular momentum conservation issues. Observations indicate that the specific angular momentum of cloud cores is six orders of magnitude larger than the material on the surface of typical stars. The tendency of collapsing materials to preserve specific angular momentum causes the infalling material to form a flattened structure or disk around the protostellar core (the accretion disk; see also "► Protoplanetary Disk"). Observations suggest that this disk can range from a few hundred to a few thousand AU in diameter. The initial mass of the protostar is only 0.01 $M_\odot$, not enough to increase the internal temperature to the stage of nuclear ignition. The embryonic star will have to accrete more material from the disk in order to build up mass. Material in the disk can fall into the star only if it loses angular momentum. Viscous accretion can result in the net outward transport of angular momentum, thereby allowing material to fall in (Lyndon-Bell and Pringle 1974). However, we still have the problem that material at the inner edge of the accretion disk has higher angular momentum compared to the star. Nature invented bipolar outflows to get rid of this angular momentum problem.

Bipolar outflows (see "► Bipolar Flow") are a manifestation of primary winds generated by the protostar itself. Close to the surface of the star, the wind appears as highly collimated circumstellar jets. These jets are hot and ionized and emit radiation at optical and centimeter wavelengths. Such jets are often seen to terminate in

bow-shock structures called Herbig-Haro (HH) objects. Further away from the star, these winds sweep up massive amounts of molecular material which shows up as bipolar molecular outflows.

Bipolar outflows are highly energetic and pack mechanical luminosities that are appreciable fractions of the total radiant luminosities of these objects. Observations indicate that the mechanical luminosities of these outflows are proportional to the rate at which they are accreting matter. It is becoming increasingly clear that the sizes of these outflows can completely dwarf the putative accretion disk, reaching parsec scales in many outflows. One consequence of an accretion driven outflow is that this expanding material tends to disperse the surrounding material, thereby ultimately limiting the mass accreted onto the star.

During the earliest phases of protostellar evolution, the young star is completely surrounded by the disk and envelope structure and emits like a blackbody with its peak in the far infrared. This stage is called the Class 0 phase. As the putative outflow disperses the surrounding material and the accretion disk and the embedded star are revealed, at least from the polar directions, the spectral energy distribution (SED) shifts its peak into the near infrared and subsequently into the optical part of the spectrum, with a large infrared excess compared to regular main sequence stars. These phases are called Class I, II, and III. Observationally, the early stages are best studied at submillimeter wavelengths. Gradually, as the circumstellar material is dispersed, the protostar becomes revealed in the mid to near infrared, which may be studied with sensitive observations with space telescopes like Spitzer and Herschel.

Planet formation probably commences quite early in the evolution, with the infalling dust settling down into the midplane of a circumstellar disk due to drag forces resulting from interaction with the gas in the disk (e.g., Lissauer 1993). Micron-sized dust particles collide and merge together to form increasingly more massive and larger particles. Once they reach kilometer size, they are called planetesimals. Planets are theorized to form from the mutual accretion of planetesimals. Such planets can grow massive enough to create gaps in the circumstellar disk which can be observable using high-angular resolution millimeter-wavelength observations using ▶ ALMA in the future.

See Also

- ▶ Bipolar Flow
- ▶ Interstellar Medium
- ▶ Molecular Cloud
- ▶ OB Association
- ▶ Protoplanetary Disk
- ▶ Protostars

References and Further Reading

Evans NJ (1999) Physical conditions in regions of star formation. Annu Rev Astron Astrophys 37:311
Lada EA (1992) Global star formation in the L1630 molecular cloud. Astrophys J 393:L25
Larson RB (1981) Turbulence and star formation in molecular clouds. Mon Not R Astron Soc 194:809
Lee CW, Myers PC (1999) A catalog of optically selected cores. Astrophys J Suppl 123:233
Lissauer JJ (1993) Planet formation. Annu Rev Astron Astrophys 31:129
Lyndon-Bell D, Pringle JE (1974) The evolution of viscous discs and the origin of the nebular variables. Mon Not R Astron Soc 168:603
Shu FH, Adams FC, Lizano S (1987) Star formation in molecular clouds – observation and theory. Annu Rev Astron Astrophys 25:23
Snell RL, Loren RB, Plambeck RL (1980) Observations of CO in L1551 – evidence for stellar wind driven shocks. Astrophys J 239:L17

Star Formation, Theory

Patrick Hennebelle
Service d'Astrophysique, CEA, Saclay, Gif-sur Yvette, France

Keywords

Collapse; Giant molecular clouds; Stars; Interstellar medium; Magnetic field; Turbulence; Instabilities; Numerical simulations

Definition

The theory of star formation aims at understanding the physical processes, which drive the evolution of the interstellar medium from a very dilute gas into a dense medium in which nuclear reactions take place. It covers a very broad range of spatial and temporal scales that go from the giant molecular clouds to the stars themselves. It is believed that this evolution is largely triggered by gravity, magnetic field, turbulence, and thermodynamics.

Overview

The interstellar medium within galaxies is filled by a gas, out of which stars eventually form. This gas presents a complex structure and relatively large temperature and density variations. However, it generally remains fairly uniform over large spatial scales in stark contrast with the stars themselves that occupy a tiny fraction of the galaxy volume but contain most of their (baryonic) mass. The star formation theory (Stahler and Palla 2005; Ward-Thompson and Whitworth 2011) aims to understand exactly how this transition, from a continuous to a discrete media, arises. This question bears important consequences for our universe. Not only stars are its building blocks but they strongly influence the evolution of galaxies through the feedback that the most massive stars exert during their life time, in particular at the end of their life when they explode in supernovae. Low-mass stars are also fundamental for it is well established now that they are hosting planetary systems like ours. Last but not least, stars synthetize heavy elements such as carbon and oxygen that drastically modify the thermal properties and the structure of the galactic gas and eventually permit the existence of complex molecules and life.

Historically a few outstanding questions have dominated the field of star formation although eventually many more should be addressed. The first challenge is to understand the efficiency at which star formed in our Galaxy, a quantity also called the star formation rate. The second major issue is to understand the mass distribution of stars. Indeed, the properties of stars are largely determined by their masses. The mass distribution of stars is usually called the initial mass function. Finally, many stars are not isolated but are binary that is to say possess at least a companion whose distance may vary from less than an astronomical unit to a fraction of parsec. Understanding exactly how this happens as well as the characteristics of binary systems is another challenge for star formation theory. More recently with the discovery of extrasolar planets, which form within circumstellar disks, the question of the disk formation, closely connected to the formation of binary systems, also became a major topic.

Various physical processes are triggering the evolution of the interstellar medium and eventually determine the star formation process (MacLow and Klessen 2004; Mckee and Ostriker 2007). First of all, the gravitational force induces the formation of self-gravitating entities such as molecular clouds and dense cores that eventually collapse to form stars. An important concept has been inferred by Jeans (1902), the so-called Jeans length (Ward-Thompson and Whitworth 2011), which determines the spatial scale above which a cloud of a given density and temperature is prone to gravitational instability. To determine whether a cloud collapses or not, one must compare the time needed for this cloud to contract gravitationally (the freefall time) with the time needed for the sound waves to cross it. If this time is shorter than the freefall time, then the sound waves are unable to erase the density perturbations, which develop under the influence of self-gravity. Second, supersonic turbulence (Elmegreen and Scalo 2004; Scalo and Elmegreen 2004; Hennebelle and Falgaorne 2012) is playing a major role in the interstellar medium, particularly in molecular clouds. On one hand, turbulent eddies tend to disperse their gas, thus contributing to reduce the efficiency of star formation. Indeed, if there were no support to resist the gravitational force, the number of stars formed each year in the Galaxy would be around 300, hundred times more than what is currently observed. However, turbulence is playing a dual role because it also

compresses the gas locally through shocks. The spectrum of density fluctuations, which is then generated, may have fundamental consequences by setting the mass of the stars and being at the origin of their mass spectrum. Magnetic field is another physical process that likely has important consequences. Indeed, it has even been believed that magnetic field could be strong enough to be entirely responsible for the low star formation rate measured in the Milky Way (Shu et al. 1987). The idea was that because the ionization of the molecular clouds is rather low, most of the gas is not subject to the magnetic Lorentz force; thus, ionized species could drift away carrying with them the magnetic field lines and reducing the magnetic intensity to the point where magnetic field would not be dominant anymore. Although this remains a controversial issue, the recent observational measurements seem to indicate that magnetic fields, while not negligible, are not dominant. Magnetic field however is having nevertheless a significant impact on the star formation process because it may contribute to reduce somehow the star formation efficiency. It also modifies the statistical properties of the supersonic turbulence, and finally during the collapse, it contributes to reduce the rotational support by transporting the angular momentum of the gas from the inner to the outer part of the collapsing cloud. As the collapse proceeds, the centrifugal force becomes more and more important and stops the gravitational infall, thereby leading to the formation of centrifugally supported disks. This process known as the centrifugal barrier requires the existence of various mechanisms to transport the angular momentum (Bodenheimer 1995; Hennebelle et al. 2013) and to permit the accretion onto the protostars. Angular momentum is at the origin of binary stars and planets. Indeed, the formation of a few objects orbiting around their center of mass constitutes an efficient way to store the angular momentum of the cloud. In the solar system, for example, the angular momentum of Jupiter is by far the dominant contribution. It is comparable to the angular momentum, which is believed to be typical for the prestellar core that led to the formation of the sun.

Finally, it is now well established that the feedback induced by the massive stars during their life, such as powerful wind or ionizing radiation, and particularly as they die and explode in a powerful supernovae, plays a major role in star formation (MacLow and Klessen 2004). First of all, this feedback is most probably an important source for the galactic turbulence. Second, the stellar feedback likely disperses the cloud in which the massive stars have formed and therefore significantly limits the star formation efficiency which otherwise would be far larger than the value deduced from observations.

Basic Methodology

Star formation appears to be a complex multi-scales and multi-physics problem. As such, it is necessary to combine various approaches to make progress in this field. First of all, high-resolution observations must be carried out using the most accurate telescopes at various wavelengths. Second, due to the complexity of the equations, which govern the fluid evolution, star formation theory makes extensive use of the numerical simulations. These calculations are performed on massively parallel supercomputers around the world. They require millions of computer hours and generate terabytes of data. To solve the fluid equations accurately, complex algorithms have been developed such as Riemann and Poisson solvers (Teyssier 2002; Springel 2005). In parallel, one also needs to develop simpler analytical calculations for some of the key processes and to confront the results and the predictions with the numerical simulations. Such approach is necessary to assess the simulation results but also to identify and understand the nonlinear phenomena at play.

The numerical models take into account the microphysical properties of the chemical elements contained in the interstellar medium and determine, for example, the rate at which it cools or forms complex molecules (Le Petit et al. 2006). The knowledge of these microphysical processes is also a challenge, which requires dedicated observations, laboratory experiments,

and heavy calculations. Third, the confrontation between observations and theory is another necessary and complex step. To achieve this goal, it is sometimes necessary to produce synthetic observations using the models. That is to say, one needs to simulate the luminous signal, which would be observed if an object like the model was observed with a telescope (Commerçon et al. 2012).

See Also

- ▶ Accretion, Stellar
- ▶ Ambipolar Diffusion
- ▶ Dense Core
- ▶ Fragmentation of Interstellar Clouds
- ▶ Initial Mass Function
- ▶ Interstellar Cloud
- ▶ Magnetic Fields and Star Formation
- ▶ Magnetohydrodynamics
- ▶ Molecular Cloud
- ▶ Protoplanetary Disk
- ▶ Protostars
- ▶ Shock, Interstellar
- ▶ Star Formation, Theory
- ▶ Star Formation, Triggering
- ▶ Turbulence, Interstellar

References and Further Reading

Bodenheimer P (1995) Angular momentum evolution of young stars and disks. Annu Rev Astron Astrophys 33:199
Commerçon B, Launhardt R, Dullemond C, Henning T (2012) Synthetic observations of first hydrostatic cores in collapsing low-mass dense cores. I. Spectral energy distributions and evolutionary sequence. Astron Astrophys 545:98
Elmegreen B, Scalo J (2004) Interstellar turbulence I: observations and processes. Ann Rev Astron Astrophys 42:211–273
Hennebelle P, Falgaorne E (2012) Turbulent molecular clouds. Astron Astrophys Rev 20:55
Hennebelle P, Fromang S, Matthis S (2013) Angular momentum during star formation and early evolution. EAS Publ Ser 62:3
Jeans JH (1902) The stability of a spherical nebula. Philos Trans R Soc Lond 199:1–53
Le Petit F, Nehmé C, Le Bourlot J, Roueff E (2006) A model for atomic and molecular interstellar gas: the meudon PDR code. Astrophys J Suppl Ser 164:506
MacLow M-M, Klessen R (2004) Control of star formation by supersonic turbulence. Rev Mod Phys 76:125
McKee CF, Ostriker EC (2007) Theory of star formation. Ann Rev Astron Astrophys 45:565
Scalo J, Elmegreen B (2004) Interstellar turbulence II: observations and processes. Ann Rev Astron Astrophys 42:275–316
Shu FH, Adams FC, Lizano S (1987) Star formation in molecular clouds – observation and theory. Ann Rev Astron Astrophys 25:23–81
Springel V (2005) The cosmological simulation code GADGET-2. Mon Not Roy Astron Soc 364:1105
Stahler SW, Palla F (2005) The formation of stars. Wiley Interscience, New York. ISBN 3-527-40559-3
Teyssier R (2002) Cosmological hydrodynamics with adaptive mesh refinement. A new high resolution code called RAMSES. Astron Astrophys 385:337
Ward-Thompson D, Whitworth AP (2011) An introduction to star formation. Cambridge University Press, Cambridge. ISBN 9780521630306

Star Formation, Triggering

Annie Zavagno
CNRS, LAM (Laboratoire d'Astrophysique de Marseille) UMR 7326, Aix Marseille Université, Marseille, France

Keywords

Star formation; Young stellar object (YSO); HII region

Definition

Star formation takes place in ▶ molecular clouds and occurs via two ways that can be either spontaneous or triggered. In the triggering case an external agent (compression) acts as a precursor. This extra pressure has different origins and favors the collapse of molecular condensations to form stars. One mechanism of triggered star formation is based on the expansion of HII region around massive stars, but massive stars also impact on their surrounding via winds and supernova explosion at the end of their life. Recent infrared large-scale surveys have shed light on

star formation processes and revealed how important feedback processes may be.

Overview

Massive stars ($M > 8M_{\odot}$) are rare and evolved rapidly but they play a crucial role in the chemical and dynamical evolution of galaxies. They produce a high amount of ultraviolet photons that can ionize the surrounding medium, especially neutral hydrogen (HI). This leads to the creation of an ionized (HII) region that expands in the surrounding medium, due to the temperature difference between the hot inside region and the cold surrounding gas (Dyson and Williams 1997). Massive stars also impact on their surrounding via winds and supernova explosion at the end of their life. They create heavy elements that are expelled and enrich the surrounding interstellar medium. Blaauw and Morgan (1953) first observed a sort of "in chain reaction" in the formation of massive stars, suggesting that the massive star HD34078 was formed in a compression region of a nebula that might have been itself pushed away from the Orion region. In a subsequent review Blaauw (1964) observed spatial separation of OB subgroups with different ages. This observation leads Elmegreen and Lada (1977) to propose a mechanism of triggered star formation based on the expansion of HII regions. This mechanism has been called the collect and collapse model as a layer of material is collected during the expansion of the ionized region and then collapses to form fragments where new stars may form. With the progress made in infrared detectors and all-sky infrared surveys, it becomes clear that an over-density of young stellar objects is observed at the edges of HII regions in our Galaxy and in external galaxies. In 2005, Deharveng et al. published a paper where they studied in the infrared using the results from the Spitzer telescope a series of Galactic HII regions where triggered star formation was likely to occur. Starting from this study, many international groups have worked on this subject with the aims to characterize the physical mechanisms responsible for this way of forming stars and to quantify its importance.

Multiwavelength large-scale surveys together with pointed observations reveal active ongoing star formation at the edges of Galactic and extragalactic HII regions (Deharveng et al. 2005; Zavagno et al. 2007; Galametz et al. 2013). In the study of triggered star formation by expanding HII regions, the key question is to establish the causal link, if any, between a given HII region's expansion and the star formation observed at its edges. One also wants to understand the physical mechanisms that control this way of forming stars and to quantify the importance of this phenomenon on a galactic scale.

Massive stars form ionized regions. These regions expand in the surrounding medium at a supersonic speed ($v \sim 10$ km/s) creating a shock front preceding the ionized front. During the expansion of the HII region, neutral material accumulates between the ionization front and the shock front. A layer of dense neutral material builds up around the ionized region. With time, this layer becomes massive and a new generation of stars may form in it. This phenomenon is called triggered star formation by the expansion of ionized regions (Fig. 1).

Basic Methodology

In the study of star formation triggered by the expansion of HII regions, the first step is to detect and to characterize the properties of YSOs that are observed at the edges of HII regions. Images give two-dimensional information and the observed young stellar objects (that are stars in the process of forming) may not be associated with the observed HII region we are looking at but may be a by-chance projection observed on the line of sight. Complementary spectroscopic data give information on the velocity of the YSOs and the ionized region and allow to demonstrate the real association of the YSO with the ionized region. The physical properties of the YSOs (luminosity, mass, age, evolution stage) can be obtained by measuring their flux at different wavelengths covering a large spectral range

Star Formation, Triggering, Fig. 1 RCW 120: a Galactic HII region with active star formation observed with the infrared Herschel satellite and the PACS and SPIRE instruments (Credits: ESA/PACS & SPIRE Consortium, Dr. Annie Zavagno, LAM, HOBYS Key Programme Consortia)

(ideally from the optical to the millimeter) and by fitting the complete set of fluxes with theoretical models that predict their evolution. The early stages of star formation are also characterized by a strong dynamical and chemical evolution. Such information is obtained with spectroscopic data and is also crucial in our determination of young stellar objects' age. Indeed, the triggered star formation mechanism supposes that the first generation of massive star(s) that create the ionized region has to be older than the YSOs observed at its edges, if a causal link exists between the expansion of the ionized zone and the further formation of YSOs observed on its edges.

Key Research Findings

Many recent infrared and submillimeter surveys have shown that we are living in a "bubbling Galactic disk" where thousands of ionized regions are observed with bright YSOs sitting at their edges (Deharveng et al. 2010; Kendrew et al. 2012). These authors have shown that triggered star formation seems to be an efficient way of forming massive stars as about 30 % of the massive YSOs are observed at the edges of HII regions in the Galaxy. Deharveng et al. (2010) have shown that many physical mechanisms can be responsible for triggered star formation at the edges of HII regions. Among these are small-scale gravitational instabilities, large-scale gravitational instabilities that lead to the formation of high-mass fragments, ionizing radiation acting on a turbulent medium, and radiation-driven compression of preexisting dense clumps. All these mechanisms can act at the edges of a given ionized region.

Herschel observations of Galactic HII regions compared with results of numerical simulations show that the expansion of the ionized region has a real impact in increasing the density at the edges of the ionized gas and that compression from the ionized gas really impacts on star formation (Minier et al. 2013; Tremblin 2012). However, these last results are still debated and other numerical studies (Dale et al. 2013) show that it is very difficult to separate the preexisting and triggered star formation at the edge of ionized regions. Herschel data provide a lot of key information especially on the structure of the dense regions that surround HII regions that should allow us to really characterize the role of these regions in the star formation observed at their edges. Billot et al. (2011) used a minimum spanning tree algorithm to characterize the spatial distribution of Galactic far-IR sources and derive their clustering properties using the results of the Herschel infrared GALactic (Hi-GAL) plane survey (Molinari et al. 2010). They show that protostars surrounded by warm molecular material and detected at short infrared wavelengths tend to be clustered in dense and compact groups around HII regions. Detailed studies of Galactic ionized regions such as Gum 31 (Ohlendorf et al. 2013) show that the location of associated YSOs in the photodissociation region is suggestive of their being triggered by a collect and collapse scenario. However, the study of an infrared dark filament in interaction with an HII region (Tackenberg et al. 2013) shows that the evidence for triggered star formation there is not obvious, even if a

massive (preexisting) clump is observed. The difficult point remains to prove that the collapse that will lead to star formation is really favored by the expansion of the ionized region. Statistical studies on a large sample of sources observed in the far infrared with the Herschel satellite should help us to answer this question.

Future Directions

The wealth of data provided by the Herschel satellite, combined with other available (and forthcoming) data, will allow an in-depth study of the star formation in our Galaxy and in external galaxies in the near future. The global view we have with large imaging and spectral surveys will allow to study the triggered star formation phenomenon and to quantify its importance on galactic scales. This global view will be complemented with detailed, high-resolution pointed observations in the infrared with ground- and space-based facilities and in the millimeter with the ALMA interferometer. The idea with high-resolution pointed observations is to go in depth in our understanding of the physical mechanisms that control star formation on small spatial scales, whatever the way (either spontaneous or triggered) of the forming star is. Future observing facilities either ground and space based go in this direction of high resolution. The James Webb Space Telescope (JWST) and the European Extremely Large Telescope (E-ELT) will play a crucial role in this context, hopefully complemented by space-based large far-infrared interferometer such as the FIRI project. All the knowledge that will be gained with these observations will help in further constraining the theoretical models that describe with more and more details the mechanisms that control star formation at the edges of ionized regions.

Some of the key questions that still have to be addressed are:

- How important is this way of forming stars? Herschel images revealed highly embedded sources that were not detected before at the edges of HII regions. This means that these sources were not "counted" and that their presence, if firmly related to the impact of the ionized region, will increase the efficiency of this way of forming stars. Spectroscopic studies show that most of the young sources observed at the edges of HII regions are physically associated with them (Martins et al. 2010). However, recent results show that in some cases, the sources are not associated with the ionized region, contrary to what two-dimensional images seem to show. This result also changes the statistics, as soon as a non-associated YSO may be counted (as being under the influence of the ionized region) if no spectroscopic information exist for it. The existence of spectroscopic large-scale surveys will improve this situation, allowing a clear association between YSOs and HII regions.
- What are the mechanisms that control star formation at the edges of HII regions? Observations and comparison with numerical simulations will help in understanding the different physical processes that take place to favor star formation. The role of turbulence and magnetic field at small and large scale is still not clear in this specific way of forming stars. Moreover, massive stars are also associated with winds and this can play a role in this process.
- What is the impact of HII region in the mass distribution of young stars that form at their edges? The study of the initial mass function (IMF) is a key question in astrophysics. A systematic study of young clusters at high resolution has to be done to address this question.
- What is the importance of this phenomenon in external galaxies? High resolution allows to study this phenomenon in external galaxies and to see how it proceeds under specific environment, including low-metallicity galaxies. If massive stars can trigger the formation of a new generation of massive stars, this phenomenon may be important for cosmology and the formation of the first massive stars in the universe.

See Also

- ▶ Herschel, William
- ▶ Protostars
- ▶ Star Formation, Theory
- ▶ Star Formation, Observations

References and Further Reading

Billot N, Schisano E, Pestalozzi M, Molinari S, Noriega-Crespo A, Mottram JC, Anderson LD, Elia D, Stringfellow G, Thompson MA, Polychroni D, Testi L (2011) Clustering properties of far-infrared sources in Hi-GAL science demonstration phase fields. ApJ 735:28

Blaauw A (1964) The O associations in the solar neighborhood. Annu Rev Astron Astrophys 2:213–246

Blaauw A, Morgan WW (1953) Note on the motion and possible origin of the O-type star HD 34078 = AE Aurigae and the emission nebula IC 405. BAN 12:76–79

Dale JE, Ercolano B, Bonnell IA (2013) Ionization-induced star formation – V. Triggering in partially unbound clusters. MNRAS 431:1062–1076

Deharveng L, Zavagno A, Caplan J (2005) Triggered massive-star formation on the borders of Galactic H II regions I A search for "collect and collapse" candidates. Astronomy & Astrophysics 433:565–577

Deharveng L, Schuller F, Anderson LD, Zavagno A, Wyrowski F, Menten KM, Bronfman L, Testi L, Walmsley CM, Wienen M (2010) A gallery of bubbles. The nature of the bubbles observed by Spitzer and what ATLASGAL tells us about the surrounding neutral material. Astronomy & Astrophysics 523:idA6, 35 pp

Dyson JE, Williams DA (1997) The physics of the interstellar medium, 2nd edn. Institute of Physics Publishing, Bristol

Elmegreen BGG, Lada C (1977) Sequential formation of subgroups in OB associations. ApJ 214:725–741

Galametz M, Hony S, Galliano F, Madden SC, Albrecht M, Bot C, Cormier D, Engelbracht C, Fukui Y, Israel FP, Kawamura A, Lebouteiller V, Li A, Meixner M, Misselt K, Montiel E, Okumura K, Panuzzo P, Roman-Duval J, Rubio M, Sauvage M, Seale JP, Sewiło M, van Loon JT (2013) The thermal dust emission in N158-N159-N160 (LMC) star-forming complex mapped by Spitzer. Herschel LABOCA MNRAS 531:1596–1617

Kendrew S, Simpson R, Bressert E, Povich MS, Sherman R, Lintott CJ, Robitaille TP, Schawinski K, Wolf-Chase G (2012) The Milky Way project: a statistical study of massive star formation associated with infrared bubbles. ApJ 755: (Issue 1) article id 71 15 pp

Martins F, Pomarès M, Deharveng L, Zavagno A, Bouret JC (2010) Near-IR integral field spectroscopy of ionizing stars and young stellar objects on the borders of H II regions. Astronomy & Astrophysics 538: idA32

Minier V, Tremblin P, Hill T, Motte F, André P, Lo N, Schneider N, Audit E, White GJ, Hennemann M, Cunningham M, Deharveng L, Didelon P, Di Francesco J, Elia D, Giannini T, Nguyen Luong Q, Pezzuto S, Rygl KLJ, Spinoglio L, Ward-Thompson D, Zavagno A (2013) Ionisation impact of high-mass stars on interstellar filaments. A Herschel study of the RCW 36 bipolar nebula in Vela C, Astronomy & Astrophysics 550: idA50, 14pp

Molinari S, Swinyard B, Bally J, Barlow M, Bernard J-P, Martin P, Moore T, Noriega-Crespo A, Plume R, Testi L, Zavagno A, Abergel A, Ali B, Anderson L, André P, Baluteau J-P, Battersby C, Beltrán MT, Benedettini M, Billot N, Blommaert J, Bontemps S, Boulanger F, Brand J, Brunt C, Burton M, Calzoletti L, Carey S, Caselli P, Cesaroni R, Cernicharo J, Chakrabarti S, Chrysostomou A, Cohen M, Compiegne M, de Bernardis P, de Gasperis G, di Giorgio AM, Elia D, Faustini F, Flagey N, Fukui Y, Fuller GA, Ganga K, Garcia-Lario P, Glenn J, Goldsmith PF, Griffin M, Hoare M, Huang M, Ikhenaode D, Joblin C, Joncas G, Juvela M, Kirk JM, Lagache G, Li JZ, Lim TL, Lord SD, Marengo M, Marshall DJ, Masi S, Massi F, Matsuura M, Minier V, Miville-Deschênes M-A, Montier LA, Morgan L, Motte F, Mottram JC, Müller TG, Natoli P, Neves J, Olmi L, Paladini R, Paradis D, Parsons H, Peretto N, Pestalozzi M, Pezzuto S, Piacentini F, Piazzo L, Polychroni D, Pomarès M, Popescu CC, Reach WT, Ristorcelli I, Robitaille J-F, Robitaille T, Rodón JA, Roy A, Royer P, Russeil D, Saraceno P, Sauvage M, Schilke P, Schisano E, Schneider N, Schuller F, Schulz B, Sibthorpe B, Smith HA, Smith MD, Spinoglio L, Stamatellos D, Strafella F, Stringfellow GS, Sturm E, Taylor R, Thompson MA, Traficante A, Tuffs RJ, Umana G, Valenziano L, Vavrek R, Veneziani M, Viti S, Waelkens C, Ward-Thompson D, White G, Wilcock LA, Wyrowski F, Yorke HW, Zhang Q (2010) Clouds, filaments and protostars: the Herschel Hi-GAL Milky Way. Astronomy & Astrophysics 518:L100

Ohlendorf H, Preibisch T, Gaczkowski B, Ratzka T, Ngoumou J, Roccatagliata V, Grellmann R (2013) Discovering young stars in the Gum 31 region with infrared observations. Astronomy & Astrophysics 552: A14

Tackenberg J, Beuther H, Plume R, Henning T, Stil J, Walmsley M, Schuller F, Schmiedeke A (2013) Triggered/sequential star formation? A multi-phase ISM study around the prominent IRDC G18.93-0.03. Astronomy & Astrophysics 550:A116

Tremblin P (2012) Ionization impact on molecular clouds and star formation numerical simulations and observations. Ph.D. Thesis, Université Paris Diderot – Paris 7
Zavagno A, Deharveng L, Comerón F, Brand J, Massi F, Caplan J, Russeil D (2006) Triggered massive-star formation on the borders of Galactic H II regions II evidence for the collect and collapse process around RCW 79. Astronomy & Astrophysics 446:171–184
Zavagno A, Pomarès M, Deharveng L, Hosokawa T, Russeil D, Caplan J (2007) Triggered star formation on the borders of the Galactic H ii region RCW 120. Astronomy & Astrophysics 472–835

Stardust Mission

Hugues Leroux
Unité Matériaux et Transformations (UMET), University Lille 1, Ronchin, Nord-Pas-de-Calais, France

Keywords

Accretion; Comet; Meteorites; Primitive material; Solar system; Spacecraft mission

Definition

Stardust is a spacecraft mission which returned to Earth samples from the ▶ comet Wild 2. The main objective of the mission was to contribute to the understanding of the evolution of the solid matter which marked the passage of the interstellar matter in the solar nebula and constrain models of formation and evolution of dust particles in the protoplanetary disk.

Overview

Stardust is a ▶ NASA mission whose main objective was to collect samples in the coma of the comet Wild 2. The spacecraft was launched on February 1999 and returned to Earth on January 2006. It is the first sample return mission to collect cometary dust. These cometary particles are believed to be relicts of the primitive material of the early solar system. Their sojourn in a comet nucleus probably allowed the preservation of primordial signatures. The main scientific objective of the mission was to understand the evolution of solid matter which marked the passage of the interstellar matter in the solar nebula and constrain models of formation and evolution of dust particles in the protoplanetary disk.

The cometary dust in the coma was trapped at a relative velocity of 6.1 km/s using a dust collector which contains ultralow-density aerogel trays. The role of the aerogel was to reduce the particle speed gradually in order by the temperature rise to minimize the physical and chemical alteration due to the high-velocity capture. A large number of particles were returned to Earth and were studied using various investigation techniques by several international laboratory consortia.

The impact of particles in aerogel generated deceleration tracks in which the cometary material is unevenly distributed in various proportions. The largest particles were found well preserved from the hypervelocity impact. Their study showed that most of them display clear evidence for high-temperature processes that likely occurred at the inner edge of the ▶ protoplanetary disk before the accretion on the comet. On the opposite, the fine-grained material shows clear evidences of thermal modification in addition to strong intermixing with the aerogel due to the capture process at very high velocity. This thermally modified material originates from fine-grained, loosely bound, dust aggregates for which the composition is close to the solar photosphere or the most primitive ▶ meteorites.

Particles returned by the Stardust spacecraft show that the comet Wild 2 accreted "cold" dust from the icy parts of the outer solar system and also thermally processed particles coming from the inner region close to the Sun. The protoplanetary disk at the accretion stage of the ▶ solar nebula period was thus animated by large radial mixing.

See Also

▶ Comet

References and Further Reading

Brownlee DE (2012) The Stardust comet mission: studying sediments from the solar system's frozen attic. Elements 8:327–328
Brownlee DE et al (1996) Stardust: comet and interstellar dust sample return. In: Gustafson BAS, Hanner MS (eds) Physics, chemistry, and dynamics of interplanetary dust, vol 104. ASP Conference Series, San Francisco, pp 223–226
Brownlee DE, Joswiak D, Matrajt G (2012) Overview of the rocky component of Wild 2 comet samples: insight into the early solar system, relationship with meteoritic materials and the differences between comets and asteroids. Meteorit Planet Sci 47:453–470
Hanner MS, Zolensky ME (2010) The mineralogy of cometary dust. In: Henning T (ed) Astromineralogy, vol 815, 2nd edn, Lecture notes in physics. Springer, Berlin, pp 203–232
http://stardust.jpl.nasa.gov/overview

Šteins

Ekkehard Kührt
Institute of Planetary Research, German Aerospace Center, Berlin, Germany

Definition

2867 Šteins is a main belt asteroid of the rare spectral E-type with an effective spherical diameter of 5.3 km and a rotation period of about 6 h. On September 5, 2008, the Rosetta space probe flew by Šteins at a distance of 800 km with a speed of 8.6 km/s and collected a great amount of scientific data.

History

2867 Šteins was discovered in 1969 by the Soviet and Russian astronomer Nikolai S. Chernykh. It is named after Kārlis Šteins, a Soviet and Latvian astronomer.

See Also

- ▶ Asteroid
- ▶ Taxonomy

Stellar Cluster

Steven W. Stahler
Department of Astronomy, University of California, Berkeley, CA, USA

Definition

Stars located in the same region that move together through space must be physically related and indeed must share a common origin – such stars form a stellar cluster. Within our own galactic neighborhood, all stellar clusters are relatively young and eventually disperse. In some groups, called open clusters, the coherence is maintained by the mutual gravitational attraction of the member stars. In others, called T associations, the stars are gravitationally bound to a parent ▶ molecular cloud. OB associations, a third type, are unbound and actively dispersing. The very youngest stars are in groups so deeply embedded in cloud gas that they can be detected only in the infrared or submillimeter wavelength ranges.

See Also

- ▶ Globular Cluster
- ▶ Molecular Cloud
- ▶ OB Association
- ▶ T Association

Stellar Evolution

Patrick Eggenberger
Geneva Observatory, University of Geneva, Geneva, Switzerland

Keywords

Stars; Stellar physics; Internal stellar structure

Definition

Stellar evolution refers to the changes of the internal and global properties of stars during their lifetime.

Overview

Stars are fundamental entities providing light and energy in the Universe, as well as producing most of the chemical elements. The study of their internal structure and evolution is thus at the basis of astrophysics. In addition, since many stars host planetary systems, their study is a basic aspect of astrobiology. In this entry, the basic concepts of stellar evolution are first introduced by deriving the equations describing the evolution of the internal structure of a star. These equations are then used to obtain simple analytical estimates of stellar properties and to qualitatively understand the different phases of stellar evolution in terms of basic physical considerations. The evolutionary scenarios obtained by numerically solving the equations of stellar evolution are then discussed for stars with different initial masses. In addition to this global view of standard stellar evolution, the inclusion of nonstandard stellar physics is finally briefly discussed together with the future developments expected in the field. Since this entry only provides a brief overview of stellar evolution, readers interested in a more in-depth description of the subject are referred to the books already available in the literature (e.g., Kippenhahn and Weigert 1990; Prialnik 2000; Hansen et al. 2004; de Boer and Seggewiss 2008; Maeder 2009).

Basic Methodology

Hydrostatic Equilibrium

To understand stellar evolution, we first note that most stars are in such long-lasting evolutionary phases that no significant changes of their global properties can be directly observed. Indeed, during the main part of their life, stars are in mechanical equilibrium or hydrostatic equilibrium. This implies that all forces acting on a given element of the star compensate each other. To prevent the gravitational force from accelerating a mass element toward the center, a force of the same absolute magnitude must be acting outward. This force is due to pressure and, more precisely, to the pressure gradient present in stellar interiors. The equation expressing the hydrostatic equilibrium of a star can be very simply derived by considering a thin shell in a spherically symmetric star between a radius r and $r + \mathrm{d}r$ with pressures of P and $P + \mathrm{d}P$, respectively. The radius r is defined here as the distance to the stellar center. The difference of pressure $\mathrm{d}P$ between r and $r + \mathrm{d}r$ is then balanced by gravitation such that

$$\mathrm{d}P = -\rho g \mathrm{d}r, \tag{1}$$

with ρ is the density and g the magnitude of the vector gravity directed toward the stellar center. By defining M_r as the total mass interior to the radius r, Newton's Law of Gravitation gives $g = GM_r/r^2$ where G is the constant of gravitation, and then,

$$\frac{\mathrm{d}P}{\mathrm{d}r} = -\frac{GM_r}{r^2}\rho. \tag{2}$$

This equation of hydrostatic equilibrium constitutes the first basic equation describing the structure of a star. It simply means that at any point in the interior of a star at equilibrium, the pressure gradient sustains the stellar matter against the gravity force.

The second basic equation governing the structure of a star concerns the variation in mass within a star and is directly related to the conservation of mass. In spherical symmetry, the change of the mass M_r contained in a sphere of radius r is given by

$$\mathrm{d}M_r(r,t) = 4\pi r^2 \rho \mathrm{d}r - 4\pi r^2 \rho v \mathrm{d}t. \tag{3}$$

The first term on the right-hand side of this equation corresponds to the change of mass resulting from a variation in the radius r at a given time t, while the second term represents the flux of mass

out of the sphere of radius r due to a motion with velocity v. At equilibrium, this velocity v equals 0, and we are left with the following equation:

$$\frac{dM_r}{dr} = 4\pi r^2 \rho. \quad (4)$$

This is the second basic equation describing the internal structure of a star. It is interesting to note that if the pressure P is a function of the density ρ alone, Eq. 4 together with Eq. 2 form a complete set of equations describing the structure of the star. However, under normal stellar conditions, pressure also depends on temperature. This means that the presence of a pressure gradient required to achieve hydrostatic equilibrium also results in a gradient in temperature inside the star. The central layers of a star are then found to be hotter than the superficial layers. Recalling that a higher temperature leads to a larger amount of energy contained per unit volume in the radiation field, an energy flow will take place from the central parts to the stellar surface so that a star continuously loses energy. The luminosity (total energy radiated per unit time) of the star is then a direct consequence of hydrostatic equilibrium: stars evolve because they lose energy in order to counteract the gravitational force and to achieve hydrostatic equilibrium. The sources of this stellar energy will directly influence the evolution of the star and the duration of the various evolutionary phases.

Energy Production

Gravitational contraction is a major source of stellar energy. By a global contraction, a star can indeed directly extract energy from the gravitational potential. Conversely, an expansion of the star leads to an absorption of energy and a decrease of its luminosity. This production of energy takes place on a characteristic timescale called the Kelvin-Helmholtz timescale τ_{KH}. This timescale can be simply calculated from elementary physics, such that the global gravitational energy Ω of a star of mass M and radius R is given by $\Omega = -qGM^2/R$ (with $q = 3/5$ for a constant density). The star will then be able to produce an average luminosity L at the expense of its gravitational energy on a timescale given by this energy divided by the energy production per second:

$$\tau_{KH} = \frac{\Omega}{L} \approx \frac{GM^2}{RL}. \quad (5)$$

For the Sun, this gives a typical value of about 3×10^7 years. This lifetime of a few tens of million years is of course too short to be in agreement with our knowledge of the past history of the Earth. This indicates that another main source of stellar energy exists.

In addition to gravitational contraction, a star can produce energy by thermonuclear reactions in its central layers where the physical conditions in terms of temperature and density needed for such processes to occur are met. The timescale of energy production through nuclear reactions can be simply estimated from the hydrogen-burning phase, the longest phase of stellar evolution, during which the fusion of hydrogen into helium occurs (astronomers refer to nuclear fusion as "burning"). The hydrogen burning transforms four protons into one helium nucleus with a release of energy due to a relative mass defect of about 0.007. Simply speaking, this means that 1,000 g of hydrogen are converted into 993 g of helium, while 7 g are transformed into energy, where $E = mc^2$. The characteristic timescale associated with this reaction can then be expressed as the ratio of the total energy that can be created by this process to the stellar luminosity, the analogue of Eq. 5. If nuclear reactions would take place in the whole star of total mass M, this energy would be equal to $\Delta Mc^2 = 0.007$ M (with c the speed of light). However, nuclear reactions only take place in the central parts of the star, so that this energy estimate has to be corrected by a factor q_c equal to the fraction of the stellar mass where nuclear reactions occur. This leads to the following timescale of energy production by nuclear reactions:

$$\tau_H \approx 0.007 \frac{q_c Mc^2}{L}. \quad (6)$$

For the Sun, this estimate gives a typical lifetime of 10 billion years (with $q_c = 0.1$), which is in agreement with our knowledge concerning the past history of the Earth. These very simple estimates of characteristic timescales for the stellar energy production show that nuclear reactions are of major importance to understanding how a star can shine during long durations. Nuclear energy is, however, not absolutely necessary to explain the observed stellar luminosities, since a star can be shining even without nuclear reactions in its core (but only on limited timescales) thanks to the energy production by gravitational contraction. The role of nuclear reactions is of course not limited to the energy equilibrium of the star, since nuclear reactions transform chemical elements in stellar interiors and are therefore at the basis of stellar nucleosynthesis.

The energy conservation in a star leads to the third basic equation for stellar structure. It simply implies that the gain of energy in a mass element is equal to the difference between the energy produced and the energy escaping. With the hypothesis of spherical symmetry of the star, it can be shown that the equation of energy conservation can be written as

$$\frac{\partial L_r}{\partial r} = 4\pi r^2 \rho \left(\varepsilon + \varepsilon_{\text{grav}}\right), \tag{7}$$

where L_r is the luminosity at radius r, ε is the energy produced by nuclear processes per unit of time and mass, and $\varepsilon_{\text{grav}}$ is the energy provided to the system due to a change of structure.

Energy Transfer

Like the mechanical equilibrium of the star, its energetic equilibrium plays a key role in determining its structure and evolution. This equilibrium describes the balance between the energy production discussed in the preceding section and its transport to the stellar surface. The energy production rate of a star regulates itself to reproduce the radiative losses at the surface. In this sense, a star can be considered as a self-controlled nuclear reactor. Assuming that more energy is produced in the stellar center than what can be transported to the surface would lead to an accumulation of energy in the central layers resulting in an expansion of the star. The internal pressure and temperature would then decrease as a result of this expansion, thereby reducing the energy production rate by nuclear reactions. The transport of energy in the interior of a star is thus of prime importance to determine its structure. The transport by photons, or radiative transfer, plays the main role. Convection is another important process for the transport of energy, but it generally occurs only over limited zones of the stellar interior, while radiative transfer is present in the whole interior. Conduction by electrons is the third process for the transport of energy; it only plays an important role in degenerate conditions (e.g., in white dwarfs).

To discuss radiative transfer in stellar interiors, we first consider a photon emitted in the central layers of a star. This photon will be rapidly absorbed by an atom, then re-emitted in a random direction, reabsorbed by another atom, re-emitted, and so on until it reaches the stellar surface. The length of the mean path of this photon between two interactions, which is called the mean free path, is much smaller than the stellar radius. In the case of the Sun, this mean free path is indeed approximately equal to 0.01 cm in the center and 1 cm in the envelope (near the surface, this value may of course be much larger given the very low density of the external layers). Thus, some time will be spent before a photon emitted in the stellar core reaches the surface; in the case of the Sun, this value is typically of the order of 10 million years.

In addition to the photon mean free path, another quantity is important in the context of radiative transfer: the mean gradient of temperature inside the star. This value can be roughly estimated by using the solar values of radius and central temperature:

$$\left\langle \left| \frac{\mathrm{d}T}{\mathrm{d}r} \right| \right\rangle \approx \frac{T_{\text{central}} - T_{\text{surface}}}{R} \approx \frac{T_{\text{central}}^{\text{sun}}}{R_{\text{sun}}} \approx 10^{-4}\ \text{K cm}^{-1}. \tag{8}$$

Comparing this value with the photon mean free path and recalling that temperatures in the internal layers of the Sun are typically of the order of 10 million K, we see that the relative variation of the temperature is very small over the mean free path of a photon. This implies that the radiation field in a star can be well described by the radiation of a blackbody with the local value of temperature T: this is called local thermodynamic equilibrium (LTE). From this, we can ultimately derive the fundamental equation of radiative transfer:

$$F = \frac{L_r}{4\pi r^2} = -\frac{4acT^3}{3\kappa\rho}\frac{\mathrm{d}T}{\mathrm{d}r}. \tag{9}$$

where κ is the opacity or absorption coefficient of the stellar matter and the radiation constant a is equal to $4\sigma/c$, with σ = Stefan's constant. The radiative flux F is thus proportional to the thermal gradient.

In addition to radiation, convection can also transport energy in stellar interiors. These convective motions take place in stellar regions where a heat excess is present that cannot be transferred by radiation alone. Since the treatment of convection is a difficult task involving the complexity of turbulent motions, we only give here the basic transfer equation describing adiabatic convection, which applies in the deep stellar layers:

$$\frac{\mathrm{d}T}{\mathrm{d}r} = \nabla_{\mathrm{ad}}\frac{T}{P}\frac{\mathrm{d}P}{\mathrm{d}r} \quad \text{with } \nabla_{\mathrm{ad}} = \frac{P\delta}{C_P\rho T}, \tag{10}$$

where C_P is the specific heat and $\delta = -\left(\frac{\partial \ln\rho}{\partial \ln T}\right)_P$.

Key Research Findings

Basic Equations of Stellar Evolution

In the preceding section, the fundamental concepts of stellar evolution have been introduced to obtain the four equations that describe the evolution of the structure of a star (when rotational and magnetic effects are ignored):

- Hydrostatic equilibrium:

$$\frac{\mathrm{d}P}{\mathrm{d}r} = -\frac{GM_r}{r^2}\rho \tag{11}$$

- Mass conservation (continuity equation):

$$\frac{\mathrm{d}M_r}{\mathrm{d}r} = 4\pi r^2\rho \tag{12}$$

- Energy conservation:

$$\frac{\partial L_r}{\partial r} = 4\pi r^2\rho\left(\varepsilon + \varepsilon_{\mathrm{grav}}\right) \tag{13}$$

- Transport equation:

$$\frac{\mathrm{d}T}{\mathrm{d}r} = -\frac{3\kappa\rho}{4acT^3}\frac{L_r}{4\pi r^2} \text{ in radiative zones} \tag{14}$$

$$\frac{\mathrm{d}T}{\mathrm{d}r} = \nabla_{\mathrm{ad}}\frac{T}{P}\frac{\mathrm{d}P}{\mathrm{d}r} \text{ in convective zones} \tag{15}$$

The properties of the stellar matter appear through the following physical ingredients, which are required to solve these equations:

- The nuclear reaction rates are needed to evaluate the corresponding production of energy.
- The equation of state expresses the relation between the three physical parameters P, T, and ρ. For a given chemical composition, the equation of state is required to determine the third physical parameter from the two others and to obtain the thermodynamic quantities needed for the computation of a stellar model.
- The opacities are required to calculate the energy transport by radiative transfer and to determine the radiative gradient. A prescription for the energy transport by

S

convection is also required to calculate the temperature gradient in a convective zone. In particular, the hypothesis of adiabaticity is correctly justified in deep stellar layers but becomes inadequate for outer convective zones. In this case, an appropriate approximation has to be used, as, for instance, the standard mixing-length theory (Böhm-Vitense 1958).

Finally, together with this system of equations, the equations of the evolution of chemical element abundances are solved.

Simple Estimates of Stellar Properties and the Mass-Luminosity Relation

The general equations governing stellar evolution are of course too complicated to be solved analytically. The structure and evolution of a star is thus computed by numerically solving this system of equations. It is, however, interesting to notice that very simple estimates of some basic stellar properties can be directly deduced from these equations. For instance, using the equation of hydrostatic equilibrium, one can readily obtain an order-of-magnitude estimate of the pressure and temperature inside a star. First, the pressure gradient of Eq. 11 is approximated by

$$\left|\frac{\mathrm{d}P}{\mathrm{d}r}\right| \approx \frac{P_{\mathrm{center}} - P_{\mathrm{surface}}}{R} \approx \frac{P_{\mathrm{center}}}{R}. \tag{16}$$

By also taking simple average values for the other quantities appearing in Eq. 11, $M_r \sim M/2$, $r \sim R/2$, and $\rho \sim 3\,\mathrm{M}/(4\pi R^3)$, one obtains an estimation of the pressure in the central parts of a star:

$$P_{\mathrm{center}} \approx \frac{3}{2\pi}\frac{GM^2}{R^4}. \tag{17}$$

The corresponding rough estimate of the central stellar temperature can then be obtained by assuming a chemically homogeneous star with the perfect gas law:

$$P = nkT = \frac{\rho}{\mu m_{\mathrm{u}}}kT, \tag{18}$$

with k the Boltzmann constant, m_{u} the atomic mass unit, μ the mean molecular weight (i.e., the average number of atomic mass units per particle), n the number of particles per unit volume, and ρ the density. Combining this relation with the above estimate of the central pressure (Eq. 17), we obtain

$$T_{\mathrm{center}} \approx \frac{\mu m_{\mathrm{u}}}{k}\frac{GM}{R}. \tag{19}$$

In the case of the Sun, these crude estimates give values of about 5.5×10^{15} g s^{-2} cm^{-1} and 3×10^7 K (assuming a mean molecular weight of $\mu = 0.5$ corresponding to ionized hydrogen) for the central pressure and temperature, respectively. This shows that very high values of pressure and temperature are encountered in the deep stellar interior. These simple estimates also are significant in that they illustrate the functional dependence of these internal stellar properties on the global stellar parameters M and R.

While simple estimates of internal stellar properties can be derived from the relation of thermodynamic equilibrium, an estimate of the fundamental relation between stellar luminosities and masses can be obtained from the equation of radiative transfer. Starting from Eq. 14 with a simple approximation of the radiative pressure gradient expressed in terms of temperature

$$\begin{aligned}\frac{\mathrm{d}P_{\mathrm{rad}}}{\mathrm{d}r} &= \frac{\mathrm{d}}{\mathrm{d}r}\left(\frac{1}{3}aT^4\right) = \frac{1}{3}a\frac{\mathrm{d}T^4}{\mathrm{d}r} \\ &\approx \frac{1}{3}a\frac{T^4_{\mathrm{surface}} - T^4_{\mathrm{center}}}{R} \\ &\approx -\frac{1}{3}a\frac{T^4_{\mathrm{center}}}{R},\end{aligned} \tag{20}$$

and with approximations for the quantities $L_r \sim L$ (with L the total luminosity) and $r \sim R/2$, one obtains

$$L \approx \frac{\pi ac}{3}R\frac{T^4_{\mathrm{center}}}{\kappa\rho}. \tag{21}$$

Using the estimate for the central temperature derived above (Eq. 19) and the mean value of the stellar density $\rho \sim 3\,M/(4\pi R^3)$, this finally leads to

$$L \approx \frac{4\pi^2 ac}{9}\left(\frac{Gm_u}{k}\right)^4 \frac{\mu^4 M^3}{\kappa}. \qquad (22)$$

This fundamental relation between L and M is called the mass-luminosity relation. Equation 22 is of course only a crude estimation of the relation. However, it enables us to clearly illustrate some fundamental stellar properties. First, the luminosity is found to rapidly increase with the stellar mass. This increase, which is proportional to the third power of the mass, correctly reproduces the properties of stars during the long-lasting main sequence phase of core hydrogen burning. Second, the luminosity is found to depend on the opacity κ but not on the nuclear energy production. This nicely illustrates the fact briefly discussed above that nuclear reactions enable the star to shine during long periods of time but that its luminosity depends on the ability of photons to travel through the stellar matter to reach the stellar surface.

Evolution in Degenerate and Nondegenerate Conditions

After briefly studying how basic stellar properties can be simply derived from the general equations of stellar structure, we are now interested in investigating how these properties evolve during a stellar lifetime. As discussed above in the section devoted to stellar energy production, two main sources of energy are available for a star: thermonuclear reactions and gravitational contraction. Consequently, the evolution of a star can be schematically represented as a succession of phases during which the energy is mainly produced by nuclear reactions and phases during which the energy production related to gravitational contraction dominates. Indeed, as soon as all the nuclear fuel present in the core of a star has been burnt by nuclear reactions, energy is mainly produced by gravitational contraction until the physical conditions in the stellar center enable it to ignite a new series of nuclear reactions. Thus, the temperature and density increase in the central parts of a star during its evolution as a result of the succeeding contractions. This can lead to significative changes in the physical properties of stellar matter with a transition from nondegenerate to degenerate conditions.

We recall here that degeneracy pressure is of nonthermal origin and results from quantum-mechanical effects. According to Pauli's exclusion principle, each quantum cell of the six-dimensional phase space $\{x, y, z, p_x, p_y, p_z\}$ cannot contain more than two electrons (x, y, z correspond to the space coordinates of the electrons with volume $dV = dxdydz$, while p_x, p_y, p_z correspond to the momentum space). The volume of such a quantum shell is defined by $dp_x\,dp_y\,dp_z\,dV$ and is equal to h^3, with h the Planck constant. When the density increases, the volume dV is reduced so that some electrons will exhibit large impulses. These electrons with large velocities will then exert a new sort of pressure that solely depends on density and not on temperature. Note that this holds not only for electrons but also for other fermions like the neutrons.

Interestingly, the two main sources of energy production, nuclear reactions and gravitational contraction, lead to completely different effects when the stellar matter is degenerate compared to the nondegenerate case. Indeed, in nondegenerate conditions, a contraction leads to an increase of the central temperature of the star, while in degenerate conditions, a contraction may produce a cooling of the stellar matter. To illustrate these different behaviors, we first consider a uniform contraction of a given mass M. This results in a variation δr of the radius together with variations in pressure δP and density $\delta\rho$. Using the equation of hydrostatic equilibrium, the relation between the variations in pressure and radius is given by

$$\frac{\delta P}{P} = -4\frac{\delta r}{r}. \qquad (23)$$

The equation of mass conservation leads to the following relation between the variation in density and radius:

$$\frac{\delta\rho}{\rho} = -3\frac{\delta r}{r}. \tag{24}$$

Combining these equations, we obtain the relation between the variations in pressure and density:

$$d\ln P = \frac{4}{3} d\ln\rho. \tag{25}$$

We then use the general form of the equation of state

$$\mathrm{d}\ln\rho = \alpha \mathrm{d}\ln P - \delta \mathrm{d}\ln T, \tag{26}$$

with $\alpha = \left(\frac{\partial \ln\rho}{\partial \ln P}\right)_T$ and $\delta = -\left(\frac{\partial \ln\rho}{\partial \ln T}\right)_P$ to obtain the relation between the variations in temperature and density:

$$\mathrm{d}\ln T = \frac{4\alpha - 3}{3\delta} \mathrm{d}\ln\rho. \tag{27}$$

This relation between the changes in temperature and density during a slow contraction is sensitive to the equation of state of the stellar matter through the coefficients α and δ. For a perfect gas, $\alpha = \delta = 1$, and this relation simply gives

$$\mathrm{d}\ln T = \frac{1}{3} \mathrm{d}\ln\rho. \tag{28}$$

This means that during a slow contraction in nondegenerate conditions, the star evolves along a straight line with a slope of one-third in the diagram showing the variation of the central values of log T versus log ρ. This situation approximately applies during the contraction of the star on a Kelvin-Helmholtz timescale before the ignition of hydrogen and also between the main nuclear burning phases when gravitational contraction provides the needed energy.

It is interesting to note that a slope of one-third in the log T_c versus log ρ_c diagram implies that the star can enter the domain of degenerate matter during its evolution. Indeed, the frontier between nondegenerate and degenerate conditions is defined by a straight line with a slope of two-thirds. This can be readily understood by recalling that for a completely degenerate nonrelativistic gas, degenerate electronic pressure is related to density by $P \sim \rho^{5/3}$. Since $P \sim \rho T$ for a perfect gas, we then obtain $\rho T \sim \rho^{5/3}$ and hence $T \sim \rho^{2/3}$ when the perfect gas pressure of electrons equals the degenerate pressure. When a star approaches the domain of complete electron degeneracy, the values of the coefficients α and δ tend to 3/5 and 0, respectively. During this transition, α becomes therefore smaller than four-thirds before δ equals 0, so that the coefficient relating the density to the temperature variation in Eq. 27 above becomes negative. For a star entering the degenerate domain, a contraction does not produce an increase of the temperature as in the nondegenerate case but can instead result in a cooling of the stellar matter.

The effects of nuclear reactions are also completely different in degenerate conditions. Contrary to the nondegenerate case, an excess of energy production in the stellar center will not result in an expansion of the star when the matter is degenerate. In this case, an increase of temperature occurs in the center, but this increase does not produce a corresponding increase of the central pressure, which is solely determined by density in degenerate conditions. Consequently, nuclear reaction rates increase further and produce more and more energy leading to a flash or an explosion. While nuclear reactions are stable in nondegenerate conditions, they are thus found to be unstable in degenerate conditions.

Applications

By numerically solving the equations of stellar structure derived above, the evolution of the internal and global properties of stars is obtained. This evolution can be quite different depending on the initial mass and chemical composition of the star. The evolutionary tracks in the theoretical Hertzsprung-Russell (HR) diagram showing the variation of the luminosity of the star as a function of its temperature is given in Fig. 1 for stars with a solar chemical composition. Different evolutionary scenarios can be distinguished according to the initial stellar mass.

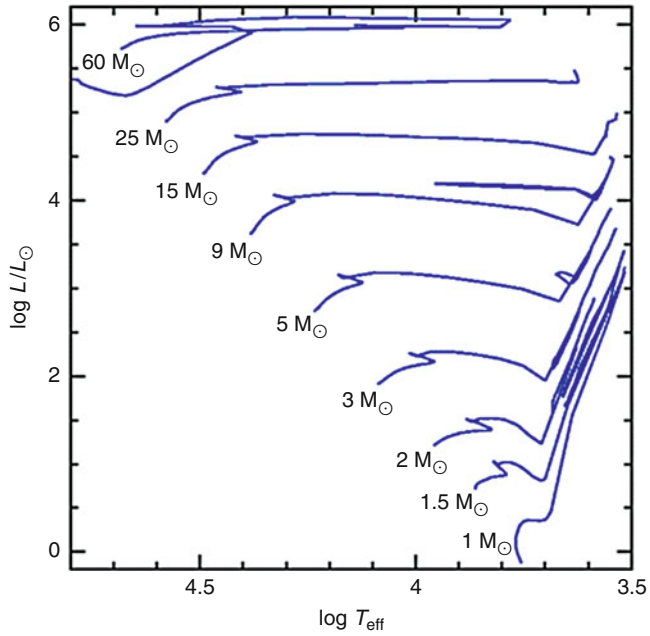

Stellar Evolution, Fig. 1 Evolutionary tracks in the HR diagram for stars with a solar chemical composition and masses between 1 solar mass and 60 times the solar mass

Substellar Objects

Objects with initial masses below about 0.08 $M_\odot$ never reach the central temperature required for hydrogen-burning ignition. These objects enter the degenerate regime during their contraction phase, leading to further contraction and cooling of the central layers as explained above. They are the progenitors of brown dwarfs. Note that for masses larger than about 0.012 $M_\odot$, deuterium burning occurs. This nuclear energy release is, however, not sufficient to compensate for the radiative energy losses, so that these objects continue to cool down.

Stars in a Mass Range of 0.08–0.5 $M_\odot$

Stars with initial masses between about 0.08 and 0.5 $M_\odot$ enter the phase of hydrogen burning. During this main-sequence phase, the energy production is due to the release of nuclear binding energy by transforming four hydrogen nuclei into one helium nucleus. As briefly mentioned when estimating the typical timescale of nuclear energy production, this corresponds to a mass defect of about 0.7 %, which is approximately ten times the energy that may be liberated by other fusion processes. This fusion can take place through two main series of reactions: the proton-proton chain (pp chain) and the ▶ CNO cycle. The pp chain is named after its first reaction, which requires two protons to form a deuterium nucleus ^{2}H. The deuterium then reacts with another proton to form ^{3}He. The formation of ^{4}He can be achieved through three different branches: pp1, pp2, and pp3. For the pp1 chain, two ^{3}He nuclei are needed to obtain ^{4}He, while the other chains require that ^{4}He already exists. The relative frequency of the pp branches is sensitive to the temperature, density, and chemical composition of the stellar layers. Having larger temperature sensitivity than the pp1 chain, the pp2 and pp3 chains will then dominate when the temperature increases.

The CNO cycle is the second main series of reactions for hydrogen burning. In this case, isotopes of C, N, and O are needed to obtain ^{4}He. The temperature sensitivity of the CNO cycle is much higher than for the pp chain. Consequently, the pp chain will dominate over the CNO cycle at low temperatures (for temperatures typically lower than about 15×10^6 K), while it becomes negligible compared to the CNO cycle for higher temperatures. Thus, hydrogen burning will mainly occur through pp chains for lower-mass stars (typically for stars with masses lower than

about 1.5 $M_{\odot}$) and CNO cycle for more massive stars.

After hydrogen exhaustion, the helium core becomes electron degenerate before reaching a temperature sufficient for helium ignition. Consequently, these stars only go through the hydrogen-burning phase and end up as helium white dwarfs. The duration of the hydrogen-burning phase is much larger than the age of the Universe for these stars, which are still burning hydrogen in their core. The observed helium white dwarfs are thus thought to come from more massive progenitors whose evolution has been radically changed by belonging to close binary systems.

Stars with an Initial Mass Between About 0.5 and 2.3 $M_{\odot}$

These stars enter both the hydrogen and the helium burning phases. During the main sequence, these stars exhibit small convective cores or no convective core (for masses smaller than about 1.2 $M_{\odot}$). After central hydrogen exhaustion, there will be a transition from central hydrogen burning to hydrogen fusion in a shell surrounding the core, resulting in a slow increasing of the mass of the helium core. At this point, the temperature of the core is still far from being high enough for helium ignition: the star is in a phase of hydrogen shell burning. Together with the core contraction, there is an expansion of the hydrogen-rich envelope resulting in a shift in the HR diagram toward lower surface temperatures. The star then begins to ascend the ▶ red giant branch. The densities in the central layers are high enough for the electron gas to become degenerate. At the tip of the red giant branch, helium ignites in degenerate conditions leading to a strong temperature rise within a very short time interval (of the order of the dynamic timescale) that is called the helium flash. This temperature rise stops when the temperature is high enough to lift the degeneracy of the electron gas. The helium flash removes therefore the degeneracy in the stellar core and enables the helium-burning phase to continue in nondegenerate conditions.

Helium burning requires temperatures higher than about 10^8 K. The fundamental reaction at the basis of the formation of ^{12}C from three ^4He nuclei is the triple alpha reaction. Note that the star is not totally disrupted by the helium flash, since the massive shell surrounding the helium zone is able to damp the explosive shock wave produced in the internal layers. After the helium flash, the star finds a new equilibrium configuration either on the horizontal branch in the HR diagram (at low metallicity) or on the so-called red clump (at solar and higher metallicity) where core helium burning takes place. After the helium-burning phase, the star evolves along the asymptotic giant branch (AGB) until the outer envelope is removed by wind and thermal pulses and a planetary nebula forms around the white dwarf.

Stars with an Initial Mass Between About 2.3 and 8 $M_{\odot}$

The beginning of the evolution of stars with an initial mass in the mass range of 2.3–8 $M_{\odot}$ is similar to the evolution of lower-mass stars undergoing a helium flash. Their evolution differs after the exhaustion of hydrogen in the central stellar core. This difference is mainly due to the fact that hydrogen burning for these more massive stars occurs in well-mixed convective cores leading to a helium core with a non-negligible mass at the end of the main sequence. Due to the absence of a central energy source, the helium core tends to become isothermal, while hydrogen shell burning occurs at the bottom of the surrounding hydrogen-rich envelope. The star then rapidly crosses the HR diagram to become a red giant. The contraction of the core proceeds approximately on a Kelvin-Helmholtz timescale and goes with an expansion of the hydrogen-rich envelope. The core contraction occurs in nondegenerate conditions resulting in the heating of the central layers. The central temperature rises until it reaches the temperature required to ignite helium (about 10^8 K). This results in a new source of central energy that stops the rapid contraction of the core: the star is then again in a phase of complete equilibrium, which terminates when ^4He is entirely

transformed into ^{12}C, ^{16}O, and ^{20}Ne. Evolving along the asymptotic giant branch, the star experiences a prolonged phase of thermal pulses leading either to the ejection of the envelope and the formation of a carbon-oxygen white dwarf, as in the case of the lower-mass stars experiencing the helium flash, or with carbon ignition in degenerate conditions if the carbon-oxygen core reaches the Chandrasekhar limit of about 1.4 $M_{\odot}$. In this case, the star is probably completely disrupted by a supernova explosion. This point is, however, still subject to major uncertainties. Indeed, estimates for the maximum initial mass able to form a white dwarf coming from observations of white dwarfs in clusters lead to values of about 8 $M_{\odot}$, which is approximately the minimal mass of a massive star. This means that the mass interval possibly leading to carbon detonation supernovae is very limited.

Massive Stars

Massive stars can be simply defined as stars that go through all nuclear burning phases: hydrogen, helium, carbon, neon, oxygen, and silicon burning. The minimum initial mass for a star to proceed through this whole sequence of nuclear phases is approximately of 8 $M_{\odot}$. This series of nuclear burning phases comes to an end with the formation of an iron core since no further exothermic fusions are then possible. The evolution of the central layers of these stars can be simply viewed as following succeeding cycles of nuclear burning, exhaustion of nuclear fuel, core contraction, and heating enabling the ignition of the next burning phase. As a result of these succeeding evolution cycles, heavier elements gradually accumulate near the center of the star. This leads to the characteristic "onion-skin structure" of the interior of evolved massive stars, where heavier elements are present on separated mass shells as the distance to the stellar center decreases.

Mass loss plays a major role in the evolution of massive stars. Indeed, these stars are characterized by a high temperature-to-density ratio resulting in a high radiation-to-gas pressure ratio, which favors mass loss by ▶ stellar winds. Wolf-Rayet stars nicely illustrate the effects of mass loss on massive stars. These stars exhibit high mass loss rates and strong emission lines with highly nonsolar chemical abundances. The abundance anomalies observed at the surface of Wolf-Rayet stars clearly indicate that a mechanism is able to efficiently remove the surface layers of the star. This can either be done through stellar wind losses in single stars or through Roche lobe overflow in binary systems.

Massive stars end their lives in supernovae explosions, enriching the interstellar medium in processed material and leaving a neutron star or a black hole as a remnant, depending on the mass of their iron core. When the mass of the core exceeds the so-called Oppenheimer-Volkoff mass (around 2 $M_{\odot}$), a black hole is formed. Otherwise, the pressure of degenerate neutrons is able to stop the collapse and leads to the formation of a neutron star.

Future Directions

The classical view of stellar evolution described above is based on many simplifying hypotheses: stars are considered as spherical systems in hydrostatic and radiative equilibrium, where mixing only occurs in convective zones. In particular, the effects of rotation and magnetic fields are neglected. This classical theoretical description correctly accounts for many astronomical observations. However, with the increasing amount of observational data, quantitative discrepancies appear between observations and theoretical predictions of standard models. For instance, standard stellar models are unable to reproduce neither the observed abundance anomalies of helium and nitrogen at the surface of massive stars nor the observations of light element abundances at the surface of solar-type stars. This suggests that other transport mechanisms take place in stellar radiative zones. Rotation is one of the key physical processes that have a deep influence on all aspects of stellar structure and evolution. The effects of magnetic fields on the internal stellar structure need also to be taken into account to obtain a coherent picture of stellar evolution. Consequently, various theoretical

models of these physical processes have been developed and compared to observational data in order to make progress in our understanding of stellar physics. These comparisons are, however, somewhat limited by the fact that classical astronomical observations only give us access to properties of the surface of the star, such as the effective temperature, luminosity, and surface chemical composition. Indeed, the opacity of a star is so large that only a tiny layer surrounding the star, the photosphere, can be observed. This is insufficient to compare and constrain a whole theoretical structure of the stellar interior, where complex physical processes are taking place. Obtaining direct observational constraints on the internal properties of stars is thus required. In this context, the rapidly developing field of ▶ asteroseismology offers a valuable opportunity to make significant progresses in our understanding of stellar structure and evolution.

We finally note that the evolution of binary stars can be quite different from the classical single-star evolutionary scenarios briefly described above. All physical processes discussed here for single stars also apply to binary stars but with a higher degree of complexity due to possible mass transfers, tidal interaction and mixing, tidal generation of gravity waves, etc.

See Also

- ▶ Asteroseismology
- ▶ Binary Stars, Young
- ▶ CNO Cycle
- ▶ Chronological History of Life on Earth
- ▶ Hertzsprung-Russell Diagram
- ▶ High-Mass Star
- ▶ Low Mass Star
- ▶ Nucleosynthesis, Stellar
- ▶ P-P Chains
- ▶ Red Giant
- ▶ Star Formation, Observations
- ▶ Star
- ▶ Stellar Population
- ▶ Stellar Rotation
- ▶ Stellar Winds

References and Further Reading

Aerts C, Christensen-Dalsgaard J, Kurtz DW (2010) Asteroseismology. Springer, Dordrecht

Böhm-Vitense E (1958) Über die Wasserstoffkonvektionszone in Sternen verschiedener Effektivtemperaturen und Leuchtkräfte. Z Astrophys 46:108–143

Crowther PA (2007) Physical properties of Wolf-Rayet stars. Annu Rev Astron Astrophys 45(1):177–219

de Boer K, Seggewiss W (2008) Stars and stellar evolution. EDP Sciences, Les Ulis

Hansen CJ, Kawaler SD, Trimble V (2004) Stellar interiors: physical principles, structure, and evolution, 2nd edn. Springer, New York

Kippenhahn R, Weigert A (1990) Stellar structure and evolution. Springer, Berlin

Maeder A (2009) Physics, formation and evolution of rotating stars. Springer, Berlin

Prialnik D (2000) An introduction to the theory of stellar structure and evolution. Cambridge University Press, Cambridge

van den Heuvel EPJ (1994) Topics in close binary evolution. In: Heuvel EPJ (ed) Saas-Fee advanced course 22: interacting binaries. Springer, Berlin, pp 263–474

Vanbeveren D (2004) Massive close binaries. EAS Publ Ser 13:141–161

Stellar Oscillation

▶ Stellar Pulsation

Stellar Population

Leticia Carigi
Instituto de Astronomía, Universidad Nacional Autónoma de México, México, DF, Mexico

Keywords

Galaxies; Initial mass function; Metallicity; Stars; Stellar evolution

Definition

Astronomers use the terms Populations I, II, and III to refer to groups of stars whose mass fraction

of elements heavier than helium is similar to the Sun (Population I), much less than the Sun (Population II), or negligible (Population III, not yet observed but hypothesized to be the earliest generation of stars). In general, stars with greater abundances of heavier elements are younger than those with lower abundances.

Overview

One of the more common classifications of stellar populations is based on the age and metallicity, where metallicity is the proportion of the stellar mass made up of chemical elements other than hydrogen and helium. In that classification, the stars are divided into Populations I, II, or III. The stellar populations show a continuum of properties, and it is difficult to place some stars in a given population. Population III stars are hypothesized to be the first ones formed in the Universe, when the composing gas was only H and He. Since no stars of zero metallicity have been observed, these stars would have had masses higher than 1 $M_{\odot}$; in other words, they followed a different ▶ initial mass function compared to the present one. When the most massive of those stars exploded as supernovae, they ejected heavy chemical elements into the interstellar medium where subsequently the very metal-poor Population II stars formed. In the ▶ Milky Way, Population II stars are mainly located in the halo. These stars are older than about 10 Gyr and have metallicities between 1/40,000 and 1/10 of the solar value. Most ▶ globular clusters and dwarf galaxies contain Population II stars.

Population I stars are located in the disk; these stars are the youngest of the galaxy and show metallicities between about one-tenth and three times the solar value. All observed stars with planetary systems, including the Sun, are Population I stars, and most of these stars harboring planets have metallicities higher than the solar one.

There are some stars that do not follow these rules: (1) elliptical galaxies, bulges, and the inner disk of spiral galaxies show metal-rich stars that are older than 10 Gyr and (2) dwarf irregular galaxies and the outer disk of spiral galaxies show metal-poor stars that are younger than 1 Gyr.

Another common classification of stellar populations is based on the photometric properties: stellar groups dominated by blue stars are called early-type populations and those dominated by red stars are called late-type populations. Yet another concept of stellar population commonly used in the evolution of stellar groups, like a galaxy or a galactic component, is the Simple Stellar Population (SSP). In an SSP, all stars have the same age and the same metallicity; in addition they are born in the same region of space. Since a galaxy is formed by diverse types of stars, a galaxy can be studied as a combination of SSPs of different ages, metallicities, and masses. Therefore, the SSPs allow observational astronomers to infer the age, the metallicity, and the mass of the stars that shine in a galaxy.

See Also

- ▶ Exoplanets, Discovery
- ▶ Globular Cluster
- ▶ Initial Mass Function
- ▶ Metallicity
- ▶ Milky Way
- ▶ Star
- ▶ Stellar Evolution
- ▶ Supernova

S

References and Further Reading

Akerman CJ et al (2004) The evolution of the C/O ratio in metal-poor halo stars. Astron Astrophys 414:931–942

Bruzual G, Charlot S (2003) Stellar population synthesis at the resolution of 2003. MNRAS 344:1000–1028

Sparke L, Gallagher J (2007) Galaxies in the universe: an introduction. Cambridge University Press, Cambridge

Tolstoy E, Hill V, Tosi M (2009) Star-formation histories, abundances, and kinematics of dwarf galaxies in the local group. Annu Rev Astron Astrophys 47:371–425

Stellar Pulsation

Patrick Eggenberger
Geneva Observatory, University of Geneva, Geneva, Switzerland

Synonyms

Stellar oscillation

Definition

Stellar pulsations or oscillations are periodic variations of the size, brightness, and temperature of the star induced by some internal physical processes. These pulsations can be either radial, with symmetric expansions and contractions over the whole stellar surface, or non-radial when the spherical symmetry of the star is not preserved. Stellar pulsations provide us with a valuable opportunity to study the internal properties of stars that are not accessible otherwise and to obtain a cosmic distance scale by calibrating the luminosity of stars with their pulsation periods.

See Also

► Asteroseismology

Stellar Rotation

Sylvia Ekström
Observatoire Astronomique de l'Université de Genève, Faculté des Sciences, Université de Genève, Versoix, Switzerland

Keywords

Spectral type; Stars; Stellar formation; Stellar evolution

Definition

The fact that a star rotates induces changes in its evolution. The centrifugal force brings an additional component which adds to pressure in sustaining the star against its own gravity. Rotation induces instabilities which in turn induce mixing. The mixing leads to larger cores and longer lifetimes, and also modifies the nucleosynthesis. For the most massive stars, fast rotation can modify the dynamics of the final supernova, breaking the spherical symmetry during the collapse. From an observational point of view, rotation modifies the spectral type and luminosity class inferred for the star. It also widens the absorption lines, because of the differing Doppler velocity of the approaching versus the receding side of the star.

Overview

Roughly summarized, a star is a sphere of ionized gas held in hydrostatic equilibrium by the competition between gravitation and pressure. Any additional force will modify the equilibrium and thus the characteristics of the object. Rotation brings such an additional force.

During star formation, a molecular cloud with a typical radius of 0.1 pc contracts to form a newborn star with a reduction of radius through six orders of magnitude. Angular momentum conservation implies that the slightest rotation movement in the cloud will convert into fast stellar spin. It is not yet clear how the excess angular momentum is driven away so that the star can actually form, probably through magnetic interactions between the star and the ► protoplanetary disk, or through the formation of binary stars, where angular momentum is transformed into orbital motion.

If the angular momentum kept by the young star is high enough, the centrifugal force that it experiences becomes nonnegligible and adds a sustaining force against gravity see (Fig. 1). At the very beginning of its evolution, the star behaves as if its mass were smaller: the luminosity and effective temperature are shifted to lower values. As the evolution proceeds, rotation

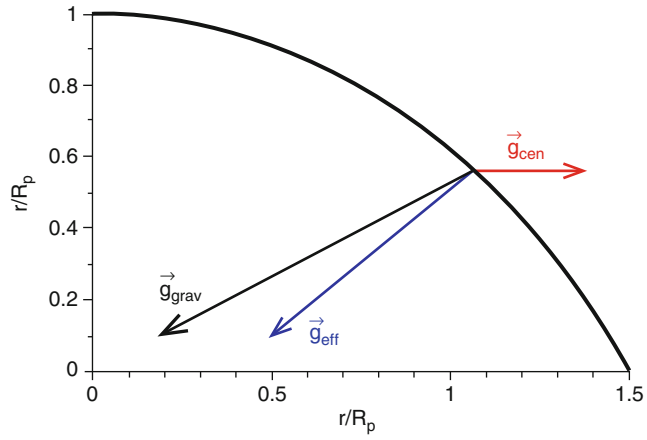

Stellar Rotation, Fig. 1 Maximal surface deformation of a rotating star (Courtesy C. Georgy). The *x-axis* and *y*-axis are the radius, normalized to the polar one. The gravitational force is in *black*, the centrifugal force in *red*, and the resulting effective gravity in *blue*

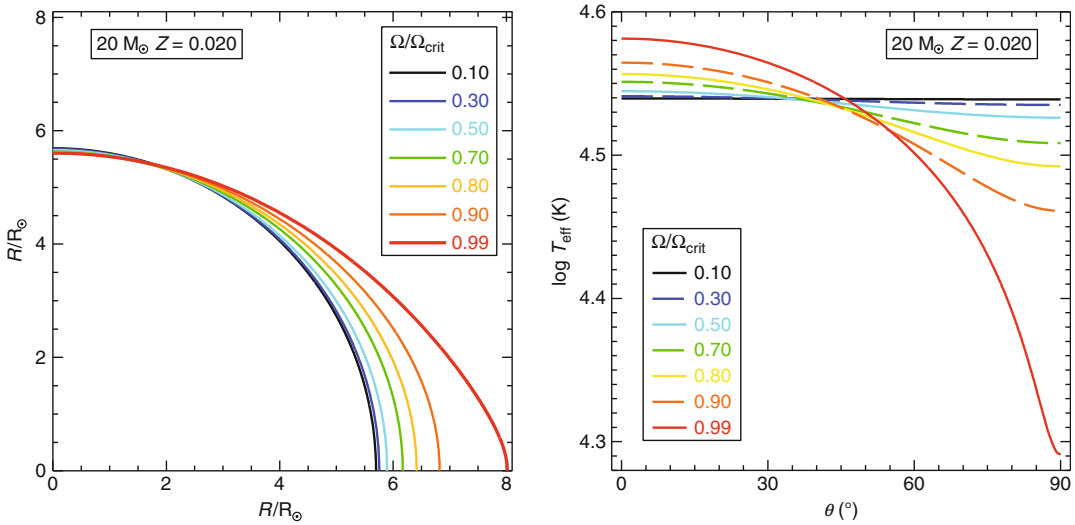

Stellar Rotation, Fig. 2 (*Left*) Deformation of the surface of 20 M_{sol} rotating stellar models. The *curves* are for increasing (from *black* to *red*) ratios of the angular velocity to the critical one, which is the angular velocity at which the outer layers of the star are no longer gravitationally bound. At critical velocity, the equatorial radius (*x*-axis) is 1.5 times the polar one (*y*-axis). (*Right*) Effective temperature as a function of the colatitude (pole: $z = 0°$; equator: $\theta = 90°$) for the same models. Fast rotation leads to hotter poles and cooler equator, the difference amounting to a factor of 2 at critical rotation (From Ekström et al. 2008)

triggers various instabilities inside the star, among which:

- The *shear instability*: as the star does not rotate like a rigid body, the differential rotation induces a shear between layers with different angular velocities. The shear drives a turbulent mixing of the chemical species through the different layers.
- The *Eddington-Sweet circulation*: rotation deforms the star (Fig. 2), so except at the equator, the centrifugal force is not parallel to gravity: the resultant effective gravity is not radial, as shown in Fig. 1. The radiative flux, which depends on the local effective gravity, is not constant on equipotential surfaces. According to von Zeipel (1924), the star cannot be in hydrostatic and radiative

equilibrium at the same time. This drives a large-scale current, also known as the *meridional circulation*, which mainly transports the angular momentum inside the star.

The main observable characteristics of the star (effective temperature, gravity, luminous flux) become colatitude-dependent, a feature which can now be observed by interferometric techniques (Domiciano de Souza et al. 2003).

The shear mixing brings fresh hydrogen into the burning core which grows, enhancing the luminosity of the star. Since more fuel is available, the duration of the main sequence is increased. Rotation enhances the mass loss by radiative winds through three mechanisms:

- The stronger effective gravity at the poles induces a stronger flux in that direction.
- The lower effective temperature at the equator increases the opacity and thus the atomic-line-driven winds.
- Later during core He-burning, rotational mixing brings freshly synthesized heavy elements to the surface, increasing the effective ▶ metallicity of the star.

Generally, rotation favors a redwards evolution in the HR diagram. Its inclusion in stellar evolution codes has improved the match between models and observations in many aspects, such as the evolution of the surface abundances during the main sequence (Heger and Langer 2000; Maeder and Meynet 2000), the variation with metallicity of the red- to blue-supergiants ratio (Maeder and Meynet 2001), and of the Wolf-Rayet to O stars ratio (Meynet and Maeder 2003; Vink and de Koter 2005).

Shear mixing induces a transport of elements between the burning core and the burning shells, modifying the nucleosynthesis. For example, the transformation of carbon produced in the He-burning core into nitrogen in the H-burning shell is supposed to be the origin of the primary nitrogen observed at very low metallicity (Meynet and Maeder 2002).

By modifying the geometry of the explosion, rotation influences strongly the supernova dynamics. It is thought that the collapse of a fast rotating massive star is at the origin of the long-duration Gamma-ray bursts (Woosley 1993; Woosley and Bloom 2006).

See Also

- ▶ Diffusion
- ▶ Hertzsprung-Russell Diagram
- ▶ Main Sequence, Star
- ▶ Metallicity
- ▶ Protoplanetary Disk
- ▶ Star Formation, Theory
- ▶ Stellar Evolution
- ▶ Supernova

References and Further Reading

Domiciano de Souza A, Kervella P, Jankov S, Abe L, Vakili F, di Folco E, Paresce F (2003) Astron Astrophys 407:L47–L50
Ekström S et al (2008) Astron Astrophys 478:467–485
Heger A, Langer N (2000) Astrophys Journal 544:1016–1035
Maeder A (2009) Physics, formation and evolution of rotating stars. Springer, Berlin
Maeder A, Meynet G (2000) Evolution of rotating stars. Annu Rev Astron Astrophys 38:143–190
Maeder A, Meynet G (2001) Astron Astrophys 373:555–571
Meynet G, Maeder A (2002) Astron Astrophys 390:561–583
Meynet G, Maeder A (2003) Astron Astrophys 404:975–990
Vink J, de Koter A (2005) Astron Astrophys 442:587–596
Woosley SE (1993) Astrophys Journal 405:273–277
Woosley SE, Bloom JS (2006) The supernova gamma-ray burst connection. Annu Rev Astron Astrophys 44:507–556
von Zeipel H (1924) MNRAS 84:665–683

Stellar Seismology

- ▶ Asteroseismology

Stellar Winds

Steven W. Stahler
Department of Astronomy, University of California, Berkeley, CA, USA

Keywords

Young star; High mass star

Definition

The tenuous outer layers of stars can be driven off into space, creating the flows known as stellar winds. In main-sequence stars like the Sun, the winds are driven by thermal pressure in the hot stellar corona. The wind, being guided by the star's magnetic field, is anisotropic. More massive stars and red giants propel gas by radiation pressure. Young stars have especially vigorous winds that are responsible for dissipating ambient cloud gas and circumstellar disks, thus ending planet formation. Here, gas is believed to be flung out centrifugally along magnetic field lines embedded in the star and its surrounding disk.

Overview

Stars of all masses and all evolutionary phases slough off their outermost layers of gas. The resulting, low-density flow is known as a stellar wind. The most familiar example is the solar wind, which has been extensively studied by satellites and other spacecraft for half a century. Ionized gas from the Sun flows past the Earth at an average speed of 500 km/s. Some ions become trapped in the Earth's magnetic field, creating the auroral glow seen near both the north and south poles.

The solar wind is driven by the pressure of very hot gas of several million degrees at the base of the Sun's corona. Other main-sequence stars with the Sun's mass and below are thought to generate similar winds. The most massive winds from main-sequence objects are produced by O stars, which also have the highest luminosity. These winds are driven by the radiation pressure from ultraviolet photons acting on ionized gas in the stellar atmosphere. The gas piles up periodically and creates internal shocks, which are detected by the X-rays they emit.

Aging stars that have left the main sequence also attain large luminosities and emit relatively massive winds. Here, the driving force is radiation pressure from infrared photons. The pressure is exerted not on the gas itself, but on dust grains that condense in the flow. Indeed, dust grains throughout interstellar space ultimately arise from nucleation within the winds of red giants.

Young stars, even those of low mass, produce vigorous stellar winds. The winds from classical ▶ T Tauri stars are seen by characteristic P Cygni line profiles in the stellar atmosphere and by spatially extended jets. These stars have strong magnetic fields and also rotate relatively fast. Accordingly, the winds are driven by material being flung out along magnetic field lines. The field is anchored in the stellar surface and the innermost region of its circumstellar disk. Similar winds of even greater strength must arise from embedded protostars.

Whatever their origin, the winds from young stars play a fundamental role in star and planet evolution. Those emitted by protostars dissipate the surrounding molecular clouds, thus ending the accretion of gas and revealing the star optically. Winds from ▶ pre-main-sequence stars are responsible for driving off their circumstellar disks, terminating the process of planet formation.

See Also

- ▶ Bipolar Flow
- ▶ High-Mass Star
- ▶ Pre-Main-Sequence Star
- ▶ Skumanich Law
- ▶ T Tauri Star

References and Further Reading

Edwards S, Ray T, Mundt R (1993) In: Levy EH, Lunine JI (eds) Protostars and planets III. University of Arizona Press, Tucson, p 567
Holzer TE (1987) In: Pizzo VJ, Holzer TE, Sime DG (eds) Proceedings of the sixth international solar wind conference. NCAR, Boulder, p 3
Lamers HJGL, Cassinelli JP (1999) Introduction to stellar winds. Cambridge University Press, Cambridge

Stellar Yield

Nikos Prantzos
Institut d'Astrophysique de Paris, Paris, France

Definition

The mass of nuclides ejected by a star into the interstellar medium, at the end of or during its life (through the final explosion or its wind, respectively) may be called the stellar yield. For instance, a star of $\sim$20 $M_\odot$ ejects $\sim$1 $M_\odot$ of oxygen. In general, lighter elements are produced during the hydrostatic evolution of the star, while heavier elements are produced by the final explosive nucleosynthesis. The *net* stellar yield is the difference between that quantity and the amount of the nuclide incorporated in the star at its formation (i.e., the amount of newly synthesized nuclei) and contributes to the chemical evolution of the galaxy. Stellar yields depend on the mass of the star but also on its initial ▶ metallicity, mass loss, rotation, etc. They are theoretically calculated but rarely validated by observations (the only case being supernova SN1987A, a 18–20 $M_\odot$ star, which produced 0.07 $M_\odot$ of ^{56}Fe, as inferred from the evolution of its luminosity).

See Also

- ▶ Metallicity
- ▶ Star
- ▶ Stellar Winds
- ▶ Supernova

Steranes, Rock Record

Jennifer Eigenbrode
NASA Goddard Space Flight Center, Greenbelt, MD, USA

Keywords

Biomarkers; Biosignatures; Eukaryotes; Hydrocarbons; Molecular fossils

Synonyms

Steroids

Definition

Steranes is a class of four-ringed cyclic compounds derived from steroids or sterols via diagenetic degradation and thermal maturation. The sterane structure is fully saturated with hydrogen atoms (Fig. 1) and makes up the hydrocarbon core of all steroids and sterols. Steranes are often regarded as molecular fossils of eukaryotic organisms, particularly those having a side chain at the C-24 position.

Overview

The precursor compounds of steranes, steroids and sterols, are essential lipids for maintaining rigidity and permeability of membranes in all eukaryotes. Steroids are isoprenoids and synthesized from squalene in complex biosynthesis in which multiple steps require reactions with molecular oxygen.

Most variations in steroid structures (i.e., position and number of double bonds, hydroxyl groups, and other functional groups) are lost during the diagenesis and thermal maturation.

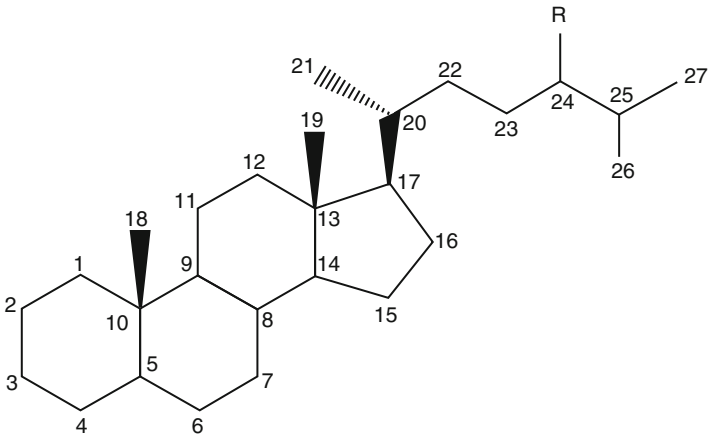

Steranes, Rock Record, Fig. 1 Core structure of steranes composed of C-C bonds (lines) and saturated with hydrogen atoms (not shown). The key stereochemical variants occur at C-5, C-14, C-17, and C-20 positions. Additional methylation is common at C-2, C-3, C-24, and C-23. R = H, methyl, ethyl, *n*-propyl, and isopropyl groups

However, structural variants with alkyl side chains are preserved over geological timescale in bitumen and oils and as constituents in kerogen of Cenozoic to Archean rocks. Although most sterol structures are widespread among eukaryotes, some alkylated structures are specific to particular taxonomic groups (e.g., sponges and algal groups) and may be distinguishable in the molecular fossil record as different steranes.

Steranes and their precursors are three-dimensional structures. Despite the 100s of possible stereochemical variations in the structures, steroid biomolecules are very specific (especially at C-5, C-14, C-17, and C-20 positions). Steroid and sterol stereochemistry is regarded as a classic example of stereochemical specificity of biomolecules in general – a fundamental biosignature of life. During diagenesis and thermal maturation, the specific biomolecular stereochemistry is lost and other isomers are formed. The relative abundances of some sterane isomers are commonly used to indicate particular geological or thermal conditions.

Most molecular fossils including steranes are thermally released from kerogen in ancient rocks, either naturally to form bitumen and oil or artificially in the laboratory. The sterane composition of bitumen and oils is typically determined by extracting hydrocarbons from rock or directly from oil using a nonpolar organic solvent (such as hexanes) and then analyzed via gas chromatography mass spectrometry instrumentation.

See Also

- ▶ Biomarkers
- ▶ Bitumen
- ▶ Eukarya
- ▶ Eukaryotes, Appearance and Early Evolution of
- ▶ Hydrocarbons
- ▶ Isoprenoids
- ▶ Kerogen
- ▶ Membrane
- ▶ Molecular Fossils

S

References and Further Reading

Brocks JJ, Logan GA, Buick R, Summons RE (1999) Archean molecular fossils and the early rise of eukaryotes. Science 285:1033–1036

Eigenbrode JL (2007) Fossil lipids for life-detection: a case study from the early Earth record. Space Sci Rev 135:161–185

Love GD, Grosjean E, Stalvies C, Fike DA, Bradley AS, Bhatia M, Meredith W, Snape CE, Bowring SA, Condon DJ, Grotzinger JP, Summons RE (2009) Fossil steroids record the appearance of Demospongiae during the Cryogenian period. Nature 457:718–721

Peters KE, Walters CC, Moldowan JM (2007) The biomarker guide: biomarkers and isotopes in petroleum

systems and Earth history. Cambridge University Press, Cambridge, p 704
Summons RE, Walter MR (1990) Molecular fossils and microfossils of prokaryotes and protists from Proterozoic sediments. Am J Sci 290-A:212–244
Summons RE, Volkman JK, Boreham CJ (1987) Dinosterane and other steroidal hydrocarbons of dinoflagellate origin in sediments and petroleum. Geochim Cosmochim Acta 51:3075–3082
Summons RE, Bradley AS, Jahnke LL, Waldbauer JR (2006) Steroids, triterpenoids and molecular oxygen. Philos Trans R Soc B 361:951–968
Summons RE, Albrecht P, McDonald G, Moldowan JM (2007) Molecular biosignatures: generic qualities of organic compounds that betray biological origins. Space Sci Rev 135:133–157
Volkman JK (1986) A review of sterol markers for marine and terrigenous organic matter. Org Geochem 9:83–99

Stereochemistry

Gilles Bruylants
Engineering of Molecular NanoSystems,
Universté Libre de Bruxelles, Brussels, Belgium

Definition

Stereochemistry refers to the relative spatial arrangement of atoms within molecules. Also known as 3D chemistry, it spans the entire range of organic, inorganic, biological, physical, and supramolecular chemistries. Stereochemistry focuses on ▶ stereoisomers, molecules that have the same chemical formula and in which the atoms have the same connectivity but different spatial distributions. If two stereoisomers are mirror images of each other, they are called ▶ enantiomers. If they are non-mirror images of each other, they are diastereoisomers.

See Also

▶ Achiral
▶ Chirality
▶ Enantiomeric Excess
▶ Enantiomers
▶ Isomer
▶ Racemic Mixture
▶ Stereoisomers

Stereoisomers

Robert Hazen
Geophysical Laboratory, Carnegie Institution of Washington, Washington, DC, USA

Keywords

Chiral pairs of molecules; Enantiomeric pairs of molecules; Mirror symmetric pairs of molecules

Synonyms

Stereomers

Definition

Stereoisomers are molecular ▶ isomers, in which two or more molecules have identical molecular formulas and atomic connectivities, but in which the atoms are arranged differently in space. Stereoisomers thus contrast with constitutional isomers, which have identical molecular formulas but differing atomic connectivities.

Stereoisomers are divided into two important groups. Conformational isomers are interchangeable by a rotation around a single bond. By contrast, configurational isomers are not readily transformable from one to the other; bonds must be broken to achieve such a transformation.

Configurational isomers are further subdivided into enantiomers (mirror image pairs of molecules) and diastereomers (which are not related by mirror symmetry). ▶ Enantiomers, unlike diastereomers, display many identical properties, including

density, vapor pressure, melting and boiling points, and other thermochemical properties.

See Also

- ► Enantiomers
- ► Enantiomeric Excess
- ► Isomer

Stereomers

- ► Stereoisomers

Steric Effect

Henderson James (Jim) Cleaves II
Earth–Life Science Institute (ELSI), Tokyo Institute of Technology, Meguro–ku, Tokyo, Japan
Institute for Advanced Study, Princeton, NJ, USA
Blue Marble Space Institute of Science, Washington, DC, USA
Center for Chemical Evolution, Georgia Institute of Technology, Atlanta, GA, USA

Definition

In chemistry, a steric effect is an influence on a reaction's course or rate determined by the fact that all of the atoms within a molecule occupy space; thus, certain collision paths are either disfavored or favored. When atoms are brought close together, there is an associated cost in energy due to overlapping electron clouds, and this may affect the molecule's preferred conformation and reactivity. Steric effects are frequently contrasted with electronic effects in explaining chemical reactivity. Steric effects can play a significant role in ► molecular recognition.

See Also

- ► Molecular Recognition

Sterile

Catharine A. Conley
NASA Headquarters, Washington, DC, USA

Definition

A sterile spacecraft or environment is one that contains no viable organisms, as measured by a specific assay.

Sterility Assurance Level

Catharine A. Conley
NASA Headquarters, Washington, DC, USA

Definition

The sterility assurance level describes the probability that an object could be non-sterile after it has been subjected to an accepted sterilization process.

Sterilization

Catharine A. Conley
NASA Headquarters, Washington, DC, USA

Definition

For ► planetary protection, sterilization is a process that actively reduces the ► bioburden on flight hardware so that the hardware is nearly free (consistent with the appropriate specifications) of viable ► microorganisms.

See Also

- ▶ Bioburden Reduction
- ▶ Disinfection
- ▶ Inactivation
- ▶ Pasteurization

Steroids

- ▶ Steranes, Rock Record

Sticking Coefficient

William M. Irvine
University of Massachusetts, Amherst, MA, USA

Definition

The probability that an incident atom or molecule will stick to a solid surface, as of an ▶ interstellar dust grain, is called the sticking coefficient.

See Also

- ▶ Interstellar Dust

Stirling Range Biota

Stefan Bengtson
Department of Palaeozoology, The Swedish Museum of Natural History, Stockholm, Sweden

Keywords

Eukaryotes; Multicellular; Paleoproterozoic; Trace fossils

Definition

The Stirling Range biota is a Paleoproterozoic biota found in the Stirling Range formation of southwestern Australia and composed of disk-shaped fossils and trace-making organisms about 1.8–2.0 Ga old. The biota lived in a near-shore marine environment and is thought to have included motile multicellular eukaryotes.

Overview

The Stirling fossils were discovered in southwestern Australia in the 1990s and were interpreted to represent metazoans (animals)

Stirling Range Biota, Fig. 1 Discoidal fossil of uncertain affinity (From Bengtson et al. 2007)

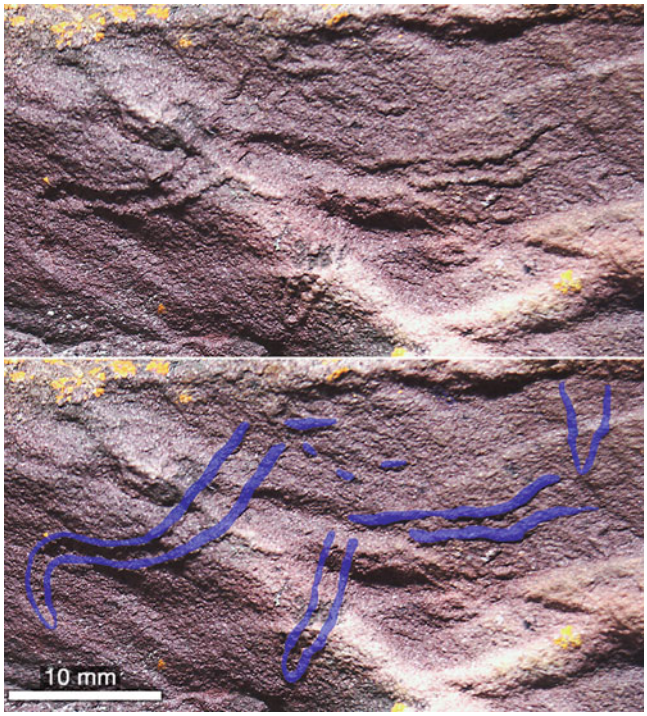

Stirling Range Biota, Fig. 2 Hairpin-like structures interpreted as traces of motile, multicellular organisms (From Bengtson et al. 2007)

belonging to the ▶ Ediacaran biota, less than 600 Ma old (Cruse and Harris 1994; Cruse et al. 1993). Subsequent radiometric dating of the sandstones containing the fossils showed that the Stirling Range biota is considerably older than the Ediacaran, between 1.8 and 2.0 Ga old (Rasmussen et al. 2004).

The biota contains disk-shaped fossils of unknown affinities (Fig. 1) and paired ridges interpreted as traces of moving organisms (Fig. 2). The traces have a characteristic hairpin shape, with one end closed and the other end usually slightly flaring. The tracemaker has been reconstructed as a motile multicellular or syncytial/multinucleate eukaryotic organism of unknown affinity (Bengtson et al. 2007; Rasmussen et al. 2002). The organism probably had a bulbous resting shape but stretched out into a more elongate body form, 1–2 mm in width, when in motion. Moving along the sea floor, the organism left sediment-entrained mucus ridges behind on both sides. The occasional presence of ridge pairs with crossed-over ridges suggests that the ridges represented two sides of a coherent band and that the organism laid down a string of mucus as it was crawling, much like today's ribbon worms or garden snails.

Because of its considerable age, more than three times that of the earliest uncontroversial trace fossils - made by metazoans - in the rock record, the interpretation of the Stirling structures as traces of moving organisms has been questioned (Budd and Jensen 2003; Conway Morris 2002; Seilacher 2007). No tenable alternative interpretation has yet been offered; however, a recent discovery of giant amoebas making similar traces on modern sea floors off the Bahamas has confirmed that other organisms than metazoans are able to make such traces (Bengtson and Rasmussen 2009; Matz et al. 2008).

The Stirling Range biota, if correctly interpreted, represents early experiments into the energy-craving life mode of motile multicellular organisms. The question why it took more than a billion years before the

multicellular life forms became an important component of the biosphere has yet to be convincingly answered but may be connected to the fluctuating oxygen levels of the ancient atmosphere.

See Also

- ▶ Cambrian Explosion
- ▶ Ediacaran Biota
- ▶ Eukaryotes, Appearance and Early Evolution of
- ▶ Proterozoic Eon
- ▶ Stirling Range, Australia

References and Further Reading

Bengtson S, Rasmussen B (2009) New and ancient trace makers. Science 323:346–347

Bengtson S, Rasmussen B, Krapež B (2007) The Paleoproterozoic megascopic Stirling biota. Paleobiology 33:351–381

Budd GE, Jensen S (2003) The limitations of the fossil record and the dating of the origin of the Bilateria. In: Donoghue PCJ (ed) Telling the evolutionary time. Molecular clocks and the fossil record. Taylor & Francis, London, pp 166–189

Conway Morris S (2002) Ancient animals or something else entirely? Science 298:57–58

Cruse T, Harris LB (1994) Ediacaran fossils from the Stirling Range Formation, Western Australia. Precambrian Res 67:1–10

Cruse T, Harris LB, Rasmussen B (1993) The discovery of Ediacaran trace and body fossils in the Stirling Range Formation, Western Australia – implications for sedimentation and deformation during the Pan-African orogenic cycle. Aust J Earth Sci 40:293–296

Matz MV, Frank TM, Marshall NJ, Widder EA, Sönke J (2008) Giant deep-sea protist produces bilaterian-like traces. Curr Biol 18:1849–1854

Rasmussen B, Bengtson S, Fletcher IR, McNaughton N (2002) Discoidal impressions and trace-like fossils more than 1200 million years old. Science 296:1112–1115

Rasmussen B, Fletcher IR, Bengtson S, McNaughton N (2004) SHRIMP U-Pb dating of diagenetic xenotime in the Stirling Range Formation, Western Australia: 1.8 billion year minimum age for the Stirling Biota. Precambrian Res 133:329–337

Seilacher A (2007) Trace fossil analysis. Springer, Berlin, p 226

Stirling Range, Australia

Stefan Bengtson
Department of Palaeozoology, The Swedish Museum of Natural History, Stockholm, Sweden

Definition

The Stirling Range is a 60-km long range of hills in southwestern Australia, about 330 km SE of Perth. It is built up of a ca 1.6 km thick Paleoproterozoic sequence of siliciclastic sediments, the Stirling Range Formation. The sediments, mostly sandstones and shales, were deposited between 1.8 and 2 Ga ago along an ocean-facing shoreline influenced by storms, long-shore currents, and tidal currents. The rocks were subjected to low-grade metamorphism about 1.2 Ga ago. The Stirling Range Formation houses a fossil biota of disk-shaped and trace-making organisms, the ▶ Stirling Range Biota.

See Also

- ▶ Stirling Range Biota

Stochasticity

- ▶ Chance and Randomness

STONE

André Brack and Frances Westall
Centre de Biophysique Moléculaire CNRS, Orléans Cedex 2, France

Keywords

Artificial meteorites; Atmospheric entry; Biosignatures; Martian sedimentary rocks; Panspermia; Endolithic cyanobacteria

Synonyms

Artificial meteorite

Definition

STONE is a series of experiments to test the survivability of terrestrial sedimentary rocks, analogues of Martian sediments, embedded in the heat shields of Foton capsules during entry into the Earth's atmosphere at a velocity of 7.6 km/s (meteoritic entry speeds being higher at 12–15 km/s). At the same time, the ► panspermia hypothesis was tested with live endolithic microorganisms protected by 1–2 cm of rock thickness, as well as the survival of organic and morphological biosignatures encapsulated within the sediment. A dolomite, a siltstone, a volcanic sandstone, and a ► basalt control sample survived entry into the atmosphere, as did organic and morphological biosignatures away from the fusion crust. The ► endolithic microorganisms did not survive.

Overview

Of six STONE experiments, only three were successfully carried to completion. STONE-1 flown in 1999 tested a basalt (in flight control), a dolomite (sedimentary rock), and artificial Martian regolith. Only the dolomite sample survived, having lost 70 % of its original thickness. Some kinetic isotopic fractionation accompanied the thermal degradation of the dolomite during reentry (Brack et al. 2002). STONE-5, 2005, carried dolerite (an igneous rock), sandstone (a sedimentary rock), and gneissic impactite from Haughton Crater that were loaded with bacterial *Bacillus subtilis* spores, fungal *Ulocladium atrum* spores, and photosynthetic endolithic cyanobacteria *Chroococcidiopsis* sp. Despite intense ablation resulting in deeply eroded samples, all rocks in part survived atmospheric reentry. Temperatures attained during reentry were high enough to form fusion crusts on the exposed gneiss and dolerite surface, thus strengthening the link with real meteorites. None of the microorganisms survived, and it was concluded that atmospheric transit acts as a strong biogeographical filter to the interplanetary transfer of photosynthetic microorganisms (Brandstätter et al. 2008; Cockell et al. 2007). STONE-6, 2007, tested a silicified volcanic sand, 3.446 ga old, containing cryptic traces of fossil life (Westall et al. 2006), a Devonian mudstone containing organic biomarkers, and an Eocene basalt from Austria. The basalt was lost but the two sedimentary rocks survived, severely ablated. Mineralogical changes indicated that entry temperatures exceeded ~1,800 °C that resulted in the fusion of both sediments. The 3.446-Ga-old microfossils survived furthest from the fusion crust while the organic carbon in the Devonian laminite sample was altered and thermally matured. Dried biofilms of *Chroococcidiopsis* pasted onto the underside of the rocks did not retain viability although the cells survived in a carbonized form (Foucher et al. 2010).

Although the speed of entry of these artificial meteorites was not as high as that of natural meteorites, 7.6 km/s as opposed to 12–15 km/s, it was close enough to produce fusion crusts on some of the sediments and to provide useful information relating to potential Martian sedimentary meteorites. Martian rocks having compositions typical of the terrestrial sediments tested could arrive on Earth as meteorites, providing they survive impact escape from Mars. Organic and morphological biosignatures in the Martian rocks could also survive. Heat flux calculations in the 3.446-Ga-old volcanic sand indicate that at least 5 cm rock thickness is necessary to protect extant organisms from heat shock.

See Also

► ALH 84001
► Panspermia

References and Further Reading

Brack A, Baglioni P, Borruat G, Brandstätter F, Demets R, Edwards HGM, Genge M, Kurat G, Miller MF, Newton EM, Pillinger CT, Roten CA, Esche E (2002) The artificial Martian meteorite experiment Stone-1. Planet Space Sci 50:763–772

Brandstätter F, Brack A, Baglioni P, Cockell CS, Demets R, Edwards HGM, Kurat G, Osinski GR, Pillinger JM, Roten C-A, Sancisi-Frey S (2008) Mineralogical alteration of artificial meteorites during atmospheric entry. The STONE-5 experiment. Planet Space Sci 56:976–984

Cockell CS, Brack A, Wynn-Williams DD, Baglioni P, Brandstätter F, Demets R, Edwards HGM, Gronstal AL, Kurat G, Lee P, Osinski GR, Pearce DA, Pillinger JM, Roten C-A, Sancisi-Frey S (2007) Interplanetary transfer of photosynthesis: an experimental demonstration of a selective dispersal filter in planetary island biogeography. Astrobiology 7:1–9

Foucher F, Westall F, Brandstätter F, Demets R, Parnell J, Cockell CS, Edwards HGM, Bény J-M, Brack A (2010) Testing the survival of microfossils in artificial Martian sedimentary meteorites during entry into Earth's atmosphere: the STONE 6 experiment. Icarus 207:616–630

Westall F, de Vries ST, Nijman W, Rouchon V, Orberger B, Pearson V, Watson J, Verchovsky A, Wright I, Rouzaud JN, Marchesini D, Severine A (2006) The 3.466 Ga Kitty's Gap Chert, an early Archaean microbial ecosystem. In: Reimold WU, Gibson R (eds) Processes on the early Earth, vol 405, Geological Society of America Special Paper., pp 105–131

Stopping Power

► Linear Energy Transfer

Stratigraphy

Felix M. Gradstein
University of Oslo, Blindem, Oslo, Norway

Keywords

Correlation; Fossils; Geochronology; Geological strata; Sedimentary rocks

Definition

Stratigraphy is the scientific discipline dealing with the nature, relative order, and physical and paleontological content of the rock record on Earth. Stratigraphy ("description of strata"), like most geologic sciences, is essentially a natural philosophy rooted in a body of organized cumulative observations, governed by a series of accepted principles and rules, and has three main attributes: (1) The irreversible flow of time, often called the arrow of time; (2) superposition of successively younger strata, often referred to as Steno's law, after the seventeenth century Danish scientist Nicholas Steno who first formulated this principle from observation in the hills of Italy; (3) the evidence of events as fossilized in Earth's sedimentary record, and their spatial and temporal relations.

Overview

Correlation of the rock record plays a major role in stratigraphy. To the geologist such correlation often requires the hypothesis that correlated units have the same age. Without correlation, the rock record and its succession in time derived in a single area are unique, and contribute nothing to understanding the Earth history elsewhere. Stratigraphy has developed several main components or subdisciplines, each with their own scientific specialists (Rawson et al. 2002; Rey and Galeotti 2008): Lithostratigraphy, biostratigraphy, chronostratigraphy, magnetostratigraphy, cyclostratigraphy, organic and inorganic isotopic chemostratigraphy, and, in the subsurface, seismostratigraphy and well-log stratigraphy. Seismostratigraphy is a special type of lithostratigraphy using acoustic remote sensing and visualization; well-log stratigraphy uses specialized tools to record down-hole physical and chemical properties. All stratigraphies strive to assign (often unique) attributes to an individual rock unit that makes it distinguishable from lateral, underlying or overlying rock units, and thus assist with its correlation. When properly stacked, described, and correlated, the rock record in sedimentary basins, flat or hilly landscapes, and

mountain ranges may thus reveal their history through geologic time.

See Also

- ▶ Geochronology
- ▶ Geological Timescale

References and Further Reading

Rawson PF et al (2002) Stratigraphical procedure. Geological Society, London, p 57
Rey J, Galeotti S (eds) (2008) Stratigraphy – terminology and practise. Editions Technip, Paris, p 163

Stratosphere

William M. Irvine
University of Massachusetts, Amherst, MA, USA

Definition

In a planetary atmosphere the region of the atmosphere above the top of the ▶ troposphere (the tropopause, where on Earth the temperature is at a minimum) is called the stratosphere. On Earth the stratosphere (from "stratus" = layered) consists of stable, cooler air lying below warmer air and is therefore stably stratified. The dominant energy transport in the stratosphere is via radiative transfer. The temperature reaches a local maximum at the top of the Earth's stratosphere (the stratopause) as a result of heating, either by absorption of solar photons by ozone (for Earth) or by aerosols (for, e.g., Jupiter) or/and possibly (in the case of the ▶ giant planets) by gravity waves or/and high energy particles. In the case of the Earth, the mesosphere (from "mesos" = middle) is the region above the stratosphere, in which the temperature systematically decreases due to less ozone heating and efficient radiative cooling. In the case of Mars and Venus there is no stratosphere, so that the mesosphere is located directly above the troposphere.

See Also

- ▶ Atmosphere, Structure
- ▶ Atmosphere, Temperature Inversion
- ▶ Giant Planets
- ▶ Troposphere

Stratospheric Ozone

- ▶ Ozone Layer

Strecker Synthesis

Jeffrey Bada
Scripps Institution of Oceanography, La Jolla, CA, USA

Definition

The Strecker synthesis is a chemical reaction inadvertently discovered in 1850 by Adolph Strecker (Strecker 1850) during an attempt to synthesize lactic acid from a mixture of acetaldehyde, HCN, and ammonia. Instead of lactic acid, however, Strecker found that the amino acid alanine had been synthesized. This represented the first successful demonstration of the synthesis of an amino acid in the laboratory.

The overall reaction sequence shown below is now generally referred to as the Strecker synthesis:

$$R_1C(O)R_2 + NH_3 + HCN \rightarrow R_1CR_2(NH_2)COOH$$

where in $R_1C(O)R_2$, R_1 and R_2 may be either a proton (H) or various substituted or non-substituted alkyl chains. Thus, both aldehydes and ketones can be starting materials for the Strecker synthesis, and depending on the nature of the aldehyde or ketone, amino acid products with different R_1 and R_2 substitutions can be generated.

This is generally accepted to be one of the principle mechanisms by which amino acids are synthesized in prebiotic simulations such as Miller-Urey synthesis and is likely one of the pathways for amino acid formation in ▶ carbonaceous chondrites.

See Also

▶ Amino Acid
▶ Miller, Stanley

References and Further Reading

Strecker A (1850) Über die künstliche Bildung der Milchsäure und einen neuen, dem Glycocoll homologen Körper. Ann Chem Pharm 75:27

Strelley Pool Chert (Amended)

▶ Strelley Pool Formation

Strelley Pool Formation

Kenichiro Sugitani
Graduate School of Environmental Studies, Nagoya University, Nagoya, Japan

Keywords

Stromatolite; Microfossils; Shallow subaerial environment; Hydrothermal; Archean; East Pilbara terrane; Pilbara Craton

Synonyms

Strelley Pool Chert (amended)

Definition

The Strelley Pool Formation (SPF) is a 3,426–3,350 Ma sedimentary succession that occurs in 11 greenstone belts in the East Pilbara Terrane (EPT) of the ▶ Pilbara Craton in Pilbara, Western Australia. The SPF is underlain and overlain unconformably by the dominantly volcanic Warrawoona and Kelly Groups, respectively. Its name is derived from a small pool known as the Strelley Pool occurring in the Pilgangoora Syncline. Its depositional area is assumed to cover more than 30,000 km^2, and the depositional environment ranges from shallow submarine to terrestrial. The SPF is known to contain morphologically diverse ▶ stromatolites and microfossils whose biogenicity has been examined through extensive analyses.

Overview

Previously known as Strelley Pool Chert, the SPF was first described and named for the chert unit of the Strelley Pool occurring approximately 30 km west of ▶ North Pole Dome (Lowe 1980). It was initially correlated to the Towers Formation (not used now) of the Warrawoona Group of the Pilbara Supergroup. This chert unit is now placed independently between the two volcanic units, the Warrawoona and the Kelly Groups (e.g., Hickman 2008; Van Kranendonk et al. 2006). In contrast to the other units of the Pilbara Supergroup in the East Pilbara Terrane (EPT) that are dominated by volcanic rocks, the SPF is composed predominantly of sedimentary rocks including sandstones, conglomerates, volcaniclastics, carbonates, evaporites, and cherts. Its depositional age is constrained by the ages of the underlying felsic volcanics of the ▶ Panorama Formation (3,433–3,427 Ma) and the overlying basalts of the Euro Basalt (3,350 Ma). The basal unconformable contact includes a subaerial erosional unconformity (Buick et al. 1995; Van Kranendonk et al. 2006). The SPF is currently identified in 11 greenstone belts in the EPT (Hickman 2008), and its thickness ranges from 10 to 1,000 m. Lithostratigraphic subdivisions of the SPF, which were proposed by Lowe (1983) on the basis of five measured sections, ascend in the following stratigraphic order:

Member 1: basal quartzose sandstone
Member 2: cherty unit of laminated flat stromatolite, conical stromatolite, and silicified evaporate
Member 3: stratified unit of stromatolite, black chert, silicified evaporite, and an evaporate solution layer
Member 4: coarse, intraformational conglomerate and breccia
Member 5: a cap unit of volcaniclastic debris

Such subdivisions are representative of the SPF, and as reported by Hickman (2008), this formation has significant lithostratigraphic variations both on regional and local scales. Lindsay et al. (2005) argued that the SPF was deposited in a relatively deep marine setting under the influence of hydrothermal activities, based on the observation that dykes composed of chert after barite, black massive chert, and dolomitic carbonates extend up to 1.7 km downward from the SPF in the East Strelley greenstone belt. The authors also raised questions about the biogenicity of carbonaceous matter in the stratified cherts and dolomitic stromatolites of the SPF. However, it is widely accepted that the SPF represents shallow-water to subaerial environments, including shallow-water marine, coastal, and estuarine and nonmarine such as lacustrine, fluviatile, and sabkha (Hickman 2008; Van Kranendonk et al. 2003; Lowe 1983; Allwood et al. 2006, 2007). Data of trace elements including rare-earth elements and Y (REE + Y) in cherts and carbonates suggest precipitation from a mixed hydrothermal and Archean normal seawater solution of various degrees, including seawater end-members (Allwood et al. 2010; Van Kranendonk et al. 2003) (Fig. 1).

The SPF is one of the most important and extensively studied Precambrian sedimentary successions because it contains Paleoarchean stromatolites and microfossils. The first description of the stromatolites in this formation was made by Lowe (1980), who reported finely laminated conical mounds in SPF chert at McPhee Creek in the East Strelley greenstone belt, which was correlated to *Conophyton* common in the Proterozoic. However, the author later revised

Strelley Pool Formation, Fig. 1 Stromatolite cones at the Trendall locality in the Panorama greenstone belt

his interpretation and suggested that except for simple cones, the structures are most likely abiogenically controlled precipitates formed under evaporitic conditions (Lowe 1994). An outcrop displaying extensive conical to pseudocolumnar stromatolitic structures in the Panorama greenstone belt was later discovered by A. F. Trendall (the Trendall locality). Hofmann et al. (1999) emphasized that purely chemical processes are insufficient for explaining several SPF stromatolite features such as (1) the combination of steeply conical forms modified by second-order corrugate lamination; (2) the coexistence of cones with branching pseudocolumns; and (3) the juxtaposition of uniform laminae in cones with uneven wispy, lenticular horizontal laminae in intercone areas. The authors also mentioned the morphological similarity of SPF stromatolites to younger varieties such as *Jacutophyton* and *Thyssagetes* and suggested that microbial activity was involved in the formation of SPF conical stromatolites. The biogenicity of SPF stromatolites suggested by this pioneering work is nearly confirmed by Van Kranendonk et al. (2003), Van Kranendonk (2007, 2011), Allwood et al. (2006, 2007, 2009), and Wacey (2010). For example, Allwood et al. (2006) described seven morphological types of stromatolites, which the authors related to the variation in sedimentary environments determined through detailed mapping that covered

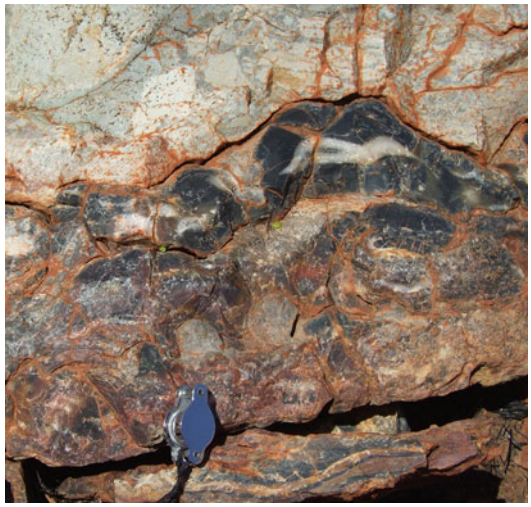

Strelley Pool Formation, Fig. 2 Black chert layer containing abundant morphologically diverse microfossils in the Goldsworthy greenstone belt

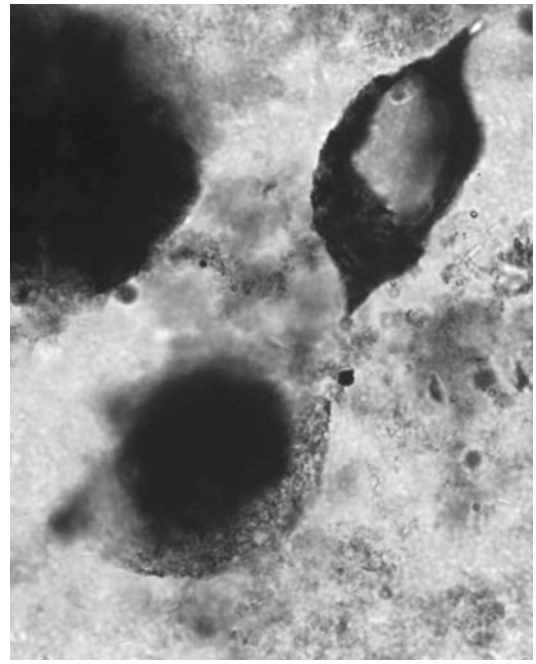

Strelley Pool Formation, Fig. 3 Flanged lenticular microfossils that characterize the SPF microfossil assemblage. The *upper* specimen shows the equatorial view, whereas the *lower* one shows the inclined polar view of the Goldsworthy greenstone belt

several kilometers of outcrops. This macroscale study was followed by microscale analyses that described textures likely related to microbial mat formation (Allwood et al. 2009; Wacey 2010). Shale-normalized patterns of REE + Y in SPF carbonates show signatures such as light REE (LREE) depletion and a strongly superchondric Y/Ho ratio that are commonly reported in other Archean marine precipitates (Allwood et al. 2010; Van Kranendonk et al. 2003) (Figs. 2 and 3).

Fossil-like microstructures have been reported in several localities of the SPF. Schopf and Packer (1987) described carbonaceous spheroids in chert assigned to SPF that were interpreted as sheath-enclosed colonies of coccoids (also see Schopf 2006). This first report of SPF microfossils and their geological context has been debated by several authors (e.g., Brasier et al. 2006). While the biogenicity of the morphologies is still debated, evidence has been reported for the biological origin of the kerogen chemistry of the original samples (Derenne et al. 2008). The issue is complicated by the fact that all the studies are not necessarily carried out on the original samples, and/or the precise field locality is not well constrained. More than 20 years later, Sugitani et al. (2010) reported morphologically diverse carbonaceous microstructures from the three localities in the Panorama, Warralong, and Goldsworthy greenstone belts. Although these localities are several tens of kilometers apart, they yielded morphologically similar assemblages of microfossil-like structures. These carbonaceous microstructures include spheroids, films, and lenses. The spheroid microstructures can be divided into two diameter categories including small (<15 μm) and large (>15 μm). The former tend to occur as colony-like clusters. Lenses range from 40 to 80 μm along the major dimensions. These microstructures are similar in morphology and occurrence to microfossils reported from the ca. 3.0 Ga Farrel Quartzite (e.g., Sugitani et al. 2007; House et al. 2013). Following this discovery, Sugitani et al. (2013) reported a similar assemblage of microstructures in a new site in the Panorama greenstone belt 1 km south of the Trendall Locality, which is a representative outcrop of SPF stromatolites.

In addition to the previously reported single-sheeted films, colony-forming small spheroids, and lenses with or without flanges, tubular filaments and honeycomb-shaped films were described for the first time. Lepot et al. (2013) performed secondary ion mass spectroscopy (SIMS) on microstructures of small spheroids and lenses from the Panorama and Goldsworthy greenstone belts previously reported by Sugitani et al. (2010, 2013). They revealed that these two morphological types have significantly different $\delta^{13}C$ values. The spheroid specimens from the Goldsworthy greenstone belt have peaks between −35 and −36 ‰, whereas the average peak of the lenses is −32 ‰; inner globules are −40 ‰. These lines of evidence strongly support their biogenicity. Among the several types of microfossil morphologies, the lenticular type is particularly important. Specimens of the lenticular type often have a sheet-like appendage along the equatorial plane known as a flange. Their morphology was initially described as spindle shaped, which merely represents a two-dimensional equatorial perspective. Similar microfossils have been reported from the contemporaneous (~3,416–3,334 Ma) Kromberg Formation in the ▶ Barberton greenstone belt, South Africa (Walsh 1992), and from the middle and the upper Proterozoic rocks (Samuelsson et al. 1999; Schopf and Klein 1992), although their biological affinity is not known. Wacey et al. (2011a) also reported carbonaceous spheroids and tubular filaments in the basal carbonaceous sandstone of the SPF in the East Strelley Pool greenstone belt. The authors performed focused ion beam system–transmission electron microscope and SIMS analyses of carbon and sulfur isotopes and suggested that the specimens are fossils of sulfur-metabolizing bacteria inhabited in an Archean sandy coastal environment.

In addition to these cellular preserved microfossils, possible noncellular biosignatures are also reported from the basal sandstone. The biosignatures include (1) pristine micron-sized pyrite with a $\delta^{34}S$ spread of −12 ~ + 6 ‰ and $\Delta^{33}S$ with both positive and negative values of −1.65 ~ +1.43 ‰ and (2) detrital pyrite grains with minute spherical pits and chains of pits. The former is associated with organic material coating the framework quartz grains and is interpreted to provide evidence for microbial sulfate reduction and microbial disproportionation of elemental sulfur, whereas the latter are likely the result of microbially mediated oxidation of pyrite (Wacey et al. 2011b, 2014). Prior to these works, Marshall et al. (2007) analyzed kerogenous materials extracted from the SPF and examined them by using several spectrometric methods including Fourier transform infrared (FTIR) spectroscopy and catalytic hydropyrolysis followed by gas chromatography–mass spectrometry (HyPy–GC–MS). The authors reported similarities of molecular profiles of HyPy products between SPF kerogens and unequivocally biogenic kerogens from the Mesoproterozoic Roper Group (~1,450 Ma), and they suggested that the SPF kerogens are likely biogenic. The origins of SPF stromatolites composed exclusively of chert or of recrystallized dolomite have been extensively debated, as has the origin of relatively large and morphologically diverse organic-walled microstructures. However, the aforementioned recently accumulated lines of evidence indicate that diverse microbial communities were already been widespread in shallow marine environments as old as 3.4 Ga. However, the photosynthetic nature of the stromatolite-building microbes and the biological affinities of reported microfossils remain unknown.

See Also

- ▶ Apex Chert
- ▶ Archean Biosignatures
- ▶ Archean Environmental Conditions
- ▶ Archean Traces of Life
- ▶ Barberton Greenstone Belt, Traces of Early Life
- ▶ Chert
- ▶ Early Life
- ▶ Isotopic Traces of Life
- ▶ Microbialites
- ▶ Microfossils, Analytical Techniques

- North Pole Dome (Pilbara, Western Australia)
- Photosynthesis
- Rare Earth Elements
- Stromatolites
- Sulfur Isotopes

References and Further Reading

Allwood AC, Walter MR, Kamber BS, Marshall CP, Burch IW (2006) Stromatolite reef from the early Archaean era of Australia. Nature 441:714–718

Allwood AC, Walter MR, Burch IW, Kamber BS (2007) 3.43 billion-year-old stromatolites reef from the Pilbara Craton of Western Australia: ecosystem-scale insights to early life on Earth. Precambrian Res 158:198–227

Allwood AC, Grotzinger JP, Knoll AH, Burch IW, Anderson MS, Coleman ML, Kanik I (2009) Controls on development and diversity of early Archean stromatolites. Proc Natl Acad Sci 106:9548–9555

Allwood AC, Kamber BS, Walter MR, Burch IW, Kanik I (2010) Trace elements record depositional history of an early Archean stromatolitic carbonate platform. Chem Geol 270:148–163

Brasier MD, Green OR, Lindsay JF, McLoughin N, Steele A, Stoakes C (2005) Critical testing of earth's oldest putative fossil assemblage from the similar to 3.5 ga Apex chert, Chinaman Creek, Western Australia. Precambrian Res 140:55–102

Buick R, Thornett JR, McNaughton NJ, Smith JB, Barley ME, Savage M (1995) Record of emergent continental crust ~3.5 billion years ago in the Pilbara Craton of Australia. Nature 375:574–577

Derenne S, Robert F, Skrzypczak_Bonduelle A, Gourier D, Binet L, Rouzaud JN (2008) Molecular evidence for life in the 3.5 billion year old Warrawoona chert. Earth Planet Sci Lett 272:476–480

Hickman AH (2008) Regional review of the 3426–3350 Ma Strelley Pool Formation, Pilbara Craton, Western Australia. Geol Surv W Aust, Record 2008/15

Hofmann HJ, Grey K, Hickman AH, Thorpe RI (1999) Origin of 3.45 Ga coniform stromatolites in Warrawoona Group, Western Australia. Geol Soc Am Bull 111:1256–1262

House CH, Oehler DZ, Sugitani K, Mimura K (2013) Carbon isotopic analyses of ca. 3.0 Ga microstructures imply planktonic autotrophs inhabited Earth's early oceans. Geology 41:651–654

Lepot K, Williford KH, Ushikubo T, Sugitani K, Mimura K, Spicuzza MJ, Valley JW (2013) Texture-specific isotopic compositions in 3.4 Gyr old organic matter support selective preservation in cell-like structures. Geochim Cosmochim Acta 112:66–86

Lindsay JF, Braiser MD, McLoughlin N, Green OR, Fogel M, Steel A, Hertzman SA (2005) The problem of deep carbon-an Archean paradox. Precambrian Res 143:1–22

Lowe DR (1980) Stromatolites 3,400-Myr old from the Archean of Western Australia. Nature 284:441–443

Lowe DR (1983) Restricted shallow-water sedimentation of early Archean stromatolitic and evaporitic strata of the Strelley Pool Chert, Pilbara Block, Western Australia. Precambrian Res 19:239–283

Lowe DR (1994) Abiological origin of described stromatolites older than 3.2 Ga. Geology 22:387–390

Marshall CP, Love GD, Snape CE, Hill AC, Allwood AC, Walter MR, Van Kranendonk MJ, Bowden SA, Sylva SP, Summons RE (2007) Structural characterization of kerogen in 3.4 Ga Archaean cherts from the Pilbara Craton, Western Australia. Precambrian Res 155:1–23

Samuelsson J, Dawes PR, Vidal G (1999) Organic-walled microfossils from the Proterozoic Thule Supergroup, Northwest Greenland. Precambrian Res 96:1–23

Schopf JW (2006) Fossil evidence of Archaean life. Philos Trans R Soc B361:869–885

Schopf JW, Klein C (1992) The proterozoic biosphere. A multidisciplinary study. Cambridge University Press, New York, p 1080

Sugitani K, Grey K, Allwood A, Nagaoka T, Mimura K, Minami M, Marshall CP, Van Kranendonk MJ, Walter MR (2007) Diverse microstructures from Archaean chert from the Mount Goldsworthy–Mount Grant area, Pilbara Craton, Western Australia: microfossils, dubiofossils, or pseudofossils? Precambrian Res 158:228–262

Sugitani K, Lepot K, Nagaoka T, Mimura K, Van Kranendonk MJ, Oehler DZ, Walter MR (2010) Biogenicity of morphologically diverse carbonaceous microstructures from the *ca*. 3400 Ma Strelley Pool Formation, in the Pilbara Craton, Western Australia. Astrobiology 10:899–920

Sugitani K, Mimura K, Nagaoka T, Lepot K, Takeuchi M (2013) Microfossil assemblage from the 3400 Ma Strelley Pool Formation in the Pilbara Craton, Western Australia: results from a new locality. Precambrian Res 226:59–74

Van Kranendonk MJ (2007) A review of the evidence for putative Paleoarchean life in the Pilbara Craton, Western Australia. In: Van Kranendonk MJ et al (eds) Earth's oldest rocks, vol 15, Developments in Precambrian geology. Elsevier, Amsterdam, pp 855–896

Van Kranendonk MJ (2011) Morphology as an indicator of biogenicity for 3.5–3.2 Ga fossil stromatolites from the Pilbara Craton, Western Australia. In: Reitner J et al (eds) Advances in stromatolite geobiology, vol 131, Lecture notes in earth sciences. Springer, Germany, pp 537–554

Van Kranendonk MJ, Webb GE, Kamber BS (2003) Geological and trace element evidence for a marine sedimentary environment of deposition and biogenicity of 3.45 Ga stromatolitic carbonates in the Pilbara Craton, and support for a reducing Archaean ocean. Geobiology 1:91–108

Van Kranendonk MJ, Hickman AH, Smithies RH, Williams IR, Bagas L, Farrell TR (2006) Revised lithostratigraphy of Archean supracrustal and intrusive rocks in the northern Pilbara Craton, Western Australia. W Aust Geol Surv, Rec 2006/15
Wacey D (2010) Stromatolites in the ~3400 Ma Strelley Pool Formation, Western Australia: examining biogenicity from the macro- to nano-scale. Astrobiology 10:381–395
Wacey D, Kilburn MR, Saunders M, Cliff J, Brasier MD (2011a) Microfossils of sulphur-metabolizing cells in 3.4-billion-year-old rocks of Western Australia. Nat Geosci 4:698–702
Wacey D, Saunders M, Brasier MD, Kilburn MR (2011b) Earliest microbially mediated pyrite oxidation in ~3.4 billion-year-old sediments. Earth Sci Planet Lett 301:393–402
Wacey D, McLoughlin N, Whitehouse MJ, Kilburn MR (2014) Two co-existing sulfur metabolisms in a ca. 3400 Ma sandstone. Geology 38:1115–1118
Walsh MM (1992) Microfossils and possible microfossils from early Archean Onverwacht Group, Barberton Mountain Land, South Africa. Precambrian Res 54:271–293

Stromatolites

Nicola McLoughlin
Department of Earth Science and Centre for Geobiology, University of Bergen, Bergen, Norway

Keywords

Laminated sedimentary structures; Microbial mats

Synonyms

Fossilized microbial mats; Living stromatolites; Microbialites; Modern stromatolites

Definition

Stromatolites are morphologically circumscribed accretionary growth structures with a primary lamination that is, or may be, biogenic. They form centimeter- to decimeter-scale domes, cones, columns, and planiform surfaces made of carbonate layers. Stromatolites accrete through a combination of microbially mediated sediment trapping and binding and by the precipitation of carbonate crusts that may be due to microbial mat growth and/or be purely ▶ abiotic in origin. Stromatolites provide the oldest macrofossil evidence of ▶ life on earth and host many important ▶ microfossil occurrences. Images of macroscopically layered stromatolites obtained by rovers on other planetary surfaces may yet provide some of the first evidence of life beyond earth.

History

The term "stromatolith" was first used just over a century ago by Kalkowsky (1908) and derived from the Greek words stroma meaning bed, mattress, or layer, and lithos meaning stone. It was used to describe laminated limestones from the early Triassic, lacustrine deposits near the Harz Mountains of Northern Germany. Kalkowsky attributed the formation of these structures to simple plant-like organisms, and the term was later popularized by Pia (1927) as a type of fossil produced by the calcium carbonate precipitation. The term was translated by Krumbein (1983) who stated that "stromatolites are organogenic, laminated, calcareous rock structures, the origin of which is clearly related to microscopic life, which in itself must not be fossilised." It is now known that ▶ prokaryotes both photosynthetic and nonphotosynthetic are largely responsible for stromatolite growth (Freytet and Verrechia 1998), along with ▶ heterotrophs, algae, and metazoans.

Overview

Stromatolites are the most abundant macrofossil in the ▶ Precambrian rock record and are volumetrically very significant components of Precambrian carbonate platforms. Stromatolites can be used to reconstruct sedimentary environments,

especially paleobathymetry, paleoslopes, and current directions, and are used for biostratigraphic correlation within basins. Distinguishing the relative contribution of biological, physical, and chemical controls on stromatolite morphology can be difficult, and below the criteria that have been developed to assess the ▶ biogenicity of stromatolites are reviewed. The macromorphology and especially microfabrics of stromatolites are archives of microbial evolution that together with their carbonate geochemistry record secular changes in seawater chemistry. This review will focus on how stromatolites grow and what they can tell us about the earliest microbial ecosystems on earth and perhaps beyond.

Key Research Findings

What Is a Stromatolite?

The definition and meaning of the term stromatolite has been widely debated, especially whether the term should be used in a purely descriptive sense, to refer to laminated sedimentary structures, or should be used genetically to refer to structures that are demonstrably biogenic in origin; see reviews by, for example, Riding (1999), Grotzinger and Knoll (1999), and Bosak et al. (2013). But herein lies the problem. There are many types of related geological structures that display some or all of the features of stromatolites, and are formed in a variety of environments, but with varying and sometimes debatable degrees of biological involvement. Such structures include hot spring travertines, nonmarine tufas, laminar caliche crusts, and speleothems. The possibility that abiotic processes may solely account for stromatolite growth was reasserted by Grotzinger and Rothman (1996) who used the Kardar-Parisi-Zhang (KPZ) equation of interface growth to show that the morphologies of some stromatolites can be modeled by abiotic processes alone. This was a significant study that reinvigorated the debate surrounding the biogenicity of Precambrian stromatolites in particular and reemphasized the difficulties of disentangling biological, physical, and chemical controls on stromatolite growth. This remains a serious concern if we are one day to assess the biogenicity of laminated deposits imaged by rovers exploring other planetary surfaces.

A purely descriptive definition of a stromatolite was proposed by Semikhatov et al. (1979) and others: "an attached, laminated, lithified sedimentary growth structure, accretionary away from a point or limited surface of initiation." Many sedimentologists favor this nongenetic definition to describe a laminated sedimentary structure with positive relief. This has resulted in the usage of terminology such as "abiogenic stromatolite" to stress the absence of compelling microtextural or morphological evidence for biological participation that is often lacking in many examples due to diagenetic alteration. Strictly speaking, however, this is a corruption of the original intention. The term stromatoloid has also been introduced by Buick et al. (1981) to refer to laminated sedimentary structures, the biogenicity of which is uncertain. An alternative approach to express the uncertainty surrounding the biogenicity of a given stromatolite is to add the prefix "probable" or "possible" or "dubio" stromatolite, as appropriate – this approach is applied to other biosignatures such as microfossils. Genetic definitions, on the other hand, have been proposed by, for example, Awramik and Margulis (1974), to mean an "organosedimentary structure produced by sediment trapping, binding, and/or precipitation as a result of the growth and metabolic activity of microorganisms, principally cyanophytes." The evidence necessary to substantiate such a biogenic definition can be difficult to obtain in the rock record, especially in Precambrian sequences that have experience diagenetic and metamorphic recrystallization – in this review the term stromatolite is therefore used in the nongenetic sense.

Some workers, meanwhile, prefer the broader term *microbialite* that was introduced by Burne and Moore (1987) to describe both laminated and nonlaminated microbially mediated sedimentary structures. They defined microbialites as "organosedimentary deposits that have accreted as a result of benthic microbial community trapping and binding sediment and-or forming the

locus of mineral precipitation." Stromatolites are thus a subset of microbialites that also include nonlaminated deposits such as thrombolites (clotted) and dendrolites (branched) (Riding 1999). This term is perhaps most useful for describing modern microbial deposits that often exhibit varied internal structure and can be composite, including stromatolitic and other microbialite microfabrics. To add further confusion, the term stromatolite has also been applied to laminated microbial deposits that are not composed of carbonate, for example, laminated silica glazes or desert varnish crusts. Here we will restrict our usage of the term stromatolite to carbonates.

Lithification of Recent Microbial Mats

Studies of modern stromatolite analogues both in nature and the laboratory have been very informative for understanding mechanisms of stromatolite growth and lithification. Many modern stromatolites are known from hypersaline settings, for instance, Shark Bay in Western Australia (Fig. 1a, b), where the hypersalinity is thought to restrict grazing on the mats. Here the stromatolites accrete at an estimated rate of $\leq$3 mm per year with microbial trapping and binding of sediment being the predominant accretion mechanisms in the intertidal stromatolites and carbonate precipitation in the subtidal stromatolites (Reid et al. 2003). Several modern stromatolite-forming microbial mat systems are also known from Lake systems such as Lake Pavilion in British Columbia and Lake Thetis in Western Australia, where elevated carbonate saturation levels are thought to promote lithification of the microbial mats. The only known modern open-marine stromatolite system comes from the Bahamas where stromatolites occur in supra-, inter-, and subtidal settings (e.g., Reid et al. 2000). Studies have found that the microbial mats are spatially and temporally very dynamic systems, with the location of primary production and lithification changing on diurnal to seasonal and annual cycles and across depositional gradients (e.g., Reid et al. 2003; Visscher et al. 2000). The distinct microenvironments, steep geochemical gradients, and diverse processes that occur within modern microbial mats are described elsewhere in this volume. Modern systems are, however, imperfect analogues for the Precambrian rock record, especially prior to the evolution of eukaryotes and metazoans, and in a water column that was anoxic for much of the Archaean and early Proterozoic. Nonetheless, the manipulation of model microbial mat systems both in the lab and in their natural environment has proved informative for better understanding the mechanisms that produce specific stromatolite features, for example, cell motility in reticulate mats and oxygenic ▶ photosynthesis in conical mats (see below).

Stromatolite Biogenicity Criteria

The rock record provides a testing ground for developing stromatolite biogenicity criteria that one day may be applied to laminated sedimentary structures on other planetary surfaces. The problem is that most of these criteria are so prescriptive that the majority of Precambrian stromatolites of widely regarded biogenic origin fail to qualify. Here a brief review of the most widely applied stromatolite biogenicity criteria is given, drawing from the classic study of Buick et al. (1981) and additional criteria (points 9–11) proposed by Hofmann (2000):

1. "The structures must occur in undoubted sedimentary or metasedimentary rocks." A viable sedimentary environment is a necessary first condition to demonstrate the biogenicity of a stromatolite.
2. "It must be demonstrated that the structures are synsedimentary." It is necessary to exclude soft sediment deformation and/or later structural deformation as contributing to the resulting stromatolite morphology.
3. "There should be a preponderance of convex upwards structures." This is a useful but very qualitative criterion and is neither necessary nor sufficient to demonstrate biogenicity as, for example, abiotic self-organizing structures such as stalagmites and agate crusts can exhibit convex-upward morphologies.
4. "Laminae should thicken over the crests of flexures." This qualitative criterion is

Stromatolites, Fig. 1 Examples of stromatolites: (**a**) submerged intertidal modern stromatolites from Shark Bay, Western Australia; (**b**) living domal stromatolites with an orange diatom-rich coating from the intertidal zone of Carbla Foreshore, W Australia; (**c**) large columnar stromatolite with smooth, convex laminae from the Neoarchean lower Transvaal Supergroup of South Africa; (**d**) microdigitate stromatolites from 2.7 Ga Tumbiana Formation of W Australia; (**e**) pseudocolumnar stromatolites from the Trendall locality of the ~3.4 Ga Strelley Pool Chert of W Australia; (**f**) plan view of simple coniform stromatolites on a bedding surface of silicified carbonate from the W Strelley locality of the Strelley Pool Chert; (**g**) domal stromatolite in a ferruginous carbonate with a silicified core from the ~3.5 Ga Dresser Formation of the North Pole Dome, W Australia. Scale bar (**a**) and (**b**) 15 cm, (**c**) 20 cm, (**d**) 1 cm, (**e**) and (**g**) 5 cm, and (**f**) 10 cm

designed to exclude abiotic, chemical crusts that are widely believed to exhibit laterally uniform thickness, i.e., be isopachous (e.g., Pope and Grotzinger 2000). However, freshwater Phormidium stromatolites, for example, are commonly isopachous and can be differentiated from abiological speleothem cements by being of uniform thickness around, for example, the entire circumference of coated tree branches, whereas abiological cement would be thicker on the undersides due to geopetal effects. In other words, crusts do not need to thicken – they may just maintain their thickness. Further discussion on the different types of stromatolite laminar geometries is given below, including the degree of vertical inheritance between laminae and their lateral continuity.

5. "If the structures are laminated the laminations should be wavy, wrinkled and/or have several orders of curvature." Again this qualitative criterion is designed to exclude abiogenic precipitated crusts that are thought to be more uniform, but no limits are placed on the extent of "crinkliness" or "curvature" which are also controlled by sedimentary rheology and overprinted by the degree of diagenetic modification.
6. "Microfossils or trace fossils should be present within the structures." This is far too rigid as the preservation potential of microbial remains is extremely low, such that this criterion would exclude more than an estimated 90 % of described fossil stromatolites. Moreover, the majority of recent stromatolites only contain microorganisms in their outermost layers. Furthermore, the presence of microfossils in a stromatolite does not confirm their active role in formation of the structure, as they may simply have been passively entombed by the accreting structure.
7. "Changes in composition of the microfossil assemblages should be accompanied by morphological changes in the stromatolite." This is an extension of criterion 6 and is extremely prescriptive as only a few instances are known where this criterion is satisfied, for example, stromatolites of the Gunflint Chert. Studies of modern stromatolites also suggest similar fabrics can be produced by more than one organism, such that morphological changes may not accompany changes in microfossil assemblage.
8. "The fossils or trace fossils must be organised in a manner indicating trapping, binding or precipitation of sediment by the living microorganisms." Again this would be desirable, but is somewhat overoptimistic. Tufted microbial filaments, fenestrae, and micropores created by the growth and decay of now absent microbes would be useful but are only found when diagenesis is minimal (e.g., Turner et al. 2000a).
9. "Brecciated mat chips accumulated in depressions between convexly laminated mounds." These are occasionally seen and have been highlighted in discussions surrounding early Archaean stromatolites, for example, from the Strelley Pool Chert (Hofmann et al. 1999). Such textures are most convincing if the mat fragments show laminated internal fabrics or microtextures that can distinguish them from fragments of brecciated seafloor crusts.
10. "Thin, rolled-up fragments as indications of the existence of coherent flexible laminae that are reasonably interpreted as microbial mats." These are desirable and occasionally seen, for example, in the Paleoproterozoic Hamersley Group of Western Australia and especially in silicified microbial mat horizons, but again require exceptional organic preservation.
11. "Distinct compositional differences between the laminated growth structures and their surrounding matrix, such as carbonate stromatolites set within terrigenous detritus." This can be a helpful criterion, but there are numerous exceptions. For instance, many of the least controversial carbonate stromatolites are found in carbonate settings, and especially those formed by trapping and binding can have a similar composition to their surrounding matrix. Whereas, in terrigenous clastic settings laminated carbonates are not always a stromatolite: many caliche crusts would meet this criterion.

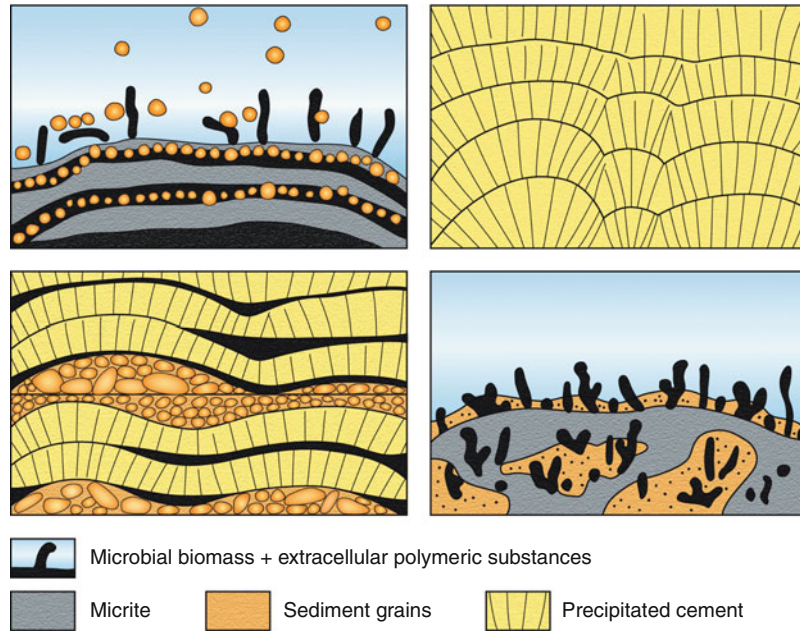

Stromatolites, Fig. 2 Mechanisms of Stromatolite Accretion: (*top left*) sediment trapping and binding by microbial mats producing laminae with micritic, detrital, and/or peloidal layers; (*top right*) chemical precipitation of carbonate producing laminae comprising "sparry crusts"; (*lower left*) a combination of these processes producing composite crusts of alternating sparry, detrital, and organic layers; (*lower right*) a skeletal stromatolite formed by calcifying microorganisms, for example, the cyanobacteria *Girvanella*

In summary, a biogenic origin is most likely for stromatolites that exhibit complex morphologies, laminae that show lateral and vertical variability (see discussion on microfabrics below), and organic bearing microfabrics. A more compelling case for a biogenic origin can be made, if it can be shown that changes in both the macro and micro features of the stromatolite correlate with biologically significant environmental gradients, such as light levels.

Mechanisms of Stromatolite Accretion

Here the processes that contribute to stromatolite accretion are summarized, also the laminar geometries and microtextures that are thought to result. A schematic of these accretionary processes is shown in Fig. 2 (modified from Shapiro 2005); these are sediment trapping and binding (top left) producing often clotted or peloidal crusts, sometimes referred to as "fine-grained crusts"; chemical precipitation of carbonate (top right) producing laminae comprising "abiogenic sparry crusts"; a combination of these processes (lower left) producing composite crusts; and a skeletal stromatolite (lower right) formed by calcifying microorganisms, most commonly ► cyanobacteria. A more detailed review of this subject can be found in Riding (2008) that focuses on the microfabrics of Precambrian stromatolites.

Sediment Trapping and Binding

In recent stromatolites, the trapping and binding of suspended sediment particles is an important accretionary mechanism. This process is controlled by the slope of the accreting stromatolite interface, the grain size and density of the sediment particles, and the size and motility of the microbes (e.g., Riding (2000) and references therein). This process is countered by the movement of sediment down stromatolite flanks under the forces of gravity and current action that are most vigorous in high-energy settings and for stromatolites with steep flanks or significant relief. Sediment trapping and binding is thought to be facilitated by biofilms that have abundant "sticky" extracellular polymer and by microbes with high motility (e.g., Golubic et al. 2000). In addition, early cementation is necessary to prevent loss of this detrital sediment off the stromatolite flanks. These processes are thought to create nonisopachous laminae that show irregular uneven layering with low inheritance and limited lateral continuity. In petrographic thin section,

preservation permitting the trapped and bound sediment grains should be visible, perhaps between the decayed remains of organic laminae that may have formed during more quiescent periods.

Trapping and binding processes are commonly associated with microbially induced carbonate precipitation (see below) that together result in so-called fine-grained crusts of Riding (2008). These can exhibit micritic, clotted, peloidal, or filamentous microfabrics, and are especially abundant in the Neoproterozoic (e.g., Turner et al. 2000b). Additional support for microbial activity can come from microfossil remains, for example, in the 1.8 Ga stromatolites of the Gunflint (Awramik and Semikhatov 1978); or in the form of micropores interpreted to be the molds of decayed microbes (Bosak et al. 2004); or palimpsest fabrics comprising vertically aligned, decayed microbial filaments (e.g., Buick 1992). The mere presence of such microbial remains is insufficient, however, to demonstrate full microbial control on precipitation, as it needs to be shown that these remains were not just passively entombed but rather actively shaped the accreting structure. In some stromatolites, the fine-grained crusts are interleaved with so-called crystalline or sparry crusts (see below) creating alternating light and dark layers conferring a streaky appearance. These are interpreted to reflect the switching between dark, fine-grained essentially microbial-mediated layers and light-colored, possibly abiotically precipitated, spar layers that are common in many conical stromatolites termed *Conophyton* (e.g., Grotzinger and Knoll (1999), and references therein).

Abiotic Chemical Precipitation

Carbonate precipitation in microbial stromatolites can be induced by the activities of living and decaying microbes (e.g., Riding 2000), but also results from pore water supersaturation generated by abiotic processes such as degassing of CO_2 and evaporation. Abiotic chemical precipitation is responsible for the growth of abiotic laminated deposits, such as agates, botryoides, crystalline crusts, and cements. These can sometimes be recognized by the expansion and ultimate coalescing of neighboring crystal fans or undulose layers with microfabrics clearly resulting from precipitation. These are termed "abiogenic sparry crusts" by Riding (2008). In discussions concerning the biogenicity of stromatolites, abiotic chemical precipitation is widely assumed to produce isopachous laminae, i.e., laminae of uniform thickness (e.g., Buick 1992). The synthetic stromatolite experiments reported in McLoughlin et al. (2008), however, together with several numerical modeling studies (e.g., Grotzinger and Rothman 1996) have shown that abiotic processes can also produce nonisopachous laminae, and therefore stromatolite imposters or pseudofossils. This is well known. For example, meteoritic cements formed in the phreatic zone, where void spaces are water filled, result in the precipitation of cements with isopachous laminae, whereas cements formed in the vadose zone have dripstone, i.e., nonisopachous geometries. Thus, the assumption that abiotic precipitation exclusively results in isopachous stromatolite laminae does not hold. This raises further concerns about our abilities to always confidently identify abiotic laminated deposits.

In the Precambrian rock record, stromatolitic growth by abiotic, surface-normal chemical precipitation is suggested by laminae that are composed of radial fibrous crystals fans (Fig. 2c) (e.g., Grotzinger and Knoll, 1999) or so-called sparry crusts (Riding 2008). These are characterized by isopachous laminae that show extreme lateral continuity and high degrees of vertical inheritance. Such structures are believed to form by direct carbonate precipitation on the seafloor and are devoid of clastic carbonate (e.g., Turner et al. 2000b; Pope and Grotzinger 2000). They are particularly abundant in Archaean and Paleoproterozoic sequences and are believed to be associated with times of high seawater carbonate supersaturation, often being associated with evaporitic sequences. They have been termed "chemical stromatolites" by Pope and Grotzinger (2000) who argued that they are largely abiotic in origin.

Biologically Induced Precipitation: Chemo- and Phototaxis

The thickening of laminae across the crests of stromatolite domes and cones is commonly believed to result from microbially accelerated growth in an upward direction due to chemo- or phototaxis. Coniform stromatolites, in particular, are taken as indicators of phototactic microbial growth by analogy to modern-tufted and peak-shaped microbial mats (e.g., Walter et al. 1976; Batchelor et al. 2004). It is envisaged that phototactic biofilms strive to gain more light and that chemotactic biofilms aim to elevate themselves in the benthic boundary layer to access more nutrients. This accelerated upward growth is accomplished by microbial motility toward topographic highs termed "upslope diffusion" by Jogi and Runnegar (2005). The exact geometries of the resulting laminae, in particular, the degree of laminar thickening in the axial zone, are likely controlled by photic zone conditions, the thickness of the benthic boundary layer, and the nature of diffusive gradient both within and above the accreting surface. Recent laboratory investigations of reticulate cyanobacterial mats have found that it is cell motility and not phototaxis that controls the shape of the mat, because upward growth was observed even when illuminated from below (Shepard and Sumner 2010).

In addition to laminar geometries, there are other microfabric clues that may indicate the phototactic growth of stromatolites. Recent laboratory experiments growing cyanobacterial-dominated microbial mats have identified the presence of contorted laminae in the axial zone of conical aggregates and preservation of enmeshed oxygen bubbles as indicators of oxygenic photosynthetic mat growth (Bosak et al. 2009). Such features are found in the central zones of well-preserved Proterozoic conical stromatolites from which these workers argue that oxygenic photosynthesis first appeared in the Paleoproterozoic. In outcrop, the observation of sinuous growth axes of 850 Ma stromatolites from the Bitter Springs Formation has also been argued to represent heliotropism, i.e., microbial mat growth that tracks the changing position of the sun (Vanyo and Awramik 1985) – this of course requires that the stromatolites were accreting and lithified at a sufficiently fast rate to record such annual variation.

Brief Review of Stromatolites Through Time

There have been many attempts to compute curves of stromatolite diversity and abundance through geological time; however, these efforts have been somewhat hampered by our inability to separate biological, chemical, and physical controls on stromatolite growth and to agree a universal definition of what constitutes a stromatolite taxa (Grotzinger and Knoll 1999). There are nonetheless, long-term, first-order trends in stromatolite morphologies and microfabrics that record evolutionary and environmental changes that are summarized briefly here.

First, there is a broad transition in the Precambrian from stromatolites formed predominantly by chemical precipitation in the Archaean with sparry microfabrics to stromatolites with fine-grained more microbially influenced microfabrics in the Neoproterozoic (Riding 2008). In the intervening Paleo and Mesoproterozoic interval, stromatolites with hybrid fabrics are most common and this is argued to reflect growth by a combination of chemical precipitation and sediment trapping and binding. This transition has been suggested to represent a long-term decline in Precambrian seawater carbonate supersaturation (Grotzinger and Kasting 1993), with a consequent switch in importance from chemical precipitation to microbial trapping and binding as the dominant mechanisms of stromatolite growth. This connection between seawater carbonate saturation and microbialite abundance has been further tested in the Phanerozoic with compilations of abundance data for calcified cyanobacteria and microbial carbonates (Riding and Liang 2005 and references therein) showing a positive correlation with marine carbonate saturation.

Second, distinctive new stromatolite morphologies and/or microfabrics can record major evolutionary events. For example, cyanobacterial biomineralization in the lower Cambrian (Riding and Voronova 1984) resulted in the formation of dendrolites and skeletal stromatolites which are most abundant in the Cambrian and

Lower Ordovician. Also thrombolites, with their clotted microfabrics, first appear in the Cambrian, and they are argued to represent "disturbed stromatolites," in which the activities of animals and ► algae have disrupted and destroyed the laminae (Walter and Heys 1985). In addition, the abundance of microbial carbonates in the Phanerozoic is generally inversed to that of marine metazoan taxonomic diversity, supporting the view that metazoan competition has progressively limited the formation of microbial carbonates. Further, stromatolite morphologies that may be diagnostic of certain periods of geological time have been recognized, although their environmental and/or evolutionary significance is yet to be fully understood. For instance, many late Archaean carbonate sequences include fenestrate microbialites, net-like masses of irregular columns, or tent shapes composed of dark organic layers encased in irregular calcite cements (Sumner 1997), but their apparently restricted time distribution is yet to be fully explained.

Third, stromatolites have been suggested as disaster taxa, namely, organisms that in the aftermaths of mass extinction events show increased abundance due to the relaxation of ecological constraints. For example, in Lower Triassic strata following the end-Permian mass extinction that was particularly devastating to benthic biota, a time period dominated by depositional systems reminiscent of the Neoproterozoic-Early Paleozoic has been reported. In particular, this includes planar microbialites, small stromatolites, thrombolites, and microbial reefs developed extensively in normal marine carbonate environments. The proliferation of these so-called disaster taxa has been attributed to a reduction in trace fossil infaunalization and metazoan grazers. But there may be other environmental factors at play, including the enhanced carbonate saturation at this time as supported by the abundance of seafloor crystal fans that would promote the lithification of benthic microbial mats. The difficulties of separating these factors yet again illustrate the complexities of separating physical, chemical, and biological controls on stromatolite growth.

The Oldest Stromatolites on Earth

The oldest known stromatolites are described from silicified carbonates of the Pilbara Craton, Western Australia. Archaean traces of life are reviewed elsewhere in this volume, and here the focus is on the macrofossil evidence provided by stromatolites. A comprehensive summary of all reported Archaean stromatolite occurrences can be found in Table 1 of Hofmann (2000). The oldest candidate stromatolites come from the ~3.49 Ga Dresser Formation of Western Australia and include wrinkled planiform surfaces, broad domes, and columnar forms (Fig. 1g). These occur at several localities in the North Pole Dome both in syn-depositional barite mounds and hydrothermal dykes and in silicified and hydrothermally altered ferruginous carbonates (Wacey 2009 and references therein). Early studies supported a biological explanation from these structures on the basis of macromorphological similarities to younger, unambiguously biological stromatolites (Walter et al. 1980). However, Lowe (1994) reinterpreted these structures as soft sediment deformation features, and Buick et al. (1981) concluded that that they were only "probable or possible" biogenic stromatolites because they failed to satisfy many of their biogenicity criteria reviewed above. More recent studies have argued largely on the basis of field relationships that these stromatolites are primary features that were constructed by hyperthermophilic microbes (Van Kranendonk 2007). The macromorphology of these stromatolites appears, however, to be largely controlled by the thickness of the precipitated barite crusts and draping chert layers, and their distribution may simply reflect the supply of supersaturated solutions from which they were precipitated. Robust microtextural and isotopic evidence for the involvement of hyperthermophilic microbial mats in the growth of these stromatolites has not yet been reported, casting doubt on their biogenicity.

Some of the next oldest putative stromatolites are described from the ~3.4 Ga Strelley Pool Chert of Western Australia; the most abundant forms are simple unbranched cones (Fig. 1f) that were initially interpreted as biogenic in origin,

but this interpretation was later rescinded in favor of an origin by abiogenic evaporitic precipitation (Lowe 1994). The discovery of large coniform stromatolites with rare flank structures and domal and laterally linked pseudocolumnar morphologies (Fig. 1e) at the Trendall locality in the North Pole Dome led to a biological origin for these structures being re-advanced (Hofmann et al. 1999). This was argued for on the basis of morphological and sedimentological evidence, especially the steep-sided cones argued to require cohesive microbial mats, the presence of detrital sediment taken to imply microbial tapping and binding, the wrinkly nature of the laminae, and microfabric differences between the stromatolites and intervening nonstromatolitic sediments (Hofmann et al. 1999). Subsequently, detailed mapping of the stromatolite macromorphologies and investigation of rare outcrops with relatively good microtextural preservation have found evidence for a spatiotemporal correlation between stromatolite morphology and microfabric and depositional environment. This has been taken to support a shallow-water carbonate platform depositional model for the Strelley Pool Chert and a phototrophic origin for the stromatolites (Allwood et al. 2009). Regionally, however, the more typical, small, unbranched coniform stromatolites of the Strelley Pool Chert do not show unambiguous biological characteristics or depth-controlled distribution and/or changes in morphology with depth (Wacey 2010). In addition, their close interrelationship with crystal fan arrays upon which they can be seen to nucleate emphasizes a strong chemical component to their growth, and their intergradation with linguoid current ripples highlights the importance of physical controls on their accretion. In short, the Strelley Pool Chert includes a spectrum of stromatolitic structures, some of which are biogenic, but we are still a long way from confidently distinguishing those that are undoubtedly biogenic from those that are not microbially mediated.

Applications

In the near future, images of layered extraterrestrial sediments will be collected by rovers or landers on other planetary surfaces, most immediately Mars. We therefore require tools for assessing if these deposits were microbially shaped and/or if their mineralogy reflects microbial involvement. One of the most promising approaches to assessing the biogenicity of extraterrestrial stromatolites involves quantitative tools to measure the degree of ▶ complexity in images of such deposits (Wagstaff and Corsetti 2010). Various protocols are being developed to evaluate the compressibility (degree of order) and entropy (spread) in images of both biogenic and abiogenic stromatolites; however, to date, a method that can consistently separate biogenic and abiogenic stromatolites is yet to be found. It is probably overoptimistic to hope that a single line of evidence can give a yes/no answer to the question of biogenicity, but such quantitative image processing tools will help to target the laminated deposits that are most likely biogenic for more detailed studies. For instance, instruments are mounted on rovers that could investigate the carbonate mineralogy or organic carbon content of stromatolites (Rividi et al. 2010).

Future Directions

Stromatolites provide one of the most abundant and richest records of microbial evolution on our planet, but we are yet to find the "rosetta stone" that fully decodes the physical, chemical, and biological processes that are encoded in their diverse shapes and microfabrics. Promising stromatolite biogenicity criteria that are being developed include the trace metal composition of microbial carbonates (Kamber and Webb 2007) and nanoscale elemental and isotopic signatures of organic matter found in some well-preserved stromatolites (Wacey et al. 2010). Together with studies that manipulate living microbial mat systems to investigate the resulting morphological and chemical signatures produced in lithified stromatolites, we are becoming better prepared to assess the biogenicity of stromatolites that may someday soon be found on other planetary surfaces.

See Also

- Algae
- Archean Traces of Life
- Belcher Group, Microfossils
- Biogenicity
- Biomarkers, Morphological
- Chemotaxis
- Chemotroph
- Complexity
- Cyanobacteria
- Eukarya
- Heterotroph
- Microbial Mats
- Microfossils
- North Pole Dome (Pilbara, Western Australia)
- Photosynthesis
- Phototroph
- Precambrian
- Shark Bay, Stromatolites of
- Syngenicity
- Tumbiana Formation (Pilbara, Western Australia)

References and Further Reading

Allwood AC, Grotzinger JP, Knoll AH, Burch IW, Anderson MS, Coleman ML, Kanik I (2009) Controls on development and diversity of Early Archean stromatolites. Proc Natl Acad Sci U S A 106:9548–9555

Awramik SM, Margulis L (1974) Definition of stromatolite. Stromatolite Newsl 2:1–5

Awramik SM, Semikhatov MA (1978) The relationship between morphology, microstructure and microbiota in three vertically intergrading stromatolites from the gunflint iron formation. Can J Earth Sci 16:484–495

Batchelor MT, Burne RV, Henry BI, Jackson MJ (2004) A case for biotic morphogenesis of coniform stromatolites. Phys A 337:319–326

Bosak T, Souza-Egipsy V, Corsetti FA, Newman DK (2004) Micrometer-scale porosity as a biosignature in carbonate crusts. Geology 32:781–784

Bosak T, Liang B, Sim MS, Petroff AP (2009) Morphological record of oxygenic photosynthesis in conical stromatolites. Proc Natl Acad Sci U S A 106:10939–10943

Bosak T, Knoll AH, Petroff AP (2013) The meaning of stromatolites. Ann Rev Earth Planet Sci 41:21–44

Buick R (1992) The antiquity of oxygenic photosynthesis: evidence from stromatolites in sulphate-deficient Archaean lakes. Science 255:74–77

Buick R, Dunlop JSR, Groves DI (1981) Stromatolite recognition in ancient rocks: an appraisal of irregularly laminated structures in an Early Archaean chert-barite unit from North Pole Western Australia. Alcheringa 5:161–181

Burne RV, Moore LS (1987) Microbialites; organosedimentary deposits of benthic microbial communities. Palios 2:241–254

Freytet P, Verrecchia EP (1998) Freshwater organisms that build stromatolites: a synopsis of biocrystallization by prokaryotic and eukaryotic algae. Sedimentology 45:535–563

Golubic S, Seong-Joo L, Browne KM (2000) Cyanobacteria: architects of sedimentary structures. In: Riding RE, Awramik SM (eds) Microbial sediment. Springer, Berlin, pp 57–67

Grotzinger JP, Kasting JF (1993) New constraints on Precambrian ocean composition. J Geophys Res 101:235–243

Grotzinger JP, Knoll AH (1999) Stromatolites in Precambrian carbonates; evolutionary mileposts or environmental dipsticks? Annu Rev Earth Planet Sci 27:313–358

Grotzinger JP, Rothman DH (1996) An abiotic model for stromatolite morphogenesis. Nature 383:423–425

Hofmann HJ (2000) Archaean stromatolites as microbial archives. In: Riding RE, Awramik SM (eds) Microbial sediments. Springer, Berlin, pp 315–327

Hofmann HJ, Grey K, Hickman AH, Thorpe RI (1999) Origin of 3.45 Ga coniform stromatolites in Warrawoona Group, Western Australia. Geol Soc Am Bull 111:1256–1262

Jogi PM, Runnegar B (2005) Quantitative methods for evaluating the biogenicity of fossil stromatolites. Astrobiology 5:293

Kalkowsky E (1908) Oolith und stromatolilith in norddeutschen Buntsandstein. Z Dtsch Geol Ges 60:68–125

Kamber BS, Webb GE (2007) Transition metal abundances in microbial carbonate: a pilot study based on in situ LA-ICP-MS analysis. Geobiology 5:375–389

Krumbein WE (1983) Stromatolites: the challenge of a term in space and time. Precambrian Res 20:493–531

Lowe DR (1994) Abiological origin of described stromatolites older than 3.2 Ga. Geology 22:387

McLoughlin N, Wilson LA, Brasier MD (2008) Growth of synthetic stromatolites and wrinkle structures in the absence of microbes – implications for the early fossil record. Geobiology 6:95–105

Pia J (1927) Abteilung: thallophyta. In: Hirmer M - (ed) Handbuch der Palaobotanik. R. Oldenbourg, Munich, pp 31–136

Pope MC, Grotzinger JP (2000) Controls on fabric development and morphology of tufas and stromatolites, uppermost Pethei group 1.8 Ga, Great Slave Lake, NW Canada. In: James NP, Grotzinger JP (eds) Carbonate sedimentation and diagenesis in the evolving Precambrian world, vol 67, SEPM Special Publication. Geological Society, London, pp 103–121

Reid RP, Visscher PT, Decho AW, Stolz JF, Bebout BM, Dupraz C, Macintyre IG, Paerl HW, Pinckney JL, Prufert-Bebout L, Steppe TF, Des Marais DJ (2000) The role of microbes in accretion, lamination and early lithification of modern marine stromatolites. Nature 406:989–992
Reid PR, James NP, Macintyre IG, Dupraz CP, Buren RV (2003) Shark Bay stromatolites: microfabrics and reinterpretation of origins. Facies 49:299–324
Riding R (1999) The term stromatolite: towards an essential definition. Lethaia 32:321–330
Riding R (2000) Microbial carbonates: the geological record of calcified bacterial-algal mats and biofilms. Sedimentology 47(Suppl 1):179–214
Riding R (2008) Abiogenic, microbial and hybrid authigenic carbonate crusts: components of Precambrian stromatolites. Geol Croat 61(2–3):73–103
Riding R, Liang L (2005) Geobiology of microbial carbonates: metazoan and seawater saturation state influences on secular trends during the Phanerozoic. Palaeogeography, Palaeoclimatology. Palaeoecology 219:101–115
Riding R, Voronova L (1984) Assemblages of calcareous algae near the Precambrian/Cambrian boundary in Siberia and Mongolia. Geol Mag 121:205–210
Rividi N, van Zuilen M, Philippot P, Ménez B, Godard G, Poidatz E (2010) Calibration of carbonate composition using micro-Raman analysis: application to planetary surface exploration. Astrobiology 10:293–309
Semikhatov MA, Gebelein CD, Cloud P, Awramik SM, Benmore WC (1979) Stromatolite morphogenesis: progress and problems. Can J Earth Sci 16:992–1015
Shapiro RS (2005) A field guide to microbialtes. In: Stevens C, Cooper J (eds) Western Great Basin geology. Pacific Section American Association of Petroleum Geologists, Fullerton, pp 68–80, Guidebook 99
Shepard RN, Sumner DY (2010) Undirected motility of filamentous cyanobacteria produces reticulate mats. Geobiology 8:179–190
Sumner DY (1997) Late Archaean calcite-microbe interactions: two morphologically distinct microbial communities that affected calcite nucleation differently. Palaios 12:300–316
Turner EC, James NP, Narbonne GM (2000a) Taphonomic control on microstructure in early Neoproterozoic reefal stromatolites and thrombolites. Palaios 15:87–111
Turner EC, Narbonne GM, James NP (2000b) Framework composition of early NeoProterozoic calcimicrobial reefs and associated microbialites, Mackenzie Mountains, N.W.T., Canada. In: Grotzinger JP, James NP (eds) Carbonate sedimentation and diagenesis in the evolving Precambrian world, vol 67, SEPM Special Publication. Geological Society, London, pp 103–121
Van Kranendonk MJ (2007) A review of the evidence for putative Paleoarchean life in the Pilbara Craton, Western Australia. In: Van Kranendonk MJ, Smithies HR, Bennett VC (eds) Earth's oldest rocks, vol 15, Developments in Precambrian Geology. Elsevier, Amsterdam
Vanyo JP, Awramik SM (1985) Stromatolites and earth-sun-moon dynamics. Precambrian Res 2:121–142
Visscher PT, Reid RP, Bebout BM (2000) Microscale observations of sulphate reduction: correlation of microbial activity with lithified micrite laminae in modern marine stromatolites. Geology 28:919–922
Wacey D (2009) Early life on earth. Springer, Dordrecht, p 274
Wacey D (2010) Stromatolites in the 3400 Ma Strelley pool formation, Western Australia: examining biogenicity from the macro to nano scale. Astrobiology 10:381–395
Wacey D, Gleeson D, Kilburn MR (2010) Microbialite taphonomy and biogenicity: new insights from NanoSIMS. Geobiology 8:403–416
Wagstaff KL, Corsetti FA (2010) An evaluation of information – theoretic methods for detecting structural microbial biosignatures. Astrobiology 10:363–379
Walter MR, Heys GR (1985) Links between the rise of metazoa and the decline of stromatolites. Precambrian Res 29:149–174
Walter MR, Bauld J, Brock TD (1976) Microbiology and morphogenesis of columnar stromatolites (*Conophyton*, *Vacerrilla*) from hot springs in Yellowstone National Park. In: Walter MR (ed) Stromatolites. Elsevier, New York, pp 273–310
Walter MR, Buick R, Dunlop JSR (1980) Stromatolites, 3, 400-3, 500 Myr old from the North Pole area, Western Australia. Nature 284:443–445

Sturtian Glaciation

▶ Snowball Earth

Subduction

Nicholas Arndt
ISTerre, Université Grenoble Alpes, France

Keywords

Active margin; Convergent margin; Dehydration; Island arc; Subduction zones; Wadati-Benioff zone

Definition

A basic tenet of ▶ plate tectonics is that ▶ oceanic crust forms at ▶ mid-ocean ridges and cycles back

into the mantle, usually at the margins of ocean basins. The latter process is called subduction, and the regions where it happens are called subduction zones. When an oceanic plate plunges beneath another oceanic plate, a chain of volcanic islands called an (*island*) *arc* is formed; when an oceanic plate plunges beneath a continent, the terms *convergent margin* and *active margin* are used.

At mid-ocean ridges, seawater penetrates the basaltic crust and converts the upper portions of the crust to an assemblage of hydrous minerals; as temperature and pressure increase during subduction, these minerals are destabilized. The released aqueous fluid triggers melting in the overlying mantle to yield the calc-alkaline magmas and explosive volcanism that characterize the arcs above subduction zones. Intermittent movement along the Wadati-Benioff zone – the contact between the subducting plate and overlying mantle – causes earthquakes. The name comes from the Japanese and American seismologists who independently discovered this inclined zone of earthquakes.

See Also

- ▶ Oceanic Crust
- ▶ Plate Tectonics
- ▶ Serpentine

Subglacial Environments

Daniele L. Pinti
GEOTOP Research Center for Geochemistry and Geodynamics, Université du Québec à Montréal, Montréal, QC, Canada

Definition

Subglacial is a term defining environments in a glaciated area that are lying directly beneath an ice mass and in close contact with the overlying ice, including cavities and channels beneath the ice that are not influenced by subaerial processes (i.e., processes that take place in open air or adjacent to the land surface). Subglacial lakes, such as ▶ Vostok Lake in ▶ Antarctica, are subglacial environments. In astrobiology, subglacial environments are studied to understand how life survives in these extreme habitats where very low temperatures and suboxic conditions prevail. It is likely that subglacial environments similar to the terrestrial ones exist in glaciated areas of ▶ Mars and in ▶ Europa and ▶ Enceladus, the icy moons of ▶ Jupiter and ▶ Saturn.

See Also

- ▶ Antarctica
- ▶ Enceladus
- ▶ Europa
- ▶ Glaciation
- ▶ Jupiter
- ▶ Mars
- ▶ Saturn
- ▶ Vostok, Subglacial Lake

Subglacial Lake Vostok

- ▶ Vostok, Subglacial Lake

Sublimation

Mark Dörr
University of Southern Denmark, Odense M, Denmark

Definition

Sublimation (Lat.: *sublimis* = "elevated," "lofty") is a special phase transition of an element or compound: the transition from a solid phase to a gas phase without intermediate liquid stage.

Sublimation is usually an ▶ endothermic phase transition that occurs at temperatures and

pressures below the ▶ triple point of a substance. The opposite of *sublimation* is *deposition*. The formation of rime is an example of meteorological *deposition*, and its sudden disappearance at temperatures below the freezing point of ▶ water is an example of *sublimation*.

See Also

▶ Endothermic
▶ Triple Point
▶ Water

Subliths

▶ Hypolithic

Submarine Hot Spring

▶ Black Smoker, Organic Chemistry

Submillimeter Wave Astronomy Satellite

Ronald L. Snell
Department of Astronomy, 517 K Lederle Graduate Research Center, University of Massachusetts, Amherst, MA, USA

Synonym

SWAS

Definition

The Submillimeter Wave Astronomy Satellite (SWAS) was a ▶ NASA mission dedicated to the study of interstellar chemistry. SWAS was launched in 1998 December and acquired data until 2004 July. SWAS was reactivated in 2005 June for a 3-month period to provide support for the Deep Impact mission. SWAS was comprised of a 54 × 68 cm off-axis Cassegrain telescope feeding two independent passively cooled heterodyne receivers. SWAS observed simultaneously the transitions of four astrophysically important species: O_2 (487.2 GHz), neutral atomic carbon (492.2 GHz), ^{13}CO (550.9 GHz), and H_2O (556.9 GHz) and it could also be tuned to observe $H_2{}^{18}O$ (547.7 GHz). The spectra were recorded using an Acousto-Optical Spectrometer (AOS) which provided a total bandwidth of 1,400 MHz for the four lines of primary interest. Observations of over 200 targets in more than 5,000 lines of sight were obtained over its lifetime and were used to study the chemistry of interstellar molecular clouds, circumstellar envelopes of evolved stars, planetary atmospheres, and comets.

See Also

▶ Deep Impact
▶ Odin

Suboxic

Daniele L. Pinti
GEOTOP Research Center for Geochemistry and Geodynamics, Université du Québec à Montréal, Montréal, QC, Canada

Definition

Suboxic is a term used for describing the oxygen concentration in the water column or any other environment where oxygen is strongly limited and shows no perceptible vertical gradients. There are no clear and agreed-upon boundaries between oxic, oxygen deficient, hypoxic, suboxic, and anoxic; however, the boundary between hypoxic and suboxic conditions is

widely taken as 10 μM of O_2, a value commonly observed in water bodies with enhanced nitrification due to an upward flux of ammonia. This level probably corresponds to the biochemical threshold below which the dominant electron acceptors are oxidized species of N (nitrate, nitrite) or of metals [Mn(IV), Fe(III)], whereas dissolved oxygen becomes an auxiliary oxidant. In the strongly stratified Black Sea, the suboxic zone is usually at 50–100 m depth and shows <3 μM in O_2 and H_2S. Suboxic zones favor denitrification which in turn removes many essential nutrients from the water column. In astrobiology, suboxic environments are of interest because they could yield clues on the development of metabolic pathways in which oxidants were limited, as was the case during the Archean and at the dawn of the Earth's oxygenation.

Substellar Objects

▶ Brown Dwarf

Substrate

Armen Y. Mulkidjanian[1,2]
and Henderson James (Jim) Cleaves II[3,4,5,6,7]
[1]School of Physics, University of Osnabrueck, Osnabrueck, Germany
[2]Moscow State University, Moscow, Russia
[3]Earth–Life Science Institute (ELSI), Tokyo
[4]Institute of Technology, Meguro–ku, Tokyo, Japan
[5]Institute for Advanced Study, Princeton, NJ, USA
[6]Blue Marble Space Institute of Science, Washington, DC, USA
[7]Center for Chemical Evolution, Georgia Institute of Technology, Atlanta, GA, USA

Keywords

Catalysis; Enzyme; Metabolite

Synonyms

Substratum

Definition

In chemistry, a substrate is a substance that is acted upon by a ▶ catalyst.

History

The word substrate is a composite of the Latin terms *sub* "below" and *stratum* "layer".

Overview

In modern organisms, protein- or RNA-based polymers (enzymes and ribozymes, respectively) serve as catalysts that act upon various substrates, or reactants, which can be organic or inorganic. Substrates and catalysts are usually distinct entities, and depending on the reaction in question, a catalyst may react with two substrates together simultaneously or act promiscuously on various structurally related substrates.

In the case of a single substrate, the substrate binds with the enzyme or catalyst ▶ active site, and a catalyst-substrate complex is formed. The substrate is then catalytically transformed into one or more products, which are then released from the active site.

$$C + S \rightleftharpoons CS \rightarrow CP \rightleftharpoons C + P$$

where C is the catalyst (a surface, enzyme, ribozyme, or other species), S is the substrate (or substrates), and P is the product (or products).

In cases with more than one substrate, these may need to be bound in a particular order, before reacting together to produce products.

In the context of astrobiology, the clear discrimination between substrate and catalysts is difficult since complex catalysts such as enzymes and ribozymes were likely not present during the first stages of chemical evolution. Accordingly, the emergence of the first substrates and catalysts

can be envisioned as their annealing from an initial network of diverse interactions between various small molecules.

See Also

- ▶ Catalyst
- ▶ Chemical Reaction Network
- ▶ Citric Acid Cycle
- ▶ Metabolism
- ▶ Organic Molecule
- ▶ Prebiotic Chemistry

Substratum

- ▶ Substrate

Subsurface Biota

- ▶ Deep Subsurface Microbiology

Succinic Acid

Henderson James (Jim) Cleaves II
Earth–Life Science Institute (ELSI), Tokyo Institute of Technology, Meguro–ku, Tokyo, Japan
Institute for Advanced Study, Princeton, NJ, USA
Blue Marble Space Institute of Science, Washington, DC, USA
Center for Chemical Evolution, Georgia Institute of Technology, Atlanta, GA, USA

Synonyms

Butanedioic acid

Definition

Succinic acid ($HOOCCH_2CH_2COOH$) is a ▶ dicarboxylic acid which plays an important role in the ▶ citric acid cycle. The name comes from Latin *succinum*, meaning amber, from which the acid was first isolated. The carboxylate anion is called succinate. Succinic acid has a melting point of 185 °C and a boiling point of 235 °C.

In the citric acid cycle, succinic acid donates electrons to FAD (flavin adenine dinucleotide) and ultimately to the electron transport chain by the reaction

$$\text{Succinate} + \text{FAD} \rightarrow \text{Fumarate} + \text{FADH}_2.$$

This reaction is catalyzed by the enzyme succinate dehydrogenase.

Succinic acid has been produced in various prebiotic experiments and has been found in carbonaceous chondrite meteorites.

See Also

- ▶ Citric Acid Cycle
- ▶ Dicarboxylic Acid
- ▶ Krebs Cycle

Sudbury Astrobleme

- ▶ Sudbury Impact Structure

Sudbury Impact Structure

Richard A. F. Grieve
University of Western Ontario, London, ON, Canada

Keywords

Impact structure; Impact melt; Hydrothermal system; Carbon; Extinction; Biological activity; Ore deposits

Synonyms

Sudbury astrobleme

Definition

The Sudbury impact structure, Canada, represents the eroded remains of an impact basin originally 150–200 km in diameter which formed ~1.85 Ga ago. It contains world-class ore deposits, associated with the Sudbury Igneous Complex, which represents the differentiated original impact melt sheet. This melt sheet was the heat engine for a postimpact hydrothermal system, which affected 20,000 km^3 of crust and may have lasted a million years. While the Sudbury impact may have had severe global environmental effects, similar to those from the ▶ Chicxulub impact 65 Ma ago, the postimpact hydrothermal activity served to enhance "local" biological activity.

Overview

The most prominent feature of the Sudbury impact structure in central Ontario, Canada, is the ~30 × 60 km elliptical basin formed by the outcrop of the Sudbury Igneous Complex (SIC), the interior of which is known as the Sudbury Basin (Fig. 1). Neither the SIC nor the Sudbury Basin is synonymous with the 1.85-Ga-old Sudbury impact structure. Although eroded, the Sudbury impact structure includes the Sudbury Basin, the SIC, and the surrounding brecciated basement rocks and covers a present area of ~15,000 km^2. From the spatial distribution of shock-metamorphic features (e.g., shatter cones, shocked quartz) and other impact-related attributes (pseudotachylite) and by analogy to equivalent characteristics at other large terrestrial impact structures, such as Chicxulub and Vredefort, the original crater rim diameter has been estimated at 150–200 km. Even larger original diameters, however, have been suggested. Considering the postimpact tectonic deformation and erosion, estimated to be ~5–10 km, which has taken place since the time of impact, it is difficult to constrain its original form but likely was a peak-ring or a multi-ring basin. The Sudbury structure is the site of world-class Ni-Cu sulfide and platinum group element (PGE) metal ores. The cumulative total worth of metals produced from Sudbury is estimated at well over $300 billion.

The SIC is the coherent impact melt sheet at Sudbury. It is differentiated and has been subdivided into a number of units. The Contact Sublayer, which has an igneous-textured matrix with inclusions of locally derived target rocks and mafic to ultramafic rocks, is discontinuous at the

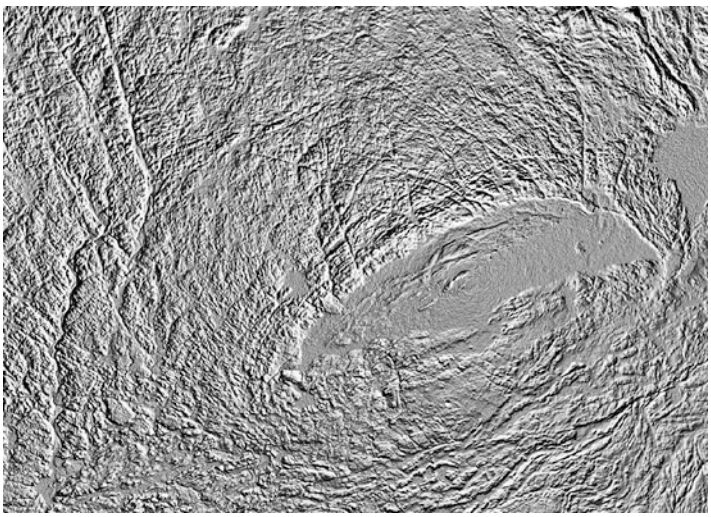

Sudbury Impact Structure, Fig. 1 Synoptic greyscale image of the topography of the Sudbury impact structure, based on the Shuttle Radar Topography Misssion. Image is illuminated from the center by an artificial sun. The most prominent feature is the 60 × 30 km elliptical trace of the Sudbury Igneous Complex and the interior, relatively smooth, Sudbury Basin

base. Associated with the SIC are the so-called offset dikes, which host 25 % of the Ni-Cu-PGE resources at Sudbury. These dikes are most often radial to the SIC, but some are concentric. Some are extensive, e.g., the Foy Offset can be traced for ~60 km from the North Range of the SIC and varies from ~400 m in width near the SIC to a few tens of meters at its most distal part. They have compositions similar to the average SIC and represent a "quenched" phase of the SIC.

The "Main Mass" of the SIC overlies stratigraphically the Sublayer. Historically, the Main Mass has been divided into a number of units: mafic norite, quartz-rich norite, felsic norite, quartz gabbro, and granophyre. These terms for these subunits are actually misnomers; however, the terminology appears "etched in stone." Only the Sublayer is gabbroic. The others fall into the quartz gabbro, quartz monzogabbro, granodiorite, and granite fields. This nomenclature confusion arises from the fact that, like most impact melts of granitic/granodioritic composition, the mafic component of the melt crystallized as ortho- and clinopyroxene although there is also primary hydrous amphibole and biotite. The contacts between the various subunits of the SIC are gradational, and details of the mineralogy, geochemistry, and geochronology support a cogenetic source for the subunits of the Main Mass of the SIC, produced by fractional crystallization of a single batch of silicate liquid (impact melt). The conclusion that the SIC is derived from melting the local crust in the target area is borne out by isotopic studies. In addition, osmium isotope studies of sulfides from several mines have confirmed their crustal origin from a binary mixture of local Superior Province and Huronian target rocks.

Various types of the ore deposits occur at Sudbury: Ni-Cu-Co "Contact" deposits associated with embayments at the base of the SIC and hosted by the Sublayer and footwall breccia, Ni-Cu-Pt-Pd-Au "Offset" deposits associated with discontinuities and variations in thickness in the offset dikes, and Cu-Pt-Pd-Au-rich "Footwall" deposits that can occur in the underlying target rock, up to 1 km away from the SIC. A fourth deposit environment is in association with the so-called Sudbury Breccia. For example, the Frood-Stobie deposit, which contained some 15 % of the entire known Sudbury resources and produced 600 million tonnes of ore, was hosted in Sudbury Breccia.

Impact structures result in upper crustal thermal anomalies as a result of the thermal effects (up to the production of superheated impact melt) of the passage of a shock wave in the crust. They physically bring originally deep-seated (hotter) target rocks to a near-surface environment. The Earth is a wet planet, and in recent years, there has been increasing recognition that terrestrial impacts produce postimpact hydrothermal systems. In the case of Sudbury, there is abundant mineralogical evidence for hydrothermal alteration, e.g., silicification, carbonization, and Ca-Na ion exchange (albitization) in the postimpact units overlying the SIC. The hydrothermal system at Sudbury is currently the largest known system associated with a terrestrial impact event and was fueled by the voluminous (calculated to have been originally on the order of 35,000 km^3) impact melt sheet. Model estimates indicate the hydrothermal system may have affected some 20,000 km^3 of the crust at its peak and lasted some 10^5–10^6 years after the impact event. The hydrothermal system in and around the SIC was complex, evolving over time and involving fluids from the SIC itself, groundwater in basement target rocks, seawater, and various mixtures of these, and included a fluid connection between the rocks above and in the SIC in its later stages of evolution. For example, the Zn-Pb-Cu ores in the postimpact sediments overlying the SIC are the result of the hydrothermal system fuelled by the heat of the SIC and involving seawater, whereas basement-derived Cl-rich brines played a role in the origin of the Footwall deposits at the base of the SIC.

Ejecta from the Sudbury impact have been found at ~20 sites in northern Michigan, Minnesota, and near Thunder Bay, Ontario, at distances up to ~900 km from Sudbury. They consist of various devitrified impact glasses, spherules, and shocked quartz and include ripped-up local bedrock. By analogy with the somewhat smaller Chicxulub impact structure, it is likely that the

Sudbury ejecta originally had a global distribution. Also by analogy with Chicxulub and its devastating effect on the global environment, including the K-Pg (previously named K-T) mass extinction event, it is speculated that the Sudbury impact event may have had global consequences. It has been noted that the Sudbury impact event appears to coincide with a significant change in sedimentation in the region, marking the end of massive iron formation deposits and the deposition of black shales.

Impact diamonds, silicon carbide, and fullerenes have all been noted in postimpact lithologies at Sudbury. The same lithologies contain some 10^{17} g of carbon which, based on its isotopic composition, is organic in nature. These deposits represent possibly the largest single burial deposit of organic carbon in the Precambrian. The Sudbury impact structure was formed in a shallow marine basin in the foreland of the Penokean orogeny. Two competing hypotheses exist to explain the copious amounts of carbon at Sudbury. The occurrence of impact diamonds, etc., points to the pre-impact presence of carbon. Thus, it has been hypothesized that, like Chicxulub, the Sudbury impact event resulted in an extinction event in the biosphere and the carbon is a record of this event. Alternatively, it has been hypothesized that the carbon is the product of enhanced biological activity resulting from the voluminous and relatively long-lived postimpact hydrothermal activity. If this was the case, the evidence from Sudbury suggests that impacts, while having the potential to destroy life, such as with the Chicxulub impact event, have also the potential to create favorable habitats which enhance biological activity. This has implications for scenarios of early Earth history, when the impact flux was much higher.

See Also

- ▶ Canadian Precambrian Shield
- ▶ Carbon
- ▶ Chicxulub Crater
- ▶ Crater, Impact
- ▶ Fullerene
- ▶ Hydrothermal Alteration
- ▶ Impact Melt Rock
- ▶ KT Boundary
- ▶ Shocked Quartz

References and Further Reading

Abramov O, Kring DA (2004) Numerical modeling of an impact-induced hydrothermal system at the Sudbury crater. Jour Geophy Res 109:E10007. doi:10.1029/2003JE002213

Ames DE, Farrow CE (2007) Metallogeny of the Sudbury mining camp. In: Goodfellow WD (ed) Mineral deposits. Geol Assoc Canada, Mineral Deposits Division, Sp. Pub. 5: pp 329–350

Ames DE, Jonasson IR, Gibson HL, Pope KO (2006) Impact-generated hydrothermal systems-constraints from the large Paleoproterozoic Sudbury crater, Canada. In: Cockell C, Gilmour I, Koeberl C (eds) Biological processes associated with impact events. Springer, Heidelberg, pp 55–100

Ames DE, Davidson A, Wodicka N (2008) Geology of the giant Sudbury polymetallic mining camp, Ontario, Canada. Econ Geol 103:1057–1077

Campos-Alvarez NO, Samson IM, Fryer BJ, Ames DE (2010) Fluid sources and hydrothermal architecture of the Sudbury structure: constraints from femtosecond LA-MC-ICP-MS Sr isotopic analysis of hydrothermal epidote and calcite. Chem Geol 278:131–150

Cannon WF, Schulz KJ, Wright Horton J, Kring DA (2010) The Sudbury impact layer in the Paleoproterozoic iron ranges of northern Michigan. GSA Bull 122:50–75. doi:10.1130/B26517.1

Suevite

Daniele L. Pinti
GEOTOP Research Center for Geochemistry and Geodynamics, Université du Québec à Montréal, Montréal, QC, Canada

S

Synonyms

Mixed breccia; Suevite breccia; Suevitic impact breccia

Definition

Suevite is a term referred to a polimictic ▶ breccia made of melt and solid fragments floating in a

fine pulverized clastic matrix. The clastic matrix contains lithic and mineral clasts in various stages of shock metamorphism produced during an impact. Initially used for describing impact breccia in the Nördlinger Ries (called also Ries crater), Germany, it is now a generalized term for describing similar brecciated rocks (impactites) found in impact craters.

See Also

- ▶ Breccia
- ▶ Crater, Impact
- ▶ Impact Melt Rock
- ▶ Impactite

Suevite Breccia

- ▶ Suevite

Suevitic Impact Breccia

- ▶ Suevite

Sulcus, Sulci

Roland J. Wagner
German Aerospace Center (DLR), Institute of Planetary Research, Berlin, Germany

Synonyms

Groove

Definition

Sulci are surface features found on ▶ Mars and on icy satellites in the outer ▶ Solar System. Sulci are subparallel grooves and ridges, generally within a structural unit that can be bounded by a major trough. On ▶ Ganymede (▶ Jupiter), numerous parallel grooves form the so-called grooved terrain on this satellite. Other icy satellites featuring sulci are ▶ Enceladus (▶ Saturn), ▶ Miranda (▶ Uranus), and ▶ Triton (▶ Neptune). Sulci are created by extensional tectonism, involving a brittle-ductile transition at comparably shallow depths (order of a few kilometers) in icy satellites.

See Also

- ▶ Chasma, Chasmata
- ▶ Enceladus
- ▶ Fossa, Fossae
- ▶ Ganymede
- ▶ Jupiter
- ▶ Mars
- ▶ Miranda
- ▶ Neptune
- ▶ Satellite or Moon
- ▶ Saturn
- ▶ Solar System, Inner
- ▶ Triton
- ▶ Uranus

Sulfaniumylidene

- ▶ Sulfur Hydrides in the Interstellar Medium

Sulfanyl

- ▶ Sulfur Hydrides in the Interstellar Medium

Sulfanylium

- ▶ Sulfur Hydrides in the Interstellar Medium

Sulfate Minerals

Nicholas Arndt
ISTerre, Université Grenoble Alpes, France

Definition

Sulfate minerals are a class of minerals that include the sulfate ion $\left(SO_4^{2-}\right)$ within their structure. Sulfate minerals occur in evaporitic depositional environments, as gangue minerals in hydrothermal veins and as secondary minerals in the oxidizing zone of sulfide mineral deposits. Common examples include gypsum ($CaSO_4{\cdot}2H_2O$) and anhydrite ($CaSO_4$) in evaporitic sediments; ▶ barite ($BaSO_4$), which is deposited from hydrothermal fluids; and anglesite ($PbSO_4$), an alteration product of lead sulfide ores. The identification of ▶ jarosite, a potassium iron sulfate hydroxide, magnesium sulfates, and possible relicts of gypsum at the Meridiani Planum landing site on ▶ Mars is suggested to be evidence of wet, oxidizing conditions in the early history of the red planet.

See Also

- ▶ Barite
- ▶ Evaporite
- ▶ Hydrothermal Environments
- ▶ Jarosite
- ▶ Mars
- ▶ Sulfur Isotopes

Sulfate Reducers

Felipe Gomez
Centro de Astrobiología (CSIC/INTA), Instituto Nacional de Técnica Aeroespacial, Torrejón de Ardoz, Madrid, Spain

Synonyms

SRB

Definition

Sulfate reducers are prokaryotic microorganisms that are able to reduce sulfate or partially oxidized sulfur compounds, such as sulfite and thiosulfate, in a non-assimilatory manner in order to obtain energy through ▶ anaerobic respiration. Sulfate reducers couple the oxidation of propionate, butyrate, lactate, and ethanol among other electron donors with the reduction of sulfate to sulfide. They are obligate anaerobes and include heterotrophs as well as authotrophs. The best known are Gram-negative bacteria, but *Desulfotomaculum* is a Gram-positive spore-forming sulfate-reducer genera closely related to *Clostridium*. There is a phylum which includes thermophilic sulfate reducers, including Thermodesulfobacteria. Different archaea, e.g., *Archaeoglobus*, are able to use sulfate as an ▶ electron acceptor for anaerobic respiration. Sulfate-reducing microorganisms are fundamental elements of the sulfur cycle.

See Also

- ▶ Anaerobic Respiration
- ▶ Biogeochemical Cycles
- ▶ Electron Acceptor
- ▶ Energy Conservation
- ▶ Respiration
- ▶ Sulfur Cycle

S

Sulfates, Extraterrestrial

Daniela Tirsch
German Aerospace Center DLR, Institute of Planetary Research, Berlin, Germany

Definition

Expression used for hydrated ▶ minerals that have been developed through the reaction of sulfuric acid with metal ions (Salt of Sulfuric Acid,

containing the sulfate ion SO_4^{2-}). These minerals primarily form in thick sedimentary beds by evaporation of ▶ water, in hydrothermal environments or as secondary minerals by the oxidation of sulfide minerals. The detection of sulfates on planets implies an acidic environment and the existence of liquid water at the time of mineral formation, but does not necessarily imply the long-term availability of liquid water. Typical sulfates found on ▶ Mars are, for example, gypsum ($CaSO_4 \cdot 2H_2O$), kieserite ($MgSO_4 \cdot H_2O$) and jarosite ($KFe^{3+}_3(SO_4)_2(OH)_6$). Typical sulfate detections on ▶ Mars are reported from Meridiani ▶ Planum and the Interior Layered Deposits at the ▶ Valles Marineris.

See Also

- ▶ Carbonate, Extraterrestrial
- ▶ Mars
- ▶ Mineral
- ▶ Phyllosilicates, Extraterrestrial
- ▶ Water

Sulfidic Oceans

Donald E. Canfield
Institute of Biology, University of Southern Denmark, Odense, Denmark

Keywords

Anoxic; Chemocline; Nitrogen fixation; Oxygen minimum zone; Sulfate reduction; Sulfide

Synonyms

Anoxic ocean; Euxinic ocean

Definition

A sulfidic ocean defines a condition where dissolved sulfide is found stably in measurable concentrations within the marine water column. Such waters contain no dissolved oxygen, but are typically found below the oxygen-containing region of the upper water column. Dissolved sulfide may or may not extend to the seafloor.

Overview

Sulfidic water-column conditions are found in permanently stratified basins such as the Black Sea and the Cariaco Basin and in numerous stratified fjords and other coastal embayments. Examples include Mariager Fjord in Denmark, Saanich Inlet in the USA, and Byfjorden in Sweden. Sulfide also accumulates in deep depressions such as the Gotland Deep in the Baltic Sea. Sulfide accumulates when the flux of oxygen by advection and diffusion is outpaced by the flux of reactive organic carbon from sinking marine biomass. The oxidation of the reactive carbon consumes all of the oxygen and then the available nitrate, after which sulfate reduction ensues with the consequent accumulation of dissolved sulfide. Sulfidic conditions are often associated with enhanced water-column stratification, as this limits the oxygen flux.

While oxygen-free and thermally stratified, sulfide is rare in oxygen minimum zones of the global ocean. This is due to a feedback loop involving the nitrogen cycle. This feedback loop checks the microbial loss of nitrate to N_2 gas in the oxygen-free waters, maintaining the waters nitrate-rich and sulfide-free. Sulfide can accumulate if ▶ nitrogen fixation (microbial conversion of N_2 to organic nitrogen) balances the loss of nitrate to N_2, but for reasons not well understood, nitrogen fixation is limited in these regions.

Sulfidic ocean conditions were very rare or absent in the distant geologic past when the Earth's atmosphere was anoxic. With no oxygen, mineral sulfides were not oxidized to sulfate on land, limiting the delivery of sulfate to the oceans and thereby limiting sulfate reduction in the oceans. The earliest reported sulfidic marine water column was 2.5 billion years ago in association with an early rise in atmospheric oxygen concentrations. Sulfide became more prevalent

after this, and from about 1.8 to about 0.8 billion years ago, sulfidic ocean conditions were apparently widespread. Sulfidic ocean conditions have decreased in magnitude over the last 500–600 million years in apparent response to rising atmospheric oxygen levels. Still, major episodes of sulfide accumulation occurred as recently 90–120 million years ago. In this case, atmospheric oxygen was plentiful and sulfide may have accumulated as result of enhanced ocean fertility or enhanced thermal stratification in a warmer climate.

See Also

- ▶ Anoxic Ocean
- ▶ Archaea
- ▶ Denitrification
- ▶ Nitrogen Fixation
- ▶ Precambrian
- ▶ Sulfate Reducers

References and Further Reading

Brüchert V, Currie B, Peard KR, Lass U, Endler R, Dübecke A, Julies E, Leipe T, Zitzman S (2006) Biogeochemical and physical control of shelf anoxia and water column hydrogen sulphide in the Benguela coastal upwelling system. In: Neretin LN (ed) Past and present water column anoxia. Springer, New York, pp 161–193

Canfield DE (1998) A new model for proterozoic ocean chemistry. Nature 396:450–453

Canfield DE (2006) Models of oxic respiration, denitrification and sulfate reduction in zones of coastal upwelling. Geochim Cosmochim Acta 70:5753–5765

Damsté JSS, Köster J (1998) A euxinic southern North Atlantic Ocean during the Cenomanian/Turonian oceanic anoxic event. Earth Planet Sci Lett 158:165–173

Johnston DT, Poulton SW, Dehler C, Porter S, Husson J, Canfield DE, Knoll AH (2010) An emerging picture of Neoproterozoic ocean chemistry: insights from the Chuar Group, Grand Canyon, USA. Earth Planet Sci Lett 290:64–73

Reinhard T, Raiswell R, Scott C, Anbar AD, Lyons TW (2009) A late Archean sulfidic sea stimulated by early oxidative weathering of the continents. Science 326:713–716

Richards FA (1965) Anoxic basins and fjords. In: Riley JP, Skirrow G (eds) Chemical oceanography. Academic, London, pp 611–645

Wilde P, Berry WBN (1980) Progressive ventilation of the oceans-potential for return to anoxic conditions in the post-paleozoic. In: Schalnger SO, Cita MB (eds) Nature and origin of cretaceous carbon-rich facies. Academic, London, pp 209–224

Sulfur

Henderson James (Jim) Cleaves II
Earth–Life Science Institute (ELSI), Tokyo Institute of Technology, Meguro–ku, Tokyo, Japan
Institute for Advanced Study, Princeton, NJ, USA
Blue Marble Space Institute of Science, Washington, DC, USA
Center for Chemical Evolution, Georgia Institute of Technology, Atlanta, GA, USA

Synonyms

S

Definition

Sulfur is a chemical element with the atomic number 16 denoted by the symbol S. It is a naturally abundant, multivalent nonmetal. In its native form, at room temperature and pressure, sulfur is a soft bright yellow crystalline solid. In nature, it can be found as the pure element and in the form of sulfide and sulfate minerals. It is found in two of the coded protein amino acids: ▶ cysteine and ▶ methionine.

Overview

The strong smell of sulfur is usually due to the presence of ▶ hydrogen sulfide (H_2S) or organosulfur compounds. Elemental sulfur is fairly insoluble in water. Common oxidation

states of sulfur include −2, +2, +4, and +6. Sulfur forms stable compounds with most elements. Sulfur forms more than 30 solid allotropes, more than any other element. Besides S_8, several other rings are known. Elemental sulfur is an equilibrium mixture of S_8, S_7, and small amounts of S_6.

Sulfur is unusual in that its viscosity in its molten state, unlike most other liquids, increases above temperatures of 200 °C (392 °F) due to the formation of polymers. Molten elemental sulfur is dark red above this temperature. At higher temperatures, its viscosity decreases as depolymerization occurs. The distinctive colors of Jupiter's volcanic moon, Io, are from various forms of molten, solid, and gaseous sulfur.

Sulfur has 25 known isotopes, four of which are stable – ^{32}S, ^{33}S, ^{34}S, and ^{36}S – with natural terrestrial abundances of 95.02 %, 0.75 %, 4.21 %, and 0.02 %, respectively. Aside from ^{35}S, all of the radioactive isotopes of sulfur are short lived.

Common naturally occurring sulfur compounds include sulfide minerals such as pyrite (iron sulfide, FeS), galena (lead sulfide, PbS), and sphalerite (zinc sulfide, ZnS), and sulfate minerals, such as gypsum (calcium sulfate, $CaSO_4$ H_2O) and barite (barium sulfate, $BaSO_4$). Sulfur occurs naturally in volcanic emissions.

Sulfur is present in many types of meteorites. Ordinary chondrites contain an average of 2.1 % sulfur, and carbonaceous chondrites may contain as much as 6.6 % sulfur. Sulfur in meteorites is normally present as troilite (FeS), but other sulfides are found in some meteorites, and carbonaceous chondrites contain free sulfur, sulfates, and possibly other sulfur compounds, including organosulfonates.

Sulfur is created in extremely large, extremely hot (over 2.5 billion kelvin) stars, by the fusion of silicon with helium.

Organosulfur compounds include thioethers (with the generic formula $R-S-R$), ▶ thiols (also known as mercaptans, with the generic formula $R-SH$), thiolates (the conjugate bases of thiols, with the generic formula $R-S^-$), sulfoxides (with the generic formula $R-S(=O)-R'$), and sulfones (with the generic formula that has the form $R-S(=O)_2-R'$).

Many organisms are able to use sulfur in its various redox states as a source of energy. Some bacteria use hydrogen sulfide (H_2S) in the place of water as an electron donor in a form of photosynthesis in which oxygen is the electron acceptor. The photosynthetic green and purple sulfur bacteria use elemental oxygen to oxidize hydrogen sulfide to elemental sulfur. Some bacteria which live around deep-sea hydrothermal vents oxidize hydrogen sulfide in this way. Sulfur bacteria use sulfate as an electron acceptor instead of oxygen and reduce various oxidized sulfur compounds to sulfides.

There are numerous sulfur-containing metabolites which are important in biochemistry, most notably the protein amino acids methionine and cysteine. Glutathione is an important sulfur-containing compound which plays a cellular role as a source of reduction potential. Several coenzymes have −SH moieties to handle reactions involving acyl-containing biochemicals, for example, coenzyme A and alpha-lipoic acid.

Some theoretical models for the origin of life have emphasized the role of sulfur compounds, for example de Duve's ▶ thioesters, with a role in an early energy transduction mechanism, or the anaerobic synthesis of pyrite from hydrogen sulfide and ferrous sulfide as the earliest source of energy and electron in primitive metabolisms as postulated by Wächtershäuser.

See Also

- ▶ Anaerobic Respiration
- ▶ Biogeochemical Cycles
- ▶ Chemolithotroph
- ▶ Cysteine
- ▶ Disulfide Bond
- ▶ Green Bacteria
- ▶ Hydrogen Sulfide
- ▶ Hydrothermal Vent Origin of Life Models
- ▶ Methionine
- ▶ Sulfate Reducers
- ▶ Sulfates, Extraterrestrial
- ▶ Sulfidic Oceans

- ▶ Sulfur Cycle
- ▶ Sulfur Isotopes
- ▶ Sulfur Monoxide
- ▶ Thioester
- ▶ Thioformaldehyde
- ▶ Thiol

Sulfur Cycle

José Luis Sanz
Departamento de Biología Molecular, Universidad Autónoma de Madrid, Madrid, Spain

Definition

The sulfur cycle, like the ▶ biogeochemical cycles of other elements, includes a series of oxidation and reduction stages of sulfur that are principally biotic and performed by microorganisms. Under certain pHs and redox potentials, some reactions of the sulfur cycle take place in the absence of microorganisms.

Overview

The sulfur cycle integrates and interconnects the different components of an ecosystem (soil, rock, sediment, aquatic phase, and atmosphere). Sulfur is present as organic sulfur (in amino acids, coenzymes, etc.) and inorganic sulfur: sulfides (S^{2-}), elemental sulfur (S^0), sulfates (S^{6+}), and a series of intermediaries of minor environmental relevance. Sulfate (SO_4^{2-}) is the major bioavailable form in nature, and is particularly abundant in marine environments, because elemental sulfur and hydrogen sulfide (H_2S) are of biological or geothermic origin and metal sulfides (MeS) are insoluble.

The sulfur cycle is complex, involving aerobic and anaerobic, auto- and heterotrophic, and chemo- and photosynthetic microorganisms. In anaerobic settings, primarily in aquatic sediments and to a lesser extent in soils (generally acidic and stagnant) or the digestive tracts of warm-blooded animals, sulfur- and sulfate-reducing bacteria (SRB) reduce sulfur and sulfates, respectively, to hydrogen sulfide. Phylogenetically, these bacteria belong to the class delta-*Proteobacteria* (*Desulfovibrio*, *Desulfuromonas*) and the order *Clostridiales* (family *Peptococcaceae*: *Desulfotomaculum*, *Desulfosporosinus*). The ▶ reduction takes place in an ▶ anaerobic respiration in which oxidized forms of sulfur (dissimilative reduction) act as electron acceptors for the oxidation of simple organic compounds (acetate, lactate, etc.) or H_2, yielding H_2S as a final product. Some ▶ archaea like *Archaeglobus* also carry out this process. Some species belonging to genera such as *Clostridium* or *Alteromonas* reduce thiosulfate ($S_2O_3^{2-}$) to H_2S. Alternatively, sulfate is converted into phosphoadenosine 5′-phosphosulfate (PAPS) by many bacteria and plants. In the form of PAPS, sulfur is used in the biosynthetic processes of living organisms (assimilative reduction).

H_2S, either released by SRB or of geothermal origin, can be used by bacteria, such as purple (*Chromatium*) or green (*Chlorobium*) sulfur bacteria, that carry out anoxygenic photosynthesis typically in anaerobic conditions such as deep aquatic systems or microbial biofilms. In both cases, H_2S acts as an ▶ electron donor, giving rise to elemental sulfur. H_2S can also be used by bacteria that carry out aerobic anoxygenic photosynthesis (*Erythromonas*, *Roseobacter*). In aerobic environments, H_2S is used by chemolithotrophic sulfur-oxidizing bacteria, such as *Thiobacillus* or *Thiomicrospira*, that accumulate extracellular elemental sulfur granules. In *Thiovulum* or filamentous bacteria like *Beggiatoa*, elemental sulfur accumulates inside their cells. In both cases, the sulfur can be further oxidized to sulfate.

Some sulfur-dependant thermophilic archaea, belonging to the order *Sulfolobales*, also carry out the oxidation of H_2S or S^0 to sulfate in the presence of oxygen (*Sulfolobus*, *Acidianus*). In the absence of O_2, a great number of thermophilic archaea – both *Crenarchaeota* (*Thermoproteus*, *Desulfurococcus*, *Pyrodictium*)

and *Euryarchaeota* (*Thermococcus* or some methanogens) – display autotrophic, myxotrophic, or heterotrophic growth during which S^0 is reduced to H_2S (although methanogens obtain no energy in the process).

Under certain circumstances, such as in the presence of oxygen and in neutral pH, H_2S is oxidized rapidly and abiotically to elemental sulfur.

See Also

- ▶ Acidophile
- ▶ Aerobic Respiration
- ▶ Anaerobic Respiration
- ▶ Archaea
- ▶ Assimilative Metabolism
- ▶ Bacteria
- ▶ Biogeochemical Cycles
- ▶ Chemolithotroph
- ▶ Crenarchaeota
- ▶ Electron Acceptor
- ▶ Electron Donor
- ▶ Euryarchaeota
- ▶ Lithotroph
- ▶ Respiration
- ▶ Sulfate Reducers

References and Further Reading

Canfield DE, Habicht KS, Thamdrup B (2000) The Archean sulfur cycle and the early history of atmospheric oxygen. Science 288:658–661

Fdez-Polanco F (2001) Combining the biological nitrogen and sulfur cycles in anaerobic conditions. Water Sci Technol 44(8):77–84

Kuenen G, Lens PNL (2001) The biological sulfur cycle: novel opportunities for environmental biotechnology. Water Sci Technol 44(8):57–66

Madigan M, Martinko J, Dunlap P, Clark D (2009) Brock biology of microorganisms, 12th edn. Pearson Benjamin Cummins, Menlo Park, pp 21–24, Chapters 15

Willey JM, Sherwood LM, Woolverton CJ (2008) The protozoa. In: Prescott, Harley and Klein (eds), Microbiology, 7th edn. McGraw-Hill, New York

Sulfur Hydrides in the Interstellar Medium

William M. Irvine
University of Massachusetts, Amherst, MA, USA

Synonyms

H_2S; Hydrogen sulfide; Mercapto radical; SH; SH+; Sulfaniumylidene; Sulfanyl; Sulfanylium

Definition

Two neutral hydrides of sulfur, H_2S and SH, and also the cation SH^+, have been detected in the ▶ interstellar medium by astronomers. Sulfur hydrides are important in many ▶ origins of life models, and two of the protein amino acids used by terrestrial life contain sulfur (▶ cysteine and ▶ methionine).

History

Whereas H_2S was one of the first triatomic molecules detected in interstellar ▶ molecular clouds (in 1972), the identification of SH^+ (in 2011) and SH (in 2012) has been much more recent. Although H_2S and SH^+ were observed using ground-based radio telescopes, radio astronomers used the SOFIA airborne observatory to detect SH (see ▶ Molecules in Space and the Web page cited there – http://www.astro.uni-koeln.de/cdms/molecules).

See Also

- ▶ Hydrogen Sulfide
- ▶ Interstellar Medium
- ▶ Molecular Cloud
- ▶ Molecules in Space
- ▶ Origin of Life

Sulfur Isotopes

James Farquhar
Department of Geology, University of Maryland, College Park, MD, USA

Keywords

Great oxygenation event; Isotopes; Isotopic ratio; Sulfates; Sulfides

Definition

Sulfur is a relatively common element in the Solar System and on Earth. It has four relatively abundant, naturally occurring, stable isotopes with masses of approximately 32, 33, 34, and 36 atomic mass unit (amu). It has a rich chemistry, and reactions involving sulfur compounds occur in the solid, liquid, and gaseous envelopes of Earth and other planets. It occurs in a variety of valence states ranging from +6 to −2, and as a result, sulfur is used in a variety of biological capacities.

Overview

Sulfur compounds are used as an energy source for metabolic activity (catabolism) by a variety of bacteria and archaea that draw upon redox transformations, using oxidized species as electron donors and reduced species as electron acceptors. Sulfur compounds are used as important electron acceptors for anoxygenic ▶ photosynthesis by green and purple sulfur bacteria. Sulfur is a constituent of both essential (▶ methionine) and nonessential (▶ cysteine) amino acids. Sulfur compounds are involved in photochemical reactions in the atmosphere, and some of these reactions can be quite complex with transformations involving a variety of bound and unbound states. The variety of bonding environments, reaction pathways, and the presence of odd and even mass nuclei that have a relatively large difference in vibrational potential energy also, ultimately, contribute to a rich isotopic chemistry.

By convention, sulfur isotope compositions are described using delta notation ($\delta^{34}S$, $\delta^{33}S$, and $\delta^{36}S$). This notation describes the deviation of an isotope ratio in a sample relative to that in an international reference material (V-CDT) and is generally expressed in permil.

A second type of notation, capital delta notation ($\Delta^{34}S$, $\Delta^{33}S$, and $\Delta^{36}S$), is used to describe the difference between the isotopic compositions of two materials expressed in delta notation. For $^{34}S/^{32}S$, $\Delta^{34}S$ is the arithmetic difference between the $\delta^{34}S$ of two materials (e.g., $\delta^{34}S_{Material-a} - \delta^{34}S_{Material-b}$), but for $^{33}S/^{32}S$ and $^{36}S/^{32}S$, the $\Delta^{33}S$ and $\Delta^{36}S$ describe the arithmetic difference between a measured $\delta^{33}S$ and $\delta^{36}S$ and a $\delta^{33}S$ and $\delta^{36}S$ that is predicted on the basis of the measured $\delta^{34}S$. Following this convention, $\Delta^{33}S = \delta^{33}S - \left[\left(1+\delta^{34}S\right)^{0.515} - 1\right]$ and $\Delta^{36}S = \delta^{36}S - \left[\left(1+\delta^{34}S\right)^{1.90} - 1\right]$. The quantities $\left[\left(1+\delta^{34}S\right)^{0.515} - 1\right]$ and $\left[\left(1+\delta^{34}S\right)^{01.90} - 1\right]$ are approximately equal to the values of $\delta^{33}S$ and $\delta^{36}S$ that would be predicted for a single-step equilibrium isotope effect. The $\Delta^{33}S$ and $\Delta^{36}S$ therefore describe deviations from an equilibrium reference frame that is anchored by the compositional reference frame, V-CDT.

The term *isotope effect* is used to describe a change in isotope ratios that is produced by a physical or a chemical process. We use the term *fractionation factor* (α) to quantify the change in isotope ratios produced by an isotope effect (e.g., $^{34}\alpha_{a-b} = (^{34}S/^{32}S)_{substance\_a}/(^{34}S/^{32}S)_{substance\_b}$). The term *fractionation* is used to describe an observed difference in the isotope ratio of sulfur in two reservoirs, and a *discrimination coefficient* ($\sum = \alpha - 1$) is used to describe the change in isotope ratios produced by one or more processes with associated isotope effects. In this context, there are a number of different types of physical and chemical processes that generate isotope

effects, and some of these produce significant variations for $\delta^{34}S$ but not for $\Delta^{33}S$ and $\Delta^{36}S$, while others produce significant variations for all three. Isotope effects have been grouped into several categories. These include (1) *classical or equilibrium isotope effects* (EIE) that arise principally because of differences in vibrational potential energy and that produce significant variations for $\delta^{34}S$ but not for $\Delta^{33}S$ and $\Delta^{36}S$; (2) *nuclear volume effects* (NVE) that arise because differences in the size and shape of the nucleus influence the nuclear charge distribution and may have an effect on the potential energy surfaces of bonding for different isotopes and that produce other types of variations for $\delta^{34}S$, $\Delta^{33}S$, and $\Delta^{36}S$; (3) *kinetic isotope effects* (KIE) that may in some cases produce other types of variations for $\delta^{34}S$, $\Delta^{33}S$, and $\Delta^{36}S$ and that arise because factors other than vibrational energy, such as nuclear spin, or level matching between bound and unbound states, or molecular symmetry, control rates of reactions involving molecules containing some isotopes more than they do the rates of reactions for molecules containing other isotopes; and (4) other *physically controlled isotope effects* that reflect the operation of physical processes such as buoyancy, gravitation, kinetic energy, and mixing processes and that produce other types of variations for $\delta^{34}S$, $\Delta^{33}S$, and $\Delta^{36}S$.

Sulfur isotope compositional variations reflect different types of isotope effects that are relevant at different times in the history of Earth and other planets and that are relevant for astrobiology. These include, but are not limited to, (1a) an observation that the range of $\delta^{34}S$ is small in the oldest terrestrial rocks and becomes larger in samples that are younger in age; (1b) an observation that there are some ancient rocks (older than ~3,000 million years old (Ma)) that exhibit larger ranges of variability for $\delta^{34}S$; (1c) an observation that the average values for $\delta^{34}S$ of sedimentary pyrite are generally near zero or slightly positive until about 550 Ma when they became negative; (2a) an observation that the variability of $\Delta^{33}S$ is largest in the oldest terrestrial rocks and becomes significantly smaller at approximately 2,400 Ma; (2b) an observation that the $\Delta^{33}S$ of proxies for seawater sulfate have risen from slightly negative values (~−0.5 to −0.10 ‰) to generally positive values (0 to +0.5 ‰) over the past 2,000 million years; and (3) an observation that samples of Martian meteorites contain sulfate and sulfide that has variable and significantly negative $\Delta^{33}S$.

The Geologic Record of $\delta^{34}S$

Monster et al. (1977) and Cameron (1982, 1983) argued that the range of $\delta^{34}S$ observed in terrestrial rocks was small in the earliest parts of Earth's history (before ~2,500–2,700 Ma) and became larger after this time. They argued that this general change in the observed variability of $\delta^{34}S$ reflects a response of sulfate-reducing bacteria to rising oceanic sulfate concentrations. They cited earlier studies of Harrison and Thode (1958) that documented a similar response in laboratory culture experiments and argued that rising sulfate concentrations was a global response to generally more oxidizing conditions for mineral weathering occurring at ~2,500–2,700 Ma. The presence of one locality at North Pole, Western Australia (~3,400 Ma), which was an exception to this general rule, exhibiting sulfides with significantly negative $\delta^{34}S$, has been argued to be evidence for the presence of ▶ sulfate-reducing and sulfur-disproportionating bacteria (bacteria capable of splitting one compound into two different compounds, in this case an electron donor and an electron acceptor) (Shen et al. 2001; Philippot et al. 2007).

Two observations made for later points in Earth history include an observation that the average values for $\delta^{34}S$ of sedimentary pyrite are generally near zero or slightly positive until about 550 Ma and that the variability for $\delta^{34}S$ increases from ~40 ‰ to ~60 ‰ starting around 800 Ma (Canfield and Teske 1996). The first observation may be attributable to a fundamental change in the way that sulfur is cycled within seafloor sediments and may reflect the initiation of significant bioturbation (displacement and mixing of sediment particles) that recycled sedimentary sulfur to seawater and allowed for the transfer of negative $\delta^{34}S$ to sedimentary pyrite (e.g., Canfield and Farquhar 2009). The cause of the amplification in the

range of observed variability of $\delta^{34}S$ at ~800 Ma is debated but includes a variety of hypotheses related to changes in the ecology of the oceans and their impacts on sulfate concentration, bioturbation, and the cycling of sulfur by a more complex biosphere.

The Geologic Record of $\Delta^{33}S$

Farquhar et al. (2000a) reported significant variability in the range of $\Delta^{33}S$ (correlated with $\Delta^{36}S$) of Archean and earliest Proterozoic rocks that disappeared at ~2,400 Ma. This variability was interpreted to reflect preservation of an imprint of atmospheric reactions that produce variations with nonzero $\Delta^{33}S$. This interpretation was based on the observation of nonzero $\Delta^{33}S$ in photolysis experiments, and in today's atmosphere, and a lack of plausible alternatives to produce similar isotope signals by liquid-phase or solid-phase reactions. The preservation of the $\Delta^{33}S$ signal in the rock record was inferred to reflect limited oxidative and reductive cycling of sulfur compared to that seen in the present-day sulfur cycle, and this was linked to atmospheric oxygen levels and therefore carried implications for ▶ oxygenation of Earth's atmosphere and surface environments. Subsequent studies by Pavlov and Kasting (2002) presented arguments that the opening of pathways for the transfer of atmospheric signals to the surface also depends on oxygen levels and were consistent with this interpretation. An atmospheric origin associated with self-shielding (large optical depths that limit photodissociation of the most abundant isotope) rather than a primary photochemical origin for the effect has been proposed by Lyons (2009) but would not change the implications. Given the cross sections, some amount of self-shielding is inescapable, but whether it is the sole reason for the sulfur isotope effect remains to be demonstrated. Recently, it has been shown that other pathways associated with some thermochemical (liquid-phase) reactions exist for the production of anomalous $\Delta^{33}S$ (Watanabe et al. 2009). It is unclear at present whether this chemistry provides an alternative explanation for the early Earth record.

The $\Delta^{33}S$ of oceanic sulfate younger than 2,400 Ma deviates slightly from a value of zero as a result of the way biogeochemical reactions are linked within the sulfur cycle. Johnston et al. (2005) demonstrated that the $\Delta^{33}S$ of oceanic sulfate rose from slightly negative values (~−0.5 to −0.10 ‰) to generally positive values (0–0.5 ‰) over the past 2,000 million years. This change was attributed to a transition from a sulfur cycle dominated by sulfate reduction to a sulfur cycle where the influence of sulfide oxidation and disproportionation was expressed. Recently Wu et al. (2010) have suggested that the $^{34}S/^{32}S$ and $^{33}S/^{32}S$ fractionations between seawater sulfate and buried pyrite may have changed approximately 300 Ma ago, suggesting a change in the oceanic cycling of sulfur that also may be linked to ocean ecology, bioturbation, and reoxidation pathways for biogenic sulfide.

Sulfur Isotope Records of Martian Meteorites

In the late 1970s and early to mid-1980s, a strong case was made that the SNC (shergottite, nakhlite, and chassingite) meteorites came from Mars (Wood and Ashwal 1981; Bogard and Johnson 1983; Mcsween 1985, 1994). While these meteorites may not themselves constitute a fully representative suite of Martian rocks, their study provides a window into aspects of Mars science that is fundamental to our understanding of Mars. Farquhar et al. (2000, 2007) reported sulfate and sulfide from these meteorites with significant and variably negative $\Delta^{33}S$ and near-zero $\Delta^{36}S$. Variations of the magnitude seen in these meteorites are larger than that seen in other types of meteorites but are smaller than those seen in ancient terrestrial samples. The origin of this signal was interpreted to reflect isotope transformations on Mars that are related to atmospheric pathways for oxidation of sulfur to sulfate. These findings point to a significant role for these atmospheric pathways in the Martian sulfur cycle. They also call for an accounting of $\Delta^{33}S$ (and $\Delta^{36}S$) in future studies that seek to use sulfur isotopes as a tracer of possible biological processing of sulfur in the search for evidence of extraterrestrial metabolic activity.

See Also

- ▶ Archean Traces of Life
- ▶ Biomarker, Isotopic
- ▶ Earth, Formation and Early Evolution
- ▶ Earth's Atmosphere, Origin and Evolution of
- ▶ Fractionation, Mass Independent and Dependent
- ▶ Great Oxygenation Event
- ▶ Green Bacteria
- ▶ Oxygenation of the Earth's Atmosphere
- ▶ SNC Meteorites
- ▶ Stable Isotopes

References and Further Reading

Bogard DD, Johnson P (1983) Martian gases in an antarctic meteorite. Science 221:651–654

Cameron EM (1982) Sulfate and sulfate reduction in early Precambrian oceans. Nature 296:145–148

Cameron EM (1983) Evidence from early Proterozoic anhydrite for sulfur isotopic partitioning in Precambrian oceans. Nature 304:54–56

Canfield DE (2001) Biogeochemistry of sulfur isotopes. Rev Mineral Geochem 43:607–636

Canfield DE, Farquhar J (2009) Animal evolution, bioturbation, and the sulfate concentration of the oceans. Proc Natl Acad Sci U S A 106(20):8123–8127

Canfield DE, Teske A (1996) Late Proterozoic rise in atmospheric oxygen concentration inferred from phylogenetic and sulphur-isotope studies. Nature 382:127–132

Farquhar J, Thiemens MH (2000) Oxygen cycle of the Martian atmosphere-regolith system: Δ17O of secondary phases in Nakhla and Lafayette. J Geophys Res 105:11991–11997

Farquhar J, Bao HM, Thiemens M (2000) Atmospheric influence of Earth's earliest sulfur cycle. Science 289(5480):756–758

Farquhar J, Kim ST, Masterson AL (2007) Implications from sulfur isotopes of the Nakhla meteorite for the origin of sulfate on Mars. Earth Planet Sci Lett 264(1–2):1–8. doi:10.1016/j.epsl.2007.08.006

Harrison AG, Thode HG (1958) Mechanism of the bacterial reduction of sulphate from isotope fractionation studies. Trans Faraday Soc 54:84–92

Johnston DT, Wing BA, Farquhar J, Kaufman AJ, Strauss H, Lyons TW, Kah LC, Canfield DE (2005) Active microbial sulfur disproportionation in the mesoproterozoic. Science 310:1477–1479

Lyons JR (2009) Atmospherically-derived mass-independent sulfur isotope signatures, and incorporation into sediments. Chem Geol 267(3–4):164–174

Mcsween HY (1985) SNC meteorites – clues to Martian petrologic evolution. Rev Geophys 23(4):391–416

Mcsween HY (1994) What we have learned about mars from SNC meteorites. Meteoritics 29(6):757–779

Monster J, Appel PWU, Thode HG, Schidlowski M, Carmichael CM, Bridgwater D (1979) Sulfur isotope studies in early Archaean sediments from Isua. West Greenland – implications for the antiquity of bacterial sulfate reduction. Geochim Cosmochim Acta 43:405–413

Pavlov AA, Kasting JF (2002) Mass-independent fractionation of sulfur isotopes in Archean sediments: strong evidence for an anoxic Archean atmosphere. Astrobiology 2(1):27–41

Philippot P, Van Zuilen M, Lepot K, Thomazo C, Farquhar J, Van Kranendonk MJ (2007) Early Archaean microorganisms preferred elemental sulfur, not sulfate. Science 317:1534–1537

Shen YA, Buick R, Canfield DE (2001) Isotopic evidence for microbial sulphate reduction in the early Archaean era. Nature 410(6824):77–81

Watanabe Y, Farquhar J, Ohmoto H (2009) Anomalous fractionations of sulfur isotopes during thermochemical sulfate reduction. Science 324(5925):370–373

Wood CA, Ashwal LD (1981) Meteorites from Mars: prospects and implications. Lunar Planet Sci XII:1197–1199

Wu NP, Farquhar J, Strauss H, Kim ST, Canfield DE (2010) Evaluating the S-isotope fractionation associated with Phanerozoic pyrite burial. Geochim Cosmochim Acta 74:2053–2071

Sulfur Monoxide

William M. Irvine
University of Massachusetts, Amherst, MA, USA

Synonyms

SO

Definition

The diatomic molecule sulfur monoxide, SO, is normally found in the gas phase. Astronomically, it has been observed in interstellar and circumstellar ▶ molecular clouds, in ▶ comets, and in the atmospheres of the Jovian satellite ▶ Io and the planet ▶ Venus.

See Also

- ▶ Comet
- ▶ Io
- ▶ Molecular Cloud
- ▶ Molecules in Space
- ▶ Venus

References and Further Reading

Gottlieb CA, Gottlieb EW, Litvak MM, Ball JA, Pennfield H (1978) Observations of interstellar sulfur monoxide. Astrophys J 219:77–94

Na CY, Esposito LW, Skinner TE (1990) International ultraviolet explorer observations of Venus SO_2 and SO. J Geophys Res 95:7485–7491

Sun (and Young Sun)

Manuel Güdel
Department of Astrophysics, University of Vienna, Vienna, Austria

Keywords

Coronal mass ejections; Flares; High-energy particles; Internal structure; Magnetic fields; Main-sequence star; Solar atmosphere; Solar radiation; Solar wind

Definition

The Sun is the central body of our solar system and the nearest star. It is a low-mass star of spectral type G2 V located on the main sequence in the Hertzsprung-Russell diagram, with an age of about 4.6 billion years. Its mass is 1.99×10^{30} kg and its bolometric luminosity amounts to 3.84×10^{26} W. The Sun shows diverse signs of magnetic activity, in particular sunspots, a warm chromosphere, a very hot magnetic corona, flares, coronal mass ejections, and the solar wind.

Overview

The Sun is a main-sequence star in the phase of core hydrogen burning, being in the midst of the longest stable phase of ▶ stellar evolution before the white dwarf phase. It is a metal-rich (population I) star with an age of approximately 4.6 billion years. It will spend another ≈5 Gyr before evolving off the main sequence. The Sun is classified as a low-mass star of spectral type G2. It entirely dominates the solar system in terms of mass and energy. Its luminosity is such that at the distance of the Earth, a total flux of 1,366 W m^{-2} is measured (the "▶ solar constant"). Some of the basic properties of the Sun are summarized in Table 1. Various appearances of the Sun and its environment are illustrated in Fig. 1.

This entry reviews our knowledge of the Sun and its environment with emphasis on features relevant for astrobiology. We therefore review the internal structure of the Sun including the magnetic dynamo and nuclear fusion in a relatively cursory way, while more emphasis is put on the escaping radiation from the solar atmosphere. We specifically focus on radiation related to solar magnetic activity, including ultraviolet and X-ray radiation. This short-wavelength radiation is crucially important for ionization, heating, and chemical reactions in planetary atmospheres and therefore for the formation and evolution of life. Important questions related to the formation of life on Earth require knowledge of the solar constitution in earlier times of solar evolution. Systematic studies of stellar samples provide this information, which we will therefore address as well.

Basic Methodology

The Sun is the only star that can be studied in spatial detail. This remains true even if a few stars have been marginally resolved by optical interferometry, by speckle interferometry, or, as far as their magnetic atmospheres are concerned, by radio interferometry. But for no other star do we

have similarly extensive methodology and diagnostics at hand as for the Sun.

Traditionally, radiation across the electromagnetic spectrum has been used to investigate all layers of the solar atmosphere. Specifically, the photospheric layers provide rich diagnostics in optical spectroscopy, including polarization diagnostics to infer strength and orientation of photospheric magnetic fields. The optically thin chromospheric and transition region layers with temperatures between 10^4 and 10^6 K reveal themselves best in ultraviolet emission lines. Million-degree coronal plasma emits in the extreme ultraviolet range and in X-rays, where again rich spectroscopic diagnostics are available to study temperature, density, and motion of coronal plasma. Nonthermal particles accelerated during flare episodes leave various traces at radio wavelengths and in hard X-rays and gamma rays. Although most of the electromagnetic spectrum is also studied routinely in solar-like stars (presently with the exception of nonthermal hard X-rays above 20 keV and gamma rays), the lack of spatial resolution has made solar studies indispensable for the interpretation of stellar atmospheres. In situ observations of high-energy particles (e.g., from flares), coronal mass

Sun (and Young Sun), Table 1 Basic parameters of the Sun

Stellar winds	Stellar winds
Mass	1.989×10^{30} kg
Radius	6.955×10^{5} km
Average density	1.41×10^{3} kg m^{-3}
Surface temperature	5,770 K
Bolometric luminosity	3.846×10^{26} W
Spectral class	G2 V
Age	4.6×10^{9} year
Sidereal rotation period	25.05 days (equator)–34.3 days (near poles)
Synodic rotation period	27.3 days at 16° latitude

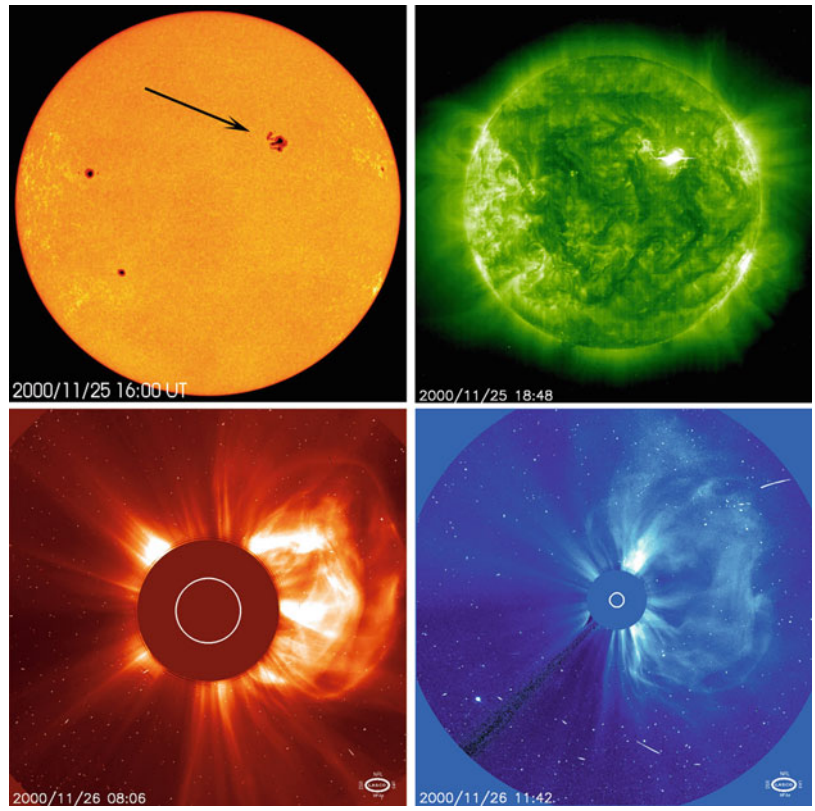

Sun (and Young Sun), Fig. 1 Images of the Sun taken contemporaneously, showing the photosphere in the *optical light* (*upper left*), the corona in the extreme *ultraviolet* range (*upper right*), and an evolving coronal mass ejection seen in optical *white light* (*lower images*) (Credit: SOHO LASCO/EIT, ESA, and NASA)

ejections, and the solar wind are of course confined to our own solar system.

Although ground-based optical solar observatories can be used to study the solar photosphere and sunspots, investigations of higher layers in ultraviolet, EUV, and X-rays require space-borne instrumentation on satellites, such as the SOHO, Yohkoh, TRACE, STEREO, or the Solar Dynamics Observatory. The same is true for observations of high-energy particles in interplanetary space and also applies to highest-energy radiation such as hard X-rays and gamma rays during flares. In contrast, the highly diagnostic radio emission is easily observed in spectral and temporal detail with relatively modest-sized ground-based telescopes.

Our understanding of the solar interior has been revolutionized by helioseismology. Helioseismology is the analog of terrestrial seismology although it probes sound waves in a gaseous environment. Convective motion in the outer layers of the solar interior excites acoustic waves, which develop standing waves. Sound waves traveling from the surface obliquely into the solar interior are refracted back to the surface owing to the increasing temperature toward larger depths and the temperature dependence of the sound velocity. Thousands of so-called pressure modes (p-modes) have been measured that together probe the internal structure in much detail except the central part of the Sun where nuclear reactions take place (there, sensitive measurements of g-modes would be required). Lower harmonics (p-mode waves with longer spatial scales) penetrate to deeper layers, while higher harmonics remain closer to the surface. Resulting oscillations of the photosphere can be recorded through Doppler shifts. The p-modes show a large spectrum of waves with an average period of 5 min. The observed oscillations can be inverted to derive the temperature and pressure profiles in the convection zone. Their detailed analysis provides much insight into the internal structure of the Sun.

Neutrinos define another important way to probe the solar interior, specifically the nuclear region. Detection of solar neutrinos has fundamentally confirmed the proton-proton chain reaction (p-p cycle; see below); although initially found to be deficient from the Sun, neutrinos oscillate between three flavors, the flavor produced in the Sun and initially detected in experiments being the electron neutrino. Considering this oscillation effect and measuring solar neutrinos of all flavors, there is no discrepancy between the standard solar model for the solar center and observations.

Magnetic fields play a major role in the solar atmosphere all the way from the photospheric layer to the corona and the solar wind. Photospheric magnetic fields are relatively easy to measure by making use of Zeeman splitting of spectral lines: magnetic fields split the atomic energy levels into sublevels, and the emitted radiation is polarized. Coronal magnetic fields can be deduced from approximate 3D extrapolations of photospheric fields based on some assumptions; alternatively, coherent radio emission diagnostics has been used to estimate field strengths in the emission region.

A key question relevant for the evolution of life refers to the long-term evolution of the Sun, its magnetic activity, and radiation spectrum. Although theoretical models of stellar evolution provide deep insight into the evolution of basic parameters (radius, surface effective temperature, etc.), the generation of magnetic activity and the solar wind is not sufficiently well understood to be modeled on evolutionary timescales. Here, stellar samples of solar analogs with known ages are used, with the goal of finding systematic trends with age.

S

Key Research Findings

The Sun's Internal Structure, Energy Production, and Composition

Our knowledge of the Sun's internal structure and physical state is summarized in the so-called standard model that calculates temperature, pressure, and density as a function of radius, fulfilling the conservation equations and the boundary conditions at the solar surface.

The central region of the Sun (within a radius of approximately 10^5 km – see Fig. 2) is

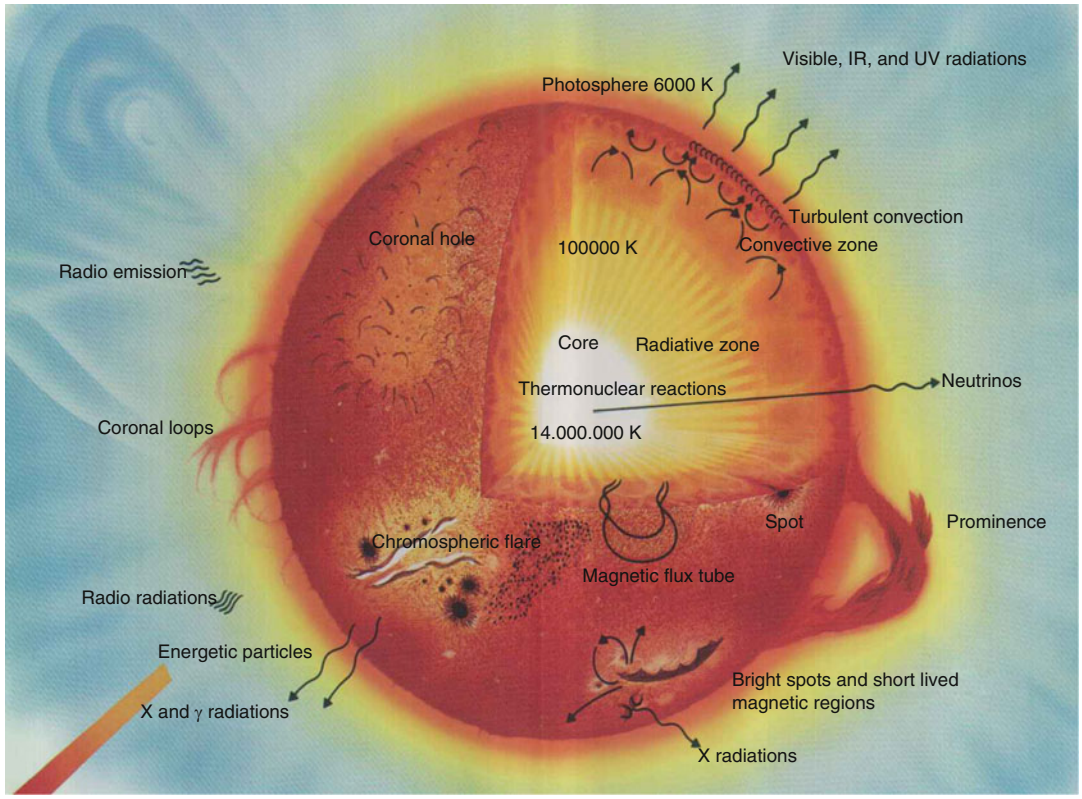

Sun (and Young Sun), Fig. 2 Schematic cross section of the Sun and sketch of features in the solar atmosphere (Credit: NASA/HEASARC)

characterized by temperatures of about 16×10^6 K and a density of 1.5×10^5 kg m^{-3}. In this core region, helium (^{4}He) is synthesized from hydrogen (p) nuclei mainly in the proton-proton chain reaction:

$$\mathrm{p} + \mathrm{p} \rightarrow {}^2\mathrm{H} + \mathrm{e}^+ + \nu_\mathrm{e}$$

$${}^2\mathrm{H} + \mathrm{p} \rightarrow {}^3\mathrm{He} + \gamma$$

$${}^3\mathrm{He} + {}^3\mathrm{He} \rightarrow {}^4\mathrm{He} + \mathrm{p} + \mathrm{p}$$

where γ stands for energy emitted in a photon and ν_e is an electron neutrino. There is also a second path to ^{4}He involving ^{7}Be, ^{7}Li, and ^{8}Be, and a small percentage of the energy is produced in the so-called CNO cycle. Within the inner $\approx$71 % of the solar radius, the energy liberated from the central fusion process is transported radiatively. Outside this region, convection plays a dominant role up to the solar photosphere.

The Sun is composed predominantly of hydrogen (approximately 70 % by mass or 91 % by number of atoms) and helium (28 % by mass or 9 % by atom number); heavy elements, predominantly carbon, nitrogen, oxygen, neon, magnesium, silicon, sulfur, and iron, contribute the remaining 2 % of the mass. The exact composition is still a matter of debate but plays an important role for the plasma opacity and therefore the radiative transport in the solar interior and the depth where energy transport becomes dominated by convective motions.

The Solar Photosphere and Sunspots

The visible surface of the Sun defines the photosphere, that is, the layer from which photons in the visible range of the electromagnetic spectrum

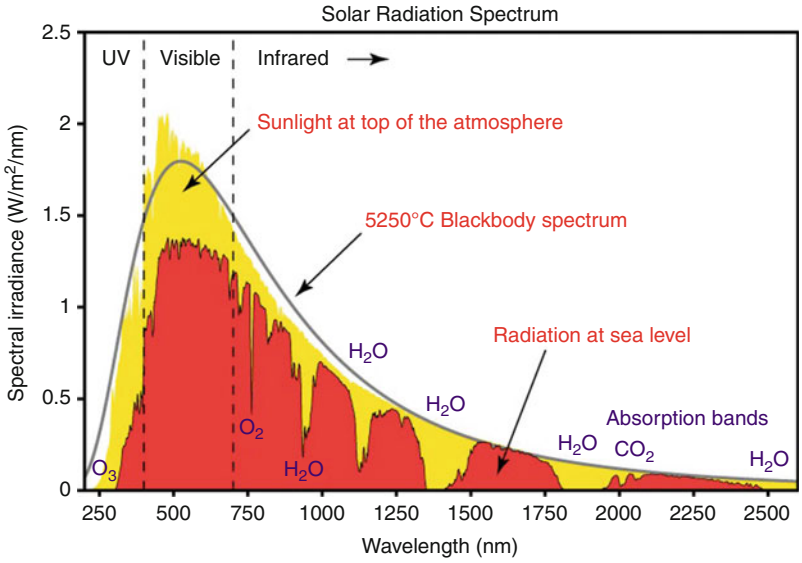

Sun (and Young Sun), Fig. 3 Solar irradiance spectrum for the ultraviolet, optical, and infrared part of the electromagnetic spectrum, both at the *top* of the Earth's atmosphere (*yellow*) and at sea level after propagation through the atmosphere (*red*) (Credit: Robert A. Rohde/ Global Warming Art project)

freely escape. This layer is only a few 100 km thick and separates the solar interior from the outer atmosphere. Its spectrum can be approximated by a blackbody spectrum corresponding to a temperature of about 5,770 K. This spectrum defines most of the solar irradiance (Fig. 3), although important contributions are added at short wavelengths as a consequence of magnetic activity.

The photosphere reflects the underlying convective motions at several scales, showing granulation structure on length scales of 100–1,000 km, mesogranulation on scales of 5,000–10,000 km, and supergranulation on scales of about 15,000–20,000 km. In individual granules, hot, subphotospheric gas flows up in the center, radiates and cools, and then flows down in the intergranular lanes. In the latter places, bright points related to magnetic flux tubes are concentrated. Concentrations of magnetic flux tubes at the supergranulation boundary form a magnetic network visible also in the overlying chromosphere.

The photosphere hosts the remarkable sunspots. These are regions in which strongly bundled, vertical magnetic fields with a field strength of about 0.2–0.3 T suppress convection and therefore impede the energy flow from below; their temperature is therefore lower, reaching typical values of 4,500 K. The sunspot core region, the umbra, is surrounded by the radially structured penumbra, which is permeated by inclined magnetic fields, and spot groups may further be surrounded by larger areas containing strong, vertical magnetic flux tubes appearing brighter than the surrounding photosphere. These latter regions, the faculae, make up for the deficit of radiation from the sunspots, such that the net brightness at times of large sunspot coverage is slightly higher than at times of small coverage; the "solar constant" therefore cyclically varies by a small amount in concert with the solar spot cycle (see below), being higher by about 0.1 % during the spot or activity maximum.

Spots appear in pairs with opposite magnetic polarity. The polarity of the spot leading in heliographic longitude is constant for one (north or south) hemisphere for a given 11-year sunspot cycle, which is an important observation that has helped formulate a dynamo theory for the Sun.

Magnetic flux tubes are also present in regions outside sunspots. Such magnetic flux elements are concentrated in intergranular lanes, where magnetic flux concentrations with kilogauss field strengths and sizes of less than 100 km are inferred. Despite their small size, their large number contributes significantly to the total solar magnetic flux.

The Solar Chromosphere

The chromosphere is a "layer" of tenuous gas above the photosphere, ranging in temperature from the temperature minimum at the top of the photosphere to about 20,000 K where it merges with the chromosphere-corona transition region. In modern concepts, the chromosphere is a complex mixture of cool and hot magnetically structured inhomogeneities subject to many forms of variability (flares, explosive events, flows, prominences, etc.). It is on average only about 2,000 km thick, but is a source of important ultraviolet emission, in particular in prominent line transitions such as Balmer lines and lines of Ca II and He I (using the standard astronomical notation of I for neutral atom, II for once ionized, etc.). Larger heights (of order 10,000 km) are reached by the jetlike hot spicules rising into the lower corona with velocities of a few tens of kilometers per second.

The chromosphere forms a dynamic network corresponding to the photospheric supergranule cells. Nearly vertical magnetic fields emerging from the photosphere in these regions rapidly fan out, forming a canopy in the upper chromosphere that seems to overlay cool, weak-field, CO-rich gas in the lower chromosphere. The canopy region itself is the anchorage region of the overlying coronal loops. The chromosphere is particularly well expressed in magnetic active regions. Around sunspots, the chromosphere is bright, defining the chromospheric plage (a continuation of the photospheric faculae). The heating of the chromospheric gas is not yet fully understood, but may involve dissipation of acoustic waves in shocks, magnetodynamic waves, or magnetic reconnection (e.g., in bright points).

Extensions of chromospheric material into the corona are seen in many large-scale filaments or prominences made of cool gas suspended by magnetic fields at coronal heights. They may reside there for weeks or months, but may also be activated and ejected, accompanied by flares or coronal mass ejections.

The Solar Transition Region

The temperature rises very rapidly above the chromosphere on length scales of only a few hundred kilometers, from 2×10^4 to 10^6 K. This chromosphere-corona transition region (TR) is a very inhomogeneous and dynamic layer, featuring flows (mostly downflows with velocities of up to 20 km s^{-1}), flares, and short explosive events involving velocities of 100 km s^{-1}; many of these processes connect to the overlying, strongly variable corona. Various physical parameters change fundamentally across the TR; helium changes from the partially ionized (below) to the fully ionized state (above), dramatically reducing the radiative losses and producing a rapid jump of the temperature to the adjacent corona. Below the TR, the plasma thermal pressure dominates plasma motion, dragging magnetic fields with it, while above the TR, the magnetic pressure dominates, such that plasma is dragged by the magnetic fields. Much of the TR is structured in magnetic loops connecting footpoints of different polarity. The TR can best be observed in emission lines at wavelengths below 200 nm (e.g., He II, C IV, O VI).

The Solar Corona

The outermost and hottest region of the solar atmosphere is the magnetically structured corona. Although the corona is well known from solar eclipses when photospheric light scattered by free electrons and dust reveals its large-scale magnetic structure, it is really a phenomenon rooted in high-energy processes in the tenuous, extended magnetic fields that are anchored in the photosphere. The corona is best observed in the extreme ultraviolet (EUV) and X-ray ranges where the hot plasma confined by closed magnetic fields emits most of its radiation or in the radio range where high-energy, accelerated electrons emit various kinds of radiation such as gyrosynchrotron radiation and a plethora of coherent radiation types. The solar coronal temperature of a few million degrees has defined one of the most persistent riddles in astronomy: among the favored theoretical concepts to explain coronal heating figures magnetic reconnection in flares, in particular also in the large number of microflares or nanoflares occurring ubiquitously across the corona.

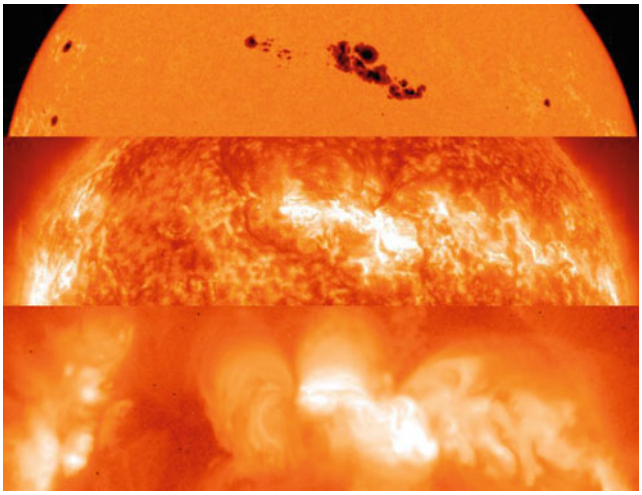

Sun (and Young Sun), Fig. 4 Three images of the solar atmosphere taken at the same time but in different wavelength regions. The *top panel* shows an optical image featuring sunspots surrounded by bright faculae. The *middle panel* was recorded in the extreme ultraviolet range showing the solar transition region. The *bottom panel* records the solar corona in X-rays (Credit: SOHO – MDI/EIT Consortia [SOHO is a project of international cooperation between ESA and NASA], Yohkoh/SXT Project [Yohkoh was a Japanese ISAS/JAXA mission, collaborating with NASA/US and PPARC/STFC/UK; its scientific operation was conducted by the international science team organized in ISAS])

The coronal magnetic fields structure the plasma into large active regions overlying magnetic sunspot groups (Fig. 4); such volumes are filled with coronal loops with both footpoint regions anchored in the chromosphere. They range from small bright points, probably simple magnetic loops above the chromospheric layer, to large-scale arcades connecting regions of opposite polarity on the solar surface. Coronal streamers may be attached to these structures, pointing outward into the solar wind region to distances of order one solar radius (Figs. 1 and 5).

Coronal active regions display a high level of variability, including flares, mass flows, and coronal mass ejections. Intermittent heating, changing magnetic connectivity in reconnection events, and magnetic instabilities define the corona as an extremely dynamic region. Various types of oscillations of magnetic coronal loops have been measured with periods in the range of seconds to minutes; propagating magnetohydrodynamic waves have been detected in the EUV range, including global waves expanding from strong flare sites.

Large volumes of the corona are not directly connected to the underlying photospheric and chromospheric active regions, but they reveal similar magnetically closed structures such as transequatorial loops or X-ray bright points and similar dynamic phenomena as in active regions, such as magnetic reconnection, mass flows, and nanoflares. These regions have traditionally been called "quiet-Sun regions" although absence of variability and dynamic phenomena are no longer implied by this term.

A physically distinct type of coronal feature emerges in regions dominated by nearly radial, "open" magnetic fields; these "coronal holes" contribute importantly to the fast solar wind but appear as very dim regions in X-ray or EUV images, as a consequence of their low densities. Prominent coronal holes are often seen in the polar regions of the Sun.

Solar Rotation, the Solar Magnetic Dynamo, and Magnetic Cycles

The Sun's rotation period, P, is a function of depth and latitude. The surface rotation period varies between about 25 days at the equator and

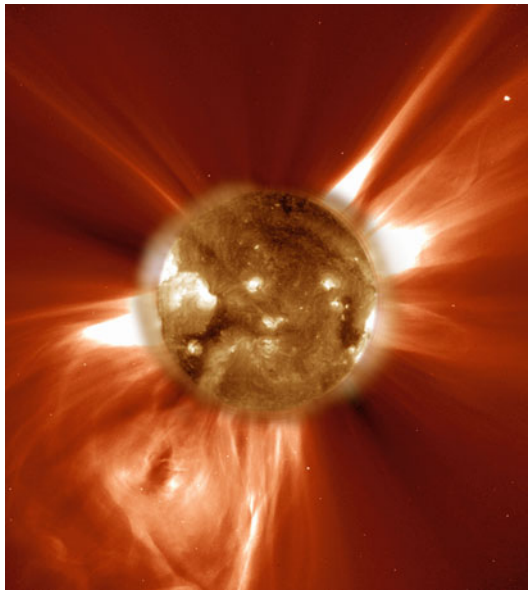

Sun (and Young Sun), Fig. 5 A coronal mass ejection (*lower left*) seen by the LASCO (Large Angle and Spectrometric Coronagraph Experiment) instrument on the SOHO satellite. Several coronal streamers (e.g., *upper right*) can also be seen. The solar disk was recorded by the EIT (Extreme ultraviolet Imaging Telescope) instrument and shows hot coronal structures (Credit: SOHO/EIT and LASCO Consortia; SOHO is a mission of international cooperation between ESA and NASA)

about 36 days near the poles, characterizing solar differential rotation. Throughout the convective zone, the rotation period determined using helioseismology methods depends on latitude in a similar way as on the surface. In contrast, the core shows approximately solid-body rotation.

The interaction between differential rotation and convection generates an internal dynamo at the base of the convection zone, in the so-called tachocline where the rapid change in rotation together with convection is held responsible for the amplification of magnetic fields. The shearing differential rotation generates toroidal fields from poloidal fields. These fields eventually rise buoyantly to the surface in the form of magnetic flux tubes; there, they become evident in a plethora of features related to magnetic activity such as bipolar sunspots and coronal magnetic loops.

There is as of yet no complete theory that explains all features of the solar magnetic dynamo. At the beginning of a magnetic cycle, spots appear at relatively high heliographic latitudes (about 35° on both hemispheres), but the regions of spot emergence slowly migrate toward the equator in the course of the 11-year sunspot cycle. A new spot cycle starts when new field concentrations appear at high latitudes. Their polarity (leading vs. trailing spot) is reversed for a given hemisphere during the new cycle, thus defining the 22-year magnetic (or Hale) cycle of the Sun.

Spot and magnetic cycles are not only evident in sunspots but can be monitored in essentially all tracers of magnetic activity, including coronal X-ray emission, the rate of flares, prominences, mass ejections, or the structure of the solar wind. The same features are used as diagnostics of solar magnetic activity, that is, the complex interplay between magnetic fields that leads to time-variable energy release, heating, acceleration, and mass motions.

Active Regions, Flares, and Coronal Mass Ejections

Active regions on the Sun are areas of enhanced magnetic flux, that is, regions where magnetic flux tubes break through the photosphere from the interior, in pairs of opposite polarity. Active regions can therefore be traced throughout all layers of the solar atmosphere, showing up, in larger examples, as sunspot groups and faculae in the photosphere, spots and chromospheric plages at chromospheric levels, and large magnetic loop systems at transition region and coronal heights. These regions are particularly prone to instabilities leading to large-scale magnetic energy release and reconnection in flares and coronal mass ejections.

Observationally, solar flares express themselves as sudden increases in electromagnetic radiation, localized in solar active regions or coronal loops in which obviously a large amount of energy is liberated following some instability. Flares may last from minutes to several hours. Flares are currently considered to be a consequence of magnetic reconnection in non-potential (mostly coronal) magnetic fields. Non-potential fields emerge in the corona as a result of convective motions of the

photospheric/chromospheric footpoints of magnetic loops. Increasingly stressed fields occasionally adjust by changing their topology, settling in a lower-energy state by liberating energy from the non-potential field. This large-scale reconnection process is induced by field annihilation once antiparallel field components (e.g., from different coronal loops) are pushed together in the corona. In the course of this process, particles are accelerated to high energies, plasma can be heated locally, and plasma jets can be ejected. Initially "open" magnetic fields may reconnect in such a way as to produce systems of closed magnetic loops, while overlying magnetic regions may "detach" and be ejected from the corona, escaping into the interplanetary space as "coronal mass ejections" (CMEs; Fig. 5), accompanied by an erupting prominence.

The size of CMEs may rapidly evolve to the order of a solar radius while they escape with a speed of 10^2–10^3 km s^{-1}. At 1 AU, a CME evolves to a typical size of 0.2 AU. It may carry of order 10^{15}–10^{16} g of material into the solar wind.

The relation between CMEs and classical flares is still a matter of debate as there is no one-to-one correlation between these expressions of magnetic energy release. Flares and coronal mass ejections may simply be two observational manifestations of large-scale coronal magnetic energy release by the reconnection process.

A large fraction of the released flare energy appears in the form of kinetic energy of highly accelerated electrons and ions. As they propagate along magnetic fields, they eventually encounter denser TR and chromospheric gas layers where they collide. The collisions result in nonthermal hard X-ray and gamma-ray radiation during the first minutes of a flare event, also known as the impulsive phase. The bulk part of the particle energy is, however, deposited as thermal energy in the chromospheric plasma, signatures of which are strong ultraviolet and optical enhancements in the magnetic footpoint regions. Electron temperatures up to about 20 million degrees are reached in the collision zone, which, as a consequence of the corresponding pressure increase, expands upward along the closed magnetic-field lines to fill coronal loops (chromospheric evaporation). This is the gradual phase of the flare when strong X-ray emission from coronal loops dominates the radiative losses. Various kinds of radio emission from the accelerated electrons (e.g., gyrosynchrotron emission from electrons spiraling around magnetic fields) or electron populations with non-Maxwellian velocity distributions can be monitored during large portions of a solar flare. Radio emission is, together with hard X-rays and gamma rays, an ideal tracer of the energy release and particle acceleration processes. Similarly, radiation in Balmer lines from chromospheric heights is prominent during extended periods of a flare. Flares are also the source of high-energy particles (protons, electrons, ions) ejected from the Sun and traveling in interplanetary space. Chromospheric filaments or prominences can be activated and ejected in the course of a flare or a coronal mass ejection.

Flares may be important contributors to the coronal heating process because they occur stochastically and in large numbers at many places in the solar corona. The distribution of their occurrence rate as a function of released energy shows a dramatic increase toward low-energy (small) events. The cumulative energy of such "micro-" or "nano-" flares could be sufficient to heat the entire coronal gas, although current debate has not converged to a clear answer.

Flares and mass ejections lead to significant interactions with planetary environments. Flare X-ray radiation increases the ionization of upper planetary atmospheres dramatically. When CMEs reach the Earth, they may interact globally with the magnetosphere and induce geomagnetic storms. Together with the solar wind, they interact with the higher atmosphere, carrying away ions and neutrals and thus contributing to atmospheric erosion.

Solar Wind

The Sun continuously loses mass in an approximately radially expanding solar wind. It consists of hot ($\approx 10^5$–10^6 K) plasma. The wind is permeated and structured by magnetic fields originating in the solar photosphere and also by shocks, waves, and turbulence. It is therefore a highly

variable structure filling the interplanetary space and interacting with planetary magnetospheres and atmospheres, leading to the removal of atoms and ions in the higher atmospheres and therefore to planetary erosion. High-energy particles (from the Sun, planetary bow shocks, and cosmic rays) and coronal mass ejections are also occasionally immersed in the solar wind.

The solar wind is a consequence of the high coronal temperatures close to the Sun, leading to coronal expansion rather than a hydrostatic structure. The processes of wind heating and acceleration are, however, still poorly understood and may involve wave dissipation and magnetic reconnection. The present-day average mass loss of the Sun in the magnetized wind is approximately 2×10^{-14} $M_\odot$ year^{-1}. The wind flow varies locally depending on whether it originates in magnetic streamer regions above the magnetically closed coronal active regions, leading to the slow wind with velocities of 300–500 km s^{-1}, or in open-field coronal holes, leading to the fast wind with velocities of approximately 600–800 km s^{-1}. This structure is further modulated by the solar activity cycle.

The volume filled by the solar wind defines the heliosphere. At distances beyond 90 AU, the solar wind collides with the interstellar medium, forming a termination shock, a heliopause, and the bow shock beyond which the undisturbed interstellar gas is encountered. Because the Sun moves relative to the interstellar plasma, the heliosphere is compressed in the direction of solar motion and elongated in the opposite direction.

The Sun in Time

The past magnetic evolution of the Sun is studied using solar analogs with different ages and therefore activity levels. For stars with masses $\leq$1.5 $M_\odot$ and ages of at least a few hundred million years, angular momentum loss by a stellar wind brakes rotation in such a way that rotation becomes nearly uniquely determined by the stellar age. Age thus becomes the only independent variable on which the rotation period and, through the internal magnetic dynamo, magnetic activity at all levels of the stellar atmosphere depend, probably also including characteristics of the stellar wind. Studying a sample of near-solar-mass stars with known ages back to stages close to the zero-age main sequence (ZAMS), age is, therefore, sufficient to approximately reconstruct the history of our Sun and the interaction of its magnetic activity with its environment.

The Evolution of the Solar Wind

Stellar equivalents of the solar wind have not yet been detected; judged from the presence of coronae in all main-sequence solar analogs, coronal winds are undoubtedly present in these stars as well. The evolutionary spin down of cool stars like the Sun is in fact the best – albeit indirect – proof of the presence of ionized, magnetized winds because such winds carry away angular momentum from the star.

Ionized ▶ stellar winds are, in principle, sources of thermal bremsstrahlung in the radio regime, but the emission is too weak to be detected even in the nearest stars with current technology. A presently more promising approach makes use of Lyman-alpha (Lyα) absorption in the so-called astrospheres, stellar analogs to the solar heliosphere. The astrospheres are permeated by neutral hydrogen with T $\approx$ (2–4) $\times$ 10^4 K. Much of this gas is piled up between the "heliopause" and the bow shock, forming a "hydrogen wall" that can be detected through excess absorption of the Lyα line. The measured absorption depths are then compared with results from hydrodynamic model calculations. It is found that the astrospheric absorption should scale with the wind ram pressure, which itself scales with the mass-loss rate assuming that the wind velocity is constant. A systematic observational study shows that dM_w/dt correlates with the stellar X-ray luminosity (L_X) and with stellar age (t),

$$dM_w/dt \propto L_X^{1.34\pm0.18}$$

and equivalently,

$$dM_w/dt \propto t^{-2.33\pm0.55}$$

The stellar-wind mass loss can therefore – in principle – be used as a genuine activity indicator. The mass loss is thus expected to be higher in young, magnetically active stars. Extrapolating the above law up to stars at the saturation limit (with an average surface magnetic flux of 2×10^6 erg cm^{-2} s^{-1}) suggests dM_{w}/dt of the youngest solar analogs to be about a thousand times higher than the present-day solar mass loss (dM_{w}/dt $\approx 2 \times 10^{-14}$ $M_\odot$ year^{-1}). The above power-law relations appear to break down for the most active stars, however. While intermediately active stars may reach mass-loss rates two orders of magnitude higher than the Sun, the most active, youngest main-sequence stars suggest loss rates no more than about ten times the present solar value. The cause for this breakdown has not been identified but could be related to the appearance of high-latitude active regions (spots) in the most active stars; if the magnetic field becomes more akin to a global dipole, then wind escape may be inhibited in such stars.

The Rotation Rate of the Young Sun

Because the magnetized stellar winds transport angular momentum away from the star, a solar analog spins down with age. The rate of change of angular momentum is related to the mass-loss rate, the rotation rate, and the Alfvén radius. For solar analogs, the rotation period is

$$P = 0.21 t_6^{0.57} [\mathrm{d}]$$

where t_6 is the age in Myr after arrival on the ZAMS and d means day. This equation implies an increase in rotation period from ZAMS age to the end of the main-sequence life by a factor of about 20.

For solar analog stars with ages of less than a few hundred million years, the ▶ stellar rotation period is not a function of age but of the pre-main-sequence history, especially the history of circumstellar-disk dispersal. Once the inner disk disappears, the lack of magnetic locking via star-disk magnetic fields and the contraction of the star toward the main sequence will spin up the star and thus determine the initial rotation period on the ZAMS. After arrival on the main sequence, the angular momentum loss in a wind will decrease the magnetic activity and presumably also the wind mass loss itself; therefore, the rotation period will eventually converge to a value that is only a function of age, as specified above.

The Evolution of the Solar Magnetic Field

Polarization measurements of the integral light from solar analog stars have provided important information on the average field strength of magnetic areas on the star, including corresponding surface filling factors. Doppler imaging methods have further deepened our understanding of the size, distribution, location, and evolution of stellar magnetic fields.

Whereas maximum magnetic-field strengths in younger solar analogs are similar to the present-day Sun, the filling factors of magnetic active regions are much higher; spot coverage of order 10 % is common and testifies to much increased magnetic activity in the young Sun. This obviously relates to an enhanced dynamo as a result of the increased rotation rate of young solar analogs.

Although surface spot distributions vary significantly between young solar analogs, most stars show evidence of high-latitude magnetic activity and the presence of polar spots. The origin of polar magnetic activity has been related to strong Coriolis forces acting on magnetic flux bundles that rise from the dynamo region of the star. This force would deflect rising flux to higher altitudes. Alternative models use magnetic bipoles (structures with two footpoints of opposite polarities) injected at various heliocentric latitudes and migrating along meridional flows. A high injection rate of interacting bipoles leads to the formation of nested polar rings of opposite polarity.

The Evolution of Solar Activity and High-Energy Radiation

Stellar evolution calculations indicate that the young, zero-age main-sequence Sun was bolometrically about 30 % *fainter* than at present.

This trend is related to the fact that hydrogen is slowly being converted into helium in its core, raising the density and causing corresponding increases in temperature and the rate of nuclear fusion.

This slow, evolutionary increase in optical luminosity of the Sun contrasts sharply with all radiation that is related to magnetic activity. Meteoritic evidence indicates that the Sun was magnetically much more active in its youth than at present. This direct evidence is fundamentally supported by observations of young solar analogs that show systematically higher levels of magnetic activity and related electromagnetic radiation.

The cause of this steady decline of magnetic activity during the main-sequence evolution is, as already mentioned above, the declining dynamo as a star spins down by losing angular momentum through its magnetized wind. Because magnetic activity is particularly important for the generation of short-wavelength radiation (ultraviolet emission from the chromosphere and the TR; EUV and X-rays from the TR and the corona), this part of the spectrum shows particularly strong evolutionary trends; the short-wavelength input into planetary atmospheres thus diminished significantly with time.

The young Sun showed stronger rotationally induced modulation in the optical light due to surface magnetic spots but also due to magnetic activity cycles that induced light variations up to 0.3 magnitudes in the course of spot cycles; such cycles have been found in solar-like stars, with cycle periods ranging from 2 to 13 years. The presence of excess emission from photospheric faculae outweighs the darkening by the spot area in old solar analogs, making these stars slightly brighter in optical light during activity maxima, while in young stars, spots dominate and make them fainter. Cycles are not present in all solar-like stars, however, and irregular variations abound among very active examples.

The increased magnetic activity in younger solar analogs enhances ultraviolet emission from transition regions by factors of a few, in particular in emission lines forming at temperatures around 10^5 K. Much more dramatic changes must have occurred in the evolution of the shorter-wavelength radiation from the solar corona (Fig. 6). Studies of solar analogs with ages of tens to about hundred million years in

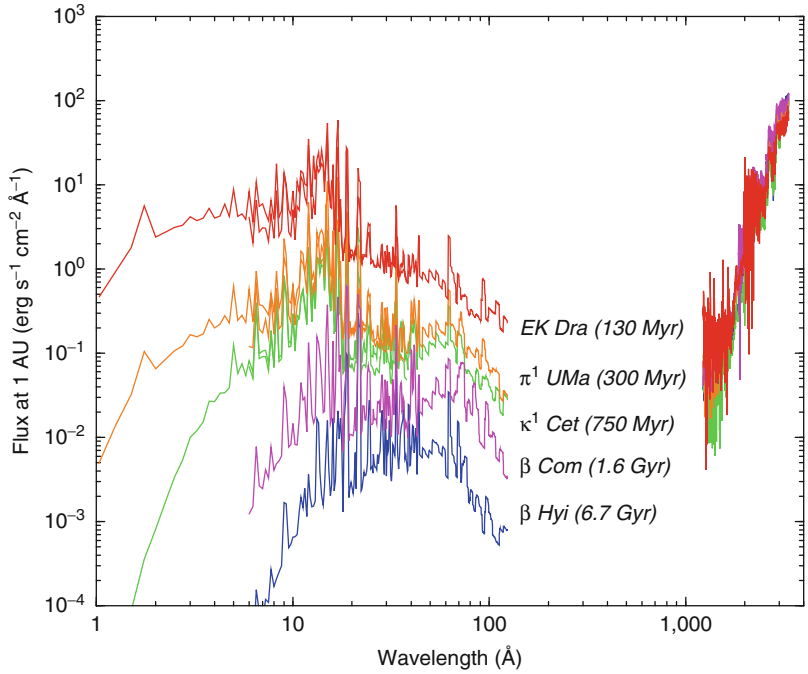

Sun (and Young Sun), Fig. 6 Solar irradiance in the ultraviolet, extreme ultraviolet, and X-ray ranges for various ages of the Sun as derived from observations of solar analogs. The irradiance refers to a distance of 1 AU from the Sun in the absence of a planetary atmosphere. Stellar names and ages are given in the middle of the figure (where radiation is absorbed by the interstellar gas) (Reproduced by permission of ASP)

young stellar clusters and in the field indicate X-ray and EUV luminosities exceeding the present-day solar output by several hundred to approximately thousand times. The same is true for stars in the younger, pre-main-sequence T-Tauri phase.

This enhanced radiation is a consequence of higher-density coronal plasma combined with a much larger filling factor of magnetic active regions. Also, the characteristic temperature of young coronae is higher, reaching average levels of 10–20 million K (Sun: 2 million K), and therefore the X-ray emission is much harder than X-rays from the present-day solar corona. How the corona can be kept three orders of magnitude more energetic and ten times hotter than the present-day solar corona is unclear; an interesting possibility is excess heating by a high rate of flares. Such "continuously flaring coronae" may be important as they also produce appreciable levels of gamma rays and high-energy particles that interact with planetary atmospheres.

The decaying trends of the short-wavelength radiation are well fitted by power laws that become *steeper toward shorter wavelengths*, as summarized in Table 2. A power-law decay law has been assumed for the rotation rate with age t, $\Omega \propto t^{-0.6\pm0.1}$. Table 3 provides numerical estimates for the solar spectral irradiance at various ages.

X-ray radiation thus suffered by far the strongest reduction (by three orders of magnitude) in the course of the Sun's history, initially achieving as much as 0.1 % of the bolometric output or (2–4) $\times$ 10^{30} erg s^{-1}. The trends are graphically illustrated in Fig. 7.

Applications

At its ZAMS stage, the Sun's luminosity was only 70 % of its present-day level. In the absence of an atmosphere, the Earth's surface equilibrium temperature would then have amounted to 255 K. Assuming an albedo and an atmospheric composition equal to values of the present-day Earth, the

Sun (and Young Sun), Table 2 Long-term trends of short-wavelength solar radiation

Radiation type	Symbol	Relation with rotation	Relation with age
UV line radiation from chromosphere	L (chrom)	$\propto P^{-1.25\pm0.15}$	$\propto t^{-0.75\pm0.1}$
UV line radiation from transition region	L(TR, UV)	$\propto P^{-1.6\pm0.15}$	$\propto t^{-1.0\pm0.1}$
FUV from transition region (920–1,180 Å)	L(TR, FUV)	$\propto P^{-1.4}$	$\propto t^{-0.85}$
EUV/X-rays from corona (20–360 Å)	L (EUV)	$\propto P^{-2.0}$	$\propto t^{-1.2}$
X-rays from corona (1–20 Å)	L_X	$\propto P^{-3.2}$	$\propto t^{-1.9}$

Sun (and Young Sun), Table 3 Enhancement factors of solar irradiance in solar history[a]

Solar age (Gyr)	Time before present (Gyr)	X-rays (1–20 Å)	Enhancement in soft X-rays (20–100 Å) / EUV (100–360 Å) / XUV (1–1,180 Å)	FUV (920–1,180 Å)	UV lines, transition region	UV lines, chromosphere
0.1	4.5	1,600[b]	100	25	50	18
0.2	4.4	400	50	14	20	10
0.7	3.9	40	10	5	7	4
1.1	3.5	15	6	3	4	3
1.9	2.7	5	3	2	2.4	2
2.6	2.0	3	2	1.6	1.8	1.5
3.2	1.4	2	1.5	1.4	1.4	1.3
4.6	0	1	1	1	1	1

[a]Normalized to zero-age main-sequence age of 4.6 Gyr before present (Table adapted from Güdel 2007)
[b]Large scatter possible due to unknown initial rotation period of the Sun

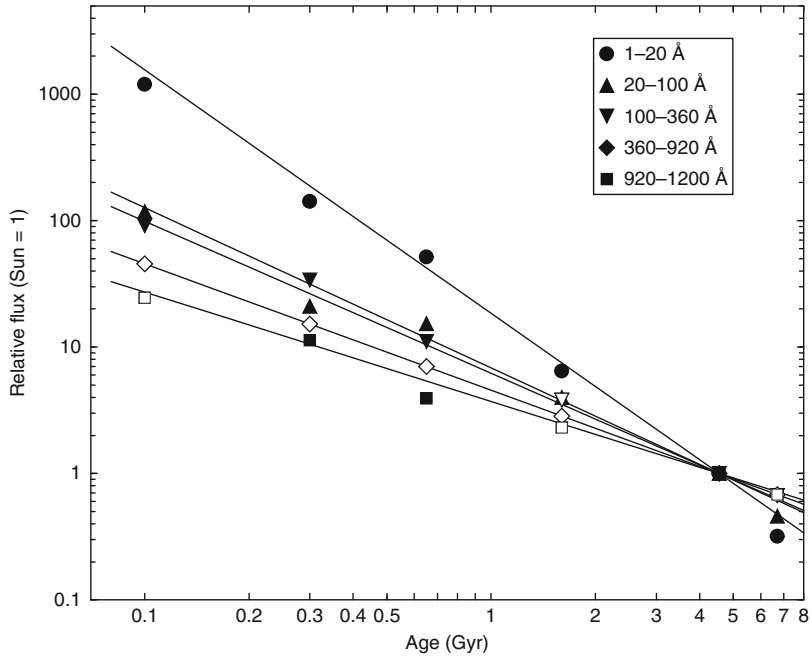

Sun (and Young Sun), Fig. 7 Decay of the irradiance in time for a solar analog for different spectral bands, normalized to the present-day levels. The decay is steepest for the shortest wavelengths (Reproduced by permission of the AAS)

mean surface temperature would have been below the freezing point of seawater until ≈2 Gyr ago. The increase of the surface temperature in the presence of an atmosphere is due to the greenhouse effect. The present-day atmosphere of the Earth raises the surface temperature by only 33 K compared to the atmosphere-free equilibrium value. Evidence for a mild early climate both on the Earth and Mars (the ► Faint Young Sun Paradox, FYSP) either requires substantially more effective greenhouse mechanisms from the presence of larger amounts of, for example, CO_2 or methane or a lower albedo (see ► Faint Young Sun Paradox).

Increased wind mass-loss rates may solve the FYSP as well. The Sun itself may have been more luminous in its past, which would imply that it had a higher mass by a few percent, having lost the extra mass by the solar wind and CMEs. However, estimates of the total wind mass loss seem to be insufficient to support this model (see ► Faint Young Sun Paradox).

The ionized and magnetized solar wind interacts strongly with planetary magnetospheres and atmospheres. Wind-planet interactions have played an important role in the formation and evolution of planetary atmospheres and consequently the formation of life on Earth. Irradiation of upper atmospheric layers by high-energy (EUV, X-ray) photons leads to atmospheric heating in the thermosphere and eventually to thermal escape from the exosphere above the thermosphere. In the exosphere, the mean free path of the particles is large; particles, in particular hydrogen atoms, with thermal energies exceeding the gravitational binding energy escape into space (Jeans escape). If in the upper atmosphere the mean particle energy exceeds the gravitational binding energy ($kT > mv_{esc}^2/2$, where v_{esc} is the escape velocity), then the exosphere becomes unstable and escapes ("blows off") into space.

Evaporation played an important role in early Venus. If surface water was initially present in large quantities, it would have evaporated due to a more efficient greenhouse (Ingersoll 1969; Kasting 1988) and subsequently dissociated in the high atmosphere due to strong solar EUV irradiation (Kasting and Pollack 1983) after which hydrogen atoms escaped to space. Hydrodynamic escape conditions for hydrogen applied as long as 250 Myr after the Sun's arrival on the

main sequence; a terrestrial water ocean could have escaped in as little as 50 Myr from Venus (Kulikov et al. 2007).

For the young Mars, there is clear evidence for a warmer climate and liquid surface water. Evidently, a strong greenhouse would be required, but its origin is debated (Chassefière and Leblanc 2004). Hydrodynamic escape conditions may have applied to Mars during the first few hundred million years for hydrogen (Kulikov et al. 2007) and possibly for heavier gases such as C, N, and O as well (Tian et al. 2009).

Atmospheric escape is also driven by the interaction of high-energy (nonthermal) particles and the solar wind; here, the escape process is related to microscopic, nonthermal mechanisms, in particular dissociative recombination or photochemical escape (in which the forming neutrals are energetic), ion pickup (in which ions produced by photons or particle irradiations are dragged along by magnetic fields), ionospheric outflow, and ion sputtering (in which newly produced atmospheric ions re-impact and eject neutral particles; see, e.g., Chassefière and Leblanc 2004; Kulikov et al. 2007; Lundin et al. 2007). These processes are thought to have fundamentally altered the atmospheres of Venus, Earth, and Mars, leading to strong loss of oxygen (Lammer et al. 2006) and therefore water after its photodissociation in the upper atmosphere. The amount of shielding depends on the strength of the wind and its ability to compress the magnetosphere. A strong magnetosphere around the Earth, shielding the lower atmospheric layers, may have been instrumental in retaining much of its water and making it habitable.

In the case of the young Venus, oxygen could have been lost from the atmosphere as a consequence of ion pickup by the solar wind in a matter of tens of million years (Lammer et al. 2006; Chassefière 1997), but a very strong solar wind – perhaps stronger than inferred indirectly for the young Sun – would have been required. A similar process as well as sputtering may have applied to the young atmosphere of Mars. But for Mars, the lack of a magnetic shield already early on in its evolution further strengthened interactions between the strong solar wind and the upper atmosphere, and escape processes were additionally enhanced by the weak gravitational potential of Mars. Some calculations indicate that a global Martian ocean of 12–15-m depth may have been lost as a consequence of such processes (Lammer et al. 2003; Chassefière and Leblanc 2004).

Coronal mass ejections (CME) add significantly to atmospheric erosion. An ejection rate of several CMEs per day acts like an enhanced solar wind and will therefore further compress planetary magnetospheres and erode the upper atmospheres (Khodachenko et al. 2007), especially in combination with enhanced exospheric heating by EUV irradiation and its consequent exospheric expansion (Lammer et al. 2007).

The future Sun will continue to affect planetary atmospheres and therefore habitability significantly, albeit in a progressively different way. As the solar bolometric output will gradually increase during the next 5 Gyr, the surface temperatures of the planets will increase. For the Earth, an increase by 60–70 K was predicted (Sagan and Mullen 1972). Beyond that phase, Sun-planet interactions will start changing fundamentally as the Sun will develop toward its giant phase. Then, it will expand considerably although its surface temperature will drop; at the same time, a strong solar wind mass loss will set in, but at that time the habitable phase of the Earth will be long gone. Eventually, a planetary nebula will be ejected from the Sun, expanding across the solar system and beyond.

Future Directions

Solar physics is an extremely rich field, involving the study of the solar interior, magnetic-field generation in a dynamo, plasma physical processes in the outer atmosphere, and various processes of particle acceleration and heating. Some of the most pressing issues in solar physics and related stellar astronomy are listed below:

- The precise solar composition in terms of chemical elements, which is of fundamental importance to test the standard model of the solar interior

- A comprehensive theory of solar magnetic-field generation in the internal dynamo
- The problem(s) of chromospheric and coronal heating by waves and/or magnetic processes, possibly involving microflares and nanoflares
- The acceleration and heating of the solar wind
- Direct detection of ionized stellar winds based on radio emission
- Improved modeling of interactions between the solar wind or solar radiation and young planetary atmospheres

See Also

- ▶ Asteroseismology
- ▶ Chronological History of Life on Earth
- ▶ Faint Young Sun Paradox
- ▶ Mass-Luminosity Relation
- ▶ Solar Constant
- ▶ Solar Luminosity
- ▶ Solar Particle Events
- ▶ Solar UV Radiation, Biological Effects
- ▶ Space Environment
- ▶ Stellar Evolution
- ▶ Stellar Rotation
- ▶ Stellar Winds
- ▶ Zero Age Main Sequence

References and Further Reading

Aschwanden MJ (2005) The solar corona. An introduction. Praxis/Springer, Chichester/New York

Chassefière E (1997) Loss of water on the young Venus: the effect of a strong primitive solar wind. Icarus 126:229–232

Chassefière E, Leblanc F (2004) Mars atmospheric escape and evolution; interaction with the solar wind. Planet Space Sci 52:1039–1058

Dorren JD, Guinan EF (1994) HD 129333: the Sun in its infancy. Astrophys J 428:805–818

Güdel M (2007) The Sun in time: activity and environment. Living Rev Sol Phys 4(3). http://solarphysics.livingreviews.org/Articles/lrsp-2007-3/

Ingersoll AP (1969) The runaway greenhouse: a history of water on Venus. J Atmos Sci 26:1191–1198

Kasting JF (1988) Runaway and moist greenhouse atmospheres and the evolution of earth and Venus. Icarus 74:472–494

Kasting JF, Pollack JB (1983) Loss of water from Venus. I – hydrodynamic escape of hydrogen. Icarus 53:479–508

Khodachenko ML, Ribas I, Lammer H, Grießmeier J-M, Leitner M et al (2007) Coronal mass ejection (CME) activity of low mass m stars as an important factor for the habitability of terrestrial exoplanets. I. CME impact on expected magnetospheres of Earth-like exoplanets in close-in habitable zones. Astrobiology 7:167–184

Kulikov YN, Lammer H, Lichtenegger HIM, Penz T, Breuer D, Spohn T, Lundin R, Biernat HK (2007) A comparative study of the influence of the active young Sun on the early atmospheres of Earth, Venus, and Mars. Space Sci Rev 129:207–243

Lammer H, Lichtenegger HIM, Kolb C, Ribas I, Guinan EF, Abart R, Bauer SJ (2003) Loss of water from Mars: implications for the oxidation of the soil. Icarus 165:9–25

Lammer H, Lichtenegger HIM, Biernat HK, Erkaev NV, Arshukova IL et al (2006) Loss of hydrogen and oxygen from the upper atmosphere of Venus. Planet Space Sci 54:1445–1456

Lammer H, Lichtenegger HIM, Kulikov YN, Grießmeier J-M, Terada N et al (2007) Coronal mass ejection (CME) activity of low mass m stars as an important factor for the habitability of terrestrial exoplanets. II. CME-Induced ion pick up of Earth-like exoplanets in close-in habitable zones. Astrobiology 7:185–207

Lundin R, Lammer H, Ribas I (2007) Planetary magnetic fields and solar forcing: implications for atmospheric evolution. Space Sci Rev 129:245–278

Murdin P (ed) (2001) Encyclopedia of astronomy and astrophysics. Institute of Physics, Bristol

Reiners A (2012) Observations of cool-star magnetic fields. Liv Rev Solar Phys 9(1). http://www.livingreviews.org/lrsp-2012-1

Ribas I, Guinan EF, Güdel M, Audard M (2005) Evolution of the solar activity over time and effects on planetary atmospheres. I. High-energy irradiances (1–1700Å). Astrophys J 622:680–694

Sagan C, Mullen G (1972) Earth and Mars: evolution of atmospheres and surface temperatures. Science 177:52–56

Schrijver CJ, Title AM (2001) On the formation of polar spots in Sun-like stars. Astrophys J 551:1099–1106

Schrijver CJ, Zwaan C (2000) Solar and stellar magnetic activity. Cambridge University Press, New York

Solanki SK (2003) Sunspots: an overview. Astron Astrophys Rev 11:153–286

Sonett CP, Giampapa MS, Matthews MS (eds) (1991) The Sun in time. University of Arizona Press, Tucson

Stix M (2004) The Sun. An introduction, 2nd edn. Springer, Heidelberg
Tian F, Kasting JF, Solomon SC (2009) Thermal escape of carbon from the early Martian Atmosphere. Geophys Res Lett 36, L02205. DOI:10.1029/2008GL036513
Wood BE (2004) Astrospheres and Solar-like stellar winds. Living Rev Sol Phys 1, lrsp- 2004-2. http://www.livingreviews.org/lrsp-2004-2

Supercontinent

Daniele L. Pinti
GEOTOP Research Center for Geochemistry and Geodynamics, Université du Québec à Montréal, Montréal, QC, Canada

Definition

A supercontinent is a landmass comprising a large fraction of the entire ▶ continental crust. It is the product of the assembly of many smaller continents into one single continent. Supercontinents form in cycles, coming together and breaking apart about every 500 million years as a result of plate tectonic movements. Examples include ▶ Rodinia (from 1,100 to 750 Ma) and ▶ Pangea (between 300 and 200 Ma). The latter split apart between 200 and 180 Ma ago to form two smaller supercontinents, ▶ Laurasia and ▶ Gondwana. The oldest putative supercontinent is Vaalbara (3.1–2.5 Ga) which regrouped ancient Archean terranes of the ▶ Pilbara Craton (Western Australia) and the ▶ Kaapvaal Craton (South Africa).

See Also

▶ Gondwana
▶ Kaapvaal Craton, South Africa
▶ Laurasia
▶ Pangea
▶ Pilbara Craton
▶ Plate Tectonics
▶ Rodinia

Supercritical Fluid

Henderson James (Jim) Cleaves II
Earth–Life Science Institute (ELSI), Tokyo Institute of Technology, Meguro–ku, Tokyo, Japan
Institute for Advanced Study, Princeton, NJ, USA
Blue Marble Space Institute of Science, Washington, DC, USA
Center for Chemical Evolution, Georgia Institute of Technology, Atlanta, GA, USA

Definition

A supercritical fluid is a substance at a temperature and pressure above its critical point. It can effuse through solids like a gas and dissolve materials like a liquid. Supercritical fluids thus have properties between those of a gas and a liquid.

Supercritical fluids have no surface tension, as there is no liquid/gas phase boundary. By changing the pressure and temperature of the fluid, the properties can become more liquid-like or more gas-like. The solubility of dissolved substances in a supercritical fluid tends to increase with the density of the fluid at a constant temperature. Since density increases with pressure, solubility tends to increase with pressure. The relationship with temperature is more complex. At constant density, solubility increases with increasing temperature. Close to the critical point, however, the density can drop drastically with slight increases in temperature. Thus, close to the critical temperature, solubility may drop with increasing temperature and then rise again.

Submarine hydrothermal vents are widely distributed on the ocean floor. Many lie at great depth where the tremendous pressure from the overlying seawater prevents the explosive release of steam and gas. In some cases, seawater can be heated to over 400–465 °C, where it becomes a

supercritical fluid depending on the ambient pressure.

The atmosphere of Venus is composed of 96.5 % CO_2 and 3.5 % N_2. The surface pressure is 9.3 MPa, and the surface temperature is 735 K, well above the critical points of both gases; thus, the atmosphere near the surface is a supercritical fluid.

Super-Earths

Nader Haghighipour
Institute for Astronomy, University of Hawaii-Manoa, Honolulu, Hawaii, HI, USA

Definition

Super-Earth is the suggested term for a diverse class of planets with masses ranging from 2 to 10 Earth masses. Prior to the operation of the *Kepler* space telescope, the value of the minimum mass of a planet was used to define the term "super-Earth." After the detection of many small planets by the *Kepler* telescope, in the interest of identifying small, rocky planets that could be habitable, in addition to mass, a radius criterion was also added to the definition. A "super-Earth" is, therefore, a planet with a mass of 2–10 Earth masses and radius of 1–2 Earth radii.

The first super-Earth around a main sequence star was discovered by Rivera et al. (2005) using the radial velocity technique. [Note that in 1992, Wolszczan and Frail (1992) discovered at least two terrestrial-sized planets around the pulsar PSR 1257+12. See the entry on ▶ Pulsar Planets.] Thanks to several ground- and space-based observational projects, to date, the number of these objects has exceeded 90. A list of the currently known super-Earths can be found in two review articles by Haghighipour (2011, 2013).

For the past few years, the formation and characteristics of super-Earths have been the subject of extensive research. This is primarily because being slightly larger than a typical terrestrial planet, these objects can have a solid surface with a solid-to-gas or liquid-to-gas phase transition at their upper boundary, similar to Earth. Super-Earths have the capability of developing moderate atmospheres and may have dynamic interiors with plate tectonics – two conditions that would render a super-Earth potentially habitable if its orbit were in the habitable zone of its host star.

Unlike Earth-sized planets, super-Earths are relatively easy to detect. Current observations of super-Earths have indicated that these objects seem to be more common around cool and low-mass stars (e.g., Dressing and Charbonneau 2013; Swift et al. 2013), where the habitable zone is in closer orbit. Two prime examples of such systems are Gliese 581, an M3V star with one or two potentially habitable super-Earths, and the M1.5 star GJ 667C, with up to three super-Earths in its habitable zone including the 4.5 Earth-mass planet GJ 667Cc.

See Also

- ▶ Atmosphere, Structure
- ▶ Biomarkers, Spectral
- ▶ Habitable Planet, Characterization
- ▶ Habitable Zone
- ▶ Habitability of the Solar System
- ▶ Mini-Neptunes
- ▶ Exoplanets, Modeling Giant Planets' Atmospheres

References and Further Reading

Dressing C D, Charbonneau D (2013) The occurrence rate of small planets around small stars. Astrophys J 767, article id. 95

Haghighipour N (2011) Super-Earths: a new class of planetary bodies. Contemp Phys 52:403–438

Haghighipour N (2013) The formation and dynamics of super-Earth planets. Annu Rev Earth Planet Sci 41:469–495

Rivera EJ, Lissaner JJ, Butter RP, Marcy GW et al (2005) A $\sim 7.5 M_{\oplus}$ Planet Orbiting the Nearby Star, GJ876. Astrophys J 634:625–640.

Swift J, Johnson JA, Morton TD, Crepp JR, Montet BT et al (2013) Characterizing the cool KOIs. IV.Kepler-32 as a prototype for the formation of compact planetary systems throughout the galaxy. Astrophy J 764, article id. 105

Wolszczan A, Frail DA (1992) A planetary system around the millisecond pulsar PSR1257+12. Nature 355:145

Superkingdom

► Domain (Taxonomy)

Supernova

Robert Mochkovitch
Institut d'Astrophysique de Paris, Paris, France

Keywords

Chandrasekhar mass; Collapse; Cosmology; Dense matter; Massive stars; Nucleosynthesis; Stellar evolution; Shock wave; Thermonuclear reactions; White dwarfs

Definition

Supernovae are cataclysmic explosions of stars at the end of their evolution. Two categories of stars are known to explode: massive ones ($M > 8$–$10\ M_\odot$; $M_\odot$ is the solar mass) and white dwarfs (the remnants of low mass stars) if they can grow by accretion in a binary system. When they explode, supernovae inject energy into the ► interstellar medium and eject ► heavy elements such as carbon, oxygen, or ► iron. Supernovae are the main contributors to the chemical evolution of galaxies.

History

Five times in the last millennium, a new star suddenly appeared in the sky. Initially very bright, it progressively declined to finally disappear after a few months or a few years. The first star, in 1006, was the brightest one, even visible during daytime. It was followed in 1054 by a new event described as a "guest star" by the Chinese astronomers. The remnant of this object is the famous Crab nebula in the Taurus constellation. Then nothing was noticed until 1572 when the Danish astronomer Tycho Brahe observed another new star in Cassiopeia and recorded his observations in Latin in his work "De ► nova stella." Only 32 years later, in 1604, Kepler studied the last one of these extraordinary events. We now know that they all were supernovae having exploded in our own galaxy, the ► Milky Way. The modern study of supernovae started during the thirties with F. Zwicky (who coined the word supernova). He launched a search for supernovae in external galaxies which was very successful with more than 100 discoveries in about 30 years. In 1987, a supernova was found in the Large Magellanic Cloud, a small irregular satellite galaxy of the Milky Way, 150,000 light years from us. Reaching magnitude 4.5 at its maximum, it was barely visible with the naked eye but still the brightest supernova since 1604.

Overview

Supernovae represent the end point of evolution of two main categories of stars: (1) the most massive ones ($M > 8$–$10\ M_\odot$) which successively fuse hydrogen, helium, carbon, oxygen, neon, and silicon in their cores, eventually leading to the formation of a central core made of iron. When this core reaches about $1.4\ M_\odot$, it becomes unstable and collapses. However, when the central density reaches a few times 10^{14} g/cm^3 (the density of nuclear matter), the core bounces and launches a strong shock wave outward which ejects the envelope at velocities exceeding 10,000 km/s. (2) The second category is white dwarfs (the remnants of stars with $M < 8\ M_\odot$), which can explode if they accrete material from a companion star in a binary system. The accretion process can occur by progressive mass transfer from the companion or by true coalescence, if the binary is made of two white dwarfs. The ► white dwarf material (a mixture of carbon and oxygen) ignites ► nuclear reactions in an explosive way and the combustion propagates to the whole star, which is entirely destroyed. The first group represents the so-called core-collapse supernovae, while the second corresponds to "thermonuclear supernovae." Besides their own interest,

supernovae play a key role in the chemical and dynamical evolution of galaxies: they synthesize the heavy elements and inject energy into the interstellar medium which triggers the formation of new stars. Cosmic rays are also accelerated in the shock waves present in their remnants. Due to their extreme luminosity (over one billion solar luminosities), they can be detected to very large distances and used for cosmological studies.

Basic Methodology

The nature of the stars ending their evolution as supernovae and the physical mechanisms responsible for the explosion are studied through a close interplay between observational and theoretical research. Spectroscopy provides clues on the progenitor stars (composition of the envelope) and energetics of the explosion (expansion velocity obtained through the Doppler effect). The light curve (i.e., the luminosity as a function of time) offers additional information on the sources of energy and constraints the mass and radius of the envelope.

The classification of supernovae was originally (and largely remains) based on spectroscopy. Hydrogen lines are absent from type I supernova spectra and present in type II. Moreover, type I supernovae have been divided into three subclasses: at maximum light (the peak of the light curve), type Ia (SN Ia) exhibits lines of intermediate mass elements (especially a bright silicon line) while they show mainly iron and cobalt lines at late times. Helium lines dominate SN Ib spectra at maximum light and are absent in SN Ic. Conversely, SN II have conspicuous hydrogen lines both at maximum light and at late times.

Population studies, which relate supernovae to their environment, show that SN Ib/c should be clearly distinguished from SN Ia. Like SN II, they are only observed in regions of ongoing star formation, contrary to SN Ia which are present in all kinds of environments, including elliptical galaxies which have not formed stars for several billion years. SN Ib/c and SN II progenitors should then be massive stars which only live a few million years and are therefore expected to explode close to their birthplace. The absence of hydrogen in SN Ib/c can be explained by mass loss due to stellar winds prior to the explosion. In SN Ib the helium layer lying below the lost hydrogen envelope remains, while in SN Ic it is also lost, leaving the "stripped" carbon and oxygen-rich core of the star.

The progenitors of SN Ia are low mass stars – the only ones remaining in an old stellar population – which should also be highly evolved to have lost all their hydrogen. This suggests an explosion scenario involving a white dwarf. White dwarfs are the remnants of low mass stars ($M < 8\ M_\odot$). They are perfectly stable when isolated but can become explosive if their mass is brought by accretion close to the Chandrasekhar limit ($1.4\ M_\odot$; see ▶ Chandrasekhar's limit).

Theoretical models of SN Ib/c and SN II supernovae invoke the collapse of the central core of the star, which becomes a ▶ neutron star or even possibly a ▶ black hole (these supernovae are now globally called "core-collapse supernovae"). Most of the gravitational energy released in the collapse is carried away by neutrinos, but less than 1 % of the total is sufficient to power the explosion. For SN Ia, a thermonuclear runaway which incinerates and destroys the whole star appears able to account for the major observational facts.

These various explosion mechanisms are studied by numerical simulations involving both a complex hydrodynamics (multidimensional treatment of the fluid motion) and input physics (equation of state of dense matter, neutrino transport). The general explosion scenarios outlined above are probably correct, but many questions remain unsolved and the study of supernovae remains an active research field.

Key Research Findings

Core-collapse and thermonuclear supernovae have very different explosion mechanisms, but the concept of Chandrasekhar mass plays a key role in both. It represents the maximum possible mass for an object "supported by electron

pressure," the interior of which is "degenerate." In degenerate matter, the usual thermal pressure is replaced by a pressure of quantum origin, resulting from the impossibility for two electrons to be in the same quantum state (Pauli's exclusion principle).

After successive episodes of nuclear burning (fusion), massive stars terminate their evolution having an "onion-shell structure" with a central degenerate iron core surrounded by nondegenerate layers of lighter elements from silicon (next to the core) to the outer hydrogen envelope, if it is present. Iron is the most stable nucleus and cannot undergo further burning. As a result of silicon burning, the core mass grows – iron nuclei being the nuclear ashes of silicon – and eventually reaches the Chandrasekhar limit where it becomes unstable. It collapses in less than 1 s until the central density reaches a few times 10^{14} g/cm^3 (i.e., 100 million tons per cm^3!). This corresponds to the density of nuclear matter, where nuclei are brought into contact with each other. Nuclear matter is strongly incompressible and provides an additional pressure which stops the collapse of the inner 0.8 $M_\odot$ of the core. The outer core violently bounces on it and acts as a piston moving outward. A strong shock wave forms and it was initially believed that it carried enough energy to power the explosion. However, it was subsequently shown that, due to energy losses behind the shock (mainly the breakup of iron nuclei into free nucleons), the bounce alone was not able to produce an outburst. Additional energy coming from the neutrinos escaping from the cooling inner core was then invoked. Neutrino interaction with normal matter is very weak, but the extreme densities encountered in the shock region may allow the transfer of a small fraction of the neutrino energy to heat the core and restart the shock propagation. Unfortunately numerical simulations of this process are so complex that no clear consensus has been reached among the different groups of experts: some get a successful explosion, while for others the material falls back.

White dwarfs are also made of degenerate material (a carbon-oxygen core surrounded by a helium layer in SN Ia progenitors) so that they become potentially explosive if their mass increases. This may happen if they receive material from a companion star by mass transfer in a binary system. Two evolutionary channels are a priori possible: slow accretion of matter outflowing from the companion or direct coalescence in a system of two white dwarfs. In the first case, carbon is ignited at the star center when the white dwarf approaches the Chandrasekhar limit. Nuclear burning in degenerate material is explosive and rapidly extends outward, the whole star being eventually destroyed. In the second case, coalescence results from the decrease of orbital separation caused by the emission of gravitational radiation from the system. At some point, the less massive of the two white dwarfs (which has the largest radius) is disrupted and coalescence ensues in about 1 min. Nuclear fuel (first helium and then carbon and oxygen) ignites in the collision region and the combustion now proceeds inward. Again, the white dwarf is entirely destroyed.

A major uncertainty comes from the difficulty of estimating the velocity of propagation of the burning front. It can be supersonic (and then called a "detonation") or subsonic ("deflagration"). Some models adopt a mixture of the two, starting with a deflagration which evolves into a detonation. Complete burning of the inner 0.6–0.8 $M_\odot$ leads to ^{56}Ni, a radioactive isotope of nickel which decays into cobalt and iron, releasing energy which powers the light curve. The outer region undergoes incomplete burning leading to elements such as silicon or sulfur. This distribution of nucleosynthetic products agrees well with the results from spectroscopy.

Applications

- If stars did not explode, all the elements formed by nucleosynthesis during their lifetime (and during the explosion itself) would stay trapped in stellar interiors. Supernovae allow most of them to be ejected into the interstellar medium, which then gets progressively enriched in heavy elements (just after

the Big Bang, the universe contained only hydrogen, helium, and very small fractions of lithium). Carbon (the elementary brick of all organic molecules), oxygen, and silicon, for example, come from core-collapse supernovae, while SN Ia are the main providers of iron. It is remarkable to realize that all the atoms from which human beings are made (except hydrogen) were formed in stars which have disappeared before the solar system formed, 4.5 billion years ago. Supernovae also inject energy into the interstellar medium. They drive strong shock waves which create bubbles filled by hot gas. At the boundaries of these bubbles, the formation of new stars is triggered.

- Supernovae are so bright that they can be detected to cosmological distances. This is especially important in the case of SN Ia which are also considered to be reasonably good "standard candles," i.e., objects which all have the same luminosity. A plot of their apparent magnitude (at maximum light) as a function of redshift, called the Hubble diagram, can then be used to constrain cosmological models. This has shown that the expansion of our universe is accelerating (and not decelerating as was previously believed), which implies that space is pervaded by some form of "dark energy," the nature of which remains unknown.

Future Directions

The details of the mechanism responsible for the explosion of core-collapse supernovae are still highly debated. Numerical simulations of the whole process are very difficult and only a few groups in the world are performing them. It has been recently realized that supernova explosions might be asymmetric due to a new kind of instability developing shortly after core bounce. It is also believed that this instability may greatly help obtaining successful explosions. A related question concerns the separation between models giving a neutron star remnant and those collapsing to a black hole. What are the key factors controlling the fate of the star? Is the initial mass the only important parameter? How critical is the amount of rotation present in the core?

In the case of SN Ia, the respective roles of detonation and deflagration in the burning mechanism are still unclear, but the main issue remains the nature of the progenitors: standard accretion from a normal star and coalescence of a system of two white dwarfs represent two possible channels. We don't know how they contribute to the rate of SN Ia in different ▶ stellar populations and even if they always both contribute.

See Also

- ▶ Black Hole
- ▶ Chandrasekhar's Limit
- ▶ Explosive Nucleosynthesis
- ▶ Heavy Element
- ▶ High-Mass Star
- ▶ Neutron Star
- ▶ Nova
- ▶ Nuclear Reaction
- ▶ Nucleosynthesis, Stellar
- ▶ Pulsar
- ▶ r-process
- ▶ Star
- ▶ Stellar Evolution
- ▶ Stellar Yield
- ▶ Supernova Remnant
- ▶ Supernova Types
- ▶ White Dwarf

References and Further Reading

Arnett D (1996) Supernovae and nucleosynthesis. Princeton series in astrophysics

Fryer C (ed) (2004) Stellar collapse. Astrophysics and space science library. Springer, Berlin

Hillebrandt W, Leibundgut B (eds) (2003) From twilight to highlight: the physics of supernovae, ESO astrophysics symposia. Springer, Berlin

Hillebrandt W, Niemeyer J (2000) Type Ia supernova explosion models. Ann Rev Astron Astrophys 38:191–230

Hillebrandt W, Janka HT, Müller E (2006) How to blow a star. Sci Am 295:42–49

Leibundgut B (2001) Cosmological implications from observations of type Ia supernovae. Ann Rev Astron Astro 39:67–98
Pagel B (2009) Nucleosynthesis and chemical evolution of galaxies, 2nd edn. Cambridge University Press, Cambridge
Smartt S (2009) Progenitors of core-collapse supernovae. Annu Rev Astron Astro 47:63–106
Woosley S, Janka HT (2005) The physics of core-collapse supernovae. Nat Phys 1:147–154

Supernova Remnant

Thierry Montmerle
Institut d'Astrophysique de Paris, CNRS/
Université Paris 6, Paris, France

Definition

In the optical domain, supernova remnants (SNR) appear as spectacular, bright filamentary nebulae, testifying to the past explosion of a star. There are two main types of SNRs, depending on the type of the explosion: (1) In "shell-type" SNRs, the nebula is hollow and filaments are arranged more or less in the form of concentric circular shells, and are interpreted as shock waves triggered by the explosion, propagating into the interstellar medium at velocities of up to a few 1,000 km/s. Famous representatives of this class are the "Cygnus Loop" and the "Medusa" in the constellation Gemini. (2) In "filled-type" SNRs, also known as "plerions" (from a Greek word meaning "full"), the nebula looks like a web of filaments of stellar origin, emanating from a bright center. Plerions contain a ► pulsar (a rotating, very condensed star called a "neutron star"). The most famous representative of the class is the "Crab nebula," illustrated in Fig. 1. Supernova remnants are also conspicuous in the radio centimetric range and in X-rays. Since these wavelengths are much less sensitive to interstellar extinction than the optical, supernova remnants are known at large distances throughout the Galaxy. Many are also known in the galaxies nearest our own, the Magellanic Clouds.

Supernova Remnant, Fig. 1 The "Crab Nebula," in the Taurus constellation is the remnant of a supernova that exploded in 1054 AD. The filaments are the remains of the parent star, and the diffuse light is due to energetic electrons accelerated by the central pulsar (Photograph ESO Very Large Telescope)

History

Today nearly 300 SNRs are known, the majority having estimated ages from several thousand to several hundred thousand years. Six supernova explosions have been witnessed with a naked eye in historical times, many being recorded by Chinese astronomers, like the Crab nebula in AD 1054. The first one was recorded in AD 185, and the last appeared in 1987 in the Large Magellanic Cloud. Two more are known to have exploded in the Milky Way during historic times (around 1671 and 1870), but were not seen because of the high interstellar dust obscuration.

See Also

- ▶ Pulsar
- ▶ Supernova

Supernova Types

Nikos Prantzos
Institut d'Astrophysique de Paris, Paris, France

Definition

▶ Supernovae are classified according to their early spectra as Type I (SNI) or Type II (SNII), depending on the absence or presence of hydrogen, respectively. SNI are further divided into SNIa (Si present), SNIb (Si absent, He present), and SNIc (Si and He absent, C present). It turns out that SNIa correspond to thermonuclear explosions of ▶ white dwarfs in binary systems, while all other types result from the gravitational collapse of the core of a massive star that has lost various amounts of its envelope (little H in SNII, all of H in SNIb, and all of H and He in SNIc). It is expected that in a galaxy like the Milky Way, 2 SN per century explode, SNIa are five times less frequent than gravitational supernovae and (SNIb +SNIc) are three times less frequent than SNII.

See Also

- ▶ Supernova
- ▶ Supernova Remnant
- ▶ White Dwarf

Superthermal

- ▶ Suprathermal

SuperWASP

- ▶ WASP

Suprathermal

William M. Irvine
University of Massachusetts, Amherst, MA, USA

Synonyms

Superthermal

Definition

Motion of particles (atoms, molecules, ions) with velocities much larger than the characteristic local thermal (Maxwellian) velocity is called suprathermal or superthermal. Processes involving magnetic fields, such as solar flares, can produce suprathermal particle motions. In the case of ▶ interstellar dust grains, suprathermal rotation has been invoked as a process involved in the grain alignment that is responsible for polarizing transmitted radiation.

Although the term suprathermal could also in principle be applied to situations like astrophysical masers, where a group of atoms or molecules

exists in a condition with more members in an excited energy state than in a linked lower energy state (thus providing a negative thermodynamic temperature and the possibility of stimulated emission of radiation), this use of the term has not been in common use.

See Also

- ▶ Alignment of Dust Grains
- ▶ Interstellar Dust

References and Further Reading

Whittet DCB (2003) Dust in the galactic environment, vol 2. Institute of Physics Publishing, Bristol

Surface Gravity

Daniel Rouan
LESIA, Observatoire Paris-Site de Meudon, Meudon, France

Definition

Surface gravity is defined as the acceleration of a test mass in free fall at the surface of a massive body under the gravitational force produced by the body. Noted g, the surface gravity for a spherical body is derived from Newton's formula $g = G\,M/R^2$, where G is the gravitational constant and M and R are the mass and radius of the massive body. Unit: m s^{-2}. The surface gravity on Earth is equal to 9.81 m s^{-2}.

Surface Plasmon Resonance

Nita Sahai
Department of Polymer Science, University of Akron, Akron, OH, USA

Synonyms

SPR

Definition

Surface Plasmon Resonance (SPR) spectroscopy is based on excitation of electronic oscillations by light at a planar interface between two materials for which the real part of the dielectric constants has opposite signs (e.g., metal/vacuum or metal/air). The electromagnetic waves that travel parallel to the interface are reflected by total internal reflection, and the evanescent wave probes the interface. The reflected intensity decays exponentially as a function of distance away from the interface. SPR is, therefore, a very sensitive probe of changes in the interfacial roughness due to adsorption of large molecules, such as polymers and proteins, on the metal surface. This technique is the basis of many lab-on-a-chip and biosensor applications.

See Also

- ▶ Biosensor

Surfactant

- ▶ Amphiphile

Survival

Gerda Horneck
DLR German Aerospace Center, Institute of Aerospace Medicine, Radiation Biology, Köln, Germany

Keywords

Dormant state; Growth; Microbial survival; Survival curves

Synonyms

Viability

Definition

The term "survival" describes a capability of individuals, communities, or whole populations of staying alive over a certain period of time. In astrobiology "survival" is mainly applied to microorganisms – individuals or communities – that withstand hostile environmental conditions. Several microorganisms are capable of forming dormant states, e.g., bacterial spores, of high resistance to temporarily unfavorable conditions.

Overview

During the about 3.5 billion years history of life on Earth, microorganisms have developed a variety of adaptive strategies to survive in environments that are toxic to most other life-forms. There are two ways of responses of microorganisms to extreme conditions: (1) capability of growth, i.e., the maintenance of an active population, which finds its optimum or near optimum conditions in those environments, and (2) capability of survival for short or even extended periods of time in a dormant state (Table 1). Examples for the latter one are spores produced by fungi and bacteria, cysts produced by various eukaryotes, and seeds produced by plants. Most of these forms are usually unicellular bodies – exceptions are seeds – which are encased by a thick protective coat. They are very resistant to environmental extremes, such as heat, ▶ desiccation, radiation, and other stresses. Bacterial ▶ spore formation represents a strategy by which a bacterium escapes temporally and/or spatially from unfavorable conditions, resulting in incredible longevity – survival times of 25–250 Ma have been reported (Cano and Borucki 1995; Nicholson et al. 2000; Vreeland et al. 2000).

Survival, Table 1 Environmental range allowing growth or survival of at least some species of microorganisms

Parameter	Growth	Survival
Temperature (°C)	−20 to +113	−262 to +113
Pressure (Pa)	10^5–10^8	10^{-7} to $\geq 10^8$
Ionizing radiation (Gy)	≈50	≤5,000
UV radiation (nm)	Depending on wavelength	Depending on wavelength
Water stress (a_w)	≥0.7	0–1.0
Salinity	≤30 %	Salt crystals
pH	1–11	0–12.5
Nutrients	High metabolic versatility, high starvation tolerance	Not required, better without
Gas composition	Different requirements (oxic or anoxic)	Better without oxygen
Time (a)	≤0.5[a]	≤ (25–250) × 10^{6}[b]

[a]Longest generation time of microorganisms recorded so far

[b]Longest survival time of microorganisms recorded so far

The survival capacity of microorganisms in response to stressors is quantified in survival curves, which give the survival rate as a function of the dose of the applied agent (Fig. 1). The bacterium *Deinococcus radiodurans* has been known as the most resistant organism in response to ionizing radiation, tolerating doses up to 4 kGy without a decrease in survival.

The exceptionally high resistance against environmental extremes over long periods of time makes bacterial spores suitable candidates for astrobiology studies, such as the likelihood of transport of life between the planets of our solar system, i.e., the hypothesis of ▶ lithopanspermia, and ▶ planetary protection considerations. Experiments in space and at ground simulation facilities as well as model calculations have shown that spores would survive a hypothetical interplanetary transfer, including shock waves

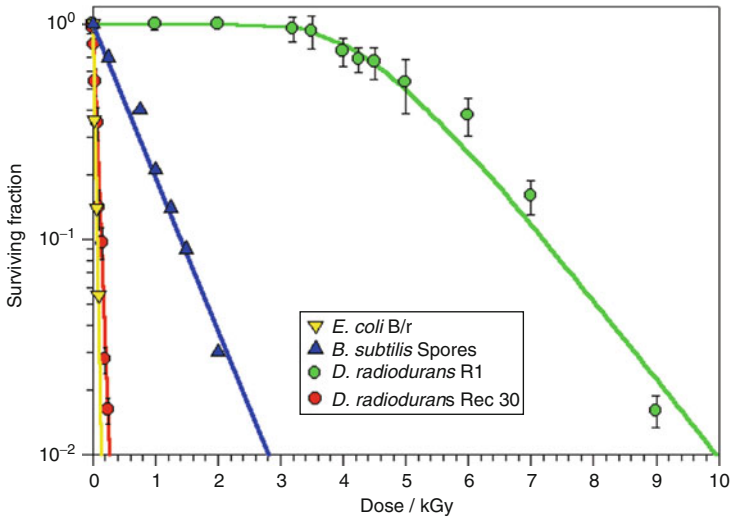

Survival, Fig. 1 Survival curves for *Deinococcus radiodurans R1* and its recombination-deficient mutant Rec 30 compared to survival curves for spores of *Bacillus subtilis* and cells of *Escherichia coli B/r* following exposure to X-rays (From Horneck and Baumstark-Khan 2002)

and high temperatures during the ejection process (Horneck et al. 2008), extreme vacuum, intense radiation, and varying temperatures during the journey in space (Mileikowsky et al. 2000), and finally accelerations and high temperatures during entry and landing on another planet (Westall and de la Torre Noetzel 2008; Horneck et al. 2010). Desiccation-resistant organisms, such as bacterial spores and ▶ lichens, survive especially well in the hostile space environment because of their low water content and the protection by outer thick layers.

See Also

- ▶ Desiccation
- ▶ Endospore
- ▶ Ionizing Radiation, Biological Effects
- ▶ Lichens
- ▶ Lithopanspermia
- ▶ Microorganism
- ▶ Panspermia
- ▶ Planetary Protection
- ▶ Spore
- ▶ Sterilization

References and Further Reading

Cano RJ, Borucki MK (1995) Revival and identification of bacterial spores in 25 to 40 million-year-old Dominican amber. Science 268:1060–1064

Horneck G, Baumstark-Khan C (eds) (2002) Astrobiology, the quest for the conditions of life. Springer, Berlin

Horneck G, Stöffler D, Ott S, Hornemann U, Cockell CS, Moeller R, Meyer C, de Vera JP, Fritz J, Schade S, Artemieva NA (2008) Microbial rock inhabitants survive impact and ejection from host planet: first phase of lithopanspermia experimentally tested. Astrobiology 8:17–44

Horneck G, Klaus DM, Mancinelli RL (2010) Space microbiology. Microbiol Mol Biol Rev 74:121–156

Mileikowsky C, Cucinotta F, Wilson JW, Gladman B, Horneck G, Lindegren L, Melosh J, Rickman H, Valtonen M, Zheng JQ (2000) Natural transfer of viable microbes in space, Part 1: from Mars to Earth and Earth to Mars. Icarus 145:391–427

Nicholson WL, Munakata N, Horneck G, Melosh HJ, Setlow P (2000) Resistance of *Bacillus* endospores to extreme terrestrial and extraterrestrial environments. Microbiol Mol Biol Rev 64:548–572

Vreeland RH, Rosenzweig WD, Powers DW (2000) Isolation of a 250 million-year-old halotolerant bacterium from a primary salt crystal. Nature 407:897–900

Westall F, de la Torre Noetzel R (2008) Meteorites: stones with stowaways? In: Looking up: Europe's quiet revolution in microgravity research. Scientific American, New York, pp 8–15. A custom publication produced in collaboration with Space Channel on behalf of the European Space Agency. J. Rennie (editor in chief)

Svedberg Unit

Henderson James (Jim) Cleaves II
Earth–Life Science Institute (ELSI), Tokyo Institute of Technology, Meguro–ku, Tokyo, Japan
Institute for Advanced Study, Princeton, NJ, USA
Blue Marble Space Institute of Science, Washington, DC, USA
Center for Chemical Evolution, Georgia Institute of Technology, Atlanta, GA, USA

Definition

A Svedberg unit (represented as S or sometimes Sv) is a non-Système Internationale unit for sedimentation rate. The unit is named after Swedish chemist Theodor Svedberg (1884–1971), who won the 1926 Nobel Prize in chemistry for his work on colloids and the invention of the ultracentrifuge. The sedimentation rate is a measure of how quickly a particle sediments from a solution or suspension under the induced gravitational field of a centrifuge.

The sedimentation coefficient is the ratio of the speed of a substance in a centrifugal field to its acceleration in comparable units. A substance with a sedimentation coefficient of 1S (10^{-13} s) will travel at 1 mm per second (10^{-6} m s^{-1}) under the influence of an acceleration of 10^6 G (10^7 m s^{-2}). Centrifugal acceleration is given as $r\omega^2$, where r is the radial distance from the rotation axis and ω is the angular velocity in radians s^{-1}.

Though the Svedberg unit is technically a measure of time (10^{-13} s), it also offers a measure of particle size, density, and shape, as these aspects of a particle contribute to sedimentation behavior. All other things being equal, larger particles tend to sediment faster and thus have higher Svedberg values.

The Svedberg has commonly been used to distinguish among the ribosomes found in the different domains of life, as well as the relative sizes of their subunits.

See Also

▶ Ribosome

SWAS

▶ Submillimeter Wave Astronomy Satellite

Swaziland Supergroup (Outdated)

▶ Barberton Supergroup

Symbiosis

Juli Peretó
Institut Cavanilles de Biodiversitat i Biologia Evolutiva, Universitat de València, València, Spain

Synonyms

Mutualism

Definition

Symbiosis is the association of two or more species, resulting in a new entity. The relationship can be metabolic or genetical and may lead to a continued association, from generation to generation. In a more restricted sense, it refers to cases in which all the associated partners obtain benefits (mutualism). But the nature of the association can be detrimental to some of the partners

(parasitism) or neutral (commensalism). The association can also be optional (facultative) or obligate. Symbiosis is widespread in nature and plays a central role in the origin of evolutionary innovations. The case of intracellular symbionts (► endosymbiosis) represents a mechanism for the origin of the eukaryotic complexity.

See Also

► Endosymbiosis
► Evolution, Biological

Synchrotron Accelerator

Henderson James (Jim) Cleaves II
Earth–Life Science Institute (ELSI), Tokyo Institute of Technology, Meguro–ku, Tokyo, Japan
Institute for Advanced Study, Princeton, NJ, USA
Blue Marble Space Institute of Science, Washington, DC, USA
Center for Chemical Evolution, Georgia Institute of Technology, Atlanta, GA, USA

Definition

A synchrotron accelerator is a particular type of cyclic particle accelerator in which the magnetic field and the electric field are carefully synchronized with the traveling particle beam. While a cyclotron uses a constant magnetic field and a constant-frequency applied electric field, both of these fields are varied in the synchrotron. By increasing these parameters appropriately as particle energy increases, the path of the particles can be held constant as they are accelerated. This allows the vacuum chamber for the particles to be a torus. A path of large effective radius can then be constructed using simple straight and curved pipe segments, unlike the disk-shaped chamber of cyclotrons.

See Also

► Synchrotron Radiation

Synchrotron Radiation

Daniel Rouan
LESIA, Observatoire Paris-Site de Meudon, Meudon, France

Definition

Synchrotron radiation is the continuous electromagnetic radiation produced by a highly relativistic plasma in a magnetic field. It can cover a very broad range of wavelengths, from gamma rays to radio wavelengths. In a magnetized ► plasma, an electron gyrates around the direction of the magnetic field because of the Lorentz force and thus radiates as does any accelerated charge. When electrons reach highly relativistic speeds, the emission comes from a narrow beam in the direction of motion, so that the observer sees extremely narrow pulses whose resulting spectrum is a continuum spread over a very broad range of frequencies. The slope of the spectrum is characteristic of the electrons' energy distribution. Synchrotron emission is seen in extreme energy environments such as the accretion disks around ► black holes, ► neutron stars, and some ultra-massive black holes at the centers of galaxies. This type of radiation is called *non-thermal*, as opposed to *thermal* radiation such as ► blackbody or free-free emission.

See Also

► Black Hole
► Continuum
► Electromagnetic radiation
► Neutron Star
► Radiative Processes

Syngenicity

Nicola McLoughlin
Department of Earth Science and Centre for Geobiology, University of Bergen, Bergen, Norway

Keywords

Antiquity; Biosignatures

Definition

Syngenicity means a feature that may be textural, chemical, mineral, or biological and that formed at the same time as the encapsulating material. In other words, a primary component is preserved contemporaneously with the deposition of the host sedimentary rock, or crystallization of the host igneous melt, or precipitation of the encapsulating mineral or ice phase(s). The demonstration of syngenicity is equivalent to the demonstration of antiquity, and this is essential to establish the history of life in our universe.

History

In economic geology, the term syngenetic has traditionally been used to refer to ore deposits formed at the same time as the enclosing rock as opposed to epigenetic that describes mineral deposits formed later. Here a definition is provided that is more generally applicable to the investigation of astrobiological materials including not just terrestrial rocks and minerals but also meteorites, interplanetary dust, and ice particles.

Overview

A syngenetic textural, chemical, mineralogical, and/or biological component is formed at the same time as the host material. Syngenetic components of low-temperature deposits are those that were stable at the ambient pressure, temperature, redox, and salinity conditions prevailing at or near the planetary surface at the time of formation. In the case of high-temperature volcanic rocks and precipitates, syngenetic components formed in equilibrium with the solidifying magma or fluid, for example, primary melt or fluid inclusions and mineral phases. Syngenicity concerns the source of a component in time. This differs from ▶ endogenicity that concerns the source of a component with regard to space. Components that are syngenetic are nearly always also endogenetic, i.e., derived from within the system. There are a few exceptions, however, for example, windblown ash particles preserved in ice cores or pollen grains entombed within desert varnish crusts.

The demonstration of syngenicity is equivalent to the demonstration of antiquity, and this is especially important to establish the history of life on planetary bodies (e.g., Wacey 2009). Syngenetic components are found within early phases in the host material and do not occur in late-stage alteration products or crosscutting veins, and this can be tested in thin section. Thus, for example, microbial remains found in superficial cracks, late-stage veins, or metastable minerals are unlikely to be syngenetic and rather, more likely, to be derived from subrecent organisms (e.g., Westall and Folk 2003). Syngenetic components should also have experienced the same degree of deformation and alteration as the host rock. Thus, for example, spherical structures should be flattened parallel to the regional deformation fabrics if these exist (e.g., Appel et al. 2003). Moreover, the distribution and abundance of syngenetic components in a system should reflect primary environmental gradients such as light levels or redox gradients. This can be investigated by meter- to micron-scale mapping to establish if there is a correlation between primary depositional or magmatic variables and the distribution of the candidate biosignatures. Sometimes it is possible to measure an absolute radiometric age for the feature of interest (e.g., Grosch and Mcloughlin 2014), or more

commonly the phase of interest can be relatively dated to mineral cements or veins of known age and placed within the chronology of processes that have affected the whole system.

See Also

- ▶ Archean Traces of Life
- ▶ Biogenicity
- ▶ Biomarkers
- ▶ Biomarker, Isotopic
- ▶ Biomarkers, Morphological
- ▶ Endogenicity
- ▶ Geochronology

References and Further Reading

Appel PWU, Moorbath S, Myers JS (2003) Isuasphaera isua (Pflug) revisited. Precambrian Res 126:309–312

Grosch EG, Mcloughlin N (2014) Reassessing the biogenicity of Earth's oldest trace fossil with implications for biosignatures in the search for early life. Proceedings of the National Academy of Sciences 111, 8380–8385

Wacey (2009) Establishing the criteria for early life on Earth. In: Wacey (ed) Early life on Earth; a practical guide, Springer, pp 47–54

Westall F, Folk RL (2003) Exogenous carbonaceous microstructures in early Archaean cherts and BIFs from the Isua Greenstone belt: implications for the search for life in ancient rocks. Precambrian Res 123:313–330

Synthetic Biology

Daisuke Kiga
Tokyo Institute of Technology, Tokyo, Japan

Keywords

What life could be; Realization of biosystems

Synonyms

Constructive biology

Definition

Synthetic biology is a biological study, in scientific and engineering fields, depending on the construction of biological systems. A living organism is a system containing multilayers such as cells, biomacromolecules (proteins, RNAs, and DNAs), and monomers (amino acids and nucleotides). Because the numbers of combinations are huge, few combinations have been tried throughout the history of the Earth. Through realization of synthetic biological systems which represent what life could be, synthetic biology allows evaluation of models and hypotheses formulated from observations. Synthetic biology thus uses the complementary approach to the analytical approach which has been used in traditional biology.

Overview

Synthetic biology relies on accumulated biological information from comprehensive analyses such as genomics and on the development of technologies for the preparation of biomolecules. One example is the creation of a bacterial cell controlled by a genome derived from chemically synthesized DNA (Gibson 2010). Although the genome sequence of this "artificial cell" is only slightly modified from the natural one, researchers can now obtain genome DNA with any sequence. In another field of artificial cell study, synthetic micro-containments consisting of lipid molecules encapsulate proteins and/or nucleic acids which confer a part of cellar function (Szostak 2001; Chen et al. 2005; Sunami 2010).

Due to the tremendously huge combination of bio-components, synthetic biology allows realization of biosystems with different properties from the one universally shared by the present life. Although natural ribozymes show a limited range of catalytic diversity, artificial evolution of RNA has uncovered a wide range of activity of aptamers or ribozymes (Ellington 1990). Creations of genetic codes containing 21 amino acids (Wang et al. 2001; Kiga et al. 2002) or

less than 20 amino acids (Amikura 2013) assist the discussion for possible codes on exoplanets or evolution toward the universal genetic code. Such a huge combination, however, invokes two potential problems.

One problem is the rarity of combinations with a proper function. Not only the ratio of amino acids sequences with biological function to that without function, but the ratio of functional biosystems containing multiple macromolecules to nonfunctional biosystems is so small that realization of the functional ones requires evolution through a long time or a rational design process. Mathematical modeling for biological systems leads to fundamental understanding in systems biology and predicts behavior of a designed system in synthetic biology. Designed genetic circuits thus have given living cells programmed bistability (Gardner 2000) or population control via cell-cell communication (Sekine 2011). Through modeling in synthetic biology, furthermore, researchers can estimate the difficulty in construction of a designed system.

The other problem is that systems without correlation to the systems in exoplanet environments or in the past Earth can be created. Thus research on the environmental conditions of exoplanets or the past Earth is crucial for applications of synthetic biology to astrobiology, in order to provide appropriate constraints.

See Also

- ▶ Aptamer
- ▶ Chemical Bistability
- ▶ Genetic Code
- ▶ Cell, Minimal
- ▶ Genome, Minimal
- ▶ Quorum Sensing
- ▶ Ribozyme
- ▶ RNA World

References and Further Reading

Amikura K, Kiga D (2013) RSC Adv 3:12512
Chen IA et al (2005) J Am Chem Soc 127:13213
Ellington AD, Szostak JW (1990) Nature 346:818
Gardner TS et al (2000) Nature 403:339
Gibson DG et al (2010) Science 329:52
Kiga D et al (2002) Proc Natl Acad Sci U S A 99:9715
Sekine R et al (2011) Proc Natl Acad Sci U S A 108:17969
Sunami T et al (2010) Methods Mol Biol 607:243
Szostak JW et al (2001) Nature 409:387
Wang L et al (2001) Science 292:498

Synthetic Cells

- ▶ Protocell
- ▶ Cell Models

System Solar Formation, Chronology of

François Robert
Laboratoire de Minéralogie et Cosmochimie du Muséum (LMCM), Muséum National d'Histoire Naturelle, UMR 7202 CNRS, Paris Cedex 05, France

Keywords

CAI; Chondrules; Chronology; Iron meteorites; Meteorites; Radioisotope; Solar system

Overview

Historical

The knowledge of the age of the Earth and of the Solar System has always been a fundamental question not only for scientists but also in most human cultures. The possibility of finding a solution to this question emerged in the beginning of the twentieth century with the discovery of radioactivity. The probability of transformation (the decay) of a radioactive nuclide (the parent) into a stable nuclide (the daughter) is constant, so that the ratio between a quantity of the parent and that of the daughter is only a function of time. Temperatures or pressures that are reached during geological or planetary processes (including

formation processes) can alter this natural clock. Since all rocks contain traces of natural radioactive elements, the age of a rock can be obtained by measuring the present-day quantity of parent and daughter isotopes, provided daughter isotopes accumulated in mineralogical sites via the decay of their parent were never transported away.

Although in principle a simple task, the determination of the age of a rock relies on a precise measurement of the isotopic ratios of the element that contains the daughter nuclide. Since radioisotopes are present only in trace amounts in most natural samples, the routine determination of the age of a rock was not possible before the early 1960s. The age of the Earth cannot be measured directly because tectonics, erosion, and weathering have eliminated any primordial sample. The age of the Solar System, in contrast, was determined in 1956 by Claire Patterson as the uranium-lead age of chondrites (undifferentiated meteorites) and iron meteorites (Patterson 1956). It is remarkable that this age is still valid within its error bars (4.54 ± 0.07 Ga; 1 Ga $= 10^9$ years). What we know of the age of the Earth comes from extinct radioactivities: the age of the Earth cannot be different by more than a few Ma from the age of the other planetary objects of the Solar System, such as chondritic meteorites. The Apollo missions returned some samples from the lunar mantle which turned out to be hardly younger than the age of the Solar System, 4.43 Ga. It is therefore accepted that this age of 4.55 Ga characterizes the formation of the Solar System. The age of the Sun calculated from nuclear physics is compatible with this value but is known only to within ± 0.15 Ga. A consequence of all these observations is that the formation of the Solar System took place within a time span of 0.1 Ga, i.e., faster than what can be defined by the analytical precision achievable 25 years ago.

The short duration of the formation of the planets prompted a massive technological effort in geochemical laboratories, beginning in the late 1980s. The motivation was to reach a precision on isotope ratios allowing us to distinguish events differing in time by a period of the order of 0.001 Ga but 4.5 Ga old! This is now achieved. New problems have nevertheless emerged simply because understanding the significance of an age measured with such a relative precision (± 0.2 ‰) is an unprecedented challenge in cosmochemistry.

Before addressing these problems, we review the analytical methods commonly used to date events that took place during the condensation of the first solids, their accretion to form small *planetoids* (sometimes referred to in the literature as planetary embryos or also as ▶ planetesimals), and the assembly of these small planetoids to form the present-day planets. Each of these stages has an age that can be deciphered in minerals.

The Concept of Radiometric Ages

The general law of radioactivity (see the detailed treatment of this problem by Albaréde 2003) is written as $P = P_0 \exp(-\lambda t)$. P and P_0 are the number of parent atoms at time t and at time 0, respectively, and λ is the decay constant, which is equal to ln 2 divided by the half-life $T_{1/2}$ (see ▶ Decay Constant, ▶ Half-Life). In cosmochemistry, long-lived ($T_{1/2} > 200$ Ma) and short-lived ($T_{1/2} < 200$ Ma) radioactivities are distinguished because most radioactive isotopes formed with the solar nebula have now disappeared. Short-lived isotopes are therefore "extinct," although minute amounts may be created by interaction of galactic cosmic rays with planetary atmospheres. The surviving long-lived nuclides may be used to obtain *absolute ages* – i.e., ages expressed relative to today – while short-lived systems are used to obtain *relative ages* between different objects. Because of their fast decay, the resolution in time offered by extinct radioactivities is usually much finer with short than with long-lived systems. In other words, the absolute ages of events dated by extinct isotopes are not known, but their time difference is accurately known. ^{235}U has an intermediate status because its half-life of 704 Ma gives the ^{235}U-^{207}Pb absolute ages a particularly high precision.

An absolute age is derived by combining the law of radioactivity and the rules of mass balance, and because thermal equilibration homogenizes isotopic abundances and not elemental

concentrations, the chronometer is formulated in terms of isotope ratios (see Chronology) where the normalizing denominator isotope is stable: $P_0 - P = D - D_0$. D stands for daughter isotope – the stable element resulting from the decay of P. In this equality, the initial quantities P_0 and D_0 are unknown since we have only access to the present-day concentrations. Using the radioactive law defined above, we derive $D = D_0 + P\exp(\lambda t - 1)$. Taking the example of the long-lived radioactive nuclide ^{87}Rb, which decays to ^{87}Sr, we have, using ^{86}Sr to normalize the concentrations, the equation

$$\left(^{87}\mathrm{Sr}/^{86}\mathrm{Sr}\right)_t = \left(^{87}\mathrm{Sr}/^{86}\mathrm{Sr}\right)_0 + \left(^{87}\mathrm{Rb}/^{86}\mathrm{Sr}\right)_t[\exp(\lambda t) - 1]$$

In this equation there are two unknowns: the age t and the isotopic composition $(^{87}\mathrm{Sr}/^{86}\mathrm{Sr})_0$ at initial time. Using several minerals from the same rock or several rocks having the same age t, the two unknowns can be determined. This equation is often displayed graphically as a linear relation referred to as an "isochron" and expressed as $y = ax + b$, with the slope a giving the age of the rock $\left(a = e^{\lambda t} - 1\right)$ and b the isotopic composition of the melt at the time of its isotopic homogenization or $b = (^{87}\mathrm{Sr}/^{86}\mathrm{Sr})_0$.

It should be stressed that the two fundamental "assumptions" of radiochronology – i.e., that the samples dated have the same age and that the system was isotopically homogeneous at some time in the past – are tested through an isochron diagram; if they fail, the linear relation $y = ax + b$ does not hold.

Relative ages are based on the same principles but the parent isotope has long disappeared. Similarly an isochron can be written using the stable isotopes to normalize the concentration. An important example is ^{26}Al ($T_{1/2} = 0.7$ Ma) which decays into stable ^{26}Mg. Normalizing to the other stable isotopes of magnesium (^{24}Mg), the isochron equation follows:

$$^{26}\mathrm{Mg}/^{24}\mathrm{Mg} = \left(^{26}\mathrm{Mg}/^{24}\mathrm{Mg}\right)_0 + \left(^{26}\mathrm{Al}_0/^{24}\mathrm{Mg}\right)$$

Using the stable isotope of aluminum (^{27}Al), the isochron equation can be rewritten as

$$^{26}\mathrm{Mg}/^{24}\mathrm{Mg} = \left(^{26}\mathrm{Mg}/^{24}\mathrm{Mg}\right)_0 + \left(^{26}\mathrm{Al}/^{27}\mathrm{Al}\right)_0 \mathrm{x}\left(^{27}\mathrm{Al}/^{24}\mathrm{Mg}\right)$$

For systems formed at the same time with homogeneous Mg isotope compositions, i.e., same $(^{26}\mathrm{Mg}/^{24}\mathrm{Mg})_0$, this equation represents a straight line in a plot of ^{26}Mg/^{24}Mg vs ^{27}Al/^{24}Mg (all values measured today). In a continuously homogenized gas that condensed Al-bearing phases, the ^{26}Al/^{27}Al ratio depends on time and decays by a factor of 2 every 0.7 Ma. Thus, two samples formed at two different times will have a different $(^{26}\mathrm{Al}/^{27}\mathrm{Al})_0$, i.e., a different slope in the isochron diagram. The time Δt elapsed between these two samples is given by $\left(^{26}\mathrm{Al}/^{27}\mathrm{Al}\right)_{0,1}/\left(^{26}\mathrm{Al}/^{27}\mathrm{Al}\right)_{0,2} = \exp(-\lambda\Delta t)$. Theoretically a relative chronology can be established for several samples, provided they originated from the same reservoir with homogeneous ^{26}Al/^{27}Al. This point can be tested by plotting Δt vs $(^{26}\mathrm{Mg}/^{24}\mathrm{Mg})_0$: in an infinite reservoir of homogeneous gas, such as the solar nebula, $(^{26}\mathrm{Mg}/^{24}\mathrm{Mg})_0$ should increase with Δt (see equation above) and its rate of change should reflect the ^{26}Al/^{27}Al of the reservoir. Recent observations on meteorites attest that the Solar System ^{26}Al/^{27}Al was indeed homogeneous.

In the last 40 years, evidence for the presence of many extinct radioisotopes has been found in meteorites (parent/daughter nuclides): ^{7}Be/^{9}Be ($T_{1/2} = 53$ days), ^{41}Ca/^{40}Ca ($T_{1/2} = 0.1$ Ma), ^{26}Al/^{27}Al ($T_{1/2} = 0.7$ Ma), ^{60}Fe/^{56}Fe ($T_{1/2} = 2.6$ Ma), ^{10}Be/^{9}Be ($T_{1/2} = 1.5$ Ma), ^{53}Mn/^{55}Mn ($T_{1/2} = 3.7$ Ma), ^{107}Pd/^{108}Pd ($T_{1/2} = 6.5$ Ma), ^{182}Hf/^{180}Hf ($T_{1/2} = 9$ Ma), and ^{129}I/^{127}I ($T_{1/2} = 15.9$ Ma). Multiple chronometric systems have been studied in meteorites with the hope of establishing a coherent relative chronology, and substantial progress has been achieved. Isotopic homogeneities of these radioactive systems in the Solar System are still in debate (Chaussidon and Gounelle 2007).

There are several sources of uncertainties on these ages (see ▶ geochronology). When minerals are formed at high temperature in a gas of

solar composition, the gas is rapidly mixed by turbulence and isotopic compositions are kept constant. As long as the gas, or the liquid in the case of molten material, is homogenized, the radioactive clock is constantly reset and does not keep the time. When the gas condenses or the liquid freezes, exchange is only achieved by molecular diffusion, a process which is extremely temperature dependent. When isotopic homogenization by diffusion stops and the parent and daughter isotopes remain in the same crystallographic location, the system is closed to exchange, the clock starts ticking, and this is the moment in time which will be dated.

The timescales of closure are also determined by the cooling rate, and for terrestrial magmas, figures of 0.01–1 Ma are not uncommon. For slow cooling, different minerals that originated from the same parent melt may exhibit substantial differences in age. Chondrules (cf. ▶ Chondrule; Zanda 2004), which are spherules constituting the main mass of chondrites, have a radius in the mm range. They probably remained molten only for minutes, and complete isotopic homogenization of the melt may not have been achieved.

In addition to analytical precision on the determination of isotopic ratios, which depends on each particular chronometer, the most often quoted sources of errors in age are (1) the difference of the closure temperature for different isotope systems and (2) the accuracy of experimentally determined decay constants, which is a serious, neutrino-related issue for β^- decay schemes.

A textbook example of (1) is the absolute age of phosphates in H ordinary chondrites determined by the uranium-lead chronometer and for which the mineralogy attests to a progressive metamorphism. The phosphates located in meteorites that experienced the higher metamorphic temperature are 60 Ma younger than their low-grade metamorphic counterpart (Göpel et al. 1994). This duration reflects the time elapsed in the planetoid that originally hosted the H chondrites to reach the closure temperature of the U-Pb chronometer: in the deepest regions of the H planetoid, the temperature reached during metamorphism was the highest, the corresponding cooling rate was the slowest, and the closure temperature for apatite was reached latest. The span in ages of H meteorites has thus no significance as far as their accretion time is concerned, but offers important clues about the thermal history of the parent body.

A second source (2) of errors is the difficulty of measuring decay constants for β^- radius activity. This problem is usually solved by cross calibration with U-Pb ages.

The Planetary Significance of Radiometric Ages

In order to obtain an isochron, the process of rock and mineral formation must efficiently redistribute the parent and daughter nuclides and induce variations in the parent/daughter ratios. Such a redistribution is controlled by the chemical properties of the minerals hosting the parent and the daughter nuclides. If the accretion of grains takes place at low temperature (typically $<400\,^{\circ}C$), the slow diffusivity of most chemical elements prevents such a parent/daughter fractionation from taking place in solids, and these solids cannot be easily dated.

Four processes have been identified that cause chemical fractionation. Some of them are related to phase changes: condensation from a gas, melting, and crystallization of minerals from a cooling silicate melt. Others are slow solid-state processes (metamorphism) and mechanical sorting. These four processes characterize four steps of planetary formation; some of them being still active today on Earth (magmatic activity and metamorphism).

Condensation fractionates parent and daughter nuclides between the solid and the gas, and its efficiency depends on the condensation temperature of each element. Refractory elements, such as Al and Ti, tend to form oxides at high temperatures (1,400–1,800 K), whereas volatile elements such as K, Na, Pb, and S condense into solids at lower temperature (700–1,000 °C).

- Crystallization or recrystallization during magmatic activity and metamorphism fractionates parent and daughter nuclides between

minerals as a function of temperature, crystallization rate, and geochemical affinity of the parent and daughter for particular minerals. Some elements tend to enter the liquid during melting, while others partition into some minerals at the early stages of the crystallization.
- Mechanical sorting also fractionates parent and daughter isotopes among silicates, sulfide, and metallic phases. Some elements are preferentially fractionated into silicates while others stay in the metallic melt. The formation of a planetary core is an example of this mechanism.

Ascribing an age to a particular process is essentially based on petrographic observations. For example, several carbonaceous meteorites contain calcium-aluminum-rich inclusions (cf. ▶ CAIs) that exhibit geochemical evidence of condensation at high temperature and – for some of them – of reactions with the surrounding volatile-rich matrix. The oldest ages of CAIs are therefore ascribed to their condensation and their younger ages to secondary heating events. Similarly, iron meteorites or basaltic meteorites result obviously from melts, and thus their ages reflect the time of solidification of these melts.

In summary, the significance of isotopic ages relies on hypotheses that may turn be difficult to test rigorously and independently.

The Age of the Solar System

It is generally accepted that the age of the oldest meteorites is a good approximation of the age of the whole Solar System. Two lines of evidence show that this statement is sound: (1) the Earth, the Moon, and most meteorites have approximately the same absolute age, and (2) this age corresponds to the astrophysical age of the Sun. The recent discovery of ^{10}Be in CAIs from carbonaceous meteorites has improved the precision on the genetic relation between the planets and the Sun (McKeegan et al. 2000). The ^{10}Be is a radioisotope produced by nuclear reactions (*spallation* reactions) between energetic solar particles (*solar flares*) and the circumsolar gas. These particles are emitted from the young Sun in its *T-Tauri phase*, which lasts no more than a few million years after its birth. The half-life of ^{10}Be being 1.5 Ma, the Sun cannot predate the CAIs by more than a few half-lives of ^{10}Be that is a few Ma.

By the same token, since CAIs contain ^{10}Be produced by solar flares, they cannot predate the Sun. Thus, it is firmly established that the minerals later incorporated into the present-day planets were contemporaneous with the Sun within approximately ±5 Ma.

This argument can be extended to ^{7}Be, whose half-life is 53 days. Although the occurrence of ^{7}Li, the decay product of ^{7}Be, in the reservoir from which CAIs formed is now confidently established (Chaussidon et al. 2006), it is not possible to ascertain if the ^{7}Be was still alive during the formation of CAIs. This analytical issue is crucial to establish a strict concordance in ages between the planetary material and the Sun.

The existence of CAIs and their mineralogical compositions were predicted thermodynamically before they were actually found. According to these calculations, they represent the first condensates appearing in the solar gas when it cooled. Their absolute ages of crystallization are indeed the oldest of all the Solar System objects. This age is known with a great precision using the combination of the two chronometers ^{235}U/^{207}Pb and ^{238}U/^{206}Pb which provide ages known as lead-lead ages. At the current level of the analytical precision, the CAIs range from 4,567.2 ± 0.6 Ma (Amelin et al. 2002) to 4,568.5 ± 0.5 Ma (Bouvier et al. 2007) and 4,568.2 ± 0.3 Ma (Bouvier and Wadhwa 2010). Scaling this age with the relative age of eucrites suggests that, to a first approximation, the formation of solids and protoplanets took place between 4,568 and 4,559 Ma ago.

Because of their short half-lives, extinct radionuclides have concentrations decreasing rapidly as a function of time and thus offer a way to establish a more precise chronology of the processes that have taken place during this short period of time, i.e., between 4,567 and 4,559 Ga.

The Chronology of Accretion

A major discovery in the field of short-lived radioactive nuclides was the finding of ^{26}Mg excesses in Allende CAIs that were positively correlated with the ^{27}Al/^{24}Mg ratio (isochron), demonstrating that the source of the ^{26}Mg excess was the in situ decay of short-lived ^{26}Al nuclide (Lee et al. 1976). Because the abundance of ^{26}Al found in most CAIs $\left(^{26}\mathrm{Al}/^{27}\mathrm{Al} = 4.5 \times 10^{-5}\right)$ is higher by at least one order of magnitude than that predicted by models of continuous galactic nucleosynthesis, the presence of ^{26}Al in the protosolar disk requires the presence of a "last-minute input." The debated question of the origin of the ^{26}Al is not discussed here: either it originated from nucleosynthesis in a massive star dying in the vicinity of the nascent Solar System or may have been produced by local irradiation of part of the protosolar disk by high-energy solar cosmic rays.

Recently, in situ analyses at micrometer scale using secondary-ion mass spectrometers (ion probes) and high-precision magnesium isotopic analyses have shown that the Earth, CAIs, and chondrules (the major high-temperature constituent of chondrites) formed from a reservoir in which the Al/Mg (parent/daughter) ratio and the ^{26}Mg/^{24}Mg isotopic ratio were homogeneously distributed across the solar nebula. At the current level of analytical precision, this homogeneity allows ^{26}Al to be used as a quite precise chronometer. In this context, high-precision ^{26}Al isochrons for chondrules reveal distinct chondrule melting events taking place between $\sim$ 1.2 and $\sim$ 4 Ma after CAIs, with formation peaks at around $\sim$ 1.5 and $\sim$ 3 Ma.

The mineralogical, textural, and chemical characteristics of chondrules indicate that these objects formed during brief and incomplete melting events of solid precursors (Hewins et al. 2005) and that they subsequently went through strong gas-melt interactions. It is not clear whether this gas was the background ▶ protosolar nebula medium or resulted from the continuous evaporation of solids at high temperature. Lead isotopes show that chondrule formation occurred over a few million years ago. For example, chondrules in the CR-chondrite Acfer have an age of 4,564.7 $\pm$ 0.6 Ma and therefore postdate CAIs by about 3.8 Ma. Chondrules in two CB chondrites have younger ages of 4,562.7 $\pm$ 0.9 Ma and are 5.8 Ma younger than CAIs. In general, the timescales given by lead isotopes are in quite good agreement with those inferred from the ^{26}Al systematics. Many chondrules, however, show no measurable record of ^{26}Al and no sign of metamorphic perturbations: they are therefore probably younger by at least ten half-lives of ^{26}Al, i.e., $\approx$7 Ma.

The problem of the significance of the chondrule ages is further complicated by the presence in Mg-rich chondrules of unequilibrated, likely relict olivines. This is clearly visible with oxygen isotopes. One of the geochemical requirements for obtaining a radiometric age is therefore not fulfilled since, upon its formation, the melt contained isotopically heterogeneous material. So far, however, no ^{26}Al isochron is known that would support a contemporaneous formation of chondrule and CAIs.

The in situ decay of ^{10}Be into ^{10}B was detected in all CAIs in which the distribution of B was not perturbed by metamorphism, alteration, or contamination, all processes that may have strong isotope effects for a trace element like boron present at the sub-ppm level. However, such a variation cannot be a priori interpreted as a chronological signature because a particularly refractory multiple oxide of Ca, Al, Ti, and Mg known as hibonite present in some rare CAIs appears to have formed with a ^{10}Be/^{9}Be ratio which is half the ratio of normal CAIs. In a condensation sequence, a refractory mineral such as hibonite should form early with respect to the other minerals from the same CAI. Therefore the ^{10}Be/^{9}Be ratio did not record the condensation time of CAIs but some other process. Because of the small number of documented cases, this conclusion should only be considered as a provisional, but it reaffirms the importance of these observations.

Lithium is very depleted in the Sun. The prevalence of irradiation processes forming ^{6}Li excesses in the protosolar disk, most likely during the T-Tauri phase of the Sun, is supported by the ^{7}Li/^{6}Li ratio of CAIs, which is lower than in chondrites. Values of ^{7}Li/^{6}Li = 9.20 $\pm$ 0.22

were observed in one Allende CAI and of 9.9 ± 1.1 in one Axtell CAI and should be compared with the chondritic value of 12.0 ± 0.3.

The ^{53}Mn-^{53}Cr extinct radioactivity is particularly useful for the early history of the Solar System. Numerous isochrons ^{53}Cr/^{52}Cr vs ^{55}Mn/^{52}Cr have been produced in meteorites. In CAIs, the parent/daughter fractionation (Mn/Cr) is a magmatic process: Mn and Cr are redistributed among various silicates and metal during melting. Therefore a ^{53}Mn/^{55}Mn age stands for the age of condensation provided that the post-formation heating events were short. As for ^{26}Al, this last point can be supported by petrological observations. On average, the ^{53}Mn/^{55}Mn ratio is 2.8 ± 0.3 × 10^{-5} in CAIs, while chondrules and whole-rock chondrites give a ^{53}Mn/^{55}Mn ratio of 9.5 ± 3.0 × 10^{-6}. The estimated age difference between CAIs and chondrites ranges between 3.7 and 10.8 Ma. This result is consistent with those obtained from ^{26}Al, although noticeable discrepancies of about ±2 Ma still exist.

Among the various short-lived radioactive nuclides, ^{60}Fe ($T_{1/2}$ = 2.62 Ma decaying in ^{60}Ni) is the only isotope that cannot be produced in the Solar System and must result from explosive nucleosynthesis in distant stars. Evidence of ^{60}Fe occurrence has been found in FeS (troilite) and in magnetite from several ordinary chondrites (Mostéfaoui et al. 2004). The highest ^{60}Fe/^{56}Fe ratio measured so far is 0.92 ± 0.24 × 10^{-6}. Somewhat lower ^{60}Fe/^{56}Fe ratios (2.2 and 3.7 × 10^{-7}) have been found in chondrules. Again, the issue of ^{60}Fe initial abundance and distribution are the subject of ongoing research.

The Chronology of Planet-Forming Processes

Mounting evidence shows that small planetoids accreted and differentiated very early around the Sun, more or less contemporaneously with the formation of CAIs, and thus earlier than chondrites. Recent models of runaway growth show that asteroids can form in a few times 10^4 to less than 10^6 years, but, until very recently, very little isotopic data from meteorites would allow us to constrain such short timescales.

Among the first evidence for an early differentiation of a meteoritic parent body was the finding of ^{26}Mg excesses in plagioclase crystals from a magmatic (melted) meteorite (the eucrite Piplia Kalan; Srinivasan et al. 1999). A ^{26}Al/^{27}Al ratio of 7.5 ± 0.9 × 10^{-7} was inferred from these data at the time of the crystallization of these plagioclases from melts produced during the melting and differentiation of the eucrite parent body, possibly the asteroid ▶ Vesta. This result implies that differentiation took place very early, some 4.6 Ma after the crystallization of CAIs. Several other similar results were found showing that the differentiation of the planetoids starts as early as ≈ 2.5 Ma after the condensation of the CAIs. The time required for the radioactive elements ^{26}Al and ^{60}Fe to produce enough heat to melt a thousand-kilometer-size asteroid has been estimated 1.8 Ma. This time represents the minimum duration taken by the planetoid to melt after its formation. Accordingly, the accretion age of these differentiated meteorites should postdate the CAI by only 2.5–1.8 = 0.7 Ma.

The extinct radioactivity of ^{53}Mn has also been used to establish a detailed chronology of the differentiation. Igneous meteorites (eucrites) define a single isochron with a slope indicative of a ^{53}Mn/^{55}Mn ratio of 4.7 ± 0.5 × 10^{-6}. This whole-rock isochron dates fractionation of Mn from Cr, which is thought to represent the isolation of the material that formed the eucrites prior to their melting. The corresponding time elapsed between the formation of the CAIs and the formation of the eucrite parent body before its differentiation is ≈ 11 Ma. Alternatively, if different minerals from a same sample are analyzed separately, the isochrons of each meteorite, the duration of the differentiation process increases to 18 Ma.

Among meteorites, iron meteorites are pure metallic bodies. They likely result from melting of asteroids followed by a gravitational segregation of the metallic and silicate melts. The metal segregates and eventually crystallizes to form the planetary cores. Debris of such cores produced by collisions among asteroids or by tidal effects in the asteroid belt are now sampled as iron meteorites. Because reducing conditions are prevalent at high temperatures, early melting of asteroids must have resulted in metal-silicate differentiation. ^{182}Hf decays to ^{182}W with a half-life of

8.9 Ma, and the ^{182}Hf-^{182}W system is a suitable chronometer to date core segregation: W fractionates into the metal and Hf into the silicate mantle. The radiogenic ^{182}W excesses measured in CAIs are used to determine that, at the time of formation of CAIs, the ^{182}Hf/^{180}Hf ratio in the protosolar nebula was $1.07 \pm 0.10 \times 10^{-4}$ and tungsten was depleted in ^{182}W by ≈ 0.35 % with respect to the Earth. Surprisingly, the ^{182}Hf-^{182}W ages of the iron meteorites are indistinguishable from those of CAIs (Kleine et al. 2005), which, taking uncertainties into account, requires that the metal-silicate differentiation took place on the parent body of magmatic irons no later than ≈ 1 Ma after CAIs. Again a picture in which small planetoids accrete very early in the protosolar disk emerges from this chronometer.

If asteroids indeed formed early – say between 0.1 and 1 Ma – most of them experienced high collision rates during the runaway growth period. Because chondrules seem, on average, to be younger than CAIs by up to a few Ma, their precursors might have incorporated fragments of the early accreted and differentiated asteroids. Such fragments were isolated recently in chondrules from the CV carbonaceous chondrite Vigarano. Oxygen isotopes show that these chondrules contain relict textures that are most likely accounted for by small fragments of olivine-rich differentiated planetoids. The different aspects of the chronology of the Solar System formation discussed in this text are summarized (Fig. 1).

Future Directions

The age of the oldest known solids of the Solar System is now known to be within ± 0.3 Ma at 4.5682. Condensation and accretion of all solid material in the Solar System took place within a few million years of this age. The presence of the in situ decay products of short-lived radioactive nuclides in both undifferentiated and differentiated meteorites demonstrates that, within a few million years or less, grains were condensed and the first planetoids were accreted and then

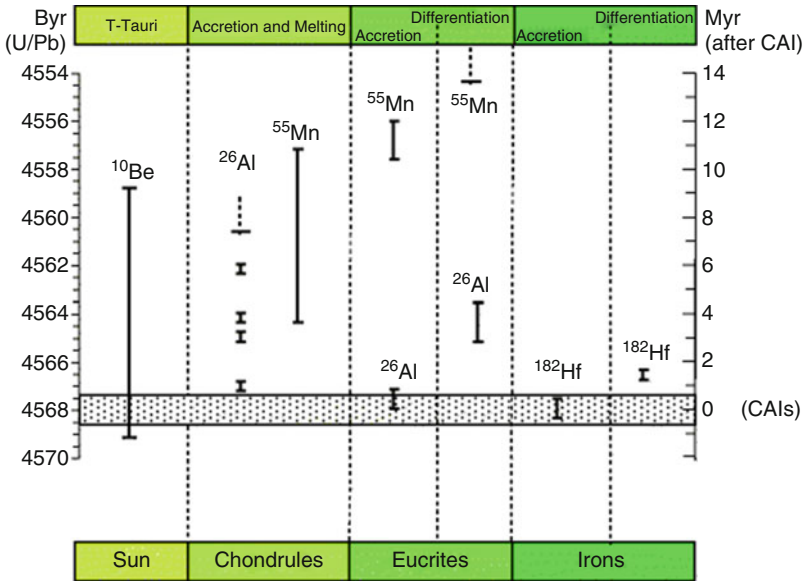

System Solar Formation, Chronology of, Fig. 1 Ages are reported for chondrules and for differentiated meteorites (eucrites and irons). The absolute age of CAIs is expressed in billions of years (Ga); all other ages are relative to CAIs and expressed in millions of years (Ma). The extinct nuclides used for these relative determinations are indicated (*dashed error bars* stand for lower limits). Contrary to chondrules that cooled rapidly, for eucrites and irons, it is possible to define an accretion age that predates their complete melting (differentiation). The age of the Sun is indirectly deduced from the presence of live ^{10}Be in CAIs, which is produced by solar flares at its birth

differentiated. Various chronometers provide an overall consistent chronology but show some discrepancies in detail. Several assumptions underlying isotopic chronometry still need validation and should be regarded as pending issues, namely: (1) Was the distribution of the various short-lived radioactive nuclides across the disk homogeneous in time and space? (2) To what extent were the observed short-lived radioactive nuclides' abundances modified by secondary processes either in the solar nebula or on the parent bodies?

See Also

- ▶ Activity, Magnetic
- ▶ CAIs
- ▶ Chondrule
- ▶ Chronological History of Life on Earth
- ▶ Cratering Chronology
- ▶ Geochronology
- ▶ Planetary Evolution
- ▶ Planetesimals
- ▶ Protosolar Nebula, Minimum Mass
- ▶ T Tauri Star
- ▶ Vesta

References and Further Reading

Albarède F (2003) Geochemistry: an introduction. Cambridge University Press, Cambridge

Amelin Y, Krot AN, Hutcheon ID, Ulyanov AA (2002) Lead isotopic ages of chondrules and calcium-aluminum-rich inclusions. Science 297:1678–1683

Begemann F, Ludwig KR, Lugmair GW, Min K, Nyquist LE, Patchett PJ, Renne PR, Shih CY, Villa IM, Walker RJ (2001) Call for an improved set of decay constants for geochronological use. Geochim Cosmochim Acta 65:111–121

Bouvier A, Wadhwa M (2010) The age of the Solar System redefined by the oldest Pb-Pb age of a meteoritic inclusion. Nat Geosci 3:637–641. doi:10.1038/NGEO941, Published Online 22 August 2010

Bouvier A, Blichert-Toft J, Moynier F, Vervoort JD, Albarède F (2007) Pb-Pb dating constraints on the accretion and cooling history of chondrites. Geochim Cosmochim Acta 71:1583–1604

Chaussidon M, Gounelle M (2007) Short-lived radioactive nuclides in meteorites and early solar system processes. C R Geosci 339:872–884

Chaussidon M, Robert F, McKeegan KD (2006) Li and B isotopic variations in an Allende CAI: evidence for the in situ decay of short-lived ^{10}Be and for the possible presence of the short lived nuclide ^{7}Be in the early solar system. Geochim Cosmochim Acta 70:224–245

Göpel C, Manhès G, Allegre CJ (1994) U-Pb systematics of phosphates from equilibrated ordinary chondrites. Earth Planet Sci Lett 121:153–171

Hewins RH, Connolly HC Jr, Lofgren GE, Libourel G (2005) Experimental constraints on chondrule formation. In: Krot AN, Scott ERD, Reipurth B (eds) Chondrites and the protoplanetary disk, vol 341. ASP conference series, pp 286–316

Kleine T, Mezger K, Palme H, Scherer E, Munker C (2005) Early core formation in asteroids and late accretion of chondrite parent bodies: evidence from ^{182}Hf-^{182}W in CAIs, metal-rich chondrites, and iron meteorites. Geochim Cosmochim Acta 69:5805–5818

Lee T, Papanastassiou DA, Wasserburg GJ (1976) Demonstration of ^{26}Mg excess in Allende and evidence for ^{26}Al. Geophys Res Lett 3:109–112

Libourel G, Krot AN, Tissandier L (2006) Role of gas-melt interaction during chondrule formation. Earth Planet Sci Lett 251:232–240

McKeegan KD, Chaussidon M, Robert F (2000) Incorporation of short-lived ^{10}Be in a calcium-aluminium-rich inclusion from the Allende meteorite. Science 289:1334–1337

Mostéfaoui S, Lugmair GW, Hoppe P, El Goresy A (2004) Evidence for live ^{60}Fe in meteorites. New Astron Rev 48:155–159

Patterson C (1956) Age of meteorites and the Earth. Geochim Cosmochim Acta 10:230–237

Srinivasan G, Goswami JN, Bhandari N (1999) ^{26}Al in eucrite Piplia Kalan: plausible heat source and chronology of formation of eucrite parent bodies. Science 284:1348–1350

Zanda B (2004) Chondrules. Earth Planet Sci Lett 224:1–17

Systems Biology

Kepa Ruiz-Mirazo[1] and Andrés de la Escosura[2]

[1]Department of Logic and Philosophy of Science, FICE, UPV-EHU, Biophysics Research Unit (CSIC – UPV/EHU), Donostia, San Sebastián, Spain

[2]Nanoscience and Molecular Materials Research Group, Universidad Autónoma de Madrid, Madrid, Spain

Keywords

Biochemical networks; Cellular metabolism; Biological complexity; Self-organization; Emergent dynamic behavior; Computational modeling

Definition

Systems biology is a young scientific discipline within the broader field of cell biology, or biology at large, whose major goal is the study of complex dynamic behaviors in biochemical and interactive networks, through the acquisition of quantitative experimental data and the complementary aid of theoretical modeling and computational tools. It is considered a more comprehensive or holistic approach than those traditionally taken in biological and biomedical research to deal with metabolic processes, regulatory networks, and adaptive cellular responses. For general references on this topic, see (Kitano 2002; Westerhoff and Palsson 2004; Boogerd et al. 2007; Camacho and Collins 2009; Klipp et al. 2009; Hübner et al. 2011).

History

Over the last century, a number of scientists and philosophers pointed out the necessity of adopting a *systems* perspective in order to make significant scientific progress, especially with regard to the challenge of biological complexity (de la Escosura et al. 2015). Von Bertalanffy was one of those pioneers, putting forward a "theory of systems" already in the 1950s and 1960s (von Bertalanffy 1950). However, he did not provide a concrete methodological framework to develop such a research program in practice, probably because the required technological advances were not available at that time yet. In addition to those early insights, various disciplines seeded the scientific soil with ideas that contributed to the later foundation of systems biology, like cybernetics and control theory, nonequilibrium thermodynamics, or the mathematical modeling of enzyme kinetics and population growth, among others. The actual term "systems biology" was coined in this context by Mesarovic (1968), followed by other relevant theoretical developments for the field, such as metabolic control analysis, biochemical systems theory, and the first stochastic simulations of complex reaction dynamics. However, the golden age of systems biology came with the advent of genomics, proteomics, and metabolomics (i.e., the "omics" revolution) in the late 1990s, which allowed gathering massive amounts of biochemical data. With the main objective of providing an adequate interpretation of those data and contributing to integrate knowledge from different levels of description of the living phenomena (in particular, from the biomolecular and cellular levels), the field of systems biology has been growing exponentially since 2000 (Hübner et al. 2011).

Overview

Systems biology, rather than a full change of paradigm, represents an important move to find a new balance in the natural sciences, a redistribution of weights in the production of biological knowledge. Oversimplifying history, during the second part of the twentieth century, the focus of biology was on the discovery of the molecular bases that could account for the complex properties and behavior of living organisms. Then, with the increased power of molecular biology's data extraction techniques (the "omics" era), the need to find criteria to interpret that huge amount of information, together with new explanatory tools to link molecular specificities with global cellular responses, became more manifest. Systems biology was the main response from the community (hand in hand with other emerging research areas, like bioinformatics, synthetic biology, or computational biology) to those new challenges. Essentially, it proposes the combination of experimental and theoretical modeling methodologies to work out possible mappings or connection routes (both "upward" and "downward") between molecular details and collective dynamic behaviors, with special emphasis on the cellular level – but also below and, potentially, beyond that level.

Some of the topics currently faced by systems biologists include the study of information processing in signaling networks, the inference of mechanistic models for intricate phenotype development, the modeling of metabolic

interactions and complex microbiomes, or the understanding of cellular dynamics and regulation. More recently, systems biology is starting to contribute significantly to the field of biomedicine, as well (e.g., in drug design and development – see Brown and Okuno 2012). It keeps a special relationship with synthetic biology, a field that was founded approximately in the same historical period and may also be instrumental to reveal basic principles of biological organization –in this case, by synthesizing and trying to assemble standardized bio-modules into more complex circuits or networks. Finally, systems biology has served as a source of inspiration for the onset of its sister discipline in chemistry, "systems chemistry," whose aim is to understand the emergence of biological phenomena from their chemical bases, namely, through the spontaneous self-organization of biomolecular components into protocells and, ultimately, living cells (de la Escosura et al. 2015).

See Also

- ▶ Genomics
- ▶ Metabolic Networks
- ▶ Proteome, Proteomics
- ▶ Protocell
- ▶ Synthetic Cells
- ▶ Systems Chemistry

References and Further Reading

Boogerd FC, Bruggeman FJ, Hofmeyr J-H, Westerhoff HV (eds) (2007) Systems biology. Philosophical foundations. Elsevier, Amsterdam

Brown JB, Okuno Y (2012) Systems biology and systems chemistry: new directions for drug discovery. Chem Biol 19:23–28

Camacho DM, Collins JJ (2009) Systems biology strikes gold. Cell 137:24–26

de la Escosura A, Briones C, Ruiz-Mirazo K (2015) The systems perspective at the crossroads between chemistry and biology. J Theor Biol (in press)

Hübner K, Sahle S, Kummer U (2011) Applications and trends in systems biology in biochemistry. FEBS J 278:2767–2857

Kitano H (2002) Systems biology: a brief overview. Science 295:1662–1664

Klipp E et al (2009) Systems biology – a textbook. Wiley, Weinheim

Mesarovic M (1968) Systems theory and biology. Springer, New York

von Bertalanffy L (1950) An outline of general system theory. Br J Philos Sci 1:114–129

Westerhoff H, Palsson B (2004) The evolution of molecular biology into systems biology. Nat Biotechnol 22:1249–1252

Systems Chemistry

Jan W. Sadownik and Sijbren Otto
Stratingh Institute for Chemistry, University of Groningen, Groningen, The Netherlands

Keywords

Molecular networks; Far-from-equilibrium systems; Dynamic combinatorial chemistry; Supramolecular chemistry; Autocatalysis; Self-replicating molecules; Oscillating reactions; Chiral symmetry breaking; Prebiotic chemistry; De novo life

Definition

Systems chemistry is an area of chemistry that seeks insight into complex networks of interacting molecules and their system-level properties. These properties emerge through the collective behavior of the system's components and cannot be attributed to the individual components acting in isolation. The way in which specific interactions between the components propagate through the system dictates these emergent properties.

History

The term "systems chemistry" was first used in 2005 by von Kiedrowski in a publication (Kindermann et al. 2005) describing the kinetic and computational analysis of a nearly

exponential organic replicator. In this paper, von Kiedrowski claims new research "could open a door to a field that may be termed systems chemistry, namely, the design of prespecified dynamic behaviour." In the same year, a systems chemistry workshop (Stankiewicz and Eckardt 2006) was held in Venice, Italy where a more detailed definition was given describing systems chemistry as "a new field of chemistry seen as the offspring of prebiotic and supramolecular chemistry on the one hand and theoretical biology and complex systems research on the other." In 2007, a new EU research network on systems chemistry (COST CM0703; European **Co**operation in **S**cience and **T**echnology) was established, which followed a similar line of reasoning. In the context of this COST Action systems chemistry is seen as the bottom-up chemical pendant of systems biology toward synthetic biology. This approach would be made feasible by a joint effort of prebiotic and supramolecular chemistry assisted by computer science from theoretical biology, theoretical chemistry, and complex systems research to tackle dynamic supersystem integration including at least one autocatalytic subsystem. In 2009, the Centre for Systems Chemistry was established at the University of Groningen, Netherlands, and an open access *Journal of Systems Chemistry* (von Kiedrowski et al. 2010) was launched through the Chemistry Central platform now part of the Springer publishing house. The 2007 COST action was followed by Action CM1304 that started in 2013.

Overview

Most chemists have traditionally focused on devising chemical transformations that produce a single, desired compound with given properties selectively. In such approaches, mixtures of compounds are undesired and eliminated with various purification techniques. This situation is no longer the case, since more complex mixtures have become tractable by the development of advanced analytical methods. Today, it is possible to move away from the reductionist approach that inspired most research in chemistry previously and develop methods to study multiple variables simultaneously paving the way for systems chemistry (Ludlow and Otto 2008; Peyralans and Otto 2009; Nitschke 2009; Stoddart 2012). Systems chemistry defines a new area of chemistry in which a few already well-established branches of chemistry come together. Many systems featured in the area incorporate phenomena under thermodynamic control such as dynamic combinatorial libraries (Li et al. 2013), molecular recognition, and self-assembly. In many cases, it is the combination and fine interplay between these elements that give rise to specific emergent properties sought for in systems chemistry research. While thermodynamically controlled molecular networks are probably easier to study and understand, kinetically controlled networks have greater relevance to biology, as life operates far from equilibrium. Some examples of studied kinetic processes in the scope of systems chemistry include autocatalytic reactions and self-replicating molecules, kinetic self-assembly, self-sorting processes, and oscillating reactions. One of the major questions that systems chemistry sets out to answer (Szostak 2009; Ruiz-Mirazo et al. 2014) is what made the transformation of a complex mixture of molecules on the prebiotic Earth into a living chemical system possible. What most researchers agree upon is that a combination of thermodynamic and kinetic processes as well as an array of auto- and cross-catalytic cycles played a major role in this development. Another aspect of this research is finding out why the particular biochemical building blocks of life that we know today were selected and how some of these biomolecules developed to have specific chirality. Systems chemistry addresses these issues by devising model synthetic systems with properties that could reflect aspects of prebiotic biogenesis. Another topic at the core of systems chemistry is the quest for de novo life. However, life is just one incredibly complex functional molecular system, and many others are conceivable, and what may be achieved with systems chemistry is ultimately only limited by the creativity of the chemist.

See Also

- Artificial Life
- Autocatalysis
- Chemical Reaction Network
- Chirality
- Complexity
- Origin of Life
- Prebiotic Chemistry
- Self-Assembly
- Self-Replication, Chemical
- Systems Biology
- Thermodynamical Chemical Equilibrium

References and Further Reading

Kindermann M, Stahl I, Reimold M, Pankau WM, von Kiedrowski G (2005) Systems chemistry: kinetic and computational analysis of a nearly exponential organic replicator. Angew Chem Int Ed 44:6750–6755

Li J, Nowak P, Otto S (2013) Dynamic combinatorial libraries: from exploring molecular recognition to systems chemistry. J Am Chem Soc 135:9222–9239

Ludlow RF, Otto S (2008) Systems chemistry. Chem Soc Rev 37:101–108

Nitschke JR (2009) Systems chemistry: molecular networks come of age. Nature 462:736–738

Peyralans JP, Otto S (2009) Recent highlights in systems chemistry. Curr Opin Chem Biol 13:705–713

Ruiz-Mirazo K, Briones C, de la Escosura A (2014) Prebiotic systems chemistry: new perspectives for the origins of life. Chem Rev 114:285–366

Stankiewicz J, Eckardt LH (2006) Chembiogenesis 2005 and systems chemistry workshop. Angew Chem Int Ed 45:342–344

Stoddart JF (2012) From supramolecular to systems chemistry: complexity emerging out of simplicity. Angew Chem Int Ed 51:12902–12903

Szostak JW (2009) Systems chemistry on early Earth. Nature 459:171–172

von Kiedrowski G, Otto S, Herdewijn P (2010) Welcome home, systems chemists! J Syst Chem 1:1–6